EFFECTS OF CARBON DIOXIDE STORAGE IN COAL ON THE PHYSICAL AND CHEMICAL PROPERTIES OF COAL

Tshifhiwa Maphala

A Thesis submitted to the Faculty of Engineering and the Built Environment, University of the Witwatersrand, in fulfilment of the requirements for the degree of Doctor of Philosophy.

Johannesburg 2012

Declaration

I, Tshifhiwa Maphala, declare that the thesis entitled:

“EFFECTS OF CARBON DIOXIDE STORAGE IN COAL ON THE PHYSICAL AND CHEMICAL PROPERTIES OF COAL”

is my own work and that all sources I have used or quoted have been indicated and acknowledged by means of references.

Signature: ……..……..

Date:……

Abstract

Unlike other carbon dioxide (CO_2) storage options, CO_2 storage in coal seams is still in its infancy, and one of the many questions that need to be answered concerns the long term effects of storing CO_2 in coal specifically on the structure and properties of the coal. Most studies on coal structural changes due to CO_2 adsorption have been done over the period of adsorption (hours or 2-3 days), and mostly at low pressures which are not representative of actual storage conditions. The aim of this study is to determine chemical and physical changes that might occur due to long term interaction of coal with CO_2 under pressurised conditions.

Air dried coal samples of different maceral groups (vitrinite and inertinite) were exposed to CO_2 in reactors under subcritical and supercritical conditions for different period of time (up to 6 months). The samples were well characterised pre- and post-CO_2 treatment. A newly-built high-pressure volumetric system was used for adsorption and desorption isotherms measurements of the coals before CO_2 sorption. The characterisation techniques used were BET, XRD, FTIR and ^{13}C NMR.

Surface area analysis of untreated and treated coal particles showed that vitrinite-rich coal samples have a greater surface area and pore size distribution change in pore structure following CO_2 treatment than the inertinite-rich coal particles. Analysis of the crystalline part of the CO_2 untreated and treated inertinite-rich particles showed that there was slight increase in the average crystallite height following CO_2 treatment, although no changes were observed for the d_{002} aromatic interplanar spacing.

In comparing the effects of subcritical and supercritical treatment on CO_2 sorption behaviour over time, the study determined that the long term effects of CO_2 storage in coal were found to be dependent on the maceral composition of the coal, with the vitrinite-rich coal showing a more pronounced structural and properties change after CO_2 storage. This change did, however, differ under subcritical and supercritical conditions. Inertinite-rich coal was found to be less prone to changes under CO_2 storage. A major implication of this finding is the inclusion of maceral composition as major criteria for determining CO_2 storage in coal capability.

The results in this study contribute significantly to the understanding of coal-CO_2 interactions and the implications for coal structure and properties changes; the results could be used by decision-makers on the effects of storing CO_2 in coal.

This thesis is dedicated to my beloved wife, Ruth Maphala, and

My parents, Elinah and Phillemon Maphala

Acknowledgements

I would like to express my sincere thanks to my supervisor, Prof. Nicola Wagner, firstly for giving me the opportunity to study towards this PhD, and secondly for her relentless guidance and support throughout this research.

I gratefully acknowledge the financial support for this work provided by the Sasol Bursary department. I would also like to thank Dr Johannes van Heerden, from Sasol Technology R&D, who was instrumental in approving this project and for his help in the first stages of my study.

I would like to thank Prof Dave Billing and his team of the Crystallography Research Group in the School of Chemistry, Wits, for his help and advice in using the x-ray diffraction facilities and at times collecting some of the data for me.

Many thanks to Willie Augustyn and Mulanga Maphada for their assistance with the volumetric high pressure adsorption.

Thanks to Gregory Okolo of the Coal group in North-West University for his assistance with data collection for the BET analysis. Thanks for your Saturdays and late nights collecting data for me. Additionally, I would like to thank Dr Dirk Prinz from RWTH Aachen University for his assistance with some of pore data collection and analysis and Dr Heidi Assumption from the University of Stellenbosch for her assistance with solid state ^{13}C NMR analysis and interpretation.

A great thank you to all my Coal and Carbon Research group colleagues, too numerous to mention, for the encouragement. Your friendship and laughter made the sometimes painful experience of studying a PhD more fun and enjoyable.

Finally a special thanks to my parents, my wife and friends for their emotional support during my studies.

Table of Contents

List of Figures

Appendices

List of Tables

Appendices

List of Abbreviations

n_{abs}	absolute number of moles
AB	Absorption isotherm
AD+AB	Adsorption + Absorption isotherm
AD	Adsorption isotherm
adb	Air dried basis
ASTM	American Society for Testing Materials
ATR-FTIR	Attenuated total reflectance-Fourier transform infrared
L_a	Average crystallite length of unit cell
L_c	Average crystallite width of unit cell
C	BET constant related to heat of adsorption
BET	Brunauer Emmett Teller
C	Carbon
CCS	Carbon Capture and Storage
CO_2	Carbon dioxide
CP	Cross Polarization
DAB	Desorption absorption isotherm
DD	Dipolar Dephasing
D-A	Dubinin-Ashkov
ECBM	Enhanced Coal Bed Methane
EOS	Equation of State
n_{exc}	excess number of moles adsorbed

AB_f	Final amount absorbed
FC	Fixed Carbon
FTIR	Fourier Transform Infrared Resonance
f_{al}	Fraction of aliphatic carbons
f_{al}^{O}	Fraction of aliphatic carbons bonded to oxygen
f_a^{S}	Fraction of alkylated aromatic carbons
f_a	Fraction of aromatic carbons
f_a^{B}	Fraction of bridgehead carbons
f_a^{CO}	Fraction of carbonyl carbons
f_a^{N*}	Fraction of non-protonated carbons and CH_3 in aliphatic region
f_a^{N}	Fraction of non-protonated carbons and CH_3 in aromatic region
f_a^{P}	fraction of phenolic carbons
f_{al}^{H}	Fraction of protonated carbons and CH_3 in aliphatic region
f_a^{H}	Fraction of protonated carbons in the aromatic region
R	Gas constant
n_{exc}	Gibbs number of excess moles adsorbed
Gt	Gigatons
S_g	Glass transition concentration
T_g	Glass transition temperature
$g.cm^{-3}$	Gram per cubic centimetre
He	Helium
H_2	Hydrogen
IRP	Integrated Resource Plan
d_{002}	Interlayer spacing of crystallites in a unit cell

kWh	kilo watt hour
kg/m^3	kilogram per metre cubed
km	kilometre
kV	kilovolts
b	Langmuir Parameter
MHz	megahertz
MPa	Megapascal
m	Metres
Mt	metric tonne (1000kg)
mA	milliamperes
mmf	Mineral matter free
M	Moisture
nm	nanometres
NIST	National Institute of Standards and Technology
N_2	Nitrogen
NLDFT	Non-local density functional density model
NMR	Nuclear Magnetic Resonance
N	Number of crystallite in a unit cell
n_o	number of sites available for adsorption
PSD	Particle size distribution
ppm	Parts per million
h^{-1}	Per hour
m^{-1}	per metre
PSD	Pore size distribution

PXRD	Powder x-ray diffraction
P_1	Pressure in the sample cell
P/P_0	Relative Pressure
P_0	Saturation pressure at adsorption pressure
SPE	Single Phase Excitation
SPE	Single Pulse Excitation
$_{ss}$NMR	Solid State Nuclear Magnetic Resonance
S.G	Specific Gravity
m^2/g	Square metre per gram
Std dvt	Standard deviation
STP	Standard Temperature and Pressure
T	Temperature
TGA	Thermogravimetric analysis
nt	total number of moles adsorbed
n_t	total number of moles of gas transferred to the cell
Rot	Total reflectance
V_t	total volume
VRr	Vitrinite reflectance
V_0	Void volume
VM	Volatile Matter
Vm	volume available for monolayer
V_{ads}	Volume of the adsorbed phase
V_{sc}	Volume of the sample cell
vol %	Volume percentage

cm^{-1}	wavenumber
wt%	Weight percentage
XRD	X-ray diffraction

List of Symbols

Å	Angstroms units
β	Beta
μ_i	Chemical potential
^oC	Degrees Celsius
ρ	density of gas in the free space
ν	Frequency of wave
γ	Gamma
λ	Lambda - wavelength of x-ray source
μm	Micrometre
ρ_a	molar density of the adsorbed phase
§	Section
δ	Solubility Parameter
θ	Theta

CHAPTER 1
INTRODUCTION

South Africa, a carbon-intensive state with 89% of the country's primary energy needs derived from fossil fuels, has recently been included in the top 20 global carbon dioxide (CO_2) emitters per kWh energy produced [1]. The country currently emits about 1% of the total global CO_2 emissions, which equates to about 400 metric tons (Mt) of CO_2 [1]. By 2026 Eskom is estimated to be producing about 485Mt of CO_2, while the South African government has set a target of 550Mt by 2025 for the whole country [2]. Given the increasingly intensive global focus on climate change, there is a growing realisation that South Africa is going to need to adopt a lower-carbon intensive energy trajectory, if it hopes to avoid the financial and social penalties that now look inevitable, not only for the developed world, but also for advanced developing countries like South Africa [3].

Given South Africa's abundance of coal, and the limitations and expense associated with renewable energy as a bulk energy supplier, much emphasis is being given to cleaner coal technologies [4]. Under the umbrella of clean coal technologies is the promising option of carbon capture and storage (CCS). Carbon Capture and Storage is a process consisting of the separation of CO_2 from industrial and energy-related sources, and transport to a storage location for long term isolation from the environment [5]. The capture of CO_2 can be applied to large point sources and the CO_2 would then be compressed and transported to a geological storage location. Geological storage of anthropogenic gas as a greenhouse gas mitigation option was first proposed in the 1970s, but little research was done until the early 1990s when the idea gained credibility through the work of individuals and research groups [5]. Over the

last decade there has been a noticeable increase in work performed in this area as evidenced by the number of literature dedicated to the subject [6]. Geological storage locations being used or under investigation include, but are not limited to, depleted oil and gas reservoirs, deep unused saline water-saturated reservoir rocks, oil shales, and deep unmineable coal seams [7].

1.1 Geological storage in southern Africa

In 2011, the world bank released a discussion paper on barriers for deployment of CCS in developing countries [8]. The study provided a business case for CCS under different scenarios of a CO_2 price. Figure 1-1 shows the estimated potential storage of CO_2 in the southern African region as estimated by the World Bank report under a US$100/Ton CO_2 price scenario.

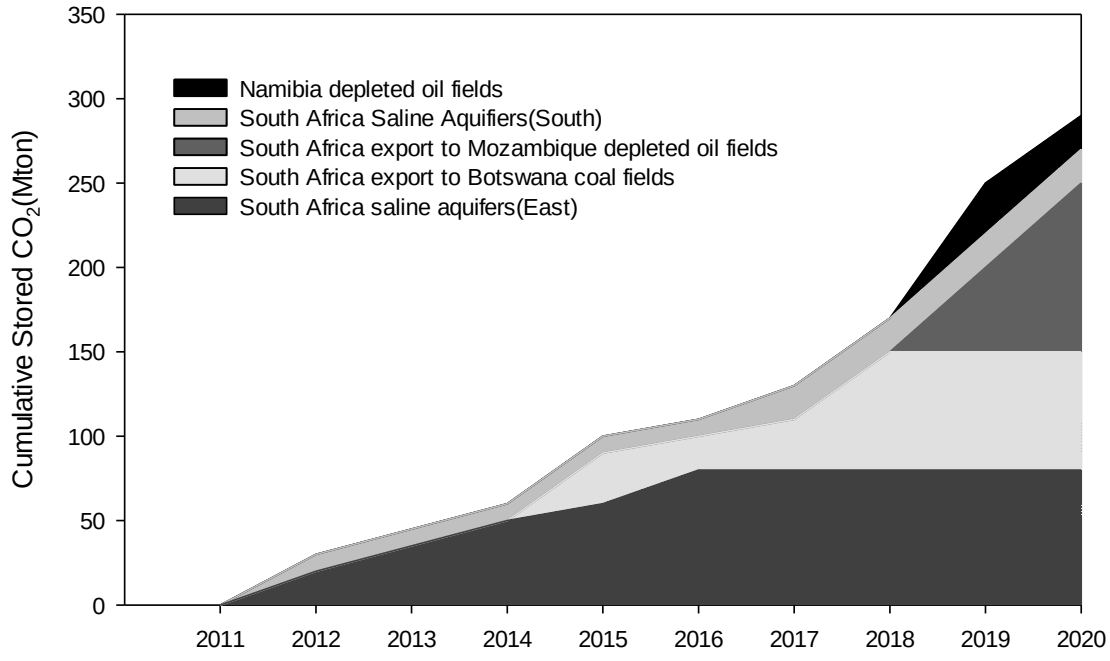

Figure 1-1: Potential storage of CO_2 in the Southern African region[8]

It is evident from Figure 1-1 that from a business perspective the economics of CCS start to make a case with a potential storage of 300Mton CO_2. The World Bank study provided a business case without providing the technical evidence for the storage potential.

In 2008, the South African Centre for Carbon Capture and Storage (SACCCS) was launched under the funding of partnerships between government and private companies with the aim of performing a feasibility study of CCS in South Africa (based on a desktop and technical assessment of South African geology). The centre recently launched Carbon Dioxide Storage Atlas to identify potential storage sites and their respective storage capacities for South Africa [9]. The Atlas provides any interested party with an opportunity to assess of the different storage options available in South Africa.

The technical study for the atlas found that the saline formation and coal seam storage possibilities for the Karoo Basins were poor, because of the very low porosity and permeability of the sandstones, the presence of extensive dolerite sills and dykes, and highly disaggregated occurrences of the coal fields [10]. The fact that there wasn't a single viable Karoo basin large enough for a storage site was a discouraging fact to many who were hoping for the contrary due to reasons explained below (§ 1.2). The study overwhelmingly supports the fact that offshore basins have the biggest potential and storage capacity, mostly in saline formations, with only limited storage potential in depleted oil and gas fields.

1.2 Potential for CO_2 storage in coal seams in South Africa

One of the major challenges offshore storage faces is the high operating costs. In a report to the South African government, Engelbrencht et al. [11] highlights the fact that the use of CCS could potentially increase electricity prices by 87%. Of the total costs involved with a CCS operation, transport is a major contributor and is calculated per kilometre i.e long distances between point sources and storage site result in higher costs. This means that the distance

from the capture point to the storage site should be minimised in order to minimise the cost. In South Africa's case, much of the CO_2 emitted is inland (see Figure 1-2(a)) and the costs for transporting it offshore for storage can make CCS uneconomical, rendering it almost impossible in South Africa [11]. Moreover, the locations of the major point source emitters in South Africa are in the vicinity of the coal reserves that can be used as storage site (see Figure 1-2).

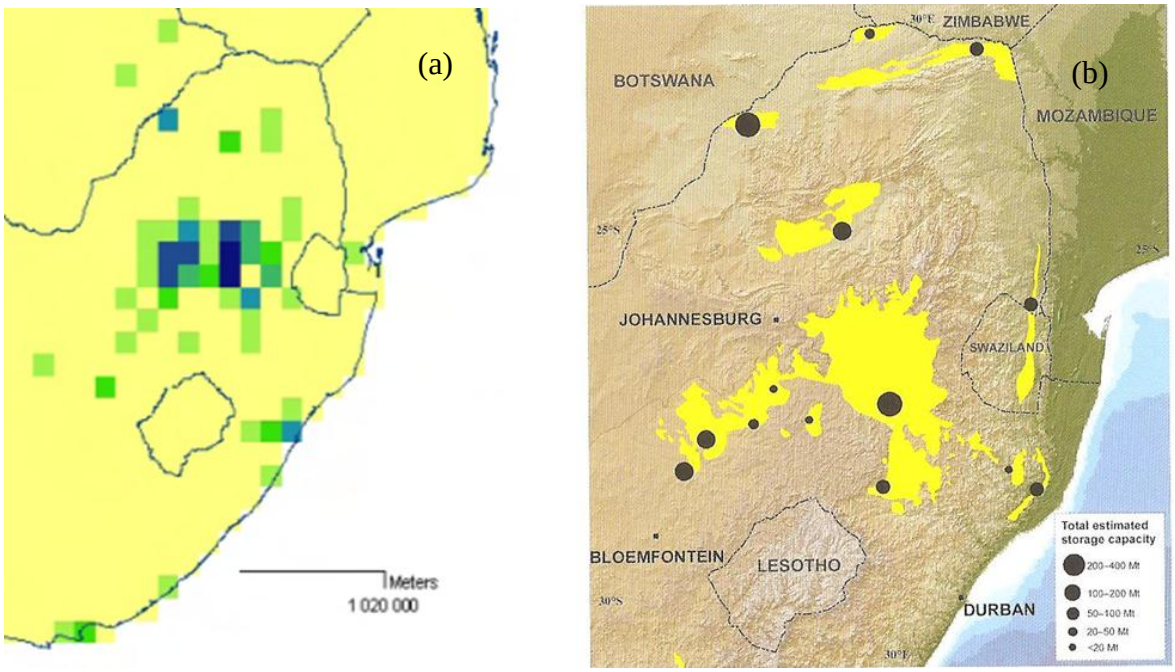

Figure 1-2: A map showing the distances between (a) CO_2 point source emitters [11] **and (b) potential for CO_2 storage in coalfields** [9]**.**

In Figure 1-2(a), the square shades represent the intensity of the CO_2 emissions with the darkest shade representing a higher CO_2 emission and a lighter representing a lower CO_2 emission. Evident from Figure 1-2(b) is that the darker shades occur in the Highveld area and Free State, where the Sasol and Eskom facilities are situated. In fact, until recently the Sasol site in Secunda was considered as the global number one point source emitter of CO_2 in the world [5].

Therefore, in terms of transportation, the ideal storage options under consideration should be inland. With so many coal reserves, a high percentage of which are "unminable" [12], South Africa is well positioned to use unminable coal reserves as storage location for CO_2. This is particularly true if a regional approach is taken on CCS in the southern African region and a funding mechanism for CCS (e.g enhanced coal-bed methane recovery (ECBM)) is available, then the storage capacity in unmineable coal seams would increase tremendously with South Africa and Botswana's estimated coal-bed methane resources [13]. According to the World Bank [8], even without ECBM revenues, CCS combined with CBM-derived gas power plants could still be economically competitive. If used with ECBM, CCS in unminable coal seams could be a value-adding technology. In addition to reducing CCS transportation costs, the storage of CO_2 in unminable coal seams can be viewed as a way of utilisation of an otherwise "unusable" resource.

Although there were reservations about the storage in unminable coal seams, as mentioned earlier (§1.1), the SACCCS storage atlas technical report also had some positive facts for CO_2 storage in coal seams in South Africa can be drawn from the [9]. Some of the points include:

- Estimated total storage capacity available for "unminable"[1] coalfields in South Africa is ~1,2GtCO_2.
- High storage capacity is estimated for both the major coal fields, Waterberg and Highveld coalfield, respectively, which is where most of the emitters are located.

With an estimated 1.2Gt storage capacity, unminable coal seams have the capacity to store "storage-ready" emissions for at least the next 30 years. Storage-ready emissions are emissions that are ready for storage without a need for a capturing technology the CO_2 before storage because the CO_2 is highly concentrated. Currently, of the 400Mt of CO_2 emitted in

[1] The definition "unminable" is under constant change and is dependent on mining technology developments. What is "unmineable" during our current times might be mineable in the future.

South Africa about 9% (about 35Mt) of it is 90-98% CO_2 concentrated [14]. Finally, the SACCCS storage atlas technical report also raised many issues and points pertaining not only CCS in unminable coal seams but CCS in general. Such issues are beyond the scope of this study and are not addressed in this study.

1.3 Research motivation

However, as promising as the argument for CO_2 storage in coal seams is, there are still some concerns with the technology and its impact on the environment. Most of the concerns raised in the public domain regarding have been on the fate and long term stability of CO_2 stored in coal seams as indicated in Box 1-1 below.

> BALI - Government is reluctant to allow Sasol, a South African petroleum company, to construct a carbon capture storage (CCS) plant in Botswana. In an interview at the ongoing United Nations climate change conference in Indonesia, senior officials, Steven Monna and Phetolo Phage said government is monitoring global developments regarding such storage plants.
>
> So far it would be too risky to embark on such a project before we know its pros and cons, *what it if the gas eventually leaks from underground*, and what happens to our water? Mr Monna asked rhetorically…In her position paper at the conference, Botswana cautions about *potential dangers such as long-term physical leakage* and points out that any uncertainties need to be fully thrashed out before any commitment could be made.

Box 1-1: Newspaper insert showing concerns for the long term fate and stability of stored CO_2 in coals seams [15]

Most of the public's concerns raised stem from a lack of data regardingthe long term fate and stability of stored CO_2 in coal seams. Although demonstration plants have been planned to address some of the concerns over long term fate and stability of CO_2 in geological storage formations [16-17], most of the currently operating and planned demonstrations are in conventional gas or oil reservoirs [5, 18] and not in coal seams.

Unlike conventional reservoirs, gas storage in coal seams are quite complex, mainly due to the extremely intricate and heterogeneous nature of the coal [19]. This complexity is

evidenced in the many studies relating to the interaction of CO_2 with coal and has been an area of great interest recently [20–22] .

However, there still much that is not understood about coal-CO_2 interactions [22–24]. A prime example of this knowledge gap is evidenced in one of the major hindrances to the full deployment of CO_2 storage in coal seams, i.e the decrease in injectivity during CO_2 injection [25]. Although swelling has been identified as the prime culprit for this observation [26], little work has been done at a fundamental scientific level to understand the CO_2-coal interaction leading to this observed phenomenon. The little work that has been done on the subject has been done in conditions that do not truly represent those in the actual storage site, that is, over the period of adsorption (hours or 2-3 days) and most at low pressures [27–29]. Such conditions are not enough to provide the understanding of CO_2-coal at a fundamental level.

Hence, this study aims to take a more fundamental approach to understanding coal-CO_2 interactions. As such, the study aims to answer the following fundamental research questions with regards to CO_2-coal interactions:

(i) What is the major coal-CO_2 interaction mechanism during CO_2 storage in coal?

It's been suggested that coal not only adsorbs but absorbs into the coal structure, but no studies have been done on what the implications of the absorption might be on the coal structure and properties and how these changes might be dependent on the maceral composition of the coal.

(ii) What effect does the coal composition, that is, maceral composition, have on the CO_2-coal interactions?

(iii) What is the long term effect of CO_2 storage on the coal structure and properties?

Unminable coal seams might be technologically and economically feasible to mine in

the future, and it would be desirable to know what the effect the stored CO_2 will have on the coal properties for mining and utilization purposes?

(iv) And whether these effects dependent on the coal maceral composition?

It should be acknowledged that although swelling of coal is a major point of discussion in the in literature[26,30–33] and to some extent in this study, it is not the focus of this study and is only discussed as a subset coal-CO_2 interaction phenomenon.

1.3.1 Aim and objectives of the study

The overall aim of the study is to contribute to the fundamental understanding of coal-CO_2 interactions and the effects thereof on the coal structure and properties. To achieve this aim the following primary objectives of the study were undertaken:

(i) To determine what the effects of storing CO_2 in coal will be on the sorption properties of the coal, and to determine the major coal-CO_2 interaction mechanism during CO_2 storage with different maceral compositions (inertinite-rich and vitrinite-rich, respectively). In order to achieve this objective the following secondary objectives are endeavoured,

a. *Design, build, and commission a high pressure volumetric adsorption instrument* – The system was able to collect CO_2 adsorption data at pressures higher than 40bar and at CO_2 supercritical conditions above 72bar and 32°C. The system is the first of its kind in South Africa.

b. *Perform high pressure adsorption and desorption isotherms on inertinite-rich and vitrinite-rich coals* – the high pressure adsorption and desorption isotherms were used to deduce the CO_2 sorption mechanisms in coal and were used to determine the adsorption capacities for the two coals.

(ii) To determine, at a fundamental level, molecular and physical structure changes occurring during CO_2-coal interactions:

a. *Long term treatment of coal with CO_2 over a relatively "long" period of time (up to 6 months) under subcritical and supercritical CO_2 conditions*

b. *Characterise the coal structure and properties before and after CO_2 saturation.*

Finally, it should be mentioned that this study will be a laboratory study and there will not be any fieldwork at a CO_2 storage location. However, references will be made to field results and inferences will be made on the applicability of findings on South Africa's potential coal seam storage sites.

1.4 Thesis layout

The thesis layout is as follows: the next chapter is a background review on the current and previous literature on coal-CO_2 interactions. Chapter 3 outlines the methodology, sample preparation and analytical techniques used in the study. Chapter 4 presents the experimental setup for the sorption experiments together with the design and commissioning of the volumetric adsorption isotherm measurement instrument. Chapter 5 presents the pre-sorption coal structure and properties characterised using techniques outlined in chapter 3, and chapter 6 and chapter 7 discusses the post-sorption structure and properties changes under subcritical and supercritical conditions, respectively. Chapter 8 presents the results from the sorption studies chapter 9 provides the summary, conclusions and recommendation for further study.

CHAPTER 2
LITERATURE REVIEW

The suitability of coals for CO_2 storage can be assessed on the basis of three criteria: technical, economic, and regulatory or resource protection [5]. The technical criterion depends on coal properties and behaviour in the presence of CO_2; economic depends on technology and economic environment; and regulatory depends on the presence of other resources, and the future use of the coal as an energy mineral, that need to be protected [5]. This literature review, if not the study, is based on the premise that the first and third criteria are linked, that is, the behaviour of coal in the presence of CO_2 will ultimately affect how the coal will behave over a long period of time. More specifically, the mechanism of CO_2 storage in coal will determine the coal's suitability for future use.

The literature review is structured so as to build up knowledge on the fundamental framework that has been developed over the past decade (and beyond) on the storage of gas in coal seams. The focus of the literature will be limited to understanding the interaction of CO_2 (and CH_4) with coal during storage, methods used to study these interactions. This chapter will also review and discuss the models that have been developed to understand the trapping/storage mechanisms and transport of the gas through the coal pore structure.

The first two sections, history of CO_2 storage in coal (§ 2.1) and factors to consider for CO_2 storage in coal (§ 2.2), form the introductory part of the review. The purpose of discussing coal storage conditions (§ 2.2) is to remind the reader that, although the current study will be at a laboratory scale, the findings and results in this review (and the study) should be interpreted in light of the field conditions of a coal seam. The second section includes a

discussion on coal structure and properties (§ 2.2.2) which includes a discussion on the current models on the coal molecular structure and how these models affect current understanding of coal-CO_2 interactions. The third section takes a step further by providing separate discussion on an important coal property in relation to coal-CO_2 interactions in coal pore structure (§ 2.3). The last three sections are a discussion on coal-CO_2 interactions, starting with a discussion on adsorption and absorption (§ 2.4) followed by a discussion on current literature on the effects of CO_2 storage in coal on the coal structure (§ 2.5.). In the last section (§ 2.6), methods used for studying these effects are reviewed.

2.1 Brief history of gas storage in coal

The idea that coal has the capacity and ability to store gas dates as far back as coal mining existed. It has been common knowledge for many years that coal seams are a geological sink for natural gas or CH_4 [33–35]. However, the idea that CO_2 can be used to displace gas was first established in 1970's by Every and Dell'osso [36] when they discovered that CH_4 can be removed from crushed coal by flowing a stream of gas at ambient temperature through the coal. In the 1980's, the idea was then used by Fulton and co-workers [37] to practically apply it in a coal seam situation. They found that they could rapidly display methane from coal when they injected CO_2 in three cycles during 90 days [37].

According to White et al. [6] the first record of this idea being developed for coal seam sequestration was proposed by Macdonald of Alberta Energy during a series of discussions with Gunter and co-workers in the early 1990's [38]. The BP-Amoco were one of the first to successfully demonstrate and patent the removal of CH_4 from deep, "unmineable" coal seams using gas and other gases [39].

The technology has since been developed over the past decade and is being considered as an option for geological sequestration. Geological sequestration (or storage) of gas in

unmineable coal seams is defined as the disposal of anthropogenic gas deep into the ground for geologically significant periods of time, with or without the concomitant recovery of natural gas [7]. Unmineable coal seams are defined as too thin or too deep and/or unsafe to mine with current coal mining or extraction technology.

2.2 Some factors affecting gas storage in coal seams

The fate and stability of stored CO_2 is a function of the manner (mechanisms) in which CO_2 interacts with coal initially during injection and the duration of sequestration [26]. These mechanisms are functions of the coal structure and properties, and the physical and chemical properties of CO_2 [5].

A brief discussion on the CO_2 properties and storage conditions is presented below. Gas storage conditions represent the actual coal seams conditions in which CO_2 storage is intended. This is important in that it defines the temperature and pressure constraints with which we are working with, even on a laboratory scale. The link between CO_2 properties and storage conditions is obvious, since gas will behave differently under different temperature and pressure conditions.

2.2.1 Carbon dioxide properties

At standard temperature and pressure, CO_2 is about 1.5 times heavier than air, with a density of around 1.98 kg/m³. Thermodynamically, CO_2 serves as the best known reference for a molecule with a strong quadrupole moment and as a testing fluid for calibration [40]. Critical to its application and uses, though, is its supercritical point.

A fluid is said to be supercritical when the temperature and pressure of the fluid are higher than the corresponding critical values. Above the critical temperature of the fluid, there is no phase transition in that the fluid cannot undergo a transition to a liquid phase, regardless of

the applied pressure [41]. At this state, it is referred to as a supercritical fluid, and will behave both as a gas and a liquid. In this way, the properties of supercritical fluids are unique.

A supercritical fluid density is a strong function of the temperature and pressure. A slight change in temperature and/or pressure will result in a large variation in fluid density [42]. A fluid, in its supercritical state, takes up much less space and diffuse better than either gases or ordinary liquids through the tiny pore spaces in storage rocks [43].

Carbon dioxide has a critical point at critical temperature at 31.1 °C, and critical pressure at 72.9 atm or 7.29 MPa [40]. Above this temperature, CO_2 will have both gas and liquid properties, that is, expanding to fill its container like a gas but with a density like that of a liquid [43].

In terms of CO_2 properties in relation to storage conditions, CO_2 will approach its supercritical state with increasing depth. The average geothermal and hydrostatic pressure gradient for a typical geological formation, including coalfields, is shown in Figure 2-1. In the figure, the likely depth for CO_2 to reach its supercritical state is shown. Evident from Figure 2-1 is that CO_2 likely to be become reach its supercritical state at depths below 800-900m [6, 35]. It also means that more CO_2 can be stored at these depths (depths >800-900m) than shallower depths when it is in gaseous phase[2].

[2] This is also to meet the "deep" criteria of unmineable coal seams. Shallower coals might be "mineable" in future

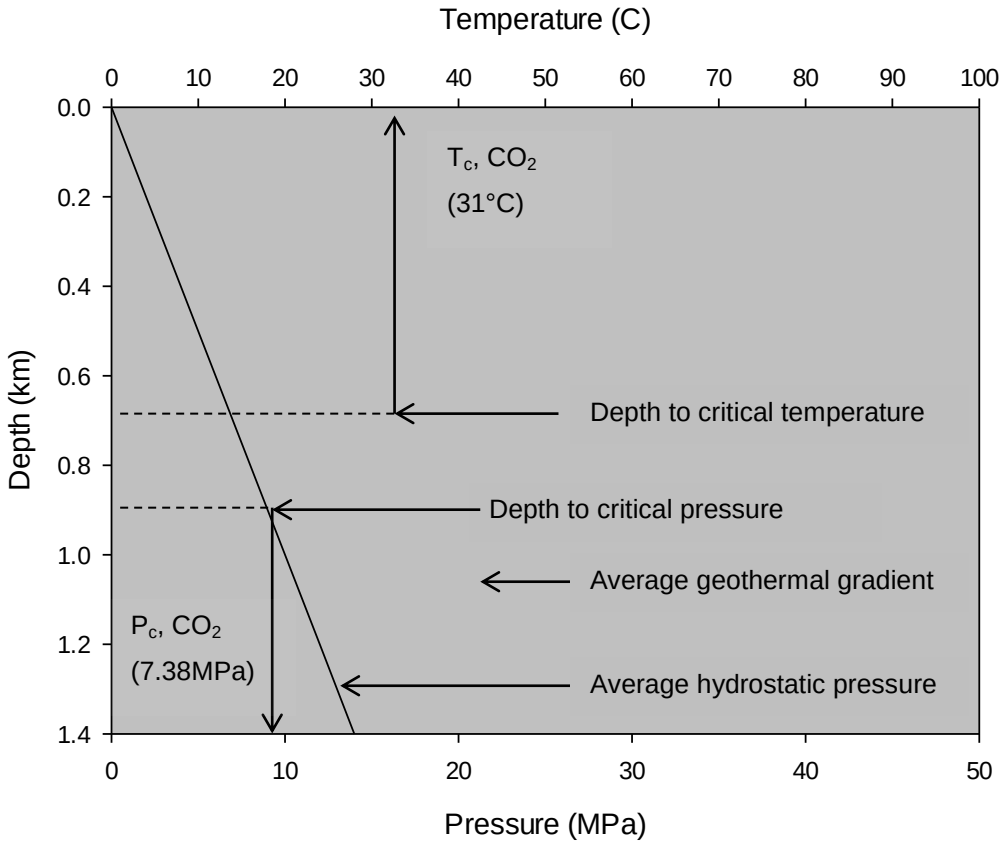

Figure 2-1: Average geothermal and hydrostatic pressure gradient for storage reservoirs ([44] **in** [43]**).**

The geothermal temperature and hydrostatic pressure of a potential CO_2 storage coal seam need to be taken into account when measuring adsorption capacity for a site as adsorption capacities of coal will differ with depths [45]. The greater the burial depth, the larger the pressure and the higher the temperature will be [35, 37]. It is also worth noting that pressure and temperature have an inversely proportional relationship. So, while increases in pressure will result in a corresponding increase in gas sorption/storage, an increase in the temperature decreases the amount of CO_2 sorption/storage [46].

2.2.2 Coal structure and properties

A major factor affecting coal-CO_2 interactions is the coal properties. Below is a discussion on coal properties; a discussion on the properties of coal is not complete if it does not begin with

an introduction to coal's standard characteristics, i.e coal rank, type, and grade. These characteristics are as a result of coal's origin and formation.

2.2.2.1 Coal origin and formation

Coal is formed from plant remains that have been compacted, hardened, chemically transformed, and metamorphosed by heat and pressure over geological time from peat forming environments [47]. In this water-saturated environment, dead mosses, leaves, twigs, and other parts of trees do not decompose completely. Instead, this plant matter becomes a layer of peat [48]. At various intervals, the swamp may be covered by sand and mud when a river floods or when ocean levels rise. Under the weight of these sediments, the peat may lose some of its water and gases, eventually turning into a soft brown coal called lignite [48]. With increasing pressures or temperatures, more water and gases are driven off, forming the common bituminous family of coals. Finally, high temperatures and pressures may cause bituminous coal to turn into a hard black coal called anthracite. This process of forming coal from peat under pressure and temperature conditions is known as lithification and gives coal its rank characteristic [49].

Figure 2-2 shows the main groups of organic matter plotted as a ratio of hydrogen-to-carbon versus oxygen-to-carbon as developed by Van Krevelen [49]. Increasing levels of heat and pressure change the physical and chemical properties of lignin. This produces the different ranks of coals shown in the figure. Note that an increase in rank from lignite to anthracite represents a rise in carbon content relative to hydrogen and oxygen.

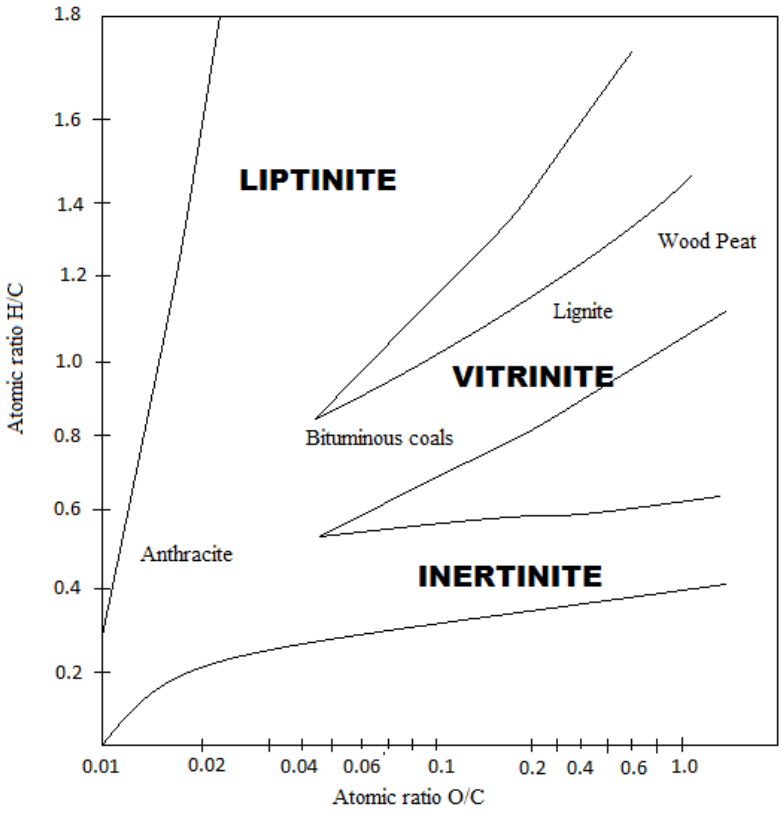

Figure 2-2: Main groups of organic matter plotted as a ratio of hydrogen-to-carbon versus oxygen-to-carbon [49]

Vitrinite inertinite and liptinite, are the coal macerals or coal type. Macerals are organic substances, or optically homogeneous aggregates of organic substances, possessing distinctive physical and chemical properties, and occurring naturally in the sedimentary, metamorphic, and igneous materials of the earth [50].

Macerals are distinguished by their physical and chemical properties; thus, even though two substances may be derived from the same kind of plant tissue, for example, cell wall material, and have a similar petrographic appearance; they would be different macerals if they had different chemical or physical properties. Coal macerals are petrographically characterised by a reflected light analysis technique using immersion oil [50].

The vitrinite group of macerals (also known as “bright” coal) are derived from plant cell wall material (woody tissue) and is the main component of most common coals. It is the most

microporous of all the macerals [50]. Vitrinite also occurs in the form of a less reactive variety, pseudovitrinite, which is characterized by a higher reflectance and a more homogeneous nature than normal vitrinite [50]. The appearance of pseudovitrinite under reflected white light is normally brighter.

The reflectance of vitrinite is intermediate compared with the other maceral groups and provides an excellent indication of the coal rank since it increases as coalification advances [47]. Accordingly, the measurement of the vitrinite reflectance on a polished coal surface has been selected as the parameter to determine the rank of a coal. Vitrinite within low rank coals exhibit a marked variation in reflectance, although such variation diminishes with increasing rank [51].

The inertinite group of macerals (also known as “dull” coal) is derived from degraded woody tissue. It has the highest reflectance and carbon content in any given coal and is usually divided into five general types. Fusinite and semifusinite are characterized by well-defined cell texture with fusinite having the highest reflectance. Semifusinite is the most abundant inertinite maceral type and has the largest range of reflectance between vitrinite and fusinite [50].

The liptinite group of macerals is derived from the resinous and waxy parts of plants such as resin, spores, and pollen. This is the least abundant maceral in coal, and, as it does not form part of this study it is thus not extensively discussed.

And finally, the coal grade is a characteristic representing the amount of non-organic mineral matter content in the coal. A coal with a low grade is associated with a high mineral matter and visa-versa.

2.2.2.2 Molecular structure of coal

Whereas the mineral matter is a well characterized and understood component of coal [52], a full understanding of the organic component is still evolving. This is primarily due to the amorphous nature of high molecular mass mixtures in the organic components. To understand the sorption mechanisms of CO_2 in coals, some background on the chemical and physical structure (organic matrix) of coals is needed.

One of the approaches used to illustrate the main molecular characteristics of coal, is the construction of molecular models of coal [53]. Models help to summarize and evaluate the consistency of various experimental data. Coal's molecular structure models have been a subject of debate that has been going for over 50 years [53–57]. But for the purposes of our study we shall review those molecular structure models that are widely accepted and discuss the implications that these models have on CO_2-coal interactions.

Despite the debate, a general agreement exists amongst coal scientists concerning coal structure, which points to the models shown in Figure 2-3 (i) a cross-linked covelantly bonded network, (ii) a physically associated structure, (iii) molecular aggregates (i+ii) [53, 58–61].

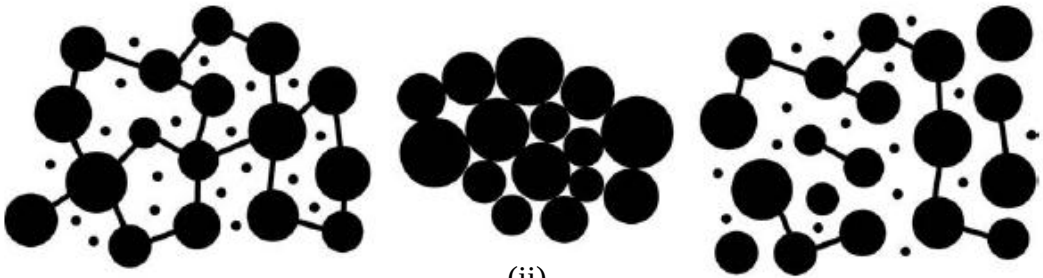

Figure 2-3: Cross-linked network (left) and a physically associated (middle) and combined (right) molecular network coal structures. Adapted from [61]

Figure 2-3(i) shows a cross-linked three-dimensional macromolecular model with the framework occluding some solvent-extractable components. The essence of this model states that only some portions (10-20%) of the mobile phase can be extracted using the regular extraction procedures because of restricted pore sizes of the immobile phase [62]. Only the smaller molecules embedded in cavities or in pores and the not very strongly cross-linked coal constituents can be dissolved by solvents to give coal extracts.

In Figure 2-3(ii), the physically associated structure is shown. It has not been experimentally proven and doubt still exists on this structure as the main molecular structure. However, it has been suggested that intra- and intermolecular (secondary) interactions will play an important role in this model [62]. The most probable structure is Figure 2-3(iii), where the structure model assumes that aromatic and hydro-aromatic structural units of, on average, three to five rings are cross-linked through short aliphatic and ether bridges to form macromolecular aggregates. It differs from the model in Figure 2-3(i) in that the network is not as continuous and three dimensional as Figure 2-3(i) is and hence could be assumed to display some characteristics of Figure 2-3(ii).

Molecular weight between crosslink junctions, the nature of junctions and 'repeating units', the ratio of covalent to hydrogen bonds and the ordering of this system of the models suggest that coal has a polymeric character [63]. This suggestion has immediate implications on the properties of coal and some have applied polymer theory for coal molecular structure studies[3] [64-65]. In polymer science, it is common knowledge that insoluble and swelling polymers are those which are cross-linked materials whilst the soluble portion of coal (like soluble polymers) cannot be cross-linked matter [66-67]. These polymer fundamentals are the basis and conclusions for the models suggested above and are used for postulations in coal sorption mechanisms.

[3] See section 2.4.2.1.1 on polymer theory applied to CO_2 dissolution in coal

An important application of these polymer fundamentals is that, when applied to coal, they can yield invaluable information regarding the coal-penetrant behaviour. Marzec [53] used these theories effectively to observe the response of coal to a swelling agent. The degree to which coal swells in the presence of a specific swelling agent was used as a measure of the solvent-coal compatibility and of the flexibility of the coal structure itself. The degree of penetrant swelling of a cross-linked macromolecular network can be used to determine the coal-penetrant thermodynamic interaction parameter and the effective number average molecular weight between crosslinks of the macromolecular coal structure as long as appropriate molecular theories are available [68].

It should be cautioned though that application of polymer theory to coal might be an oversimplification of an otherwise complex system. Whilst polymers have measurable repeating units over a long molecular range, such repeating units have not been shown in coal [60-61]. In applying these theories to coal (which is not a pure polymer), modified Gaussian network equations have been developed which accommodate the relatively short and inflexible coal macromolecular chains [63, 70]. These equations are not applicable to the current study and are not discussed.

2.3 Coal pore structure

Coal porosity is a contentious subject, with some researchers questioning the validity of the methods used for pore structure determination [39-40]. Generally, coal porosity is defined as the volume fraction of coal occupied by ‘‘empty spaces’’ [71]. It can thus, operationally, be viewed as the volume fraction of coal that may be occupied by a particular fluid [72]. Pores vary in size from micrometer to angstrom dimensions, and may be subdivided into macropores (>50 nm), mesopores (50–2 nm), and micropores (<2 nm). Micropores will have a higher surface area than meso, and macro-pores. The majority of coal’s porosity is

microporous [39, 43]. This makes coal a very high surface area material which is able to physically sorb substantial quantities of gas [73].

Macropore are controlled by fractures, fissures, and jointing. They represent the volume occupied the natural fracture system (cleats). Factors affecting cleat gas transport of desorbed gas are the total number and aperture of the cleats and their connectivity [74]. They contribute significantly to the long distance transport of fluids, and will not greatly affect the short distance transport of the fluids, which is the focus of this study [6]. A significant portion of coal's total open pore volume is located in the micropores and these structures are briefly discussed as they have a major impact on sorption or gas storage mechanisms [75].

2.3.1 Pore structure models

The models for coal pore structure[4] form the basis of most of current literature's postulations regarding sorption mechanisms and coal-gas interactions. In this subsection these pore structure models and discuss how these models have shaped our current hypotheses on coal-gas interactions are reviewed. The review shall mostly concentrate on two current models/theories on the connectivity of the micropore structure, one held by Larsen [76] and the other by Walker and others [40, 49]**,** because of their implicit effect on most of literature's interpretation of coal-gas interactions, gas diffusion, and ultimately storage mechanisms.

The 1970s and 1980s were the major period of research activity on coal porosity and most models on coal porosity were developed in this period [78]. The dominant model of coal porosity during this period was developed by Bond [79] who conceived coal as a high internal surface material having a network of slit-like pores interconnected by narrow capillary constrictions. The model was applied in one variation or another by many

[4] Other models include coal molecular structure models already discussed in section 2.2.2.2

researchers in the 1970s and 1980s. In Figure 2-4, one of these models are shown, with (C) symbolizing closed, (B)-blind, (I)-interconnected, and (R)-roughness [80].

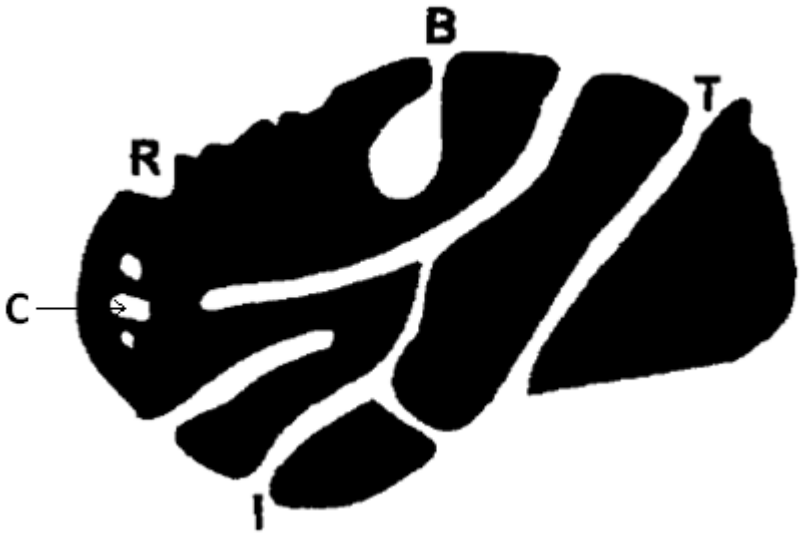

Figure 2-4: The pore structure of coal. Cross-section of a hypothetical microporous grain showing various types of pores: closed (C), blind (B), interconnected (I), together with some roughness (R)[80]**.**

Vitrinite has a more microporous system than inertinite, as was discussed earlier [51-52]. It was also observed that both molecular representations contained aromatic stacking. However, it was observed by van Niekerk and Matthews [61] who modelled inertinite rich coals and found that inertinite rich coals had a more ‘‘open” (porous) system due to a higher degree of aromaticity and covalent crosslinking, contrasting that of a vitrinite-rich model which was observed to have a denser structure. The size of the pores was not quantified. Micropores have also been found to be inter-granular and controlled by deposition and lithification [6]. In conclusion, micropores have a large storage capacity but contribute little to long distance transport of reservoir fluids.

2.3.2 Coal porosity versus coal properties

Many studies on coal porosity were built on the foundation laid by King's work on coal porosity [48-49, 54, 56]. King and Wilkins [56] postulated that, during coalification, the total porosity of the coal structure progressively decreases from about 20% at 82% carbon to a minimum of 3% at 89% carbon and again increases with rank increase.

Crosdale et al. [82] went even further than total porosity and looked at the individual porosity. They found that during coalification (increase in rank), the relative importance of the micropores increases at the expense of macropores and mesopores. This observation agrees well with other studies, where the microporosity was found to increase with rank [46, 53, 61-62] and this has been given as the reason why gas capacity increases with rank to a maximum of 89% carbon content.

Table 2-1 shows the typical pore sizes distribution according to coal rank. Pore structure development during coalification underpins the increase in adsorption capacity observed with increasing coal rank [58-59].

Table 2-1: The distribution of pore sizes classed according to rank [71]

Pore Sizes	**Coal rank (ASTM Designation D388-98a)**
Micropores (d<2nm)	High volatile bituminious coal A and higher
Mesopores (2nm<d<50nm)	High volatile bituminious (C+D)
Macropores (d>50nm)	Lignite + sub- bituminious coal

In studying individual maceral contribution to coal porosity, Unsworth et al. [81] observed that for low rank bituminous coals, inertinite is more macroporous and less microporous than their rank equivalent vitrinite. With rank increase, the mesoporosity of vitrinite decreases

considerably compared to that of inertinite. All the studied coals are multimodal with respect to pore volume distribution, but have varying proportions of micro-, meso-, and macroporosity [88]. In particular, bright coals have a greater micropore volume than dull coals of equivalent rank, whereas dull coals have a greater proportion of mesopores, as evidenced by nitrogen isotherm hysteresis loops, and an estimation of mesopore volume from Barrett, Joyner and Halenda (BJH) theory [89].

Although the findings of the current study are, in part, consistent with the Unsworth et al. [81] study for low rank bituminous coals, who found that inertinite-rich coals generally have a higher mesoporosity than vitrinite rich coals, it is probably not sufficient to state that vitrinite-rich coals have less macroporosity than inertinite-rich coal.

Gas storage in coals occurs predominantly by adsorption on the walls of the micropore network[5]. It has been postulated that at high vapour pressures, multilayer adsorption probably occurs after the micropores are filled [90]. This means that not only is the pore structure critical in understanding how gas content varies in relation to coal type and rank, but that the distribution of those pores is also important [82]. The reason vitrinite can store more gas than inertinite is because vitrinite is more microporous.

2.4 Coal and CO_2 interactions

During CO_2 storage, CO_2 migrates through macropores to mesopores and ultimately to the micropore system where it is stored. Once the gas has been transported to the coal micropore system, a trapping mechanism should exist in order to keep the gas in place. In this section the gas trapping mechanisms of coal is discussed. Figure 2-5 shows a model of CO_2's migration into a coal seam.

[5] See section 2.4.1 for a detailed discussion on adsorption on coal micropore

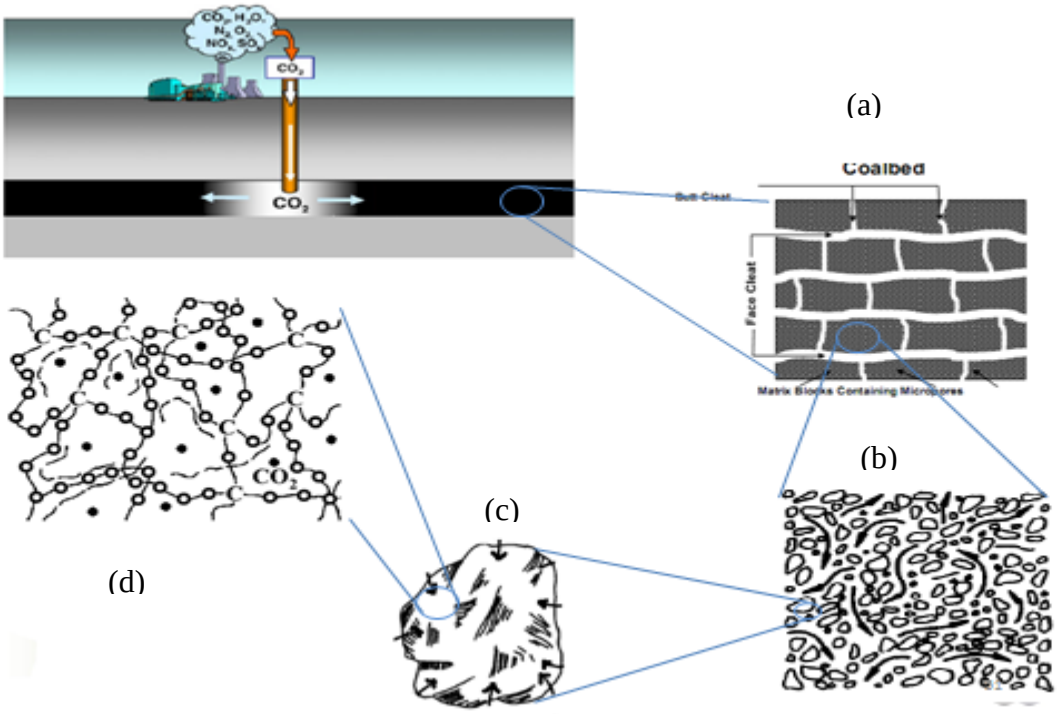

Figure 2-5: A model of CO_2 migration in a coal seam [90-91]**, (a) CO_2 migration from the macropores into cleats, (b) CO_2 migration from mesopores into the micropores (c) and ultimately into the coal matrix.**

The model in Figure 2-5(a) shows how the CO_2 migrates from the macropores within butt cleats and face cleats. Figure 2-5(b) shows the movement of CO_2 from mesopores into the micropores (Figure 2-5 (c)) and ultimately into the coal matrix (Figure 2-5(d)). A variety of mechanisms have been proposed for the trapping /storage of gases in coal as follows [92]:

(i) Adsorbed on the internal surface (adsorption) ;
(ii) Dissolved in the coal structure (absorption) and;
(iii) As a free gas compressed in the pore spaces,

Much literature reports sorption isotherms and coal-CO_2 interactions based on the assumption of adsorption being the only mechanism in operation [93–95]. Observations of coal swelling and other structural changes to coal on gas sorption have suggested otherwise [41]. Further discussion is restricted to mechanism (i) and (ii) stated above since they have been identified to be the dominant gas trapping mechanisms in coal seams. High sorption capacities cannot be accounted for by (iii).

2.4.1 Adsorption

Adsorption is defined as a process that occurs when a gas or liquid solute accumulates on the surface of a solid (adsorbent), in this case coal, forming a film of molecules or atoms (the adsorbate) [96]. Desorption is the reverse process. *Ad*sorption is different from *ab*sorption (discussed in 2.4.1.2), in which a substance diffuses into a liquid or solid to form a solution (Figure 2-6).

In cases when the adsorption and absorption are indistinguishable, it is then convenient to use the wider term *sorption* which embraces both phenomena, and to use the derived terms sorbent and sorbate [96]. The difficulty of distinguishing between the two phenomenon is well known, and presents a practical challenge to the current study as one of the objectives of the study is distinguish which of the two phenomena (absorption or adsorption) is in operation during coal-CO_2 interactions.

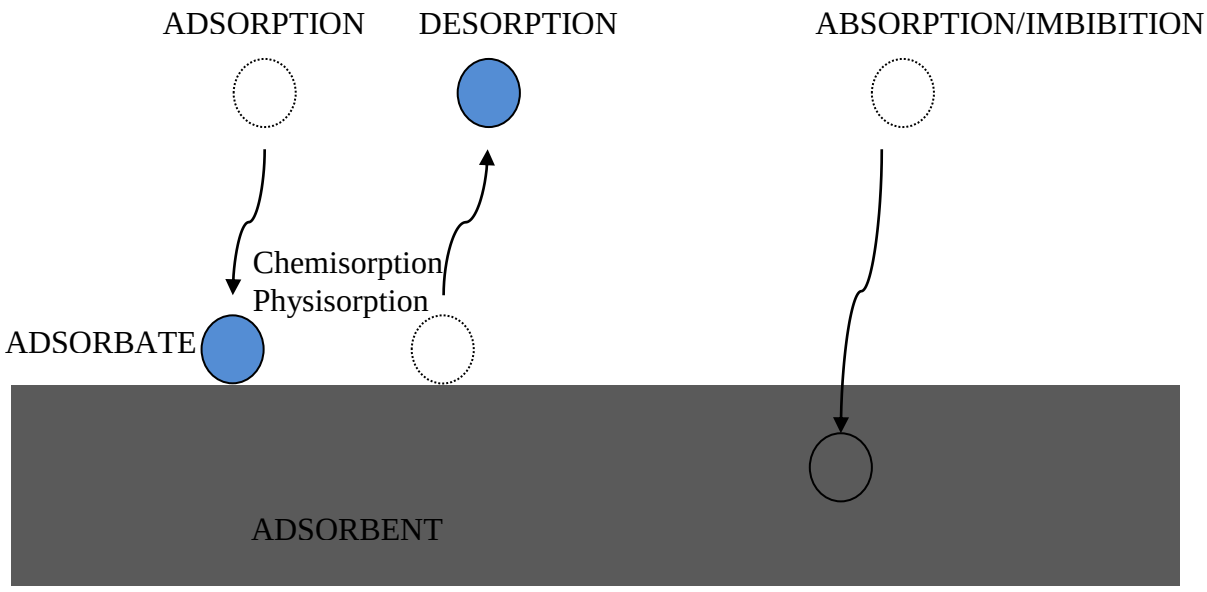

Figure 2-6: A schematic representation of adsorption, desorption, and absorption phenomenon.

There are two distinct adsorption process that are known, physical adsorption (physisorption) and chemical adsorption (chemisorption):

(i) In physisorption, adsorbing molecules are weakly bound, often by van der Waals- and/or dispersion forces due to induced dipole-dipole interactions [97]. They also can be desorbed reversibly by lowering the sorptive gas pressure or increasing the temperature. Adsorbate molecules are basically preserved and not subject to chemical reactions, that is, changes in the character of their electron shells due to interactions with the atoms and/or molecules of the sorbent [96].

(ii) In chemisorption, adsorbate molecules are normally strongly bound to the surface atoms or molecules of the sorbent material, and are subject to chemical reactions. They also cannot reversibly be desorbed from the sorbent, but only irreversibly by which the sorbent material is changed [96].

Adsorption of gases is usually described through isotherms, that is, the amount (mass or volume) of adsorbate on the adsorbent as a function of its pressure at constant temperature. A discussion on the methods used for investigating sorption of gases in solids follows.

2.4.1.1 Adsorption measurement methods

Two main methods are used to investigate sorption of gases in solids: volumetry and gravimetry. The main difference between the two methods is that volumetry is an indirect method of measuring gas sorption on solids, whilst gravimetry is a direct method of measurement [98]. Both methods have advantages and disadvantages in terms of costs, accuracy, simplicity, errors produced etc. The principles of the two methods, together with the advantages and disadvantages mentioned above, is the subject of this section and because the volumetric system was used in the current study. Volumetric method is discussed more in

detail than the gravimetric method and a detailed description of both methods is presented in [97-98].

2.4.1.1.1 Volumetric Method

Volumetry or "Manometry" is the oldest method of the two methods with some of the earliest known experiments performed by Scheele in the 18th century, Chappuis in late 19th century, and Ostwald and Langmuir in the early 20th century [101, 103]. Today's volumetric instruments are based on an instrument which was designed by R. W. Pohl in the 1940's and was called a "volumimeter" [99].

The principle of volumetric adsorption is simple, as shown in Figure 2-7 [98]. Two cells, a reference or pressure cell (V_{prc}) filled with the adsorbate gas and a sample cell (V_{sc}) with the adsorbent sample, are separated by a valve (initially closed). A given amount of adsorbate gas is expanded into the adsorption cell (V_{prc} + V_{sc}) by opening the valve. Upon expansion the adsorbate gas is partly adsorbed on the (external and internal) surface of the adsorbent material, partly remaining as gas phase around the adsorbent [97-98].

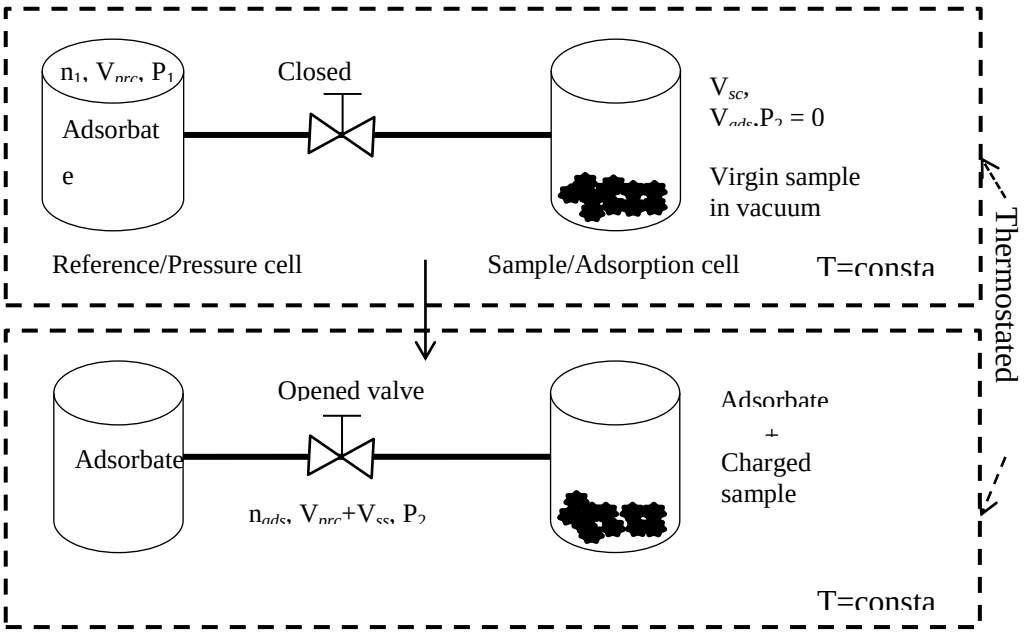

Figure 2-7: Principle of volumetric adsorption. Adopted from Belmabkhout et al.[98]

The amount adsorbed (n_{ads}) is calculated by a mass balance on the gas phase before and after adsorption (P_1, P_2, $T_1 = T_2$) using an appropriate equation of state (see § 2.4.1.2 for a more detailed discussion).

As mentioned earlier, the volumetric system has it advantages and disadvantages. Table 2-2 shows the main advantages and disadvantages of the volumetric adsorption system[102-103].

Table 2-2: Advantages and disadvantages of volumetric adsorption system. Adopted from [97-98].

Volumetric system	**Item**	**Description**
Advantages	(i) Simplicity	• Instruments are fairly simple to build and do not require sophisticated high tech equipment. • Experiment in itself is simple - opening of a valve between gas storage cell and adsorption cell. • Can easily be automated and run without permanent supervision for hours and days.
	(ii) Measuring techniques	• Volumetric measurements of gas adsorption equilibria are measurements of pressures and temperatures in gas phases and a variety of high precision measuring instruments operating in a fairly wide range are readily available for use.
	(iii) Cost	• Volumetric gas adsorption instruments are relatively cheap to make
Disadvantages	(i) Amount of sorbent material	• For volumetric measurements of small amounts of adsorbent, several milligrams, has shown to be ineffective
	(ii) Approach to equilibrium	• Gas adsorption equillibria may last for seconds, hours or sometimes days.
	(iii) Wall sorption	• Upon expansion from the storage cell the adsorbate gas may not only be adsorbed on the surface of the adsorbent material but also on the walls of the adsorption cell and the tube connecting both cells. This may cause additional uncertainties in measurement. • To reduce wall adsorption all inner surfaces electropolished

	(iv) Inherent errors	• Errors are due to the indirect determination of the adsorbed quantities. The main sources of errors of the technique are: o errors in the determination of the pressure cell and adsorption cell volumes, o errors in the pressure and temperature measurements, o errors due to leakage at high pressure, the error in the sample mass and the error due to the equation of state.

2.4.1.1.2 Gravimetric method

Although the idea of comparing masses by weighing them in the gravity field of Earth is a very old technique going back to biblical times, the application of this idea in the investigation of sorption phenomena of gases in porous solids is relatively new [100]. The main reason for the delay in the application of this idea has been the lack of highly sensitive balances able to measure small relative changes in the weight of a sorbent sample. However, recent advances in mass balance technology have also enabled the application of comparing masses in investigating sorption of gases in porous solids [100].

The gravimetric method consists of exposing a clean adsorbent sample to a pure gas at constant temperature. The change in the weight of the adsorbent sample as well as pressure and temperature are measured when equilibrium is reached. This allows the direct measurement of the amount adsorbed and hence the gravimetric method is considered as an accurate technique [98].

The main advantage of gravimetry when compared to manometry is that with gravimetry it is possible to observe the approach to equilibrium during the adsorption process at the balance's data display. Therefore, one can choose arbitrarily a certain small fraction of the pure sorbent sample's mass and a certain time interval and define technical adsorption equilibrium of the

system. The main disadvantages of the gravimetric system are the relative high cost of construction and high sensitivity to external environment [96].

2.4.1.2 Construction of adsorption isotherms using volumetric methods

Volumetric adsorption measurement apparatus only measures the pressure difference in the sample cell due to adsorption. It is from this pressure difference that the amount of gas adsorbed is calculated. This is done by using the Gibbs definition for the absolute adsorbed amount, n_{abs}. In accordance to Gibbs theory [101], n_{abs}, can be calculated by subtracting the moles of free-gas in the sample cell void volume (V_i) from the total moles of gas transferred into the sample cell, n_t. The total moles of gas transferred into the sample cell from the reference cell, n_t, can be easily calculated by using the ideal gas law equation:

$$n_t = P_2 V_{SC}/RT \tag{2-1}$$

Where P_2 is the pressure in the sample cell and V_{SC} is the volume of the sample cell. Since n_t is equal to the moles in the gaseous phase plus the moles adsorbed on the substrate:

$$n_{ads} = n_t - \rho V_i \tag{2-2}$$

Where ρ is the molar density of the gas in the free space, and V_i is the "true" void volume in the sample cell; that is, the volume occupied by neither the solid adsorbent nor the volume of the adsorbed phase (V_{ads}). However, this leaves two unknowns, n_{ads} and V_i, and in order to overcome this problem, the Gibbs excess adsorption (n_{ex}) is defined employing the void volume initially estimated by He expansion, V_o:

$$n_{ex} = n_t - \rho V_o \tag{2-3}$$

Where n_t and ρ are as defined above.

The excess adsorption is the amount of gas calculated to have been adsorbed when the volume of the adsorbed phase, V_{ads}, is ignored. The relationship between the experimentally measured excess adsorption, n_{ex} and the absolute adsorption, n_{abs}, can be obtained from the difference between Eq (2-2) and Eq (2-3) such that

$$n_{ex} = n_{abs} + \rho \Delta V \qquad (2\text{-}4)$$

Where ΔV, is the difference between the void volumes in the presence and absence of the adsorbed phase, respectively. There are many isotherms that have been developed during the last period of 100 years [96], but only the most commonly used isotherms in describing adsorption of gases on coal are reviewed in the following section (§ 2.4.1.3).

2.4.1.3 Model Equations for the Absolute Adsorption (n_{abs})

The absolute adsorption, n_{abs}, is the amount of material actually adsorbed on a solid adsorbent. Many adsorption-model equations have been proposed to represent the absolute adsorption amount (See Table 2-3). Some of these equations are based on a theoretical foundation, such as the Langmuir [102] and BET [103], while others are derived to provide empirical curve fits, such as Dubinin equations [104]. Empirical equations, which are not related to physical factors, however, do not allow extrapolation beyond the range of the variables for which the parameters have been determined [105].

Model equations used to represent the amount of gas in the adsorbed phase are grouped according to the mechanism of adsorption and the surface properties of the solid adsorbent and are shown in Table 2-3. For instance, the Dubinin equation is based on a pore filling rather than surface adsorption mechanism. The modified BET (BET*n*) is based on *n* numbers of adsorbed layers rather than the monolayer adsorption or infinite numbers of adsorbed layers as in the Langmuir and BET equations, respectively [106].

Table 2-3: Models used to describe absolute adsorbed amount (V_{ads} or n_{abs}) on porous materials. Adapted from Perera el al. [107]

Model Number	Equation	Reference	Remarks
1	$$V_{ads} = \frac{V_m P_L}{1 + P_L}$$ V is the volume of gas adsorbed, P is the gas pressure, V_m and P_L are experimental coefficient. V_m is the "Langmuir volume parameter" which represents the maximum storage capacity of the coal, and P_L is "Langmuir pressure parameter", which represents the pressure at half of the maximum volume capacity of the coal	[102]	(i) Called Langmuir model. (ii) Represents only pressure effect on the sorption capacity
2	$$n_{abs} = \frac{n_0 C(P/P_0)}{\big(1 - (P/P_0)\big)\big(1 + (C-1)(P/P_0)\big)}$$ C is a constant related to the heat adsorption, P is the pressure, P_o is the saturation pressure at adsorption temperature, n_o is the maximum number of site available for adsorption and n is site available for adsorption	[103]	(i) Called the BET equation. (ii) Determine the amount of gas adsorbed for multilayer condition
3	$$V_{ads} = \left[\frac{(100 - M - A)}{100}\right] \times \frac{V_m}{V_d}[K(P)^N - b \times T]$$	[108]	(i) Used only sub-bituminous to anthracite coals to develop the model

	$\frac{V_m}{V_d} = \left[\frac{1}{0.25\times M\times 1}\right],\ T = 2.5\times\left[\frac{h}{100}\right] + T_0$ $K = 0.8\left[\frac{FC}{VM}\right] + 5.6,\ N = 0.39 - 0.013\times K$ V is the volume gas adsorbed, M is the moisture content, A is the ash content, T and T_o are the temperature and initial temperature of coal seam, V_d and V_w are the volume of gas adsorbed in dry and wet coal, h is the depth, P is the pressure, FC is the fixed carbon content and VM is the volatile matter content.		(ii) Considered more factors that affect the gas sorption in coal
4	$\log V_{ads} = \log V_0 - \frac{BT^2}{\beta^2}\left(\log\frac{P_0}{P}\right)^2$ V is the volume of gas adsorbed, V_o is the micropore capacity, B is a constant, T is the temperature, b is the affinity coefficient of the adsorbate, P_o is the saturation vapor pressure of the adsorbate	[97]	(i) Called "Dubinin–Radushkevich (D–R) equation". (ii) Cannot be used for the situations where the saturated vapor pressure does not exist
5	$\frac{V_{ads}}{1-(\rho/\rho_0)} = V_0\exp\left(\frac{-BT^2}{\beta^2}\left(\log\frac{\rho_0}{\rho}\right)^2\right) + \frac{K_H\rho}{\left(1-(\rho/\rho_0)\right)}$	[28]	(i) Can be used, when the saturated vapor pressure does not exist

	ρ is the gas density and ρ_o is the density of adsorbed phase, K_H is the Henry's law constant and other factors are similar to Sakurovs et al. (2007)		
6	$V_{ads(daf)} = (48.9 + 26.9\ln(P))M^{(-0.0038P^2+0.0636P-1.2832)}$ $V_{ads(daf)} = \frac{T}{(0.9890P^{-0:778})T - 1.7447P^{-0.268}}$ $V_{ads(daf)}$ is volume of gas adsorbed in dry average fracture basis, with moisture content M and with temperature T, P is the pressure	[109]	(i) Shows the effect of moisture content and the temperature on the gas adsorption in coal seams. (ii) Two equations are fully empirical and tested for only two types low rank coal

When a particular adsorption equation is used for the n_{abs} term, the fit of the experimental adsorption data provides physically meaningful constants, such as the adsorption capacity (n_o) and the affinity coefficient (K) of the solid adsorbent can be calculated [105].

2.4.1.3.1 Langmuir isotherm

The most commonly used adsorption isotherm in describing adsorption gas capacity on coal is Langmuir isotherm [106]. The Langmuir model describes the maximum number of moles that are adsorbed for a particular porous solid material. The simplified classical form of the isotherm as published in 1916 by Langmuir is [102]:

$$V_{ads} = V_m \frac{bP}{1 + bP} \qquad (2\text{-}5)$$

Where V_{ads} is the volume of the gas adsorbed, commonly reported at standard temperature and pressure (STP); V_m is the volume available for monolayer covering (at constant T and P→∞), P is the equilibrium gas or vapour pressure, b is the Langmuir parameter which is an emperical constant.

The Langmuir model is based upon the assumption that a state of dynamic equilibrium exists (at constant T and P) between adsorbed and non-adsorbed species, and that adsorption is restricted to a single monolayer [74-75]. In addition, the adsorbent surface is assumed to be energetically homogeneous with respect to adsorption. This assumption has been shown to be violated by coal surfaces which are highly heterogeneous [111].

2.4.1.3.2 Branauer, Emmett and Teller (BET)

The BET model is an extension of the Langmuir model that accounts for the formation of multilayers [103]. The model was developed for the interpretation of Type II isotherms and the reversible part of Type IV isotherms.

The BET equation has the following form:

$$\frac{\mathrm{p}}{(\mathrm{p_0}-\mathrm{p})\mathrm{m^a}} = \frac{\mathrm{C}-1}{\mathrm{Cm_1}}\left(\frac{\mathrm{p}}{\mathrm{p_0}}\right) + \frac{1}{\mathrm{Cm_1}} \qquad (2\text{-}6)$$

Where P/P_0, is the relative pressure, and C is a constant related to the net heat of adsorption. A plot of the left-hand side of equation (2-6) versus relative pressure should yield a straight line in the relative pressure range $0.05 < P/P_0 < O.35$. The BET isotherm works better for physisorption for non-microporous surfaces and is usually applied to measure the surface area of coal [96].

2.4.1.3.3 Dubinin's pore filling

As discussed earlier, coals are microporous materials with a relatively high surface area, and with such materials, it is often useful to distinguish between the external and internal surface. The external surface is usually regarded as the envelope surrounding the discrete particles or agglomerates, but is difficult to define precisely because coals are rarely smooth on an atomic scale [112]. The suggested convention is that the external surface be taken to include all the distinctions, and also the surface of those cracks which are wider than they are deep. The internal surface then comprises the walls of all cracks, pores, and cavities which are deeper than they are wide and which are accessible to the adsorbate.

In practice, the demarcation of external and internal surface is likely to depend on the methods of assessment and the nature of the pore size distribution. Because the accessibility of pores may depend on the size and shape of the gas molecules, the area of, and the volume enclosed by, the internal surface as determined by gas adsorption may depend on the dimensions of the adsorptive molecules (molecular sieve effect). The roughness of a solid surface may be characterized by a roughness factor, i.e. the ratio of the external surface to the chosen geometric surface [112].

Pore-filling mechanisms are dependent on the pore shape and are influenced by the properties of the adsorbate and by the adsorbent-adsorbate interactions. The whole of the accessible volume present in micropores may be regarded as adsorption space, and the process which then occurs is micropore filling, as distinct from surface coverage which takes place on the walls of open macropores or mesopores. Micropore filling may be regarded as a primary physisorption process (see Figure 2-8); on the other hand, physisorption in mesopores takes place in two more or less distinct stages (monolayer-multilayer adsorption and capillary condensation) [112].

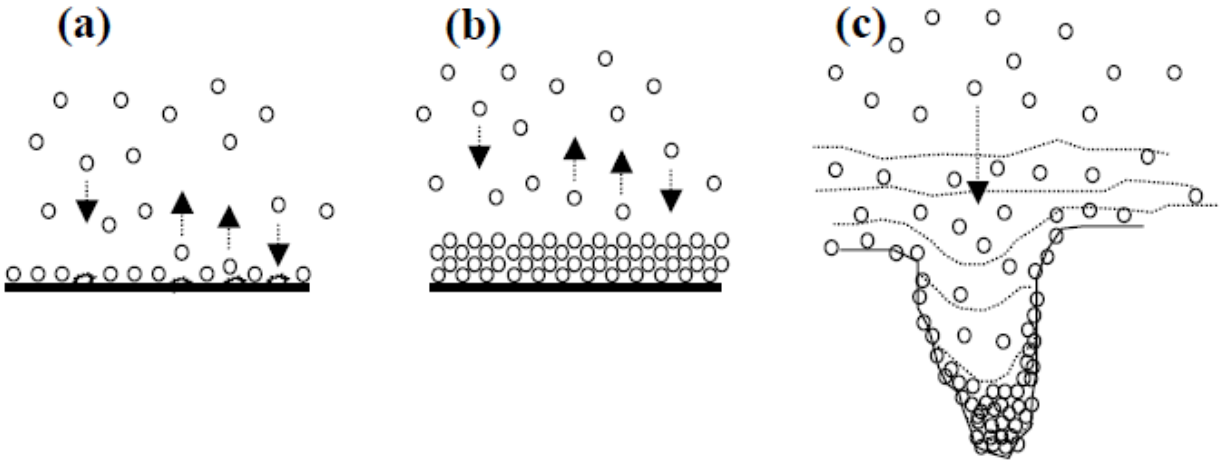

Figure 2-8: A schematic representation of adsorption mechanisms (a) Langmuir's adsorption model (b) BET's multilayer adsorption model (c) Dubinin's pore filling model [105]**.**

In the case of micropore filling, the interpretation of the adsorption isotherm in terms of surface coverage may lose its physical significance. It was to account for this that Dubinin et al developed a theory for micropore filling [72, 75–77, 113]. The theory conveniently defines a monolayer equivalent area as the area, or specific area, respectively, which would result if the amount of adsorbate required to fill the micropores were spread in a close-packed monolayer of molecules.

For this reason, Dubinin theory of adsorption of vapours in micropores is commonly used instead of Langmuir [112]. In the Langmuir theory, the sorbed phase is assumed to occupy a monolayer on the adsorbent surface, which is in turn assumed to be homogeneous. Dubinin theory, however assumes that, in micropores, the adsorbate fills the adsorption space via the mechanism of volume filling and hence does not form discrete monolayers in the pores [114].

There are other models for gas sorption used to describe coal-gas interactions which are not covered in this review. A summary of the equations that are most relevant to the current study are presentedby Perera et al. [107] and are shown in Table 2-3

2.4.1.4 Coal quality parameters and their effect on adsorption

In this section, an evaluation of the standard coal quality parameters, that is, rank, maceral content, moisture content, and mineralogy, and their effect on storage mechanisms follows. In the late 70's and 80's, studies of adsorption and the effect of coal properties on the adsorption capacity of coal because of safety issues associated with the mining of gassy coal seams [83, 115]. Much of the fundamental knowledge built on coal interactions with gases has been built on the interaction of coal with CH_4, most notably coal's CH_4 sorption capacity. It is only recently that more work has been conducted on CO_2-coal interaction due to the interest in ECBM and CO_2 sequestration [27, 107, 116]. As such, the bulk of the literature review correlating coal-gas interactions to coal qualities will include CH_4 adsorption/desorption.

Literature shows that there is still uncertainty on the relationship between standard coal qualities on gas sorption and attempts to correlate these coal properties with gas sorption capacities has failed to produce any conclusive agreement [82, 117-118]. Below is a brief summary on the relationship between rank, maceral content, moisture content and mineral matter content. In this summary, a high sorption capacity is indicative of the strong gas-coal interaction and a low sorption capacity indicative of weak gas-coal interactions. But since the

current understanding on coal-gas interactions is based on coal-CH_4 interactions, much of the literature reviewed will be concentrated on coal-gas interaction in general, including coal-CO_2 interactions.

2.4.1.4.1 Coal rank and maceral composition

Gas sorption by coal is closely related to its physical and chemical properties, which are, in turn, governed by coal type and rank[6] [82]. Major rank parameters in coal include volatile matter, fixed carbon content, calorific value, and moisture and vitrinite reflectance[7].

In their study on assessing the potential for gas storage on Black Warrior Basin, Caroll and Pashin [119] found that rank is the strongest determinant of sorption capacity. Others have argued that coal rank and type are not the determinant in themselves, but rather strongly influence the pore structure development which is widely accepted to be the main factor determining coal sorption capacity [82].

In an attempt to correlate coal sorption behaviour with coal composition, Laxminaraya and Crosdale [120] made some interesting observations and drew conclusions about certain trends regarding coal rank and type in relation to gas sorption capacity. In correlating adsorption capacity with rank, they found that the Langmuir pressure (i.e adsorption capacity) decreases with increasing rank (Figure 2-9). The reason given for this is that as coal rank increases, the pore surfaces become less heterogeneous and the coverage of these surfaces is more complete. They suggested that the decrease in heterogeneity of the pore surfaces may be linked to the increased aromaticity of the coal structure by polymerization condensation and the loss of non-aromatic carbons [120].

[6] Rank refers to the maturity of a coal; is broadly classified as lignite, bituminous and anthracite. Coals are generally identified by rank prefixed with volatile content i.e high volatile bituminous

[7] These can be determined by using a standard thermogravimetric analysis (TGA) instrument for fixed carbon content, calorific value, moisture content, and volatile matter, whilst the vitrinite reflectance can be determined using petrography.

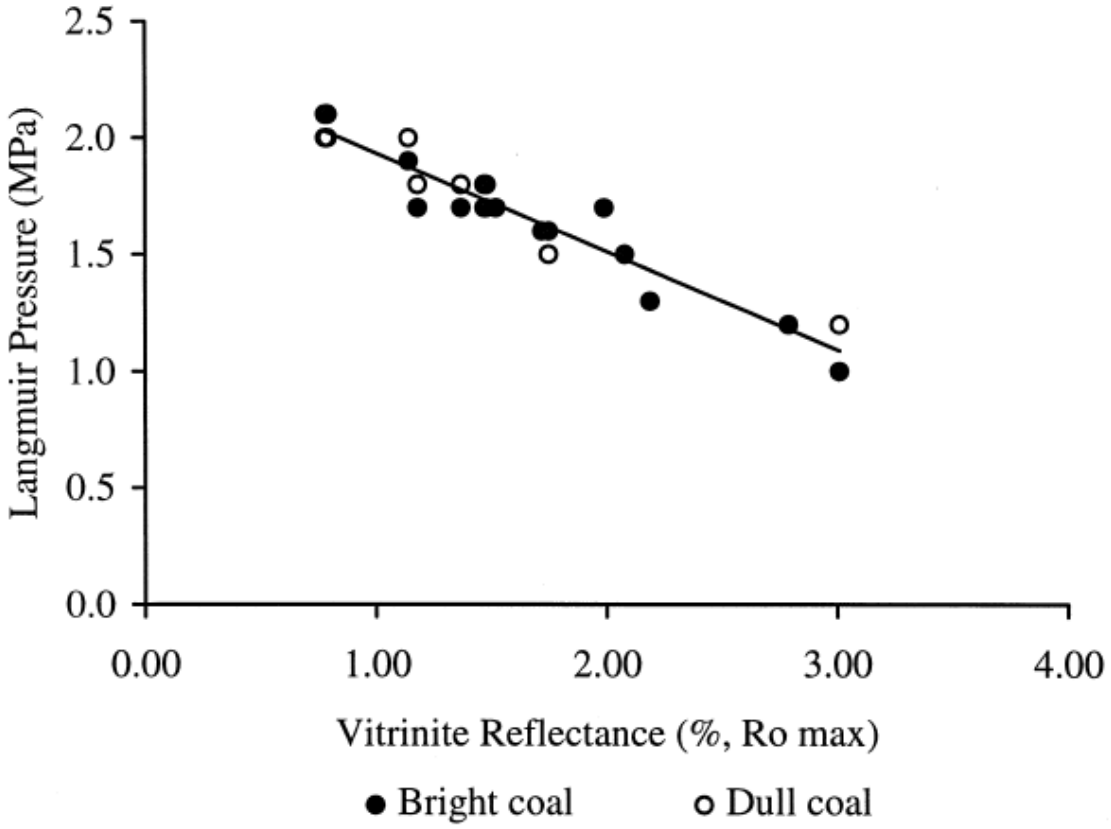

Figure 2-9: Langmuir pressure (P_L) against rank. The graph shows that Langmuir pressure (P_L) decreased with increasing rank [121].

The same trend has been observed by other researchers, not for the whole spectrum of rank from low rank to anthracite, but rather in the high volatile bituminous to anthracite rank range [115, 121]. The studies [115, 121] observed that sorption capacity and porosity decreased with rank to a broad minimum at the medium volatile bituminous stage, followed by increases with increases in rank. Others, however, have observed a trend of increasing storage capacity with increasing rank [108, 122].

Day et al. [41] also studied gas sorption for 30 coals from Australia and elsewhere covering a wide range of rank and other properties, at 53 °C and pressures up to 16 MPa. Although a broad minimum in adsorption capacity versus rank was found at a vitrinite reflectance of about 1.2 %, the study was unable to find any conclusive correlation between rank (and other properties) and gas sorption capacity.

Coal type effects on gas sorption are also poorly understood. Inertinite-rich coals at low and medium rank have been found to have higher adsorption capacity than vitrinite-rich coals, whereas at higher ranks, both coal types adsorb similar amounts [123]. Other studies, in contrast, have found vitrinite to have a greater adsorption capacity than inertinite over a wide range of ranks [82, 91, 124]. Maceral composition has also been postulated to have little influence on methane sorption properties [120].

The role of maceral composition is not fully established, but it is clear that maceral composition may affect adsorption capacity rate and not adsorption capacity [82]. An attempt to correlate maceral composition and adsorption for coals of differing maceral composition failed to produce any conclusive results, but may have some correlations for South African coals (see Figure 2-10).

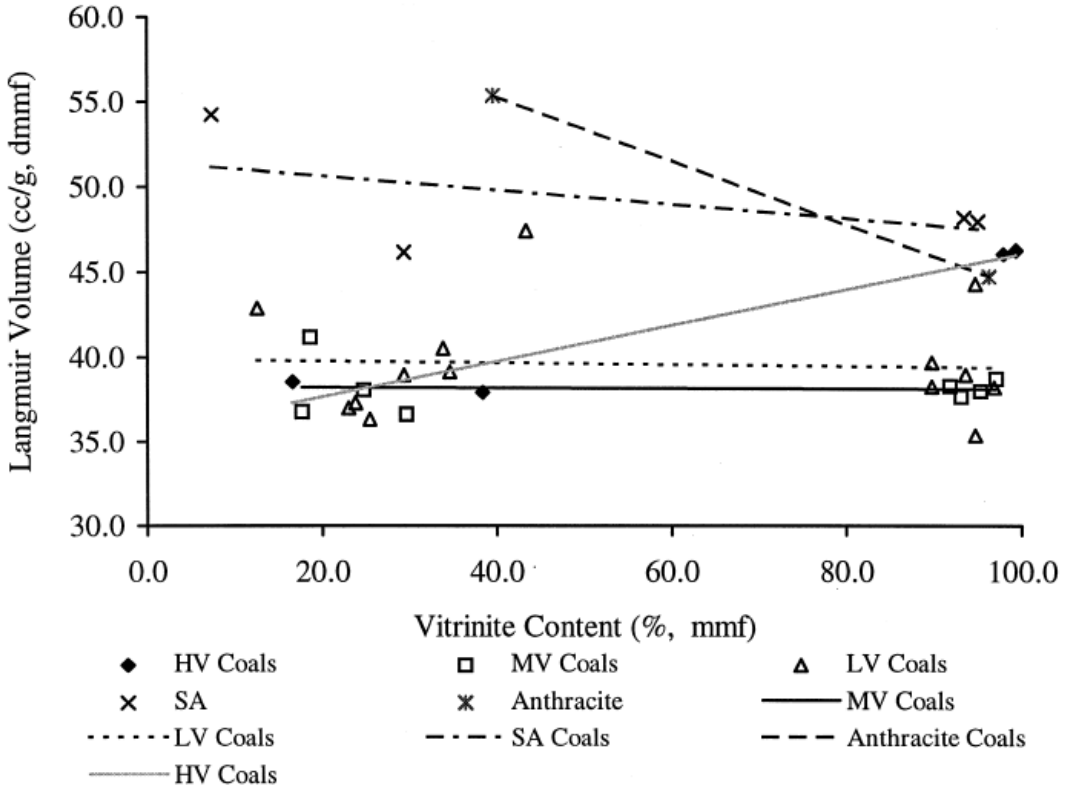

Figure 2-10: Trends in Langmuir volume in relation to vitrinite content (also showing rank influences). Maceral composition has greatest influence on gas adsorption capacity in high volatile bituminous coal, semi-anthracite, and anthracite [120]**.**

However, Karacan [32] determined that inertinite associated with kaolinite and illite clays was found to have higher adsorption capacity. The study suggests that, because the gas molecules are adsorbed on the large surface area of the clays, retained in the free volume provided by the interlayer spaces of the clays, they are then absorbed by the inertinite because of easy accessibility to these sites.

2.4.1.4.2 Mineral matter Content

No convincing relationship between gas sorption and mineral matter content and gas sorption and equilibrium moisture has been determined in literature. In a study on CO_2 and CH_4 sorption in high volatile bituminous coals from Indiana, it was found that both adsorption capacities on as received or dry ash-free basis are similarly weak, suggesting that the organic matter is the dominant control on gas sorption [125]. Those authors that have attended any

correlation have found a non-proportional relationship between coal sorption capacity and mineral matter content as shown in Figure 2-11 [86].

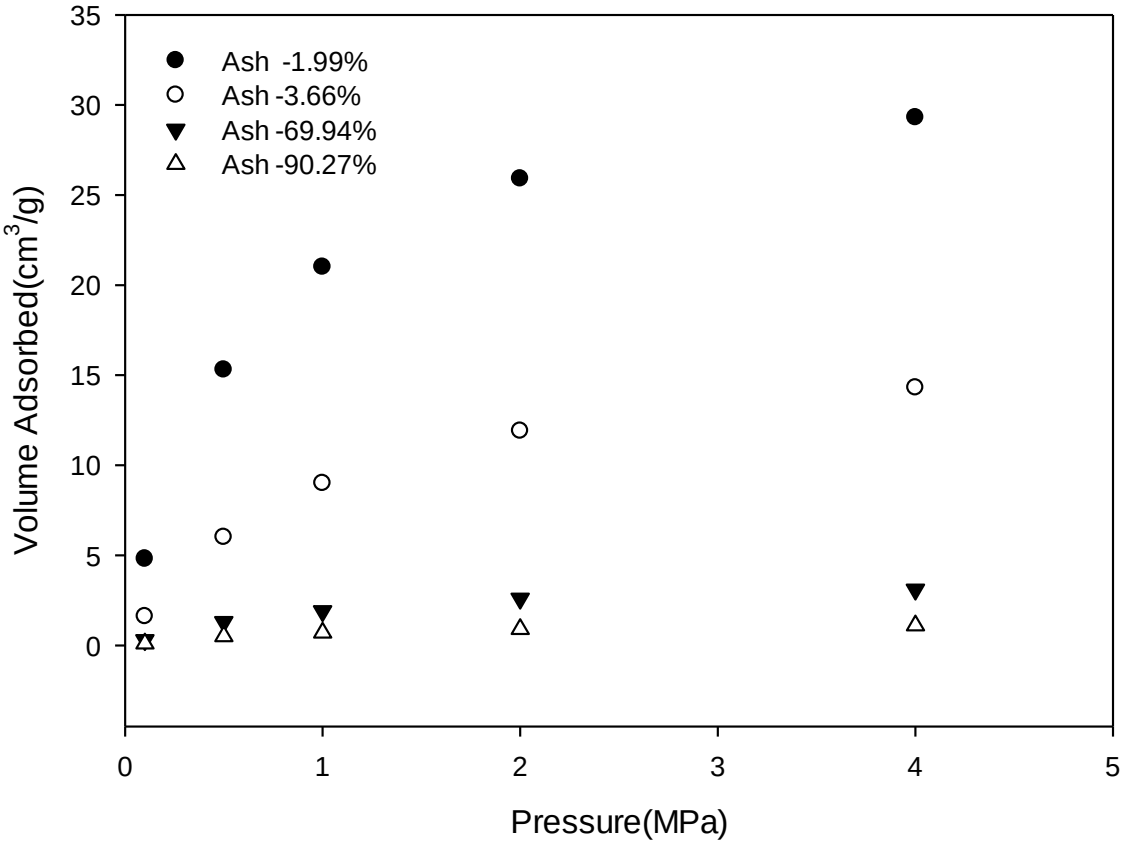

Figure 2-11: Effect of ash content on methane sorptive capacity of South Wales coalfield sample at 25°C [86]

The explanation for this trend is that the presence of mineral matter in coal takes up space that would otherwise be filled with organic matter, thus reducing the surface area and sorption capacity [126].

However, Karacan [32] found that clays associated with inertinite, specifically kaolinite and illite, provided high porosity, and hence a high sorption capacity was observed at these sites. In light of the above contrasting findings, it is suggested that different mineral matter will have different effects on sorption capacity. Clays, more specifically kaolinite, illite, and montrille, because of their porous nature, will have higher sorption capacity than say, carbonates or pyrites, because of their lack of porous nature. Detailed mineral matter

characterisation is necessary to confirm this hypothesis. The effect of mineral matter is not included in this study, but acknowledged.

2.4.1.4.3 Moisture Content

It is a well-known fact that water molecules are strongly held by the coal structure, and removal of moisture during sample pre-treatment can collapse the interconnected pore network, particularly for coals of low rank [127]. Moisture in coal occurs in different forms and before an analysis can be done on the moisture in coal and its relation to sorption capacity of coals (see Table 2-4), it is important to define the different forms in which moisture occurs in coal.

Table 2-4: Moisture in coal and their effect on gas sorption

	High effect on sorption	Little or no effect on sorption	Reference
Surface moisture	✔		[33]
Inherent moisture	✔		[54, 105]
Mineral moisture		✔	[129]

Total moisture[8] in coal is the moisture (in all forms except mineral moisture) that resides within the coal matrix [130]. *Mineral moisture* is the water which comprises part of the crystal structure of hydrous silicates such as clays and *surface moisture* represents the water held on the surface of coal particles or maceral. *Equilibrium moisture* [9] is the moisture content retained at equilibrium in an atmosphere over a saturated solution of potassium

[8] This form is the form of moisture commonly reported by proximate analysis of coal
[9] When the sample, before such equilibrium, contains total moisture at or above the equilibrium moisture, the equilibrium moisture may be considered as equivalent to inherent or bed moisture, and any excess may be considered as extraneous moisture

sulphate at 30 °C, and 96% to 97% relative humidity and is equivalent to inherent moisture [95].

The relationship between moisture in coal and gas adsorption is one that is well understood with earlier studies mainly initiated for improving safety during coal mining operations [33, 131]. These studies found that total moisture in coal had a conversely proportional relationship with sorption capacity. Sorption capacity decreases with an increase in the total moisture of coal in the sample (Figure 2-12). This relationship was followed by a 'saturation point' after which additional moisture has no effect on the sorption capacity of gas [33].

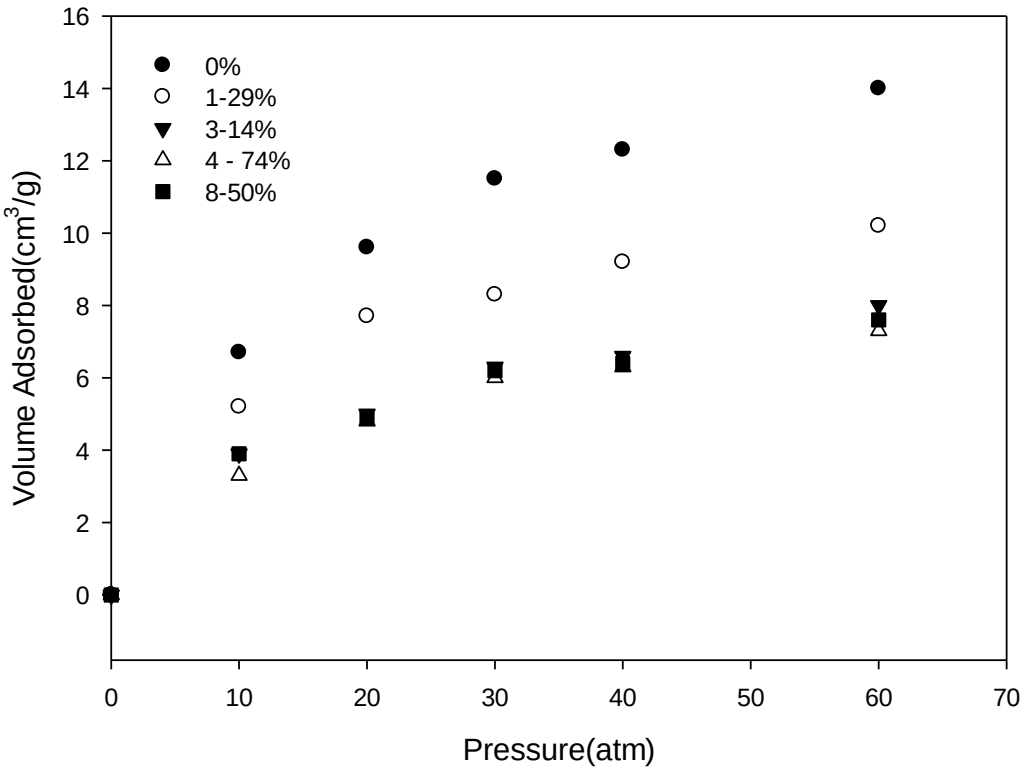

Figure 2-12: Methane adsorption isotherms for Illinois No. 6 coal at 30 °C with different moisture content [33]**.**

The findings in Figure 2-12 make scientific sense if adsorption is thought of in terms competition between water and sorbing gas for the same pore cavity or for the same binding site [131]. Pre-adsorbed water fills the pores in moist coals and occupies the pore space or the

active sites for the adsorption, which means the sorbing gas cannot penetrate into those available sites for adsorption. As a result, lower adsorption capacities should be expected in wet coals. The presence of pore water reduces the adsorption capacity of the sorbing gas by either blocking the path to or by occupying the adsorption sites within the coal matrix [128].

An interesting observation by Joubert et al. [131] is that coals with a high oxygen content generally have high moisture capabilities, and ultimately a lower sorption capacity. It is rationalised that this is because interactions between polar water molecules and surface oxygen complexes are a very strong. This was supported by the fact that the percentage reduction in gas sorption increased with increasing oxygen content; i.e more tightly bound adsorbed water is present in the higher oxygen coals when the coal is saturated with moisture. Any water molecules present in excess of the adsorbed water are probably quite mobile, or are located on the surface of the coal; these would little or no effect on gas sorption.

The correlation between oxygen content and moisture content can be used to predict sorption from rank determination because of the general trend between rank and oxygen content, that is, increasing coal oxygen content increases with decreasing coal rank and thus there is an increase in bed moisture of coal with decreasing rank. From this it can be expected that low rank coals will sorb less than higher rank coals.

Inter-laboratory comparison studies were undertaken by several researchers from the US, Australia and Europe on the reproducibility of sorption isotherms [132-133]. In the first inter-laboratory study [132], the different laboratories involved reported very high deviations in the excess sorption values and in some cases deviating by more than 100% for medium to low rank coals. The discrepancies were attributed to the varying residual moisture contents after drying of the coal samples. In the second inter-laboratory study, the comparison of sorption isotherms of CO_2 was performed this time on moisture equilibrated coals [133]. The result

was an improved agreement of the sorption isotherms data within the different laboratories up to 8MPa. At higher pressures, the sorption isotherm data deviations were significant and were not accounted for.

In Hartman and Pratt [134] CO_2 isotherm measurements were conducted on coal samples that contain moisture levels above the as-received moisture content of the coal sample. Their study indicated that excess surface moisture on the coal samples increases the CO_2 storage capacity of the coal. Their study also suggested that CO_2 dissolves in the excess surface moisture in the coal matrix causing the resultant isotherm to over-predict the CO_2 storage capacity of the coal.

Conversely, if isotherms are measured on coal samples that contain moisture levels below the as-received moisture content, as reported by the Argonne premium coal program, then a greater CO_2 storage capacity would be expected for drier coal samples. A recent study confirmed this behaviour [118].

2.4.2 Absorption

As stated earlier, when the adsorbate molecules penetrate the surface layer and enter the structure of the bulk solid, the term *absorption* is used [112]. The coal-bed methane (CBM) and gas storage community commonly states, erroneously so at times, that gas is stored on the coal's surface in a monolayer by physical adsorption. This is can be seen from the number of papers in the literature cited in the preceding section where this term was loosely used as summarised by Crosdale et al. [82]. If this is indeed the case, then there are few unexplained observations that require clarification:

(i) The observed monotonical gas content increase in coalbeds which seems to increase with rank [108], while the coal's surface area seems to exhibit a minimum at intermediate rank [135]

(ii) The swelling of the coal on gas "adsorption" [136-137] and the corresponding loss of gas injectivity and coalbed permeability at gas storage sites [138-139]

This suggests that a combination of *both* adsorption and absorption might be in operation. The fact that CO_2 dissolves in coal and causes them to swell was known as early as the 1930s [140]. However, it was not until 50 years later that Patel and Reucroft [141] suggested that CO_2 dissolution caused inaccurate estimation of surface areas measured by CO_2 adsorption. Since then, the idea that CO_2 dissolves in coal has gained popularity and is now being applied in current models for coalbed methane and CO_2 sequestration studies [27, 139, 142–144]. Although the absorbed part of a gas in coal is hardly exploitable with common technological methods on economical scale, it should be considered both from a practical standpoint due to a possibility of its gradual long-term escape, and from a theoretical standpoint in connection with swelling caused in the coal matrix by its presence [78].

2.4.2.1 Coal solubility and Swelling

The dissolution and swelling of CO_2 in coal is explained by the polymer theory [23]. Briefly, coals are glassy, strained, cross-linked materials[10] and they are not at a stable state [145]. Their brittleness has been attributed to this glassy nature in which intramolecular interactions are greater than the available thermal energy, leaving the molecules with limited freedom to move except for some small-scale vibrations and rotations [32]. In light of this view of coal as a glassy polymer, it is worth looking to polymer theory again to explain the phenomenon

[10] Details of the polymeric structure of coal are detailed in 2.2.2.2

in detail and also at some studies that have been performed with CO_2 as a plasticizer in polymers.

2.4.2.1.1 Polymers dissolution theory applied to CO_2 dissolution in coal

In polymer theory, the dissolution of a polymer into a solvent involves two transport processes, namely solvent diffusion and chain disentanglement or rearrangement (Figure 2-13). When a glassy polymer is in contact with a thermodynamically compatible solvent, the solvent will diffuse into the polymer.

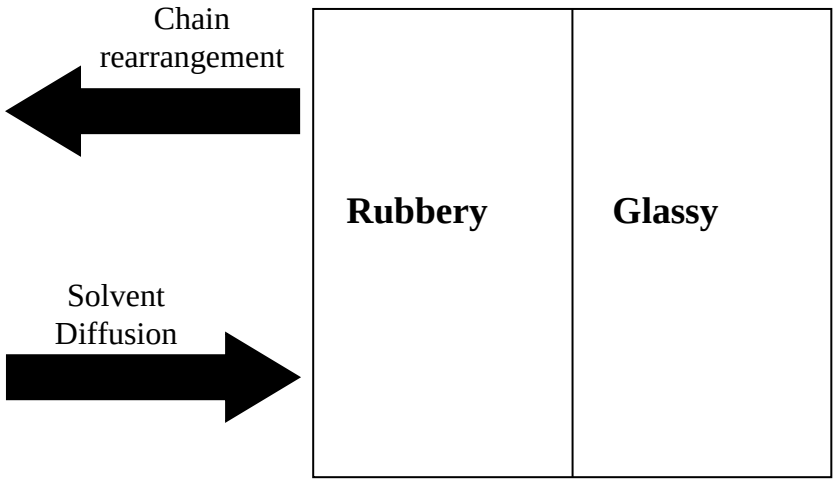

Figure 2-13: A schematic of one-dimensional solvent diffusion and polymer dissolution [146]

A polymer in the glassy state contains a free volume in the form of a number of channels and holes of molecular dimensions, and the first penetrating solvent molecules fill these empty spaces at the start the diffusion process [146]. The process is a combination of two analytically treatable cases:

(i) A Fickian diffusion (case I) mechanism [147] ;

(ii) A case II (anomalous) transport mechanism which is characterized by a well-defined diffusion front, preceded by a region of low permeate concentration, resulting from the Fickian diffusion into the glassy network, with concentration

dependent diffusivity [148]. Under conditions of enhanced solubility, bituminous coal has been shown to exhibit case II transport behaviour [149].

The transition between glass state and rubbery state is generally characterised by the glass transition temperature, Tg, which is commonly determined by an energy transition using differential scanning calorimetry [150]. At the glass transition temperature, strained cross-linkages in the macromolecular structure are disentangled or chain mobility is increased to become rubbery. It should be mentioned, though, that the glass transition temperature depends on the heating/cooling rate, molecular weight distribution and could be influenced by the nature of mobile phases in coal.

In a study, by Khan and Jenkins [151], on the plasticising abilities of different gases, CO_2 was found to the most plasticizing than the other gases in the study. Figure 2-14 shows the effects of CO_2 and Helium at elevated pressures on the softening temperature of a high rank coal. Khan and Jenkins [151] found He had no effect on the coal's softening temperature. Carbon dioxide, however, showed a drastic decrease of the glass transition temperature. The coal glass transition temperature began to drop sharply at a CO_2 pressure of 30 atm and dropped to about 300 °K at 55 atm CO_2 pressure. The 373°C decrease in glass transition temperature shows that, in the coal studied, CO_2 is a very effective plasticiser. It should be mentioned though that the existence of the glass transition temperature is one that is under debate [150].

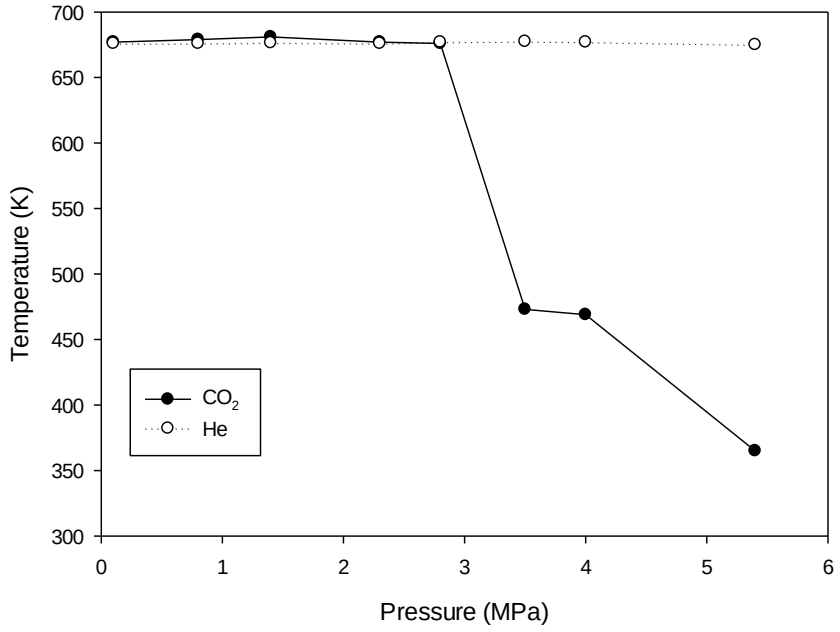

Figure 2-14: CO_2 glass temperature depression [151]

The way it works is that when CO_2 dissolves in coal it acts like a plasticiser in the sense that an equivalent amount (in mol/g coal) of dissolved gas results in the depression of Tg [152]. The rubbery cross-linked coal has sufficient freedom of motion for the molecules to rearrange themselves to adopt a new lower-energy, more highly associated physical structure (Figure 2-15). Large Tg depressions can be achieved at moderate CO_2 pressures [152].

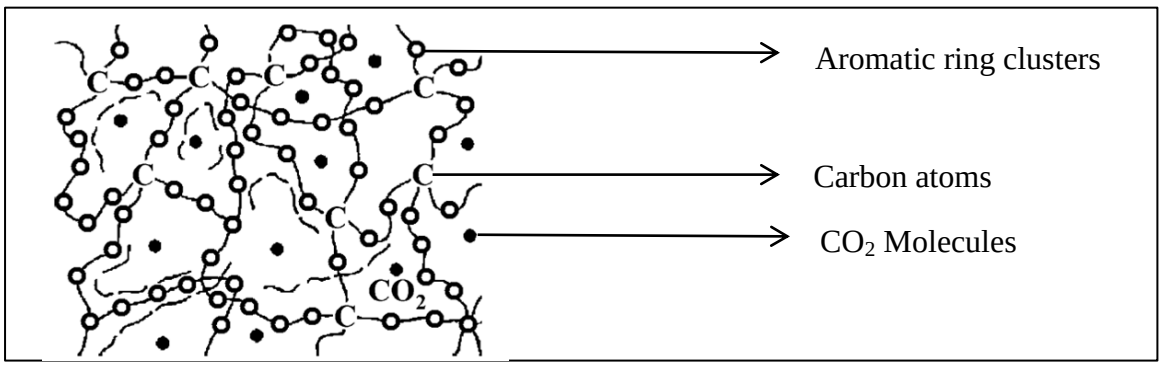

Figure 2-15: A simplified representation of the glassy-polymer structure of coal [153]**.**

Wissinger and Pauliatis [152] demonstrate that in the absence of a glass transition, the equilibrium solubility of a gas in a polymer will exhibit a maximum with increasing pressure owing to free volume effects.

A useful parameter for measuring the solubility of a solvent into a polymer is conveniently called the solubility parameter, denoted δ. A Flory parameter, χ is commonly used in polymer applications to relate a polymer's solubility parameter to that of the solvent's [154]:

$$\chi = (V_{solvent}/RT)[\delta_{coal} - \delta_{solvent}]^2 + \beta^2 \qquad (2\text{-}7)$$

Where $V_{solvent}$, is the molar volume of the solvent (a reference volume), δ_{coal}, and $\delta_{solvent}$, are the solubility parameters of the coal and solvent, respectively, and β is an empirical parameter that usually has a value of the order of 0.34 [155]. The theory also predict that dissolution will be minimal or absent if $\delta_{coal} \gg \delta_{solvent}$ or $\delta_{coal} \ll \delta_{solvent}$.

The solubility parameter of coal can be expressed on a "per carbon atom" basis by using the expression [156]:

$$\delta_c = \frac{7.0 + 63.5 f_a + 63.5\frac{H}{C} + 106\frac{O}{C} + 51.8\frac{(N+S)}{C}}{-10.9 + 12fa + 13.9\frac{H}{C} + 5.5\frac{O}{C} + 2.8\frac{(N+S)}{C}} \qquad (2\text{-}8)$$

The symbol f_a is the fraction of carbon atoms that are aromatic and for application to coal, all oxygens are assumed to behave as ether oxygens and the contribution of sulfur atoms is included (generally small) with nitrogen. These can be determined using ^{13}C NMR studies.

The solubility parameter of coal is estimated to be $\delta_{coal} \approx 10$ cal$^{0.5}$ cm$^{-1.5}$ whilst CO_2 solubility parameter is estimated to be $\delta_{co2} \approx$ 6-6.1 cal$^{0.5}$ cm$^{-1.5}$ [141].

In Reucroft and Patel [157], studies on the gas-induced swelling showed an increased swelling effect of CO_2 with increasing pressure. This correlation was attributed to the

solubility parameter of carbon dioxide approaching a value closer to that of the coal. As the pressure increases, the solubility parameter of CO_2 approaches the solubility parameter of coal resulting in an increase in solubility. Therefore, the amount of CO_2 absorbed by the coals increases with pressure as does the % of CO_2 that is dissolved (Figure 2-16).

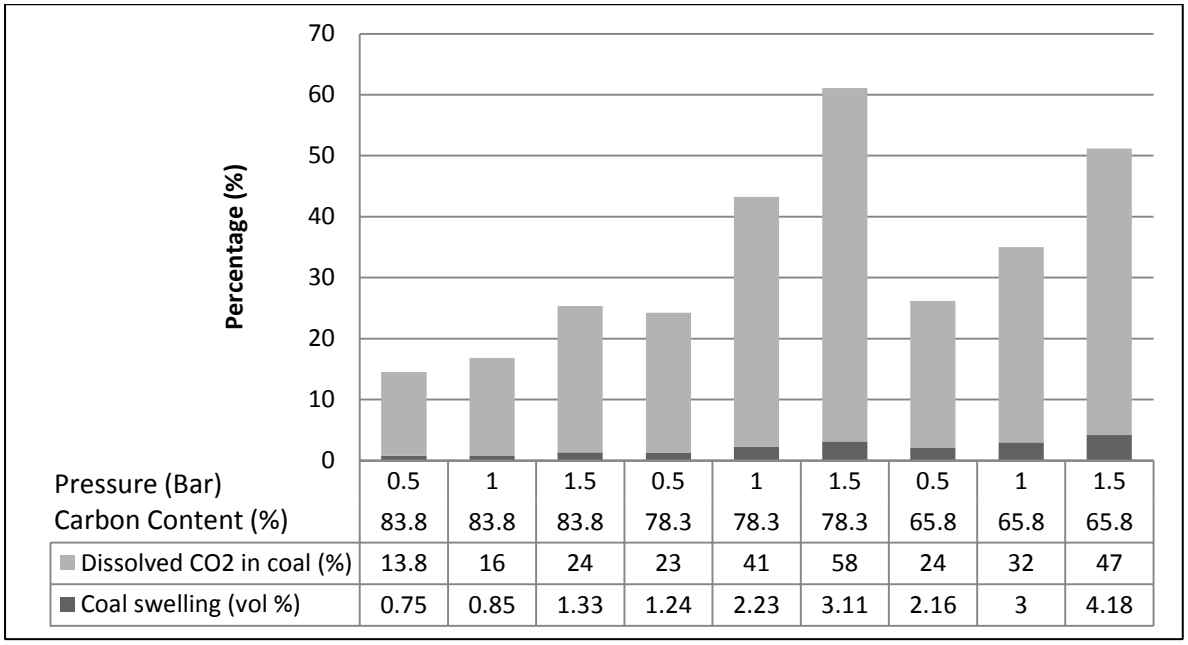

Pressure (Bar)	0.5	1	1.5	0.5	1	1.5	0.5	1	1.5
Carbon Content (%)	83.8	83.8	83.8	78.3	78.3	78.3	65.8	65.8	65.8
Dissolved CO2 in coal (%)	13.8	16	24	23	41	58	24	32	47
Coal swelling (vol %)	0.75	0.85	1.33	1.24	2.23	3.11	2.16	3	4.18

Figure 2-16: The effect of dissolved CO_2 on volume changes. The figure also shows the effect of pressure and carbon content on the dissolving CO_2 and coal swelling [157]**.**

Figure 2-16 also shows a maximum at 78.3% carbon content in the coal studied. Percentage carbon content is usually a good indicator of rank, and this relationship is explored more in detail in the next section.

2.4.2.2 Dissolution and swelling versus maceral composition

From Figure 2-16, for the amount of CO_2 dissolved increases with decreasing coal rank[11] [157]. Assuming Flory's theories on solvent-polymer interactions are true, then this observation holds true since polar interactions within the coal structure decrease with rank increase [156].

[11] Assuming carbon content is an indication of rank

In Larsen [23], swelling is shown to more pronounced in vitrinite-rich macerals in comparison to other macerals that were present in the studied coal.

However, Karacan [32] studied the effect of microlithotypes on CO_2 storage and found that volumetric strain maps of the macerals indicated that the amount of compression (an indication of swelling) in clay and inertinite layers was around 10.0–17.5%. This amount is very close to the volumetric strains created by swelling of vitrinite, suggesting that the amount of compression was a reaction to swelling and was approximate in magnitude to the strains created by the vitrinite. Volumetric strain maps were generated using x-ray CT-scan [158]

In conclusion, the observations above suggest that coal will undergo a structural rearrangement of dissolution of CO_2. This is a well-known phenomenon in polymer theory. However, the results obtained in the above studies seem to be in direct contrast to classical polymer theory, where coal structure rearrangements on the solubility of organic liquids strongly decrease subsequent sorption.

2.5 Effects of CO_2 storage on coal structure

From the previous section, it was established that coal is a glassy macromolecular structure which, when in contact with a fluid, liquid or gas, behaves in a manner that can be described using polymer theories. If this view is held to be true and the results presented in the previous section are generalised (for all coal types and rank, strained, and unstrained)[12], then pumping high pressure CO_2 into coal seams will readily dissolve the CO_2 into the coals. This may enable structural rearrangements that will decrease CO_2 solubility forcing some of the dissolved CO_2 back out of the coal. The rates of possible coal rearrangement as a function of

[12] It is the author's view that this is unlikely and this study is at least aimed at looking at maceral composition effects

CO_2 pressure, temperature, and hydrostatic pressure on the coal are not known. Additionally, the effect of structure rearrangements on CO_2 solubility in coals is not fully known. This information is crucial to understanding and evaluating the possibility of sequestering CO_2 in coal seams for geological time periods. There have been some studies done to provide insight into structural rearrangement on CO_2 sorption on coal [137, 145]. These studies, together with methods for probing these structural rearrangements are the subject of this section. We shall start the discussion on methods that can be used to distinguish between pure adsorption and a mixture of adsorption and absorption.

2.5.1 Physical structural changes: Swelling

A source of volumetric changes in coal on CO_2 adsorption is due to the compression or shrinkage of the coal at high pressures [21, 30, 159]. This is especially important for porous solids, because the calculated volume of the solid may be affected in two opposing ways. Firstly, there is a dimensional change as the solid is compressed at high pressures resulting in a net decrease in sorbent volume. Second, the constriction of pore entrances upon compression may prohibit gas molecules from accessing pores that were accessible initially, resulting in an apparent increase in solid volume. The expansion, or swelling, of adsorbents considered above may also result in a change in volume, which may be affected in two opposing ways. The dimensional increase as the solid swells results in a net increase in sorbent volume. However, the widening of the previously constricted pore entrances may enable more gas molecules to access those pores that were initially inaccessible, resulting in a net decrease in solid volume [160].

As mentioned earlier, dissolution of the adsorbing gas in the coal sample is another source for the volumetric changes. A number of phenomena, such as sorption induced swelling [141, 161-162] and dissolution of coals have indicated that the coal is an elastic material [138]. The

adsorption on coal is generally explained with a dual sorption model describing adsorption on the surface and absorption within the coal matrix as two interacting sub-processes [139, 163-164]. Dissolution of the adsorbing gas within the coal matrix may result in a volume change [160]. Whilst the issue of swelling and possible plasticity is very important to accurately calculating CO_2 adsorption volumes, it is beyond the scope of the current study and hence not discussed in any further detail.

2.6 Methods for probing structural changes

Methods and techniques for coal structure analysis have been around for since the 1940's [80, 180], however, it was only in the 1980's that more advanced techniques were used to study coal interaction with gases and liquids, mainly to study coal's surface area [115, 166]. The exponential growth in technology in the 1990's and early 2000's have also accelerated the rate and volume of studies in coal's interaction with gases and liquids using non-conventional techniques structure analysis [167–169]. The methods are discussed below and other classical methods are discussed in this section.

2.6.1 Desorption hysteresis method

Much attention has focused on the factors controlling the magnitude of sorption by coals in single-step sorption experiments [127, 171-172], while little attention has been paid to the reversibility of sorption by including desorption steps. Sorption hysteresis is the non-coincidence of the sorption and desorption branches of the experimental isotherm [144]. To build an understanding of desorption hysteresis and how it can be used *both* for elucidating sorption mechanisms and probing structural changes, we discuss the findings from studies performed on solid-liquid sorption (where sorption hysteresis has been widely used to understand sorbate-sorbent interactions) can be extrapolated for the solid-gas (supercritical fluid) under study.

In solid-liquid sorption systems, true and artificial desorption hysteresis has been observed [146]. Possible artifacts include non-equilibrium owing to intra-particle molecular diffusion limitations; removal of competing substances, such as colloids or cosolutes in the supernatant liquid just prior to the desorption step; and reaction to give covalently altered products that are either free or bonded to the sorbent [172]. True hysteresis is referred to as *irreversible* sorption. Irreversible here means, not that the sorbate is irretrievable, but that sorption and desorption follow different mechanistic pathways, i.e sorption is irreversible because sorption and desorption occur to/from different physical environments [173].

Hysteresis has also been attributed to formation of metastable states, network percolation effects, or irreversible pore deformation [173]. The first two of these causes are characteristic of capillary liquid condensation in fixed mesopores [80], whereas the last is characteristic of vapor sorption in the micropores of glassy polymers [174].

The terminology used for sorption hysteresis observed in materials containing mesopores is "high pressure hysteresis" (Figure 2-17(a)); this type of hysteresis is usually attributed to capillary condensation. For microporous solids with irreversible sorption characteristics, hysteresis which persists down to very low pressures (Figure 2-17(b) or Figure 2-17(c)) is observed, depending on whether mesopores are absent or not. This type of hysteresis is called "low pressure hysteresis" [175].

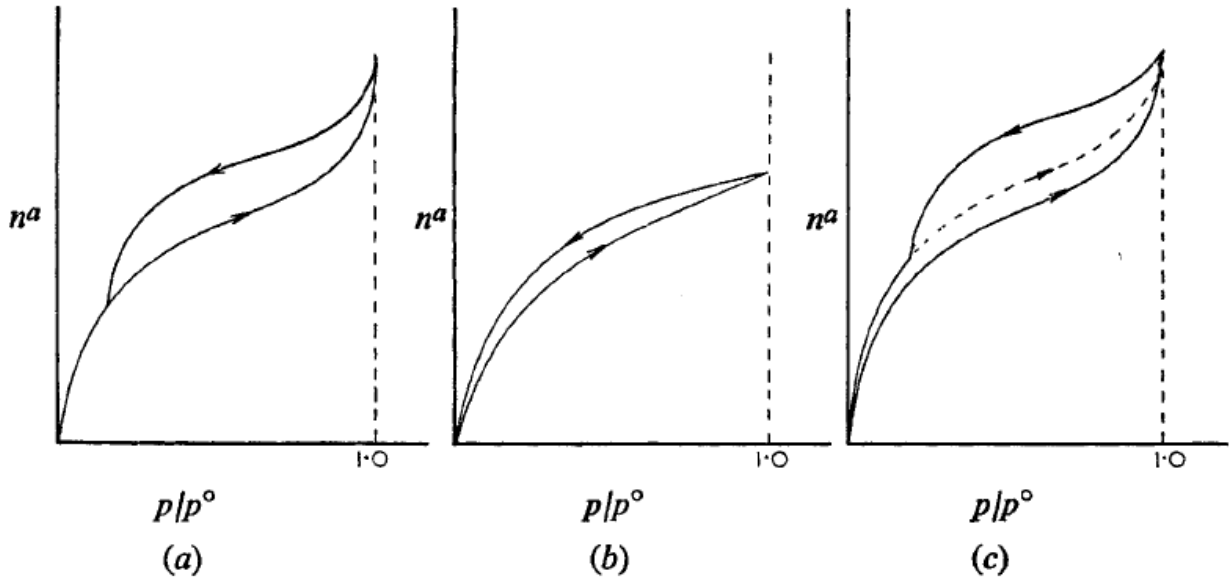

Figure 2-17: Desorption hysteresis for (a) meso and/or macroporous and (b) microporous materals. (c) a material containing both microporores and mesopores (and/or macropores) [175]

According to Sing et al. [112], this phenomenon may be associated with:

(i) the swelling of a non-rigid porous structure, or

(ii) with the irreversible uptake of molecules in pores (or through pore entrances) of about the same width as that of the adsorbate molecule, or

(iii) in some instances, with an irreversible chemical interaction of the adsorbate with the adsorbent.

In a series of studies on the study of sorption hysteresis, Rao [176–181] used sorption hysteresis to extract information on the sorbent-sorbate relationship. After four and a half months from the commencement of the first sorption (performing successive sorption-desorption experiments), it was observed that the hysteresis suffered a "drift"; which was concluded to indicate a structural change in the sorbent, resulting in the variation of the size of the capillaries [176].

Coal structural change has also been theorized by Lu and Pignatello [173]. In the study, Lu and Pignatello suggest that on sorption, pores in the sorbent may be forced to expand by the thermal motion of incoming sorbate molecules, creating new internal surface area in the solid (Figure 2-18). Molecules may even force their way into pores initially too small to accommodate them. On desorption, a lag can exist between sorbate molecules leaving their pores and relaxation of the surrounding matrix to its original state. This cycle results in irreversible sorption because sorption and desorption are occurring to/from different physical environments.

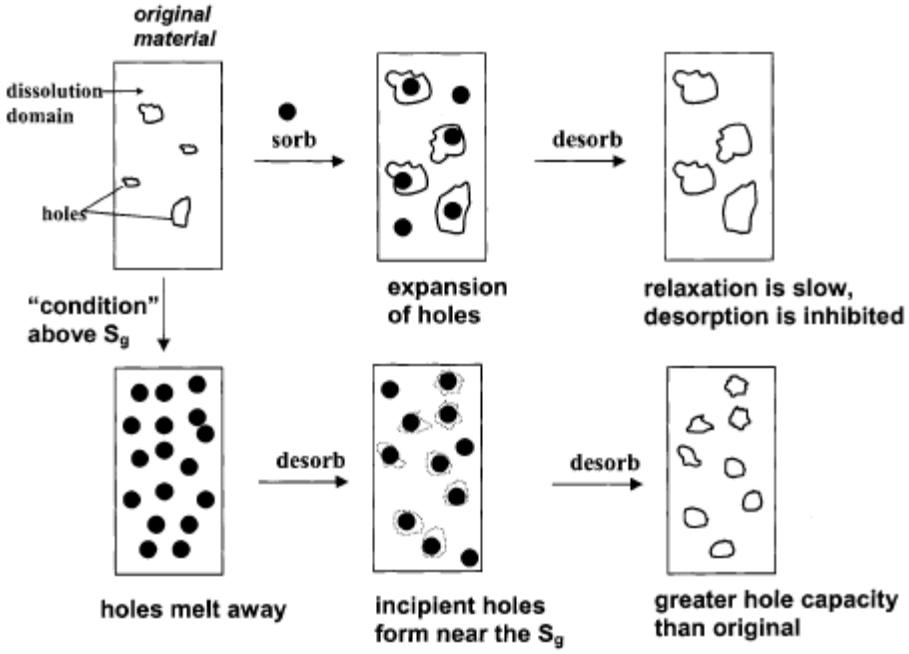

Figure 2-18: Conceptual diagram of the proposed mechanisms of desorption hysteresis and conditioning effect in natural organic matter based on glassy polymer theory. The glassy material initially contains holes interspersed in a solid-phase dissolution domain [173]**.**

For glassy polymers[13] the "conditioning effect" has been demonstrated for small hydrocarbon molecules like CO_2 [174]. In the conditioning effect, hysteresis is brought about by the infusion of the sorbate into the sorbent at a concentration above the glass transition

[13] See section 2.2.2.2 for a discussion of coal as a glassy polymer

concentration of the sorbate, S_g. In this solid-liquid sorption system, conditioning first converts the sample to a rubbery state through the effect of plasticisation, and causes the pores to disappear[14]. Then, as the conditioning agent is removed and S_g is approached from the high-concentration side, "new pores" are created in the solid. This leaves the conditioned sample with a greater pore capacity than the original sample. By this mechanism (Figure 2-18), the sorbate causes irreversible changes in the structure of internal micropores (holes) in the organic matrix upon its sorption [173].

A thermodynamic explanation for the structure deformation has been given by Bailey et al. [175]. Here, only the summarised version of Bailey et al's thermodynamic theory on the low pressure hysteresis is presented, due to structural changes of sorbent which was expanded from Everette's work [130]. In this model, the solid + adsorbate are regarded as a two-component system (solid = 1; adsorbate =2).

At constant temperature and external pressure, the Gibbs-Duhem equation for a system where the adsorbate is in equilibrium with its vapour is:

$$\mu_1 = \mu_1^{\circ} - RT \int_0^P (n_2/n_1) d \ln p_2 \qquad (2\text{-}9)$$

where is μ_1° the chemical potential of the empty solid structure. Low pressure hysteresis may be expected to occur, if at some point in the adsorption isotherm, the structure of the solid jumps irreversibly to a new configuration, which when empty has a different value of μ_1° (Figure 2-19)**.** The unperturbed lattice is represented by I, the perturbed (expanded) lattice by II, with μ_1°(II)> μ_1°(I), so that I is the stable form of the empty solid structure. In principle, conversion from I→II could occur reversibly when the adsorption process has proceeded to

[14] This (the disappearance of pores) is unlikely to occur in coal-gas systems.

point O; the existence of hysteresis suggests, however, that the strained solid I does not change until an irreversible jump occurs at some point P beyond O**.**

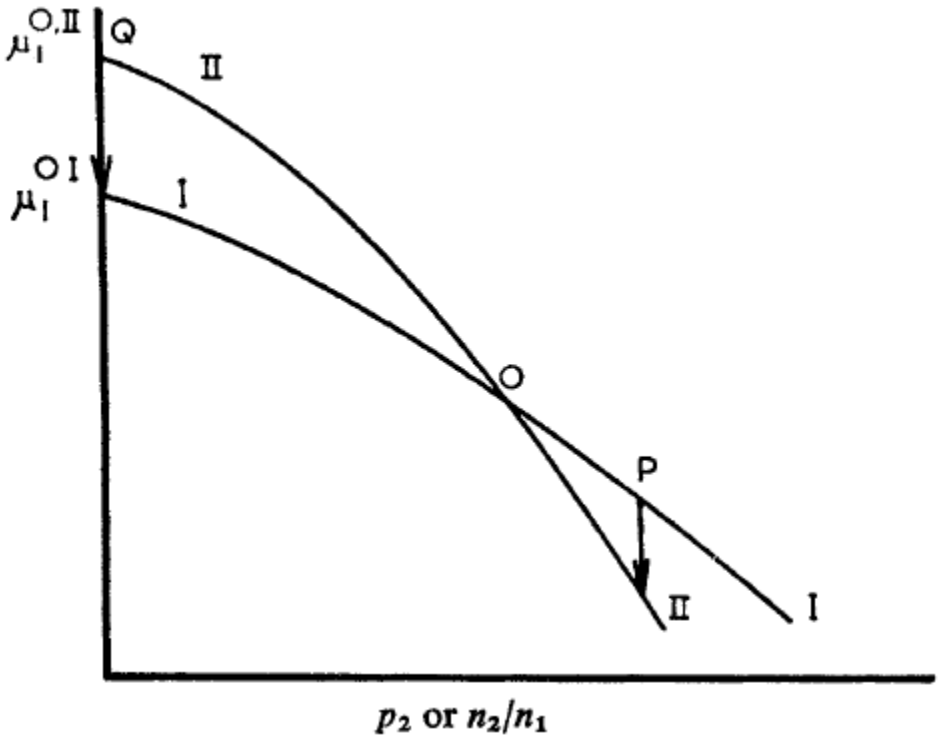

Figure 2-19: Schematic representation of chemical potentials of solid during adsorption and desorption in a system showing low pressure hysteresis [175]**.**

On desorption, the system follows curve II and the persistence of hysteresis to low pressures, and the very slow recovery by the solid to its original properties suggests that the reverse change occurs only at P=O, and even then may be retarded by an energy barrier. Since, for this mechanism to be possible,

$$d\mu_1^{II}/d(\ln p_2) > d\mu_1^{I}/d(\ln p_2) \qquad (2\text{-}10)$$

It follows that at a given:

$$n_2/n_{1_{II}} > (n_2/n_1)_I \qquad (2\text{-}11)$$

(Along the adsorption isotherms).

However, more complex materials such as porous carbon (coal as one of them) possess many local molecular structural features which can play the role of state I, and, by an appropriate modification change to state II. Bailey et al. [175] suggested that, for such complex materials, the ideas expressed above should be associated with a domain structure in which there will be many transition points P, which position varies from one region to another, without all domains necessarily behaving irreversibly.

2.6.1.1 An example of desorption hysteresis used in coal sorption studies

In Medek et al. [182], isotherms of adsorption and absorption on coal were differentiated by use of adsorption hysteresis determined on a gravimetric system. Shown in Figure 2-20(a) is the adsorption isotherm with complete reversibility, and Figure 2-20(b) is the absorption hysteresis showing a large low pressure hysteresis.

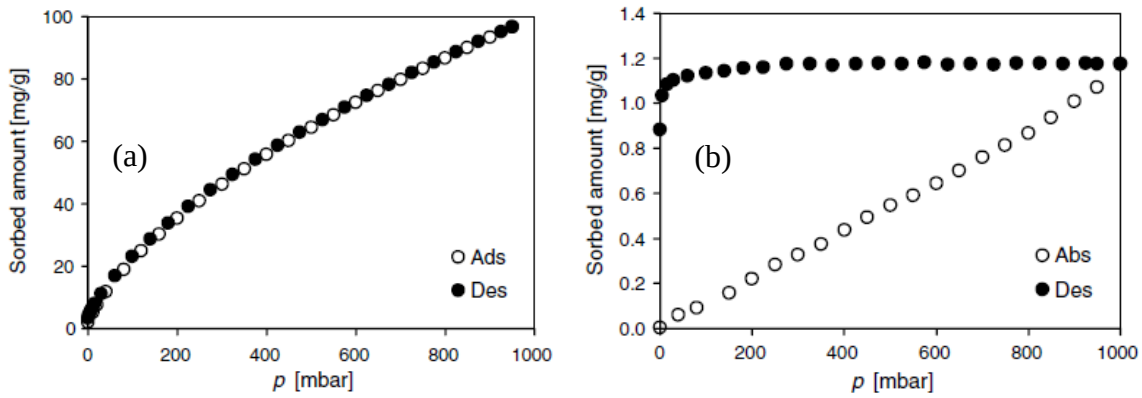

Figure 2-20: Desorption hysteresis used in the elucidating sorption mechanism [203].

The study proved useful not only in discerning sorption mechanisms, but also for calculation of sorption parameters confirming Dubinin principles of pore filling[15]. Sorption-desorption studies can also be used to study the new restructured coal structure and its sorption capacity

[15] Discussed in section 2.4.1.3.3.

or abilities. In conclusion, by use of desorption hysteresis it is not only possible to probe for structural changes but this method can also be used to elucidate trapping mechanisms.

2.6.2 Analytical methods

Goodman et al. [183] used attenuated total reflectance-Fourier transform infrared (ATR-FTIR) spectroscopy to directly observe the interaction of CO_2 on two Argonne Premium coals (Figure 2-21). Upon exposure to CO_2, a positive absorption band due to sorbed CO_2 appeared in the spectrum between 2335 and 2332 cm^{-1} ($\nu_3$antisymmetric stretching mode). As the coals were exposed to increasing CO_2 pressure, the CO_2 absorption band grew in intensity [183]. Because this technique allowed for the direct observation of sorbed CO_2, both the chemical interaction between CO_2 and coals and the isotherm shape were determined.

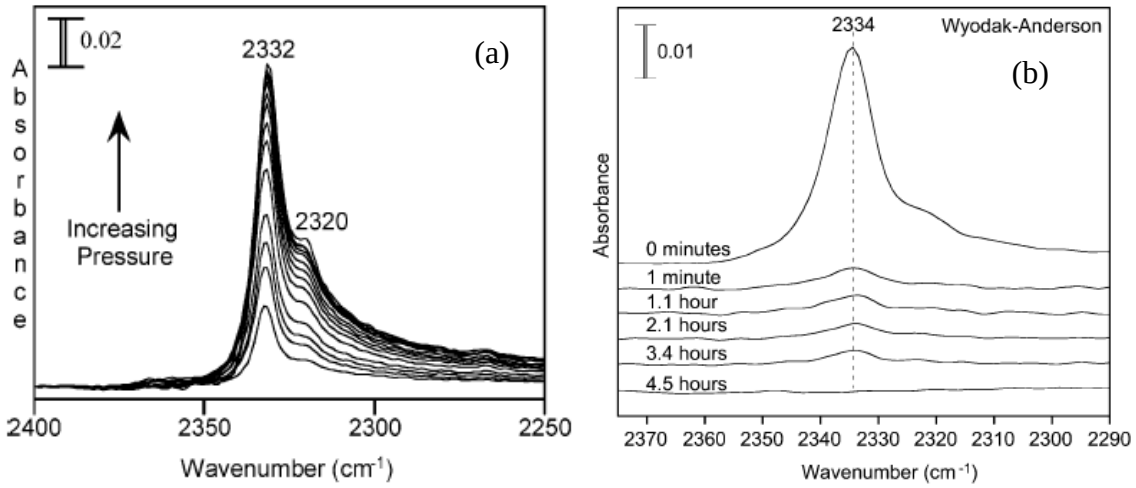

Figure 2-21: ATR-FTIR studies to investigate structure rearrangement on CO_2 sorption, (a) [183] **and (b)** [137]**.**

The study, however, determined the mechanism of CO_2 sorption to be through physical adsorption, which meant that structural rearrangement and/or a chemisorbed CO_2 main absorption band near 1400cm^{-1} was absent.

In a subsequent study, Goodman et al. [137] used the same experimental design to study structure rearrangement on CO_2 exposure over a longer period of time (4 days). In this study coal was exposed to CO_2 initially and then removed and then re-exposed the second to determine the rearranged structure's sorption capacity (Figure 2-21(b)). It was also demonstrated that the physical structure of these coals changed due to its contact with CO_2 in ways that allow more rapid CO_2 diffusion.

2.7 Chapter summary

In summary, literature and theory on coal-CO_2 interactions has been reviewed and discussed. The key point to take away from this chapter is that coal is a very complex material to study, requiring models to understand its complex structure and properties. These models have been discussed and reviewed, including the pore structure models and the molecular structure models. It was also established that the interaction of coal with gases introduces an additional complexity. However; theories, methods and techniques used for understanding this added complexity have also been reviewed. The theories discussed are coal as polymer and polymer dissolution theory, and adsorption theory. Methods discussed include volumetric method for investigating gas sorption in solids; desorption hysteresis and FTIR were established as some of key techniques to study coal-CO_2 interactions. These theories, methods and techniques discussed in this chapter have laid a solid foundation for the rest of the chapters in this study.

It also established that although there has been a lot of work done in understanding coal-CO_2 interactions there are still some gaps in understanding long term effects of storing CO_2 in coal on coal structure and properties.

CHAPTER 3
SAMPLE PREPARATION AND ANALYTICAL TECHNIQUES

In this chapter the samples and the analytical techniques used in the study are outlined. The first section is a discussion on the samples and the sample preparation used in the study. The second section is a discussion on the characterisation techniques used in the study, and the rationale for using them.

3.1 Methodology

The methodology for the study was designed as in Figure 3-1.The coal structure was characterised thoroughly prior to CO_2 adsorption for two reasons, namely:

(i) to predict the expected coal structure behaviour on CO_2 sorption based on previous literature, and

(ii) to be able to compare the structure post CO_2 sorption.

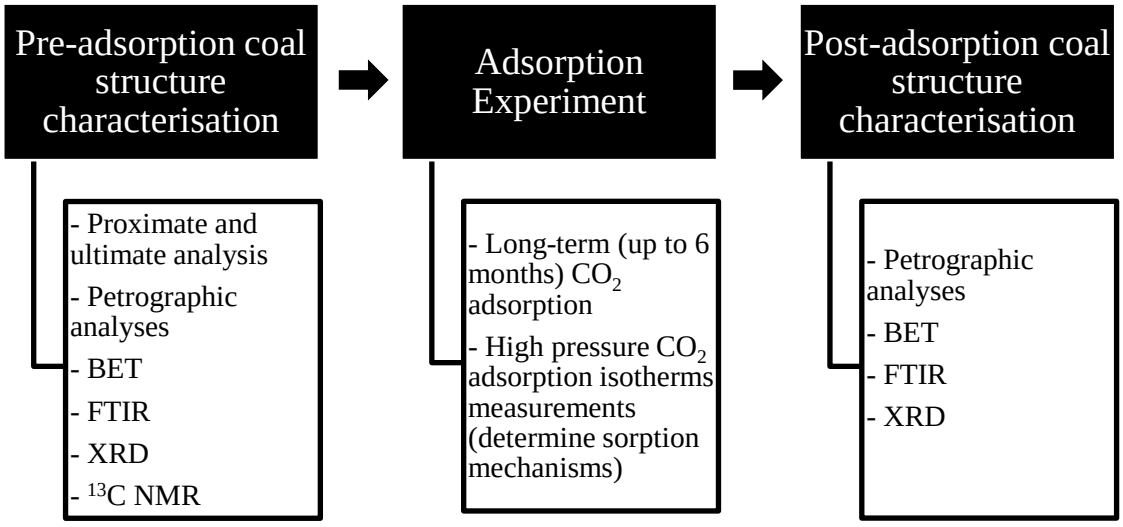

Figure 3-1: Methodology of the study

3.2 Samples

Coal samples were obtained as belt cuts from the Waterberg coalfield (numbered 14 in Figure 3-2). The Waterberg (Lephalale) coalfield is situated north-west of the Karoo basin in the Limpopo Province. The coalfield is structurally deformed, being dissected by numerous east-west and northwest–southeast trending faults. According to Cairncross [184] the faults have produced a series of horsts and grabens of which, in some areas, allow shallow coal to be mined, but in other areas, coal is too deeply buried to be economically mined. It is these inaccessible coals which make a good candidate for CO_2 sequestration and/or ECBM.

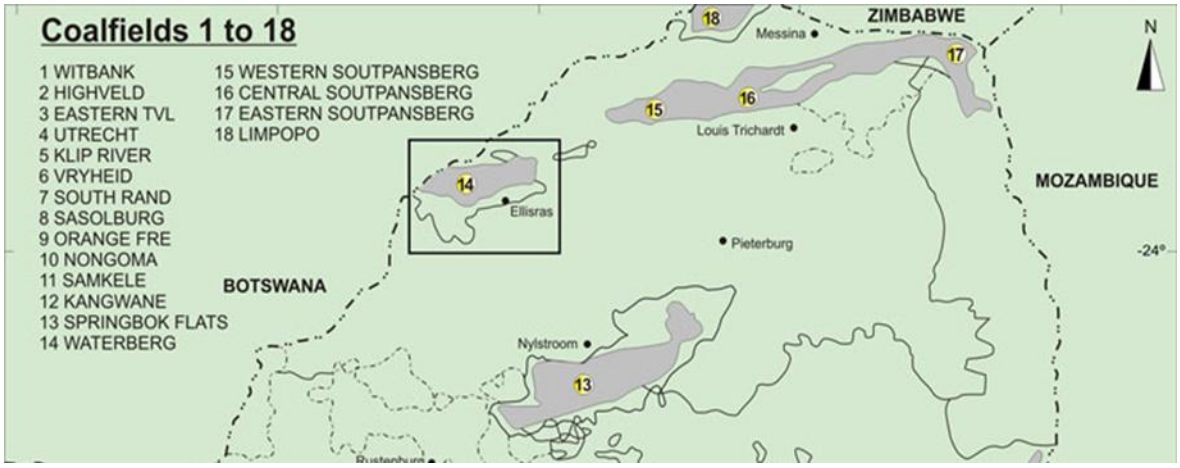

Figure 3-2: Map showing the location of the Waterberg coalfield, South Africa [12]

3.2.1 Sample preparation

Whilst coal sample origin is of interest, it is of limited value to this project. Since one of the major objectives of the study was to determine the effects of macerals on CO_2-coal interactions, attempts were made to obtain pure macerals (>90% pure maceral composition) from the coal sample. Handpicking proved to be a challenge, and it was decided to employ laboratory scale coal beneficiation techniques (density fractionation) to isolate the coal macerals.

All the samples were crushed and screened to +500-1000μm particle size fraction and stored in nitrogen-flushed containers.

The samples were then separated using solvents as a separating media. The organic solvents selected for the study were chloroform and benzene. Benzene has a specific gravity (S.G) of 0.88 g/cm^3 and chloroform an S.G. of 1.48 g/cm^3. It was suggested that the density separating media might affect the coal sample's surface properties. To account for this a study was done to determine the effect of separation media on coal surface properties [See Appendix A]. As discussed in Appendix A, the density-separated samples were characterised before and after density fractionation. The study showed that the separating media does have a slight effect on the coal's properties, with organic solvents showing a smaller effect than inorganic solvents, and hence organic solvents were chosen as the separating media.

A fraction of the density fractionated samples were demineralised. This fraction of samples were used in quantitative XRD analysis (§ 3.3.2.2 and §6.6). This was done because of the difficulty encountered in performing quantitative XRD analysis on samples with mineral matter[16]. The following procedure was used for demineralisation [168]. A weighed sample (5 g) was dispersed in 30 mL of concentrated HCl solution (36.5 wt.%). The mixture was stirred for 3 hours at 50°C before the coal was filtered and washed with distilled water. The HCl-treated sample was then mixed with 30 mL of concentrated HF solution (48 wt. %). The mixture was stirred for another 3hours at the same temperature and filtered. Finally, the treated coal was washed with distilled water and dried in the air at ambient temperature.

Following density media separation and demineralisation, each sample was dried in a vacuum-drying oven at 50°C for 24 hours before measurements were performed. Higher

[16] Demineralisation of the samples does compromise the integrity of the samples [258-259], however, it was conducted to remove mineral matter for better comparison of quantitative powder XRD analysis on the two maceral rich coals. Quantitative XRD analysis is not intended as an absolute characterisation but rather as a comparative characterisation.

temperatures will result in less drying time, and may not influence the pore analysis results [185].

3.2.2 Basic characterisation

Standard coal analyses (petrographic, proximate and ultimate analysis) were performed on the coals to determine the standard properties (maceral composition, ash, moisture etc.) of the coals before any further characterisation techniques.

3.2.2.1 Maceral analysis

For maceral analysis a standard petrography procedure was used [186]. The density fractionated coals were crushed and sieved to -1mm + 800μm and prepared into coal blocks for point count and image analysis. The coal blocks were produced by mounting the coal in an epoxy resin. After setting, the blocks were polished using a Struers TegraForce-1 polisher machine located at the University of the Witwatersrand, in the School of Metallurgical and Chemical Engineering.

The polished blocks were examined under a Leica DM4500P petrographic microscope located at the University of the Witwatersrand, in the School of Metallurgical and Chemical Engineering. Maceral group analysis was conducted on the parent coals following [187]. The analysis was conducted at a magnification of x500 with oil immersion in polarized light.

3.2.2.2 Proximate and ultimate analysis

Proximate analysis was conducted to determine the amount of moisture, volatile matter, fixed carbon and ash in the density separated coal samples. This analysis was conducted using a Thermogravimetric Analyser (TGA) at the University of the Witwatersrand, in the School of Metallurgical and Chemical Engineering.

The analysis was performed following standard methods to measure the percentage of moisture [188], ash content [189] and volatile matter. The difference between these three percentages and the mass of the original sample (100 %) is referred to as fixed carbon. To calculate the surface moisture, the percentage mass loss between the initial sample mass and the stable mass at 110 °C is measured. This can be reported as mass percent or mass.

Ultimate analysis was conducted using a standard for determination of hydrogen, sulfur, and nitrogen in the coal samples [190]. The ultimate analysis was conducted by the ALS Laboratory, Witbank.

3.3 Structural analysis techniques

The change in coal structure is central to the study and thus the integrity of the techniques used for characterising the coals before and after CO_2 saturation is important. Because of the nature of the small structural changes under study, the biggest challenge was to find the appropriate techniques with the correct detection limits and availability. Herewith are the techniques and methods used in the study:

(i) Physical properties (§ 3.3.1)

- Helium pycnometry
- Brunauer-Emmett-Teller (BET) method

(ii) Advanced Characterisation techniques (§ 3.3.2)

- Solid state Nuclear Magnetic Resonance ($^{13}C_{ss}$NMR) to understand the internal structure of the coal
- Fourier-Transform Infrared (FTIR) Spectroscopy to probe for functional properties change,
- X-ray diffraction (XRD) to observe the internal crystalline structural changes

3.3.1 Physical properties

3.3.1.1 True density measurements

The true density and porosity are important characteristics of a material, and sorption behaviour will largely be influenced these properties. Therefore, it is important that these properties are well characterised for the samples under study. A He pycnometer was used for this purpose:

(i) to determine the volume of the coal samples before the measurement of the adsorption isotherms;

(ii) as a structural change probe technique, in conjunction with BET, to probe for changes in the coal's pore properties after CO_2 sorption

A He pycnometer provides the true density of a porous material [191]. Because of its size, He is able to penetrate into smallest pores and gaps making it possible calculate the true volume of a material [192]. This volume corresponds to the exact volume occupied by the material, without porosity. The material is, after preparation and activation (degassing at elevated temperatures), put in a cell of known volume which after evacuation is filled with a known mass of He. The computations involve Archimedes' principle of fluid displacement and Boyle's law to determine the sample volume. Refer to APPENDIX B for further information regarding the theory behind this technique. Knowing the mass, the density of the material can be computed.

A Quantachrome Ultrapycnometer 1000, housed in the School of Chemical and Metallurgical Engineering, University of the Witwatersrand, was used. The density value reported is an average value of three measurements, and the standard deviation achieved is less than 0.005 g/cm^3. Before conducting density determination experiments, the samples were prepared by

removing the atmospheric gases and vapours therein by heating the samples under vaccum at 50°C. Then the samples were placed in the pycnometer and the probe gas was then added to purge all the samples for 30 min. Each experiment was carried out at room temperature. Both the purge and fill pressure were set to 17 psig [185]. Helium gases used in the adsorption isotherms were purchased from Afrox (South Africa) with a purity of 99.997%.

3.3.1.2 Surface Area (BET) and pore size distribution

A characteristic parameter of a porous material is its so-called BET surface. This is the surface of a monolayer adsorbate at boiling temperature of at namely 77.3 K. It is determined by nitrogen adsorption experiments at this temperature for pressures. The mass of the monolayer load is determined by fitting data to the adsorption isotherm equation developed by Brunauer, Emmett and Teller in 1938, originally designed for multilayer adsorbates [193].

$$\frac{p}{(p_0 - p)m^a} = \frac{C - 1}{Cm_1}\left(\frac{p}{p_0}\right) + \frac{1}{Cm_1} \qquad (1.1)$$

Here (C, m_1) are parameters to be determined by a data fitting procedure, preferably restricted to the region $0<p/p_o<0.3$. Assuming a cross section of σ_{N2} = 0.162 $(nm)^2$ per N_2 molecule[1.3], the BET-surface of the monolayer simply can be calculated as:

$$A_{BET} = \sigma_{N2} m_1 / M_{N2} \qquad (1.2)$$

M_{N2} = 28g/mol is the molar mass of nitrogen.

The BET-surface concept only should be used for nonporous or meso- and macropores including materials but not for microporous substances. The reason for this restriction is that in micropores and especially sub-micropores (diameter d < 1 nm) pore filling may occur prior to adsorption on the more “open” surfaces of meso- and macropores. Hence, part of the

nitrogen adsorbed may form linear, string like aggregates in the micropores for which the concept of surfaces becomes obsolete.

Although the model on which the above equations for BET are oversimplified, BET is still the most widely used method for analysis of porous sorbents like coal [112]. Both CO_2 and N_2 are used as adsorbent gases in the analyser. Nitrogen is commonly used as the adsorbate to examine the mesopore and macropore structure as well as larger micropores. Although its molecular diameter is similar to CO_2, N_2 is not able to penetrate the micropores because of the activation energy barrier in the micropores [74] .

Nitrogen BET-surface concept only should be used for nonporous or mesoporous and macroporous including materials, but not for microporous substances. The reason for this restriction is that in micropores, and especially sub-micropores (diameter d < 1 nm) pore filling may occur prior to adsorption on the more "open" surfaces of mesopores and macropores. Hence, part of the N_2 adsorbed may form linear, string like aggregates in the micropores for which the concept of surfaces becomes obsolete. Nevertheless, N_2 BET data are still used today for microporous materials in the technical literature. Carbon dioxide is a better sorbing gas to use in coal BET studies, because of its smaller molecular size and ability to access "micropores".

The BET analyses were conducted at the North West University, Chemical Engineering laboratories. A Micromeritics 2020 ASAP surface area analyser was used to gain information on the surface area and pore size distribution of the coal samples. The method is based on the physical adsorption of N_2 on the solid surface at 77K and CO_2 at 273K. Approximately 200 mg of sample was used for each analysis. Prior to analyses, the samples were degassed for 2h at 105°C to remove moisture and adsorbed gases on the sample surface. Then the amount of probe gas adsorbed/desorbed, as the partial pressure was gradually increased or decreased,

was measured. The surface area was then estimated by the method developed by Brunauer, Emmet and Teller (BET method). The micropore area and micropore volume of the sorbent were determined according to the thickness plot (T-plot) method. Pore diameter distributions were obtained by the H-K (Horvath-Kawazoe) method based on the desorption isotherm.

For a comparison of the accuracy of surface area properties, samples were also sent to Germany (Aachen University of Technology) for surface area and pore diameter distribution analysis. The isotherms were measured with a Quantachrome AS1 MP pore structure and surface area analyser. Carbon dioxide isotherms (36 points) were obtained at 273.15K in a water/ice bath in the relative pressure range from 1.1×10^{-5} to 2.5×10^{-2}. The model for the pore diameter distributions (PDS) determination was the Non-local density functional theory model (NLDFT) with a slit-geometry. N_2 isotherms were obtained at 77K in a liquid N_2 bath from 4.5×10^{-5} to 0.98 (48 points). For N_2 isotherms, the model for the PDS was the NLDFT with combined slit/cylinder geometry.

3.3.2 Advanced characterisation techniques

Structure (physical or chemical) affects the behaviour of coal in any application [194]. However, the molecular scale interaction of coal and CO_2 has rarely been investigated, with the exception of Pone and co-workers [195]. In this section the different characterisation techniques used for elucidating the coal structure, are discussed.

3.3.2.1 Solid state Nuclear Magnetic Resonance (^{13}C ^{ss}NMR)

To understand the internal structure of the coal, more specifically the fraction of aromatic and amorphous carbon, a solid state ^{13}Carbon Nuclear Magnetic Resonance (^{13}C ^{ss}NMR) technique was used. NMR is able to quantify the ratios of aromatic carbons and aliphatic carbons, which are important parameters in coal chemical structure analysis [167]. It utilises

the property of the magnetic moment associated with the intrinsic angular momentum or spin of nuclei. The phenomenon is restricted to isotopes with odd atomic number (Z) and mass number(A) such as ^{1}H, ^{13}C etc.

^{13}C NMR analyses were conducted at the University of Stellenbosch, Central Analytical Facility. Analyses were carried out on a Chemagnetics CMX-100 NMR spectrometer operating at a carbon frequency of 25.152 MHz and a proton frequency of 100.02 MHz. Four experiments were conducted: (1) cross-polarization (CP) magic angle- spinning ^{13}C NMR; (2) single-pulse excitation (SPE) ^{13}C NMR; (3) variable contact time NMR; and (4) dipolar dephasing. For dipolar dephasing, 27 points were obtained, from 2 μs to 1 ms for CP experiments and 11 points in the same region for SPE. The CP experiments are conducted with a 2 ms contact time. The highest points in the variable contact time experiments were between 0.4 – 0.8 ms. Both the proton and carbon T1's were measured by saturation recovery and all experiments were run with pulse delays equal to five times the longest component in additional CP or SPE based experiments.

Although there was value in performing ^{13}C NMR analysis for pre-sorption samples, the value for analysing post-sorption was in doubt. This was due to the nature of the expected changes in the coal properties not being easily detectable by ^{13}C NMR. On this basis, together with the cost constraints, it was decided to only analyse pre-adsorption samples.

3.3.2.2 Powder X-ray Diffraction (PXRD)

Following Goodman et al. [20], it was postulated that, should there be any structural changes on the coal structure, it should be detectable via powder X-ray diffraction (PXRD), by observing the change in interlayer spacing caused by the sorbed CO_2. One of the advantages of using PXRD is that it is a non-destructive and well established technique with good reproducibility. It uses a relatively large amount of sample (about 1-2g), and collects most of

the intensities scattered from the examined sample. Therefore the properties yielded represent an average for the sample rather than the properties of individual particles.

PXRD is most useful on crystalline materials; however, coal is composed of both crystalline phases and amorphous phases. The crystalline material is from both crystalline inorganic minerals and organic matrix of coal. Nevertheless, useful structural information can still be obtained from a PXRD pattern for probing structural changes on CO_2 sorption. In Figure 3-3, a schematic illustration of the organic single crystallite in coal is shown together with how it links with amorphous carbon. In the figure, d_{002} represents the planar distance between graphitic carbons, L_a and L_c is the length and width of the unit cell, respectively. These parameters can be used to probe for structural change.

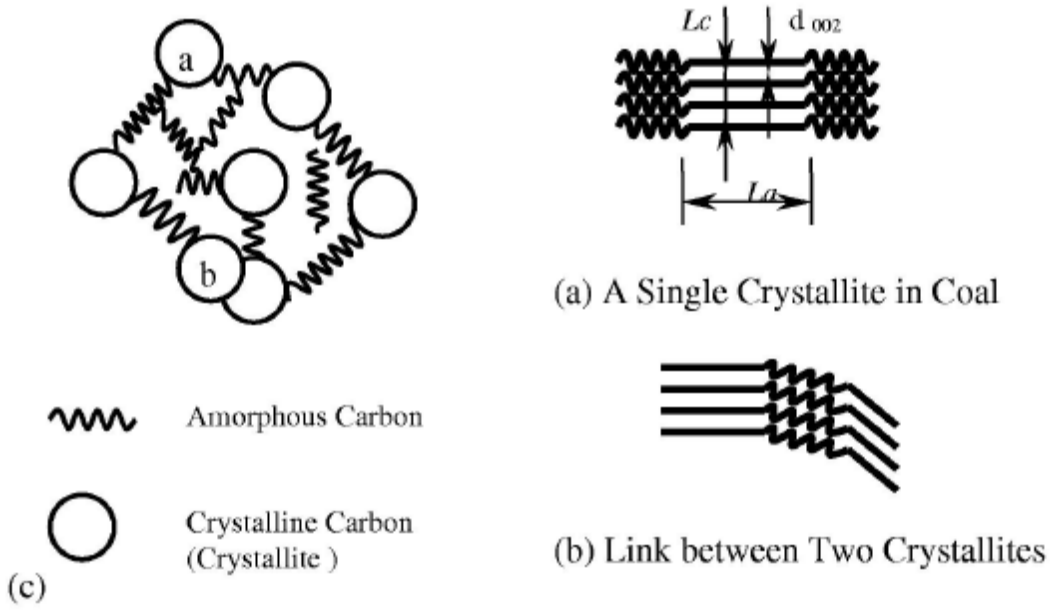

Figure 3-3: Crystalline and non-crystalline carbon structure[196]

From PXRD data, the interlayer spacing between the aromatic rings can be determined. This is done by calculating the interlayer distance between aromatic sheets (d_{002}) from a maximum of the (002) band using the Bragg equation [168]

$$d_{002} = \frac{\lambda}{2\sin\theta_{002}} \quad (3\text{-}1)$$

The average crystallite stacking height (L_c) can be computed

$$L_c = \frac{0.9\lambda}{\beta_{002}\cos_{002}2\theta} \quad (3\text{-}2)$$

In this study, PXRD data were collected using a Bruker AXS D8 (housed at the University of the Witwatersrand) equiped with a primary beam Gobel mirror, a radial Soller slit, a V Antec-1 detector and using Cu-K radiation (40kV, 40mA). Data was collected in the 2θ range 5 to 90 in 0.007 steps , using a scan speed resulting in an equivalent counting time of 439.2s.

Curve fitting was performed using the OriginLab® software curve fitting toolkit. Average structural parameters were calculated from the peak widths at half-maximum intensity (β) and the peak positions (θ) using empirical [168].

3.3.2.3 Fourier Transform Infrared Reflectance (FTIR)

Fourier Transform infrared spectroscopy (FTIR), provided it is used quantitatively, offers valuable information on the chemical structural changes of coal. Goodman et al. [183] used FTIR to study coal under CO_2 environment (see § 2.6.2). Although Goodman's study was performed in-situ, it showed the power of FTIR to probe for structural changes on CO_2 exposure. In this study FTIR was used ex-situ, but still proved as useful if there is minimal exposure of the CO_2 'treated' sample to the atmosphere [183].

FTIR spectra were obtained using a solid state Bruker FTIR spectrometer (housed at the University of the Witwatersrand) equipped with a NICPLAN microscope. A 35 x IR objective and an aperture of 30pm were used for micro-FTIR. Analyses were done in both transmission and reflected modes. All spectra were obtained at a resolution of $4cm^{-1}$ and 128

scans were co-added (a ratio to a gold plate background of 128 scans was calculated). Kramers-Kronig transformation was applied to reflectance spectra. Bands were assigned according to Painter et al. [169].

3.4 Chapter summary

In this chapter, methods used to characterise the coal samples pre- and post-sorption for the study, and the rationale for using those methods were discussed. A belt cut run-of mine sample was used to prepare density fractionated and demineralised samples. Each sample was characterised using a petrographic microscope for maceral analysis. For physical properties characterisation, each sample was characterised by a He Ultrapycnometer for density measurements, and a BET surface area analyser was used to gain information on the surface area and pore size distribution of the coal samples.

Each sample was also characterised using advanced analytical techniques to gain more in-depth understanding of the coal's structure and properties. Powder XRD, ^{13}C NMR and FTIR were used for this purpose. The techniques discussed in this chapter provide the necessary coal characteristics and properties (pre-sorption results discussed in Chapter 5) important for discussing the changes in Chapter 6, 7 and 8.

CHAPTER 4
EXPERIMENTAL METHODS

This chapter discusses the experimental methods that were used in the study. The chapter particularly focusses on the high pressure reactors (§4.1) and the newly-built high pressure volumetric adsorption system used for the adsorption isotherms measurements (§4.2). The final section of the chapter (§4.2.3.2) presents how the data collected from the high pressure volumetric system was used for construction of adsorption isotherms.

4.1 Static pressure experiments

Static pressure experiments were performed by exposing coal to CO_2 in reactors at different temperatures and pressures. Two experimental setups were utilised; (i) one Parr reactor at Sasol Technology R&D laboratories, and (ii) three High Pressure (HiP) reactors used at the University of the Witwatersrand.

The Parr reactor was readily available at the beginning of the project but could only achieve a pressure of 50 bar due to the unavailability of a pressure booster and safety restriction at the Sasol site where pressures higher than working 50 bar were not allowed due to safety concerns. Subsequently, the HiP reactors were purchased to achieve pressures up to 150 bar at the University of the Witwatersrand, hence the Parr reactor and the HiP reactors were used for the subcritical and supercritical conditions experiments, respectively.

4.1.1 Description of the Reactors

The Parr reactor used for the study was a high pressure 4551 reactor with 3.75L capacity and working temperatures of up to 225 °C and pressures up to 131 bar (Figure 4-1). Coupled with

a heater and a moveable head, the reactors are designed so that they can be opened or closed conveniently without removing the cylinder from the heater and without auxiliary handling equipment.

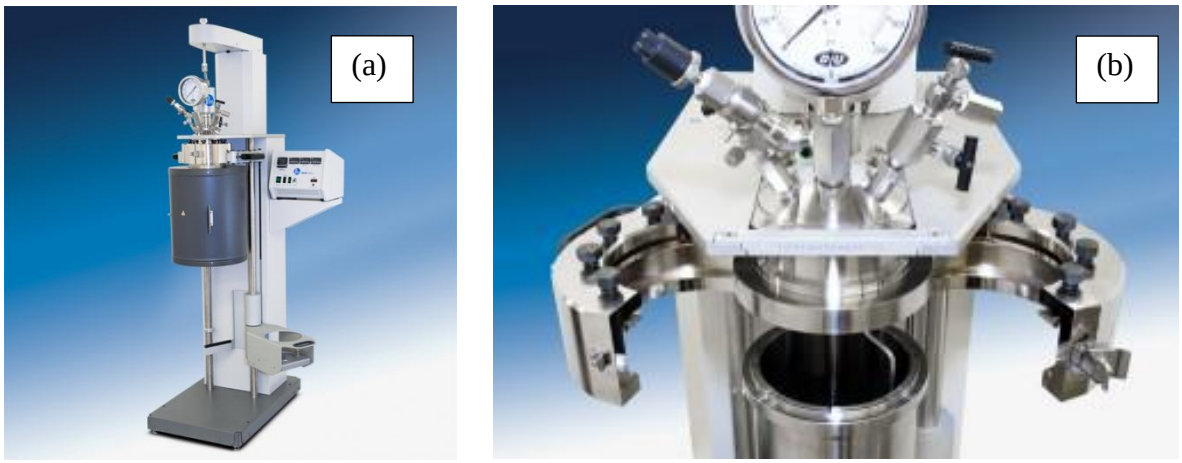

Figure 4-1: Parr reactor used for sub-critical static experiments-(a) front view of the Parr reactor, (b) split ring cover clamp.

Figure 4-1 (b) shows the split-ring cover clamp section that can be moved into place from the sides, and the cap screws can be tightened with the cell in place in its heater.

Two types of High pressure (HiP) reactors were chosen for the supercritical section of the static experiments (Bolted and OC reactors). Cost and stability at high pressures were the main criteria for choosing the reactors. Bolted closure reactors are designed to operate at maximum working pressures up to 345 bar and at temperature of up to 343°C (maximum temperature for this study is 60°C). Standard material for the body, cover, and gasket is Type 316 stainless steel. Two HiP reactors were chosen so that the two maceral enriched coals can be run concurrently thus saving time.

The OC Series provide a simple closure that is reliable and easy to assemble and disassemble. Standard material for the body and cover is Type 316 stainless steel. They operate at pressures up to 1000 bar (maximum pressure for the study is 150bar) and temperatures of up to 121°C. Both these reactors are suitable for either a gas or a liquid with a capacity of 125

ml. They were fitted with a thermocouple for temperature measurements, a pressure transducer and a safety relieve valve (see Figure 4-2). The display unit and pressure transducers and the thermocouples are then connected to through a wire respectively.

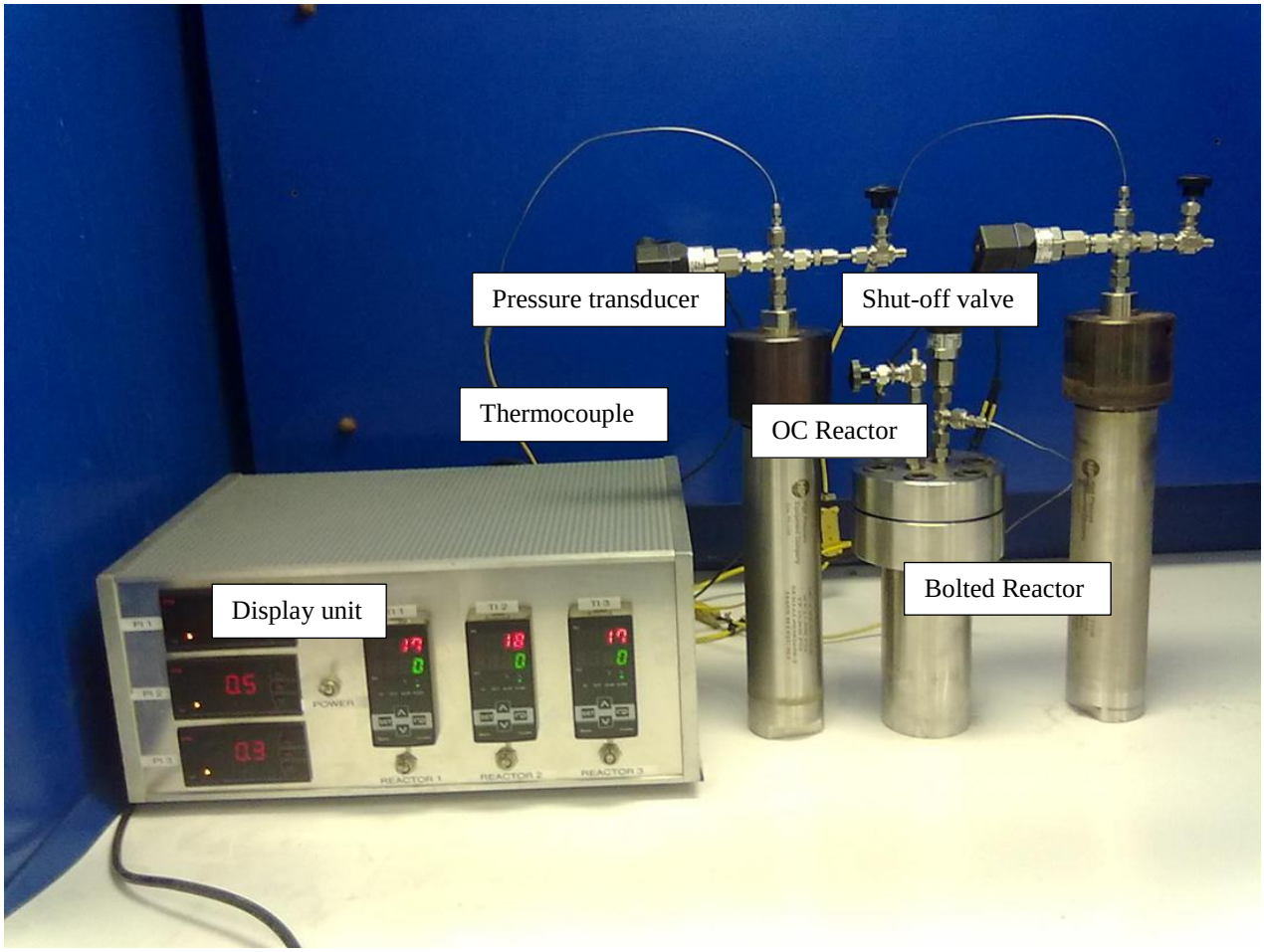

Figure 4-2: A photograph of the instrumental setup for the long term storage reactors, showing both the OC and Bolted reactors.

Reactors were also compartmentalised using stainless steel. This was done so that demineralised and non-demineralised samples can be placed in the same reactor without any interference.

4.1.2 Static reactors storage conditions

The different temperature and pressure conditions used in conjunction with the Parr and HiP reactors are shown in

Table **4-1**. The conditions were chosen to simulate the levels of a potential storage site conditions (see Figure 2-1).

Table 4-1: Experimental conditions for CO_2 treatment

Run	Reactor	Sample	Pressure (bar)	Temperature (°C)	Time (Days)	PSD (mm)	Mass (g)	CO_2 phase
1P	Parr	Coal A	45	20-30	180	+0.5-1	5	Vapour
		Coal B	45	20-30	180	+0.5-1	5	Vapour
1H	HiP	Coal A	45	25	14	+0.5-1	3.11	Vapour
		Coal B	45	25	14	+0.5-1	3.22	Vapour
2H	HiP	Coal A	125	35	180	+0.5-1	20	Supercritical
		Coal B	125	35	180	+0.5-1	20	Supercritical

The reactors were enclosed with a heating jacket to control the temperature of the reactors. They were also coupled with a PT 100 thermocouple and a pressure transducer. A displaying unit was used to monitor for leaks and any other irregularities that might have occurred in the period under study.

In order to study the internal structural changes using XRD, demineralised untreated coals were placed in the high pressure reactors for treatment with CO_2, together with non-demineralised coals. The particle sizes were selected such that there was a balance between using a sample large enough to extrapolate results for field applications, and small enough to reduce sorption time to fall within a reasonable time frame for this PhD study (with repetitions) and simultaneously meeting the study objective of observing long term effects.

The reactors were pressurised by connecting the reactors (one at a time) to the pump and pressurising to the desired pressure. Once the desired pressure was achieved, the valve on the reactor was closed to maintain the pressure within the reactor.

After the period of CO_2 treatment as specified in Table 4-1, samples were removed and either stored or prepared for post-sorption analysis. Storage conditions were at 4°C to minimise air exposure. Table 4-2 shows the analysis performed post-adsorption.

Table 4-2: Analysis performed on sample post-adsorption

Run	Reactor	Sample	Analysis (post-sorption)
1P	Parr	Coal A	Petrography, BET, PXRD, FTIR, CO_2 adsorption
		Coal B	Petrography, BET, PXRD, FTIR, CO_2 adsorption
1H	HiP	Coal A	PXRD and BET
		Coal B	PXRD and BET
2H	HiP	Coal A	Petrography, BET, PXRD, FTIR, CO_2 adsorption
		Coal B	Petrography, BET, PXRD, FTIR, CO_2 adsorption

Quantitative PXRD was performed on demineralised coals (see § 3.2.1). Samples from 1H run were only analysed for quantitative PXRD and BET. Based on BET and PXRD results, it was decided not to perform the other analysis as the samples remained relatively unchanged after 14 days.

4.2 High pressure sorption

In order to fulfil the objectives of this study, it was necessary to design a new high pressure adsorption isothermal measurement system (see § 2.4.1.1). The system chosen for the

purposes of this study was a volumetric adsorption isotherm measurement system based on the results from the criteria in Table 4-3.

Table 4-3: Criteria for the selection of adsorption system used

Criteria	Volumetric Method	Gravimetric Method
Cost	4	2
Time of Construction	4	2
Accuracy	3	4
Availability of material	4	3
Maintenance	4	3
Total	19	14

5-excellent, 4-very good, 3-good, 2-fair, 1-poor

The system was designed in-house, verified at Aachen University of Technology and constructed by Chemvak, a company based in Pretoria, South Africa. An MSc student assisted with the commissioning and verification of the equipment, and a more complete description of the equipment is provided in his dissertation [197]. The system took about two and a half years to complete from design phase to commissioning phase. A more concise design discussion follows.

4.2.1 High pressure volumetric adsorption instrument

A volumetric instrument for measurement of pure gas adsorption consists of a gas storage cell and an adsorption cell connected by a tube bearing an air controlled pneumatic valve (see Figure 4-3). Both cells are completely placed within a thermostat (oven) and provided with tubes for gas supply and evacuation, as well as with thermometers and manometers to measure the temperature and pressure inside the cells, respectively.

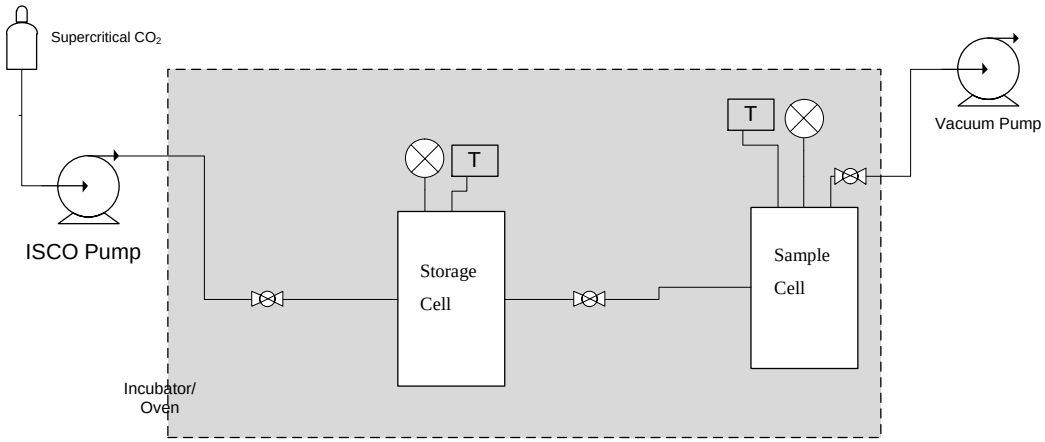

Figure 4-3: Simplified schematic of the volumetric adsorption isothermal measurement instrument

All cells and tubes were manufactured of stainless steel so that they can operate at pressures above ambient. The sealing materials were chosen according to the sorbing gases to be used (CO_2) and the ranges of temperature and pressure of operation (20°C-50°C). None of the gases used were corrosive, but the high pressures necessitated the use of metallic sealings (stainless steel). Figure 4-4 shows the final assembled high pressure adsorption instrument with the different components of the system.

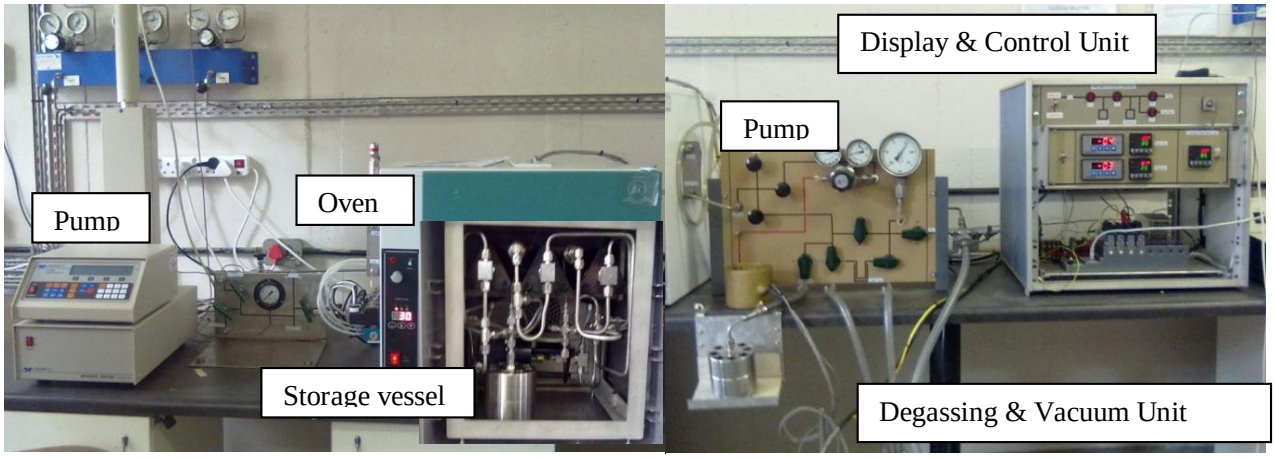

Figure 4-4: High pressure adsorption measurement system

A consideration during the design of the system was the minimisation of experimental errors. Since the estimation of void volume contributes most to experimental errors, one of the main contributions towards experimental errors, the instrument was designed such that the sample cell volume was as small as possible in order to minimize the sample volume (§4.2.2.1). Table 4-4 provides a brief description of the components used to construct the system (details are provided in APPENDIX C)

Table 4-4: Components description for volumetric apparatus

Item	Description	Supplier
Vacuum pump	Evacuating the system to under 100Pa	Edward
Cells	Interchangeable cells, stainless steel, ¼" piping, elecropolished inside. 0-160bar, -20°C to 60 °C	Manufacturer (in collaboration with Chemvak)
Valves and fittings	High pressure electro-valves. 0-200 bar, -20°C to 150 °C. 24V DC voltage Filter: +7µm retained, 0 to 413bar and 0°C to 480 °C	Fittings – Swagelok Valves - Asco
Temperature measurement	4 wire Pt100 with ¼" NPT, output: 4-20 mA DC	Thermocouple Products
Pressure transducers	0 – 250 bar(absolute and gauge), 0.075% accuracy, up to 473K,	Endress+Hauser
Data acquisition	I/O – NI 9203 8-Channel +/-20mA, 200kS/s, 16-Bit analog Input Module	National Instrument
Oven	less than +/- 0.3°C, internal height sufficient for the sample cylinders used and a hole for fittings, pipes and tubing	JP Selecta
Software and peripherals	Labview	JAD Systems

4.2.2 Instrument commissioning

4.2.2.1 Sample cell and void volume measurements

Before adsorption isotherm measurements, the empty volume of the sample cell, V_{sc}, and the void volume, V_0, must be measured (see Appendix Table C-1 for values). The void volume, which is the volume of the sample cell not occupied by the solid coal, V_0, is variable and dependent on the sample volume in the sample cell, whereas V_{sc} is a constant and only need to be measured once. During commissioning, V_{sc} is measured using the He displacement method (He is a non-adsorbing gas). The steps used in performing the V_{sc} and V_0 measurements are shown in Figure 4-5.

In the first step, the empty volume of the sample cell, V_{sc}, is estimated by filling the gas with He and by using simple ideal gas law equation. In the second step, the void volume, V_0, is measured. The density and volume of the adsorbent can also be estimated from these two measurements. In the third step, the adsorption isotherm is measured using the adsorbate gas of interest. As shown in Figure 4-5, the adsorbed phase occupies volume and this volume needs to be included in the calculation of the remaining free volume in the cell (§ APPENDIX B for equations).

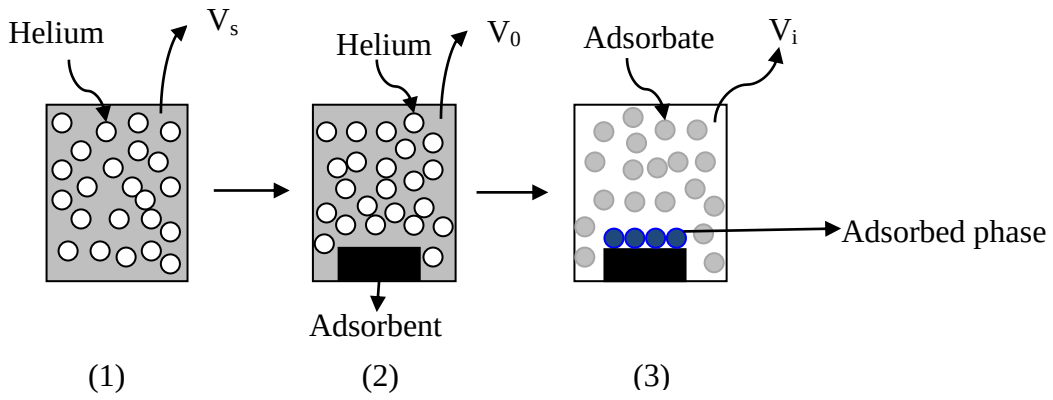

Figure 4-5: Measurement of V_{sc} and V_o [105]

4.2.2.2 Leak detection

A leak test was conducted by introducing He into the system at the desired maximum pressure of adsorption study. If not otherwise stated, this pressure was up to 45bar for adsorption study at 28 ^{o}C, and 100bar for adsorption study at 40 ^{o}C. The pressure was recorded overnight at constant temperature. Any leak occurrence was detected from the decline in the pressure recordings were, accordingly fixed by tightening the affected bolts and nuts [198].

4.2.3 Adsorption isotherm experiment

4.2.3.1 Operating procedure

In order to generate isotherms, the experiment was performed as follows. Prior to the adsorption experiment, the boosting pump system was completely flushed with liquid CO_2 so that compression to the required high pressure could be achieved. The adsorption processes for the experiment is run in a batch nature.

The experimental procedure is explained with the help of a simplified schematic of the apparatus (Figure 4-6). Before commencing with the experiment valve v_1, v_2, and v_3 were closed, and the sample cell previously filled with a sample was vacuumed. A record of P_1, T_1 and V_1 of the sample cell was conducted. Carbon dioxide gas is then pumped from the supply gas cylinders (top left corner of Figure 4-3) to the gas cell via v_1.

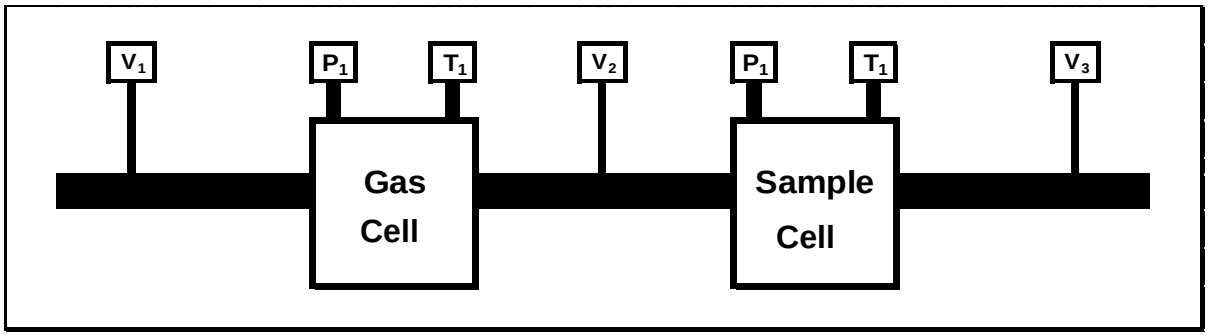

Figure 4-6: Simplified schematic of volumetric system

Immediately when the gas cell was filled to the desired pressure, v_1 was closed. Initially it was planned that the sample cell conditions would be used as the initial conditions for the experiment. But problems were encountered with v_1, concerning constant leaks. It was then decided to use the sample cell as the system boundary for the experiment. In this new system, the initial conditions (V_1, T_1, and P_1) readings were taken after V_2 was opened and closed, whilst the final readings (V_2, T_2, and P_2) were taken after equilibrium was reached. The mass balance to estimate the amount of CO_2 adsorbed was based on the difference of the number of moles between the initial and final stages (see § 4.2.3.2).

After recording the conditions in the gas cell, v_2 was opened in order to allow the gas through the pipe into the adsorbent cell where observation was made until pressure equilibrium was attained. At this new equilibrium, another record of the pressure (P_2) and temperature (T_2) readings was taken. The desorption process is the reverse of the above process.

After the adsorption and desorption readings are taken, the used coal sample was removed and the adsorption cell was cleaned. The data was then fitted into a model to obtain isothermal parameters (see APPENDIX D).

4.2.3.2 Experimental conditions and parameters

The conditions in which the isotherms were generated are 5 to 45bar and 5 to 100bar at 28°C and 35°C for subcritical and supercritical conditions, respectively. For all the experiments, 10 bar successive pressure increase were used. Each point of the isotherm was run until equilibrium adsorption was reached; hence each isotherm consisted of at least six points which where run over a period of at least 12 hours.

The particle size of the samples was +500-1000μm for the untreated samples. Properties for the post samples are described in Table 4-2. The experimental conditions and parameters used in this study are shown in Table 4-5.

Table 4-5: Experimental conditions and parameters for adsorption isotherm measurement experiments

Sample	Experimental Conditions					
	Isothermal Temp(°C)	True density (cm^3/g)	Sample mass(g)	$Void_{sample}$ Volume(l)	Vapour Pressure(P_0)	Fluid state
Coal B - untreated	28.86	1.65	1.689	0.0389	70.75	Subcritical
Coal A- untreated	28.65	1.35	0.53	0.0396	70.40	Subcritical
Coal B-CO_2 treated 6 months	28.68	1.45	0.565	0.0396	70.45	Subcritical
Coal A-CO_2 treated 6 months	28.86	1.33	0.55	0.0395	70.75	Subcritical
Coal B -CO_2 treated 6 months	32.2	1.65	0.76	0.0395	77.83	Supercritical (at 125bar)
Coal A-CO_2 treated 6 months	32.6	1.35	0.577	0.0396	77.94	Supercritical (at 125bar)

4.3 Construction of adsorption isotherms

The method for construction of adsorption isotherms from a volumetric adsorption system is well documented [67, 181] and discussed in the literature review section (see §2.4.1.2); a similar approach was employed in this study. The number of moles adsorbed at each pressure step is calculated by measuring the difference in the total number of moles injected into the sample cell and the number of moles when equilibrium was reached, at each pressure step:

$$n^{exc} = n^t - \rho V_o \qquad (4\text{-}1)$$

Where n^{exc} the excess number of moles is adsorbed, n^t is the total number of moles of gas transferred to the cell, ρ is the molar density of gas in bulk phase, and V_o is the void volume determined by He expansion

The molar density of the gas in bulk phase at each pressure step was determined by using data obtained from the National Institute of Standards and Technology (NIST) web-book [201], which uses equations of state (EOS) from Span and Wagner (see § APPENDIX D.1). The EOS is then used to calculate the difference in the molar volume of the bulk phase between the initial and final pressure reading at each pressure step (see APPENDIX D.2 for obtained data). The excess number of moles adsorbed was then plotted in MS Office Excel® and used to calculate the excess adsorbed amount and the corresponding isotherm parameters from isotherm models (see §APPENDIX D.2).

4.4 Chapter summary

In this chapter the description of reactors and conditions for static and adsorption isotherms experiments are presented. High pressure Parr and HiP reactors were chosen for the static experiments due to their ease of use and low. The Parr reactor was used for subcritical CO_2 treatment whereas HiP reactors were used for both subcritical and supercritical treatment. A new volumetric adsorption system was designed, built and commissioned for measurement of adsorption and desorption isotherms under both subcritical and supercritical conditions. The procedure and conditions for the measurement of adsorption isotherms on the new equipment was described. Finally, the equations and tools used for the construction of adsorption and desorption isotherms are presented.

CHAPTER 5
PRE-SORPTION COAL STRUCTURE CHARACTERISATION

5.1 Introduction

In order to understand the structural changes occurring in the coal particles during CO_2 storage, it was important to conduct characterisation of the coal samples before CO_2 saturation, as well as after. The characterisation was conducted to determine the major physical and chemical properties that may be affected by the interaction of CO_2 with coal. Pre-sorption characterisation results are presented here, with post-sorption characterisation results discussed in Chapter 6 and 7. The analytical techniques are explained in Chapter 3.

5.2 Petrographic, proximate, and ultimate analysis

Petrographic analysis of the samples was conducted to determine the maceral concentration following density fractionation. Results for the petrographic analysis are shown in Table 5-1. Evident from Table 5-1, coal A has high vitrinite content (97.0%) and coal B is rich in inertinite macerals (80.9%), on a mineral matter free basis. The samples are iso-rank (Medium rank C bituminous coals). Also included in Table 5-1 are the proximate and ultimate analyses. The proximate analysis was conducted to determine the amount of moisture, volatile matter, fixed carbon, and ash in the samples. The ash content is low for both samples but slightly higher for coal B.

Coal B has a higher fixed carbon content and hence a higher total carbon content than coal A. Using carbon content as an indication for the order in the internal matrix structure, it can be

assumed that coal B will be more ordered than coal A (see section 5.4.1). A more ordered structure has been shown to strongly correlate with an increase in porosity [168]. Hence, it is expected that coal B will have a higher surface area and higher micropore volume than coal A.

Table 5-1: Petrographic, proximate and ultimate analysis of coal A and coal B

Component	Coal A	Coal B
Petrographic Analysis (vol%, mmf)		
Vitrinite	97.0	15.7
Liptinite	1.3	3.4
Inertinite	1.7	80.9
Proximate analysis (wt%, adb)		
Ash content	4.9	10.4
Moisture content	3.8	3.0
Volatile content	35.6	23.4
Fixed Carbon (by difference)	55.7	63.2
Ultimate analysis (wt%, adb)		
Carbon	68.25	72.69
Hydrogen	5.14	3.90
Nitrogen	1.52	1.70
Oxygen (by difference)	15.31	7.23

Adb – air dried basis, mmf – mineral matter free

5.3 Physical properties

Low-pressure adsorption experiments with CO_2 and N_2 on dry coal samples were performed at 273 K and 77 K respectively to obtain information about surface area and pore structure.

5.3.1 Surface area and porosity

Nitrogen BET surface areas (Figure 5-1) are larger for the inertinite-rich coal (2.71 m^2/g) than for the vitrinite-rich coal (0.92 m^2/g). Surface areas lower than 1 m^2/g are considered to be a very low. However, such results are not uncommon as Gan et al. [83] similarly obtained

N_2 surface areas that were less than 1 m^2/g for some coals. The reason for such low surface areas could be that N_2 is not accessible to particulate macerals in the organic matrix of coal at low temperatures [83]. Coal B, the inertinite-rich coal has about 2.8 times N_2 BET surface area more than vitrinite-rich Coal A. Other studies have are in disagreement with this finding in that vitrinite-rich coals were found to have a higher N_2 BET surface area than inertinite-rich coals [84].

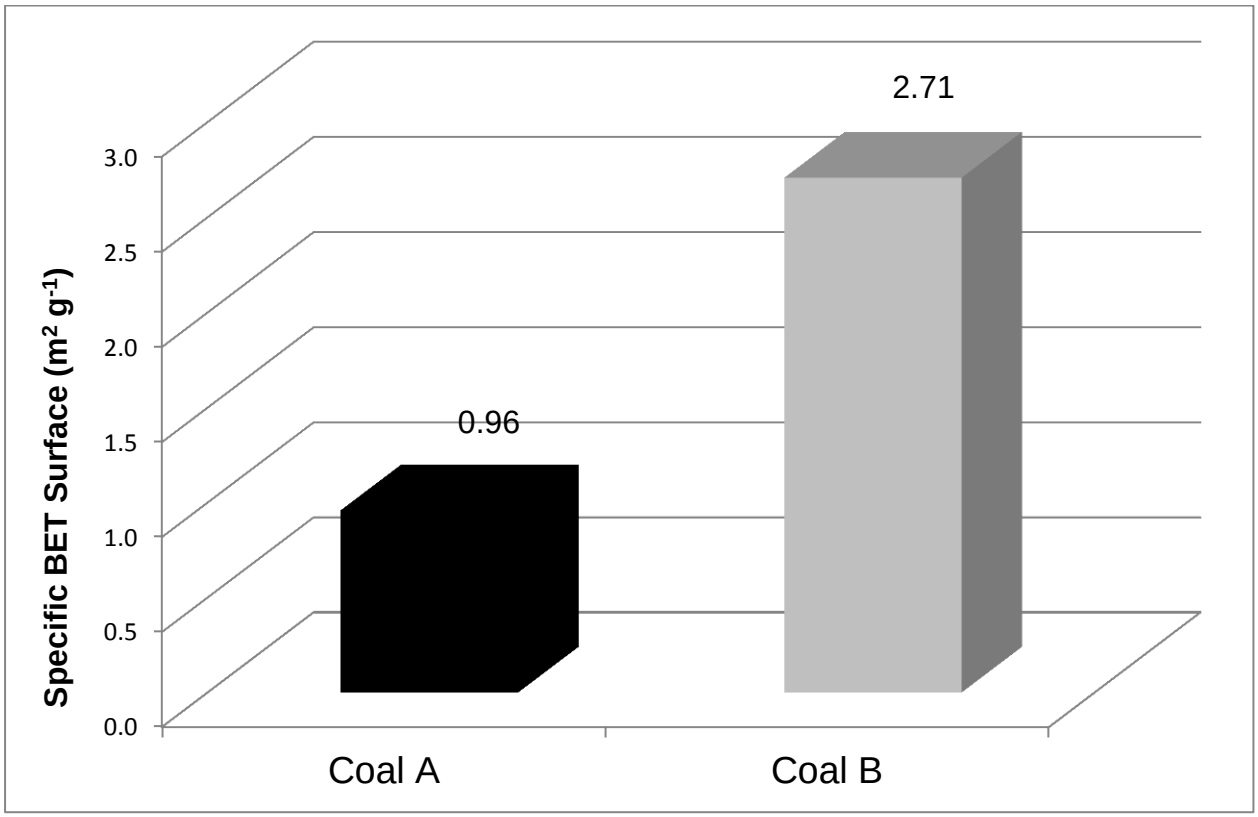

Figure 5-1: N_2 specific BET surface area for coal A and coal B

The reason for such a difference in BET surface for these two coals could be due to their respective microporous and mesoporous volumes. An analysis of the micropore volume shows a contradicting observation in that the coal A (4.96×10^{-2}) is found to have a higher micropore volume than coal B (4.20×10^{-2}) (Figure 5-2).

Micropore surface areas were in the region of 142 m^2g^{-1} and 121 m^2g^{-1} for coal A and coal B respectively. These values agree with the published data on micropores in a number of coals of other ranks [202]. There are a few reasons why the vitrinite-rich coal A has a greater micropore volume than the inertinite-rich coal B, although coal B has a higher BET surface area. One of the main reasons could be the fact that CO_2 (gas used for micropore analysis) swells coals [157]. In swelling the coal, the micropore volume is at times, inflated. This can be accounted by using "swelling factor" in the calculations for micropore volumes and surface areas using CO_2 [154, 203].

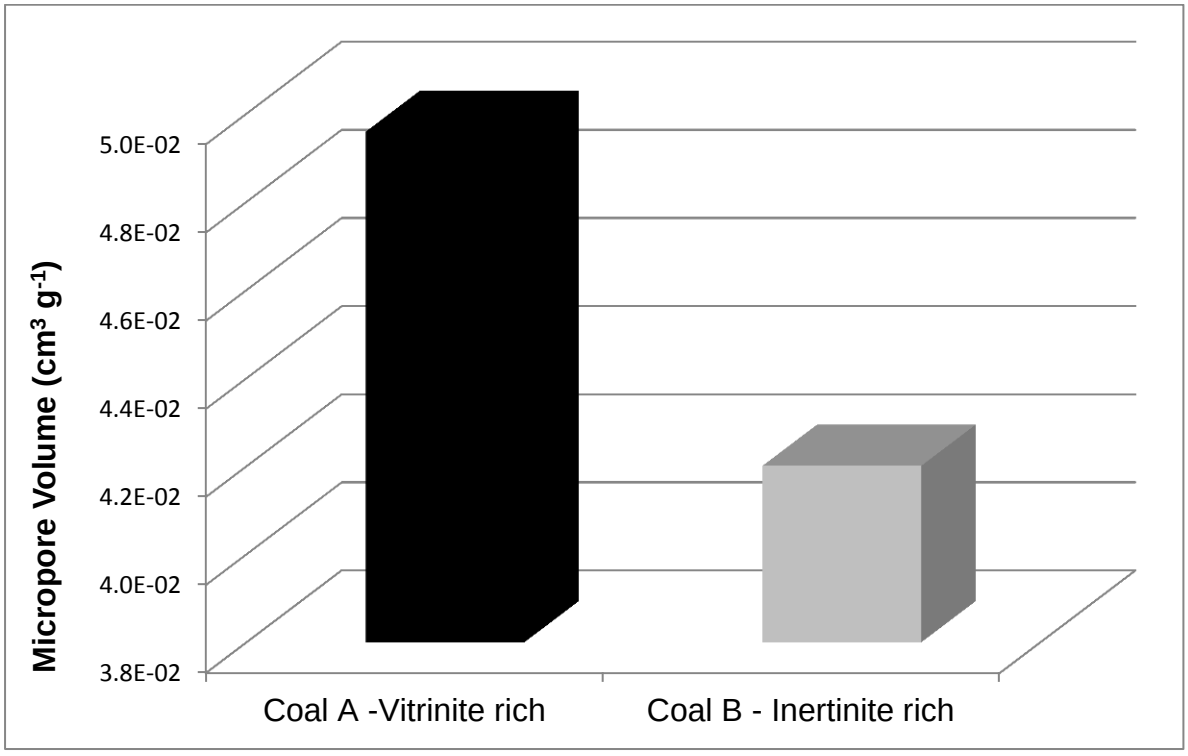

Figure 5-2:CO_2 micropore volume for coal A and coal B

An analysis of the adsorption isotherms was performed to further understand the big difference in BET surface area. The N_2 isotherms provide the best information about the meso- and macropores in the coals, because N_2 molecules at 77K cannot penetrate pores < 0.5-0.6 nm due to activated diffusion problems [74]. Hence, both CO_2 and N_2 isotherms are

used to define a pore system, because CO_2 (273K) is able to penetrate pores down to its limiting diameter (Figure 5-3).

Figure 5-3(a) shows the BET CO_2 adsorption isotherms for both coal A and coal B. According to the Brunauer, Emmet and Teller classification [204] the CO_2 adsorption isotherms are Type I for both Coal A and B. Type I isotherms are given by microporous solids having relatively small external surfaces, the limiting uptake being governed by the accessible micropore volume rather than by the internal surface area. Again, coal A has a higher adsorption capacity than coal B, but only slightly at lower relative pressures, with a wider increase at higher relative pressures.

In Figure 5-3(b), both low-pressure N_2 (77 K) adsorption and desorption isotherms are shown. The reversible Type II isotherm is the normal form of isotherm obtained for a non-porous or macroporous adsorbent. The Type II isotherm represents unrestricted monolayer-multilayer adsorption. Relative pressure 0.1, the beginning of the almost linear middle section of the isotherm, indicates the stage at which monolayer coverage is complete and multilayer adsorption begins [112].

In Figure 5-3(b), the dashed lines indicate the desorption isotherms. A low pressure desorption hysteresis is observed (extending to very low relative pressures) for coal A, which is indicative of a system containing micropores, confirming the earlier observation that coal A has a higher micropore volume than coal B.

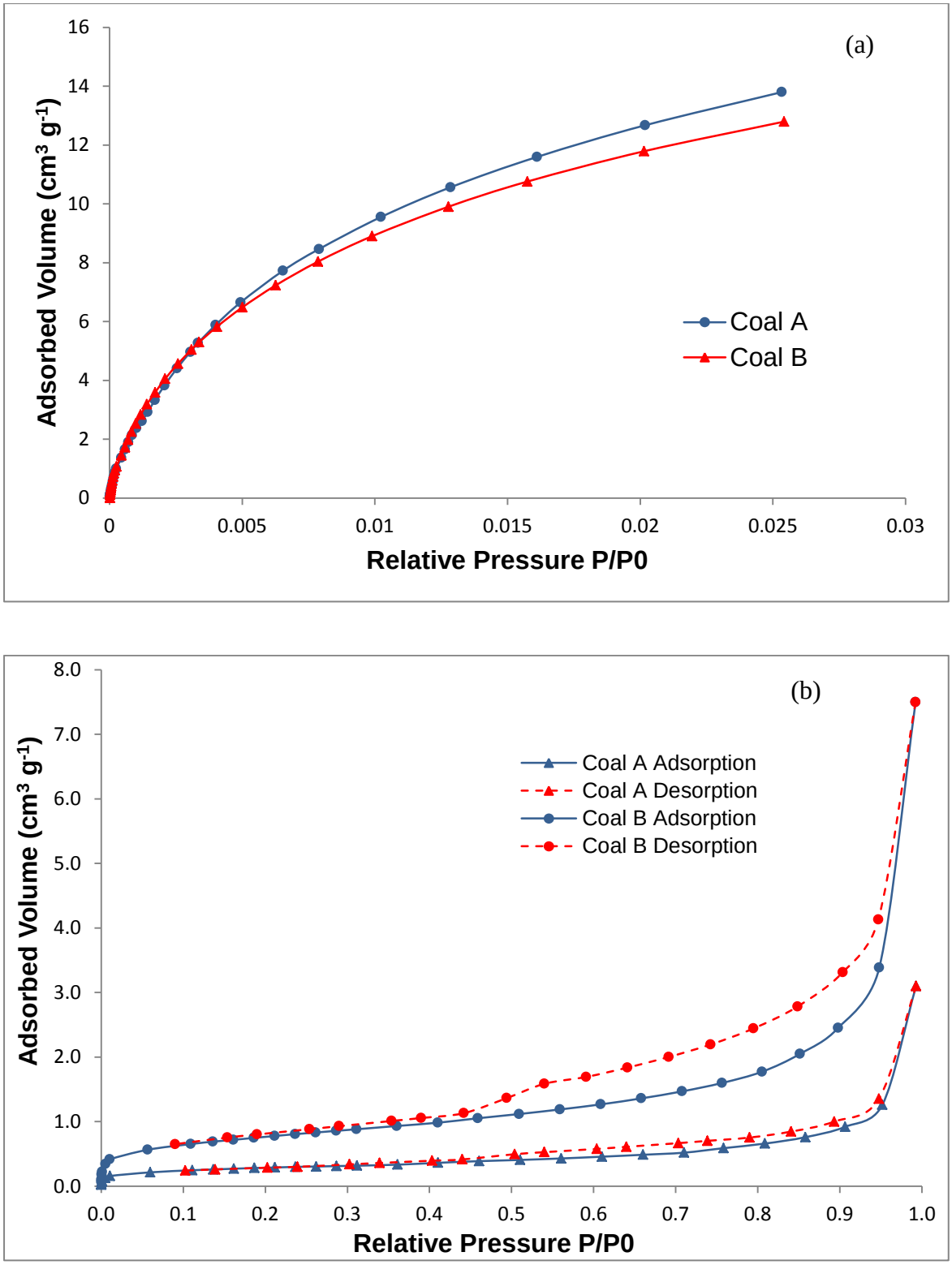

Figure 5-3: Low pressure adsorption isotherms for coal A and coal B samples. (a) CO_2 adsorption isotherms, (b) N_2 Nitrogen adsorption and desorption isotherms

The low pressure desorption hysteresis phenomenon can also be associated with the swelling of a non-rigid porous structure, or with the irreversible uptake of molecules in pores (or through pore entrances) of about the same width as that of the adsorbate molecule, or in some instances with an irreversible chemical interaction of the adsorbate with the adsorbent [112]. Due to the low temperatures, a reasonable explanation is that the above mentioned phenomenon was due to the micropore structure.

The high vitrinite coal A displays a greater amount of hysteresis than the inertinite-rich coal B. Results are given here on a mineral-matter-containing basis (mmcb) as the contribution of entrained mineral matter to N_2 adsorption is unknown.

The two different probe gases are used in this investigations, namely, N_2 adsorption at 77 K and CO_2 adsorption at 273 K are also relevant to CO_2-ECBM, with CO_2 being an important probe gas, as one would like to probe the microporous region potentially accessible by CO_2 during sequestration. Nitrogen forms a large percentage of flue gas streams and is likely to be an impurity in the CO_2 gas stream for CO_2 storage. Nitrogen adsorption also provides the baseline pore-size distribution (PSD) to compare with the PSD based on CO_2 adsorption.

5.3.2 Pore structure and pore size distribution

The use of sorption/desorption data to deduce pore size distributions (PDS), for microporous carbonaceous materials still remains, theoretically, a contentious issue due to reasons explained earlier[17] [97, 157]. Despite the theoretical uncertainties, PSDs generated from adsorption/desorption data are of great value in comparing the structural characteristics and accessibility of different pores in a given coal sample [70]. Both low pressure N_2 and CO_2 isotherms were used for constructing a complete pore structure, as mentioned earlier (§5.3.1). These isotherms were mathematically evaluated to provide meso- and micropore size

[17] See section 3.3.1.2

distribution for the coal samples (§ 3.3.1.2). Figure 5-4 (a) shows the results of the PSD analysis for the two coal samples, Coal A and Coal B, in the microporous region, which was calculated from low pressure CO_2 adsorption data. The CO_2 isotherms data (36 points) was performed at 273.15K in a water/ice bath in the relative pressure range from 1.1 x 10^{-5} to 2.5 x 10^{-2}. A non-local density functional theory model (NLDFT) with a slit-geometry was used.

As mentioned earlier, CO_2 is able to penetrate (at 273K) all pores down to its limiting diameter. In the relative pressure range measured, CO_2 gives values in the range up to 2nm. This range represents the micropore region, and, because adsorption occurs at the micropore sites, the region can also be used to define the adsorption capacity for gases using the Dubinin-Radushkevich model [85]. Hence the micropore size distribution is an important feature of coal structure.

Both coal samples have a very narrow micropore size distribution, with a modal equivalent pore diameter of 0.32-0.38 nm, and micropore volume of 0.06-0.08 cm^3 g^{-1}. The pore size distributions shown in Figure 5-4 (a) indicates a large number of pores in the size range of 0.4-0.7 nm. Coal A has a greater pore volume in this size range than coal B. This confirms the BET micropore volume results, which showed coal A to have a higher micropore volume.

The pore size distribution in Figure 5-4(b) shows results for the mesoporous region (2-50 nm) which was calculated from N_2 adsorption/desorption data. The N_2 isotherms were performed at 77K in a liquid N_2 bath from 4.5 x 10^{-5} to 0.98 (48 points).The model used to calculate PSDs is the NLDFT with a combined slit and cylinder geometry.

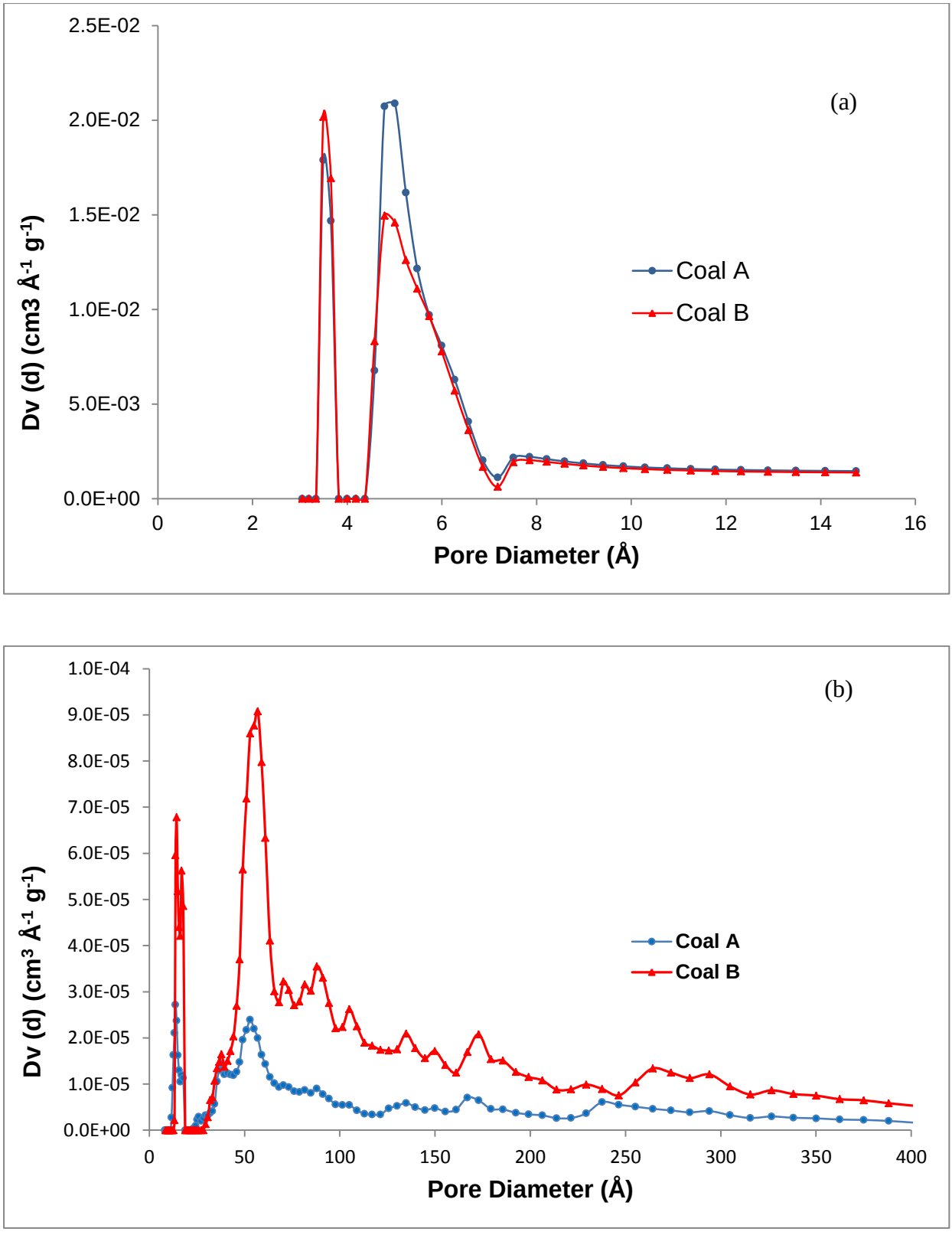

Figure 5-4: Pore size distribution for coal A and coal B. (a) CO_2 micropore size distribution and (b) N_2 pore size distribution

An observation from Figure 5-4(b) is that the difference between the two coals in the mesoporous range is great, with inertinite-rich coal B having a greater pore volume in mesoporous range (2-50 nm) than the vitrinite-rich coal A. Much of the volume in the mesoporous region is pore sizes 4-10 nm for both the coals.

This observation would corroborate with the BET studies, where the specific BET surface area for coal B was found to be higher than for coal A (see Figure 5-1). This would suggest that mesoporous volume makes a significant contribution to specific surface area of the coal (Coal A has higher micropore volume).The implication of the above observation on CO_2-coal interactions is that coal A may have a higher CO_2 adsorption than coal B since adsorption occurs in the microporous region. Additionally, the surface molecules of coal A are expected to interact more frequently with CO_2 molecules and should experience a higher structural change than coal B, because of the high microporous region. Table 5-2 is a summary and comparison of the pore size distribution for coal A and coal B.

Table 5-2: Comparison of pore structure of coal A and coal B.

	Pore size distribution	
Samples	**Micropores**	**Mesopores**
Coal A	higher	lower
Coal B	lower	higher

5.4 Surface chemical properties

The surface and pore structure properties provide a great understanding of factors affecting adsorption capacity. To gain a greater appreciation for coal-CO_2 interactions, an analysis of the coal chemical properties is necessary. Of interest, in terms of chemical properties in this

study, was the fraction of amorphous and aromatic carbons in the different coal samples. This analysis would provide an understanding of the coals internal structure behaviour on CO_2 sorption. Surface functionality group would provide information as to the surface chemistry changes on CO_2 sorption.

5.4.1 Fraction of aliphatic and aromatic carbon

The fraction of amorphous material for this study can be indirectly estimated by the determination of the fraction of crystalline material, or "crystallinity", of the petrographic constituents. Table 5-3 shows the weight percentage of the fraction of carbons bonded to aromatic and aliphatic carbons on the vitrinite and inertinite-rich samples as determined by NMR (see § 3.3.2.1).

Table 5-3: Weight percentage of the fraction of carbons bonded to aromatic and aliphatic carbons of coal A and coal B

Coal	f_a	f_{al}	f_a^{CO}	f_a^{P}	f_a^{S}	f_a^{N}	f_a^{H}	f_a^{B}	f_{al}^{N*}	f_{al}^{H}	f_{al}^{O}
A	0.64	0.36	0.04	0.06	0.11	0.23	0.41	0.07	0.08	0.28	0.06
B	0.69	0.31	0.09	0.09	0.12	0.45	0.24	0.24	0.11	0.20	0.06

*f*a = total fraction of aromatic carbons, *f*al = total fraction of aliphatic carbons, fa^{CO} = fraction of carbons bonded to carbonyls, fa^{P} = fraction of carbons bonded to phenolic esters, fa^{S} = fraction of carbons bonded to alkylated carbons, fa^{N} = fraction of non-protonated carbons and CH_3 in aromatic region, fa^{H} = fraction of protonated carbons, fa^{B} = fraction of bridgehead carbons, fal^{N*} = fraction of non-protonated carbons and CH_3 in aliphatic region, fal^{H} = fraction of protonated carbons and CH_3 in aliphatic region, fal^{O} = aliphatic carbons bonded to oxygen

From Table 5-3, coal A has a lower total fraction of aromatic carbons *(f*a)(0.64) when compared to coal B (0.69), whilst coal A (0.36) has a higher total fraction of aliphatic carbons (fal) (0.31). To clearly gain an understanding of the implication of this finding on the coal structure, it is important to refer to the ultimate analysis results (see Table 5-1)

With a 68% carbon content (Table 5-1), the vitrinite-rich coal is expected to have about 30% amorphous material. This is due to the fact that the relationship between carbon content and amorphous material has been shown to have a linear relationship, with coals having an amorphous material of about 38% for a vitrain of 57% carbon content, to about 28% for a vitrain of 83% carbon content or less [205].

The amount of amorphous material is important in the current investigation, because it contributes to the pore structure, which affects sorption behaviour. Coals with carbon content less than 85% are expected to have an open pore structure [206]; they are highly amorphous and porous; the lamellae are connected by crosslinks, and are more or less randomly oriented in all directions. Figure 5-5 shows the weight percentage fraction of aromatic and aliphatic carbons of vitrinite and inertinite-rich samples (from NMR).

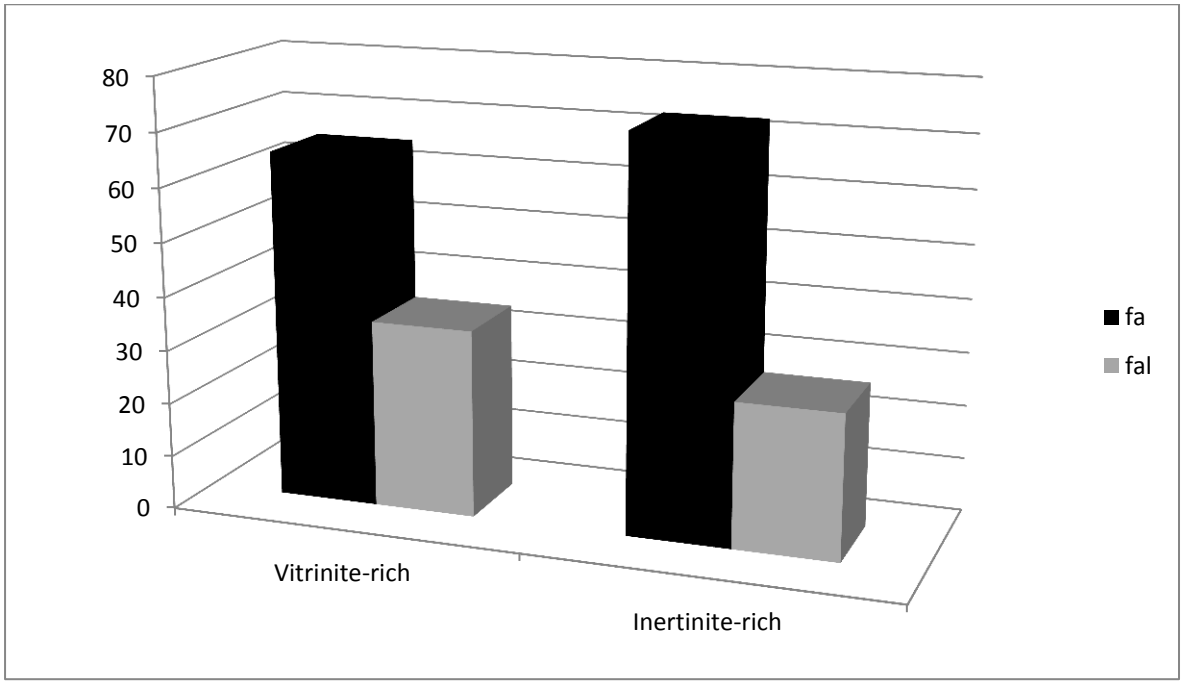

Figure 5-5: Weight percentage fraction of aromatic and aliphatic carbons for the vitrinite and inertinite-rich samples. f_a=fraction of aromatic carbons and f_{al}=fraction of aliphatic carbons

The fraction of aromatic carbons in the vitrinite-rich coal sample was found to be in agreement with those found in literature, where the f_a values have been found to be vitrinite < inertinite for any given coal [50]. These results also confirm those found by van Niekerk et al. [207], who observed that vitrinite-rich molecular models showing a less aromatic structure than the inertinite-rich models, and consist of longer aliphatic crosslinks and more aliphatic side chains. In the inertinite-rich model, it was found that the structures have more covalent crosslinks, and thus have larger molecules.

This observation would suggest that the vitrinite-rich coal would have a more microporous system than inertinite rich coal [61, 207]. This was observed in the BET surface area analysis of the two coals (see Figure 5-2). In Figure 5-2, the vitrinite-rich sample was found to have a lower microporous surface area than inertinite rich sample.

However, in contrast to this finding, Unsworth et al. [81] observed that inertinite is more macroporous and less microporous than its rank equivalent vitrinite. Results supporting Unsworth et al. [81] have also shown that microlithotypes with maceral compositions that are rich in inertite have higher porosities (both mesoporosity and microporosity) when compared to microlithotypes rich in vitrite [32].

The scheme in Figure 5-6 is a PXRD pattern for vitrinite-rich coal A and inertinite-rich coal B. Assuming that a higher XRD pattern background is directly proportional to the amount of amorphous carbon material, and a lower background is indicative of the presence of crystalline carbon, it can be concluded from the figure that inertinite has a higher degree of crystallinity compared to vitrinite. These results are in complete agreement with the NMR results, which showed that inertinite-rich sample had a higher fraction of aromatic carbon than vitrinite. A material with a high crystalline structure will generally have a more porous

structure and is less prone to structural changes than a material with a less crystalline structure [141, 208].

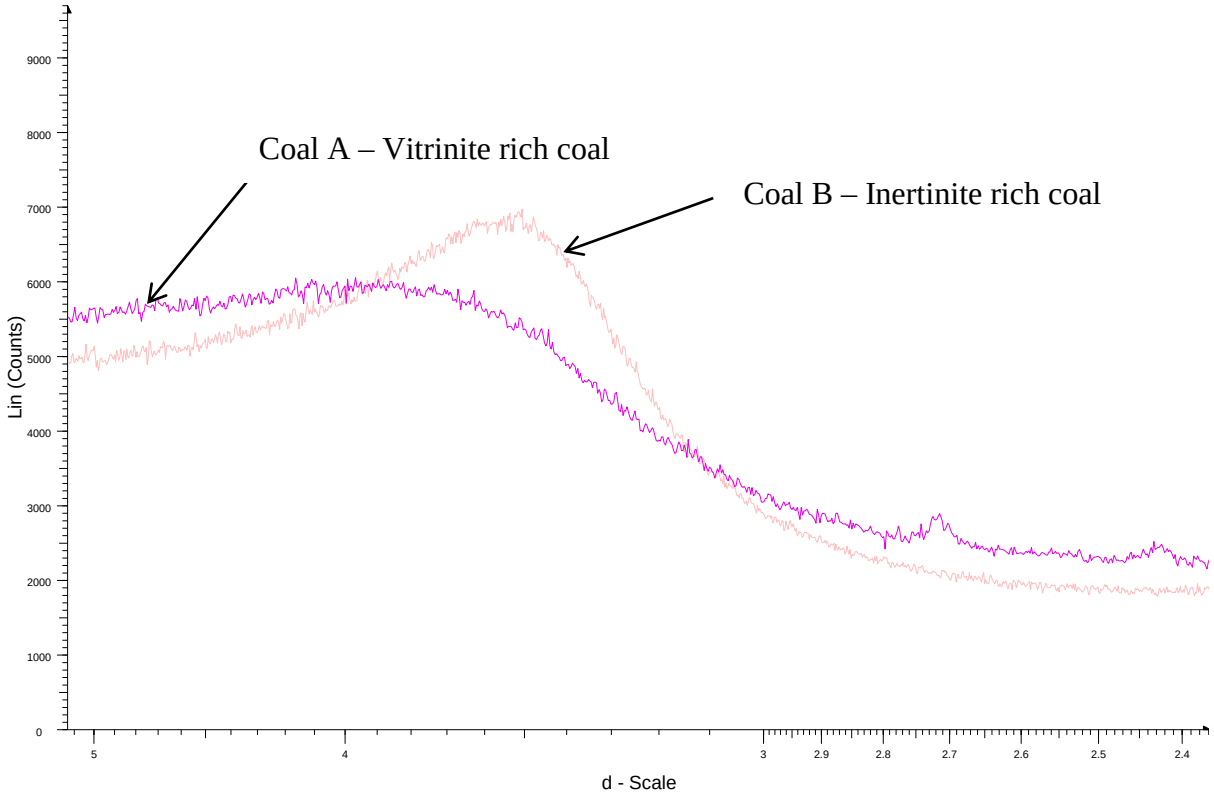

Figure 5-6: Powder XRD profile for vitrinite-rich coal A and inertinite-rich coal B coals (demineralised)

In summary, the physical and chemical characterisation is in agreement with literature. One would then expect that the vitrinite-rich sample will sorb less CO_2 than the inertinite-rich sample, as in literature. In terms of CO_2-coal interactions, the less aromatic and more aliphatic side chains there are, the easier the structural rearrangement should be. This means that it would be expected that the vitrinite-rich sample will swell more than inertinite-rich sample during CO_2 treatment, and will have a more pronounced glass transition temperature reduction (discussed in § 2.5.1).

5.4.2 Functional groups

Since CO_2 has polar bonds and a large quadrupole moment, specific chemical interactions between coal and CO_2 may make an important contribution to the adsorption process, which may well vary significantly with the composition of the coal [127].

Fourier Transform Infrared Spectroscopy provides information about functional groups in the coal samples studied, and can be used to study the chemical composition of coal. FTIR spectra for the CO_2 reacted and parent coals are presented (Figure 5-7). Similar peaks were identified for the two samples, with the exception of the peaks at 1900-2400cm^{-1} for the vitrinite-rich coal A sample.

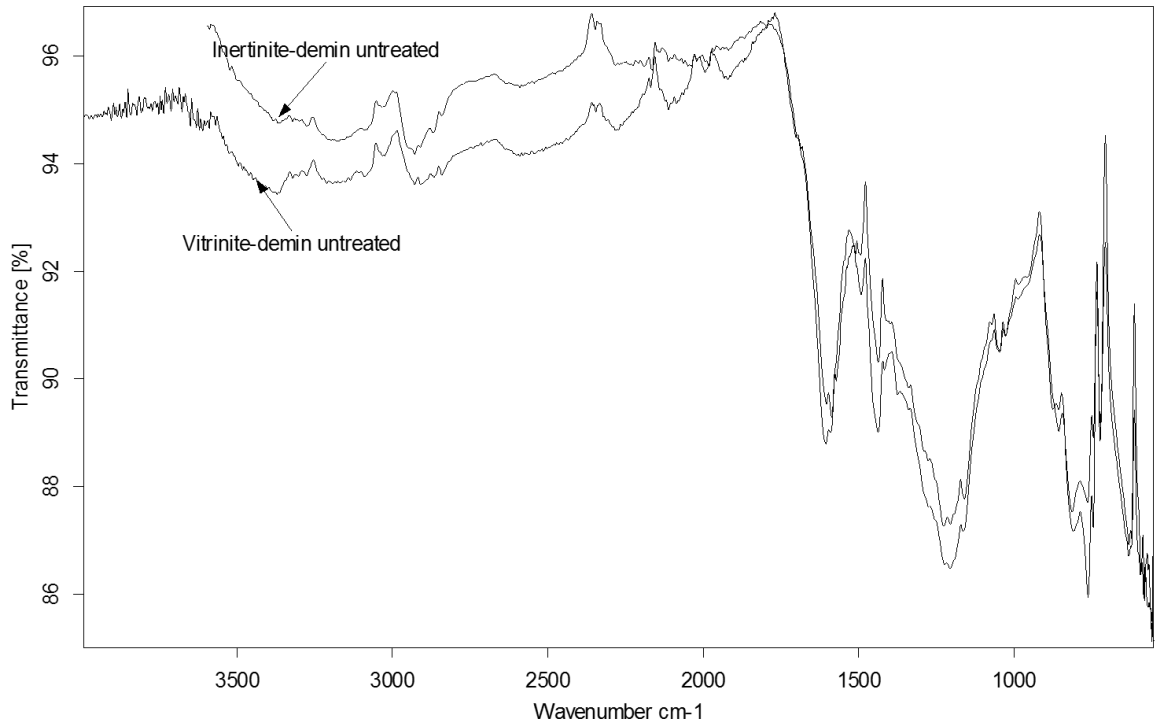

Figure 5-7: FTIR spectra for the inertinite and vitrinite (demineralized) coals

The broad absorption bands observed 3200-3600 cm^{-1} in both the coals are due to N–H and O–H groups [209]. The main features of FTIR are the strong aliphatic absorptions (2800–3000 cm^{-1}). The intensity of peaks at 2900-3000 cm^{-1} is greater than the peaks at 2800-2900

cm^{-1} for both the coal samples, and indicates the presence of aliphatic chains in both the coals. The broadness of the peaks is indicative of short aliphatic chains in both coals.

Low intensity aromatic bands were observed in 700-900 cm^{-1} regions for both coals. The peaks at 1700 cm^{-1} appears in both coals, and indicates the presence of carbonyl (C=O) contents. The oxygen containing functional groups found in coal specifically include phenols, alcohols, ethers, carboxylic acid, and carbonyls. The region of 1000–1300 cm^{-1} observed in the spectra is for C–O bonds in coal structures. The weak band at 690 cm^{-1} observed in the coal may be due to C–S bond.

5.5 Chapter summary

In summary, the petrographic analysis indicated a successful maceral separation as coal A was found to have a high vitrinite maceral content and coal B having a high inertinite maceral content. A proximate analysis showed that coal A has a slightly lower ash and carbon content than coal B.

The surface area analysis revealed that the surface area obtained is dependent on the adsorbate molecule used. For N_2 BET surface area analysis, inertinite rich coal B has a higher surface area than the vitrinite rich coal A sample. For CO_2 BET analysis, vitrinite-rich coal A has a higher surface area than inertinite coal B sample. This was interpreted as indicative of more microporous nature of the vitrinite rich coal A. A pore size distribution analysis confirmed this interpretation to be true.

In terms of surface chemical properties, coal A was found to be more aliphatic than the inertinite coal B sample, and as such more amorphous. It was hypothesised that the more aliphatic character of the vitrinite-rich coal A would be easily rearranged on long term CO_2

treatment. This means that it could be expected the vitrinite-rich sample to swell more than inertinite-rich sample, and to have an increase in its “plastic” behaviour.

CHAPTER 6
EFFECTS ON COAL PROPERTIES UNDER SUBCRITICAL CONDITIONS

6.1 Introduction

In this chapter results for coals that were treated with CO_2 under subcritical conditions (45 bar and at 28°C for up to 6 months) are presented and discussed. Results and a discussion on the effects on petrographic properties (reflectance) and surface properties morphology are presented (§ 6.3). In the second (§ 6.4) and third section (§ 6.5) effects on the physical (surface area and pore structure) and chemical properties (functional groups and crystalline structure) are presented and discussed, respectively. The last section is a discussion on the effects on the internal structure of the coal as studied by XRD (§ 6.6). In addition to determining the effects of CO_2 treatment on coal structure, this section aims to elucidate whether CO_2 interaction with coal is chemical or physical.

6.2 Experimental

The testing of CO_2 effects under subcritical conditions were conducted according to the experimental scheme presented in Chapter 4, which also gives information on the equipment used and details on the characterisation techniques used. The samples were placed in high pressure cells saturated with CO_2 for 6 months (see §4.2.3.2).

6.3 Effects on petrographic reflectance

It was not expected that the subcritical CO_2 treatment on coal would have significant effects on the petrographic properties. In Table 6-1, the vitrinite reflectance of treated and untreated

coals is shown (45 bar, 28^{o}C, 6 months). It is clear from the table that there was a minor change between the pre-CO_2 treated and post CO_2 treated coal A (vitrinite-rich) and coal B (inertinite-rich).

Table 6-1: Vitrinite reflectance for treated and untreated coal A and coal B

Samples		**Coal A untreated**	**Coal A treated**	**Coal B untreated**	**Coal B treated**
Vitrinite reflectance (RoV%)	R_{max}	0.70	0.73	0.70	0.80
	st. dev.	0.00	0.07	0.00	0.10
	R_{random}	0.67	0.69	0.60	0.70
	st. dev.	0.04	0.06	0.10	0.10
	V classes	v6 - v7	v5 - v9	v6 - v7	v6 - v9

This observation is consistent with that of other studies, where it was found that CO_2 effects on petrographic properties are very small [118]. However, the v-classes and the greater standard deviation in reflectance analysis for the treated samples may be of interest. This signifies that there might be some changes occurring, but the period under investigation might be too short to observe any significant changes. It is recommended that this aspect is reassessed during a longer term test. An increase in reflectance value may indicate a change in atomic rearrangement or alignment of strutures.

6.4 Effects on physical properties

The BET surface area (CO_2) analysis showed that Coal A (vitrinite-rich) and Coal B (inertinite rich) have surface areas typical of low rank bituminous coals. When comparing the surface area of Coal A to that of Coal B, it was found that coal A had about 10% greater surface area than coal B (Figure 6-1).

The left bar in Figure 6-1 is the non-treated surface area, and the right shows the result following 6 months treatment in CO_2 at 45 bar. The treated vitrinite-rich coal (A) shows a higher surface area than its non-treated counterpart. The inertinite sample shows no significant change after treatment.

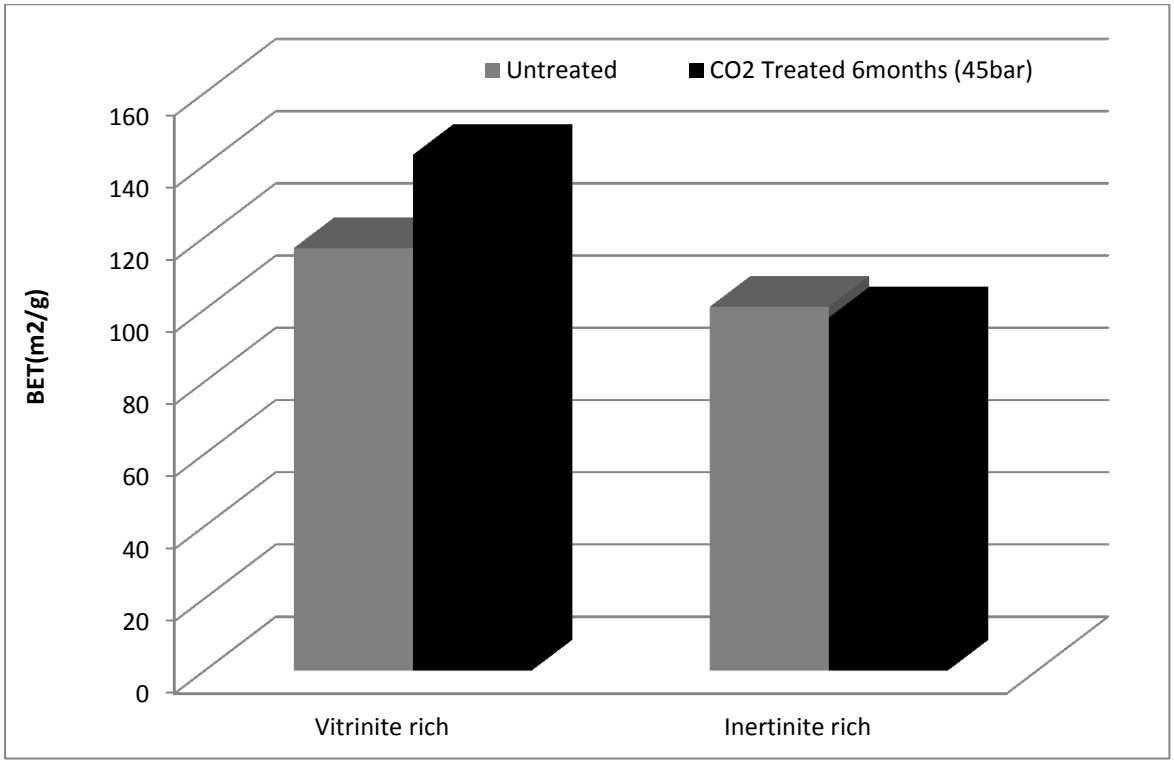

Figure 6-1: BET CO_2 surface area for non-treated and 6 months treated coals

These findings do not support a previous study's observations [210], which showed that the BET surface area and both mesopore and micropore volumes had lower values in post-CO_2 treatment samples when compared to pre-CO_2 treatment samples. A decrease in these parameters (surface area and micropore volume) was also documented after CO_2 adsorption into vitrains of coals from the Illinois Basin [211], and was interpreted to be a reflection of CO_2-induced swelling of the vitrinite matrix and subsequent post-adsorption shrinkage. A possible explanation for these observed differences might be that CO_2 treatment in the current study was over a longer period of time, or post-sorption shrinkage did not occur.

The findings in the current study contradict other studies comparing vitrinite and inertinite-rich samples where an opposite effect on the CO_2 treated coals was observed [212]. The study [212] found different responses for inertinite- and vitrinite-rich coals respectively, and postulated that if the different responses of vitrain and fusain to CO_2 are characteristic of high-vitrinite and high-inertinite coals in general, then it would suggest that high-inertinite coal would record an increase in mesopore and micropore volumes after CO_2 treatment, and high vitrinite coal would register a decrease

A possible explanation for the change in surface area observed in the current research is: (i) a change in the pore structure of the coal structure due to the long term CO_2 sorption; and/or (ii) CO_2 imbibition into the coal structure. To further investigate the cause of the surface area change, the pore size distribution for the coals was analysed. The CO_2 sorption/desorption data was used to calculate pore size distribution (PSD) using the Horvath – Kawazoe method [213]. Figure 6-2(a) shows the microporous region of Coal A (vitrinite-rich), and Figure 6-2(b) the microporous region for Coal B (inertinite-rich).

An observation that one can make is that the two samples seem to have fairly similar microporous PSDs. For both Coal A and Coal B, the 6 months treated coals show a greater PSD distribution than the untreated coals. This would suggest that some structural deformation might have occurred due to the long term CO_2 treatment period.

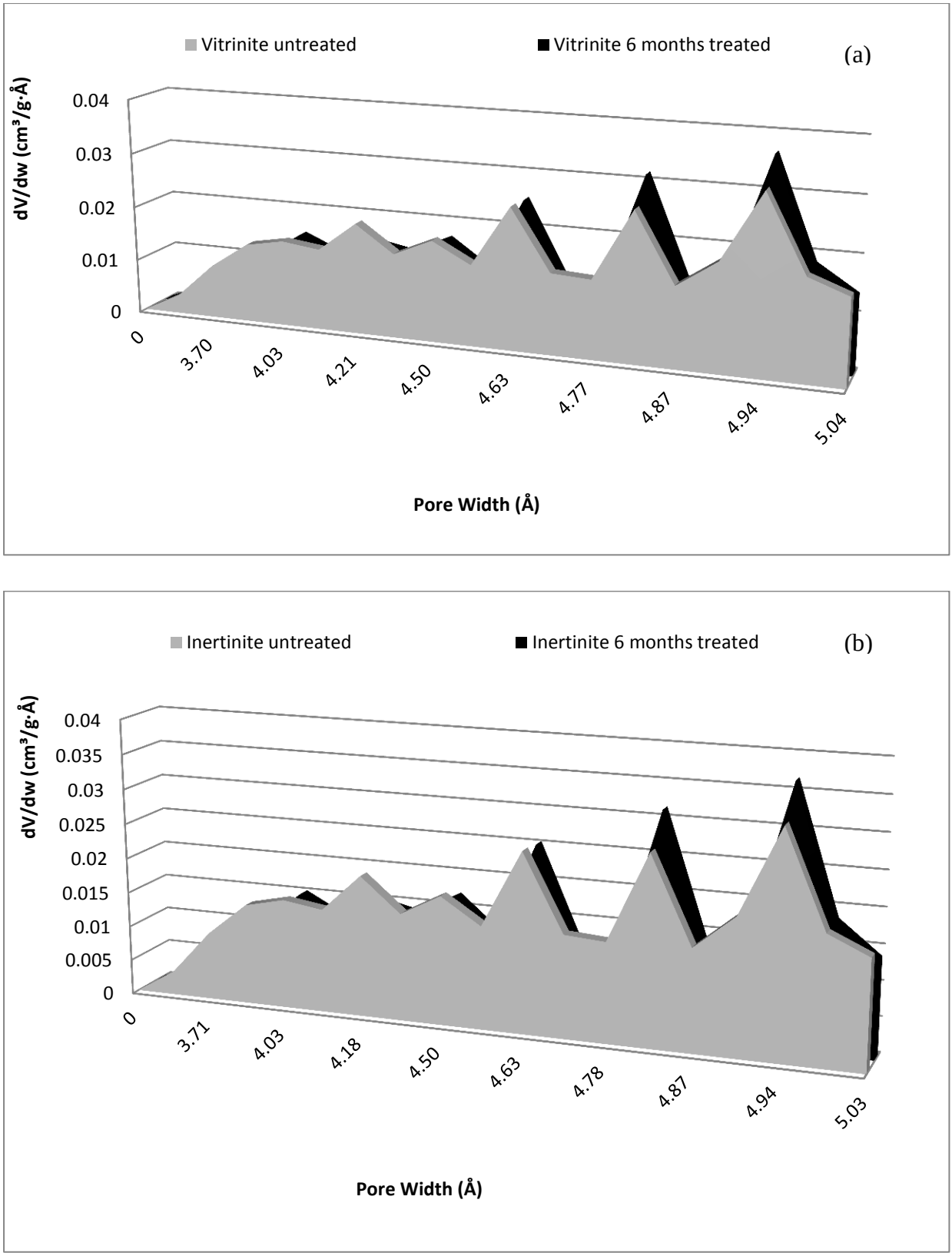

Figure 6-2: Pore Size Distribution (PSD) in full analysis for the two different coal samples. (a) Coal A (Vitrinite-rich) and (b) Coal B (Inertinite-rich)

It is also possible to deduce structural deformation from PSD's, following Kowalczyk et al. [214]. In the study, Kowalczyk et al. [214] found that adsorption induced deformation of carbon materials is dependent on the pore size distribution. Small pores of width <0.38nm (i.e., slightly wider than adsorbate molecular diameter of 0.34 nm) swell the carbon material, whilst the larger pores (>0.38 nm) contract the material.

Caution must be exercised when utilising the sorption/desorption data to deduce a PSD for microporous carbonaceous materials such as coals, as there is still some theoretical uncertainties associated with these methods. There is, however, still value in comparing PSDs for structural characterisation purposes as was done in the above paragraph [215]. It can be deduced from the above observations that there are physical changes in the pore structure and the surface area of the coal following by CO_2 sorption over 6 months.

6.5 Effect on chemical properties

Since CO_2 has polar bonds and a large quadruple moment, specific chemical interactions between coal and CO_2 may make an important contribution to the adsorption process, one which may well significantly alter the surface functional composition of the coal and its subsequent behaviour [127].

To test this, FTIR analysis of treated and untreated samples was performed to qualitatively observe if the CO_2 treated at conditions in this study resulted in any significant surface functionality changes. Figure 6-3 shows the FTIR spectra of the treated and untreated Coal A (vitrinite-rich) samples.

The most observable features of the FTIR plot in are the broad absorption bands observed between 3200 and 3500 cm^{-1} in the coals due to the N–H and O–H bond absorption. Also prominent are the strong aliphatic absorptions at 2920–2850 cm^{-1}. The higher intensity of

peaks at 2920 cm^{-1} compared to the peaks at 2850 cm^{-1} for all the coal samples is indicative of the presence of long aliphatic chains [209].

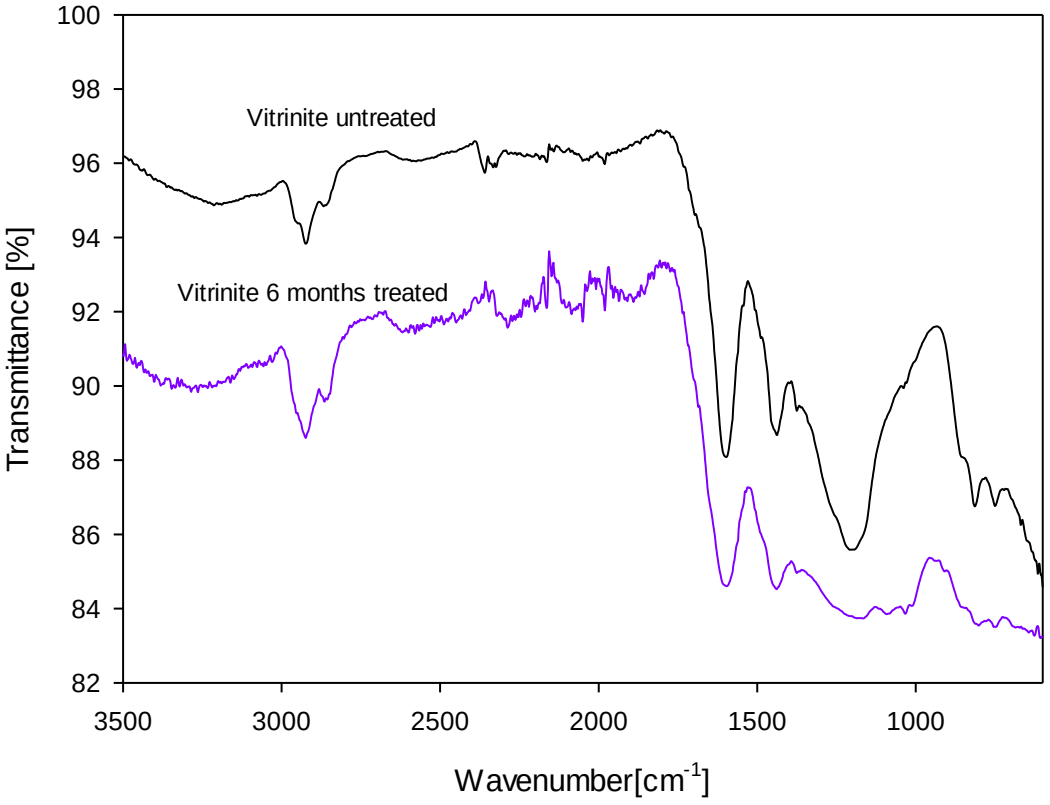

Figure 6-3: An FTIR spectra of treated and untreated Coal A (vitrinite-rich) sample

The peaks at 1670-1700 cm^{-1} are generally observed in coals and are indicative of the carbonyl (C=O) group, whilst the weak aromatic C=C ring stretching vibration and CH out of plane deformation at 1610 and 900–700 cm^{-1} [216]. The region of 1000–1300 cm^{-1} observed in the spectra is for C–O bonds in coal structures. Most of the peaks between 1100 and 400 cm^{-1} can be assigned to clay minerals [209].

Of particular interest for the current study were the hydroxyl group (3200-3600cm^{-1}) and the adsorbed CO_2 peak at 2330cm^{-1}. As stated in Saikai et al. [209], the amount of CO_2 adsorbed per square meter of the surface area and the heat of CO_2 adsorption increases with an increase

in the fraction of the surface covered by hydroxyl groups. Consequently, a high hydroxyl group on the surface would induce a higher CO_2 adsorption. Of greater interest to this study is whether this interaction would cause any functionality changes on the surface of the coal.

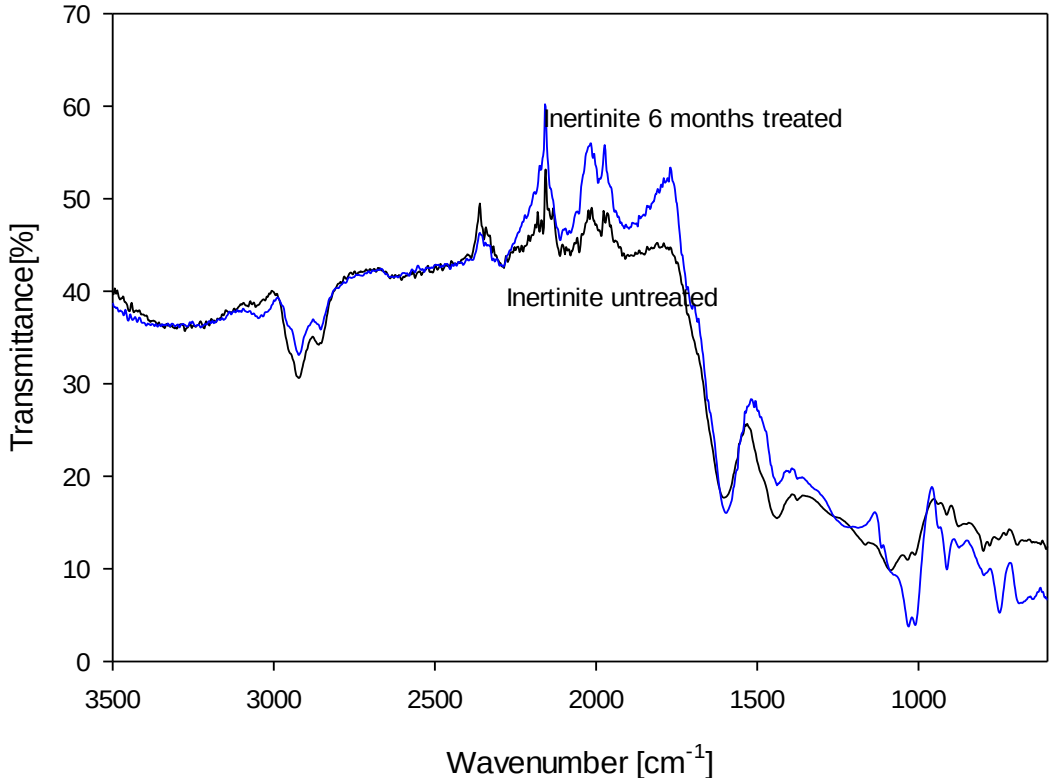

Figure 6-4: An FTIR spectra of treated and untreated Coal B (inertinite rich) sample

As shown in Figure 6-4, the hydroxyl group peak shows no changes between the treated and untreated inertinite-rich samples. In addition, the only difference between the two peaks is the change in the peaks between 2000cm^{-1} and 2500cm^{-1}. Although the region is a fingerprint for other functional groups, the notable difference is with the adsorbed CO_2 peak region at 2330cm^{-1} [20].

Goodman et al. [20] showed that absorbance intensity of the CO_2 peak was time-dependent, and increased with the length of CO_2 exposure. The Goodman et al. [20] study showed that if CO_2 is initially sorbed into the coal structure and released, as in our study, the coal structure

structural rearrangement occurs after the initial uptake. The rearrangement is not reversed as the CO_2 is removed from the coal. A similar peak increase was observed in this study, which is an indication of structural rearrangement, although not quantified here

6.6 Effects on the internal structure

As indicated earlier, coal has a very complex internal structure (§2.2.2), and this complexity makes it challenging to study the internal structural changes due to CO_2 sorption without making certain assumptions. Without delving too much into the coal structure and its complexities, it should suffice to state that, here, the internal structure refers to the crystalline structure of the coal.

Analysis of the internal structure was performed on demineralised untreated, 14 days, and 6 months treated coals. The 14 day analysis was included in this section as it enabled statistically valid correlations to be drawn from the d_{002} and L_c data in Figure 6-6 (discussed later). A pre-sorption solid state ^{13}C NMR analysis of the coals showed that Coal B (inertinite rich) had a higher fraction of aromatic carbons than Coal A (vitrinite rich) sample, as expected.

In order to study the internal structural changes, demineralised and untreated coals were saturated with CO_2, together with non-demineralised coals, as discussed in the experimental section (§2.3). Powder XRD patterns for Coal B untreated, treated for 14 days at 45 bar, and 6 months at 42 bar, are shown in Figure 6-5.

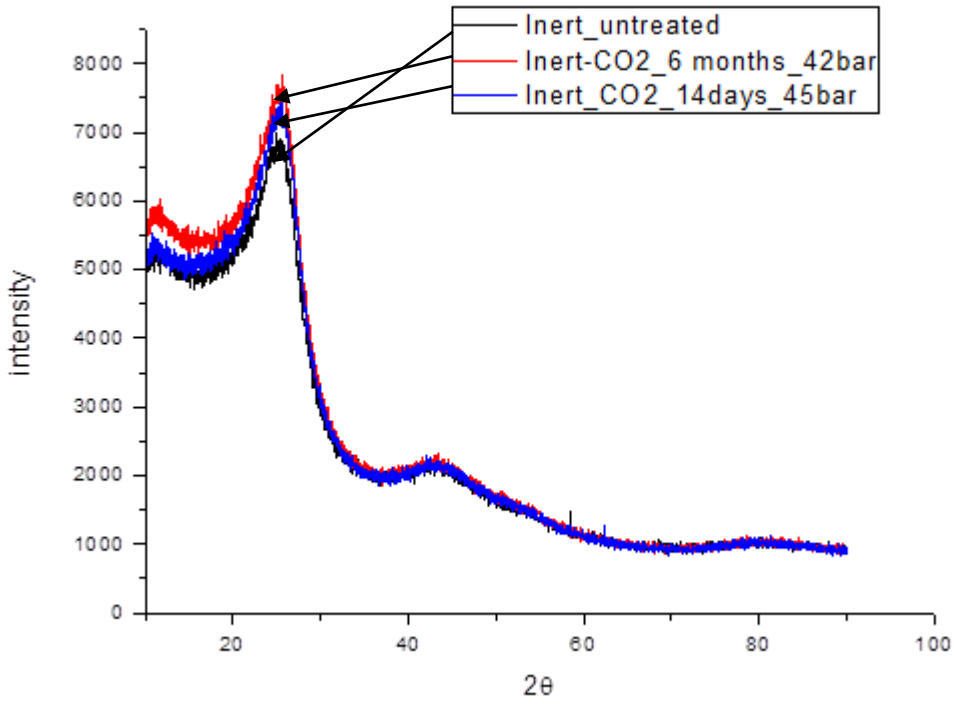

Figure 6-5: Powder XRD patterns for the untreated, 14 days treated, and 6 months treated inertinite-rich coal B

The most prominent band in an XRD diffractogram pattern of coal is the (002) band at about 2θ 23°, because it arises from the parallel stacking of planar (d_{002}) aromatic ring clusters. It is also well established that the (002) peak position changes with carbon content [205-206, 217-218].

In this study, it was postulated that, if CO_2 sorption at high pressures affected the internal structure of the coal, then the peak position and intensity of the d_{002} band can be used to observe, and, if possible, measure, the degree of change in the parallel stacking of planar aromatic clusters. Only Coal B is shown, because Coal A had a lower fraction of aromatic carbon and it was difficult to observe the d_{002} band.

From the XRD data the interlayer spacing between the aromatic rings can be determined. This is done by calculating the interlayer distance between aromatic sheets (d_{002}) from a maximum of the (002) band using the Bragg equation [168] .

$$d_{002} = \frac{\lambda}{\sin \theta_{002}} \quad (6\text{-}1)$$

The average crystallite stacking height (L_c) can be computed:

$$L_c = \frac{0.9\lambda}{\beta_{002} \mathrm{Cos}\, \theta_{002}} \quad (6\text{-}2)$$

Where β_{002} is the integral breadth or breadth at half maximum intensity of the pure reflection profile in radians, θ_{002} is the angle 002 angle, and λ is the copper wavelength, 1.54nm.

Results for the calculation of these structural parameters are shown in Figure 6-6. Evident from Figure 6-6 is the fact that the inter-planar d_{002} spacing between the samples is unchanged for the untreated, 14 days treated, and the 6 months CO_2 treated coals. This was because the d_{002} peak position did not change with CO_2 saturation. However, the average stacking height of the aromatic fringes in the coal seem to be increasing from untreated, 14 days treatment, to 6 months treatment.

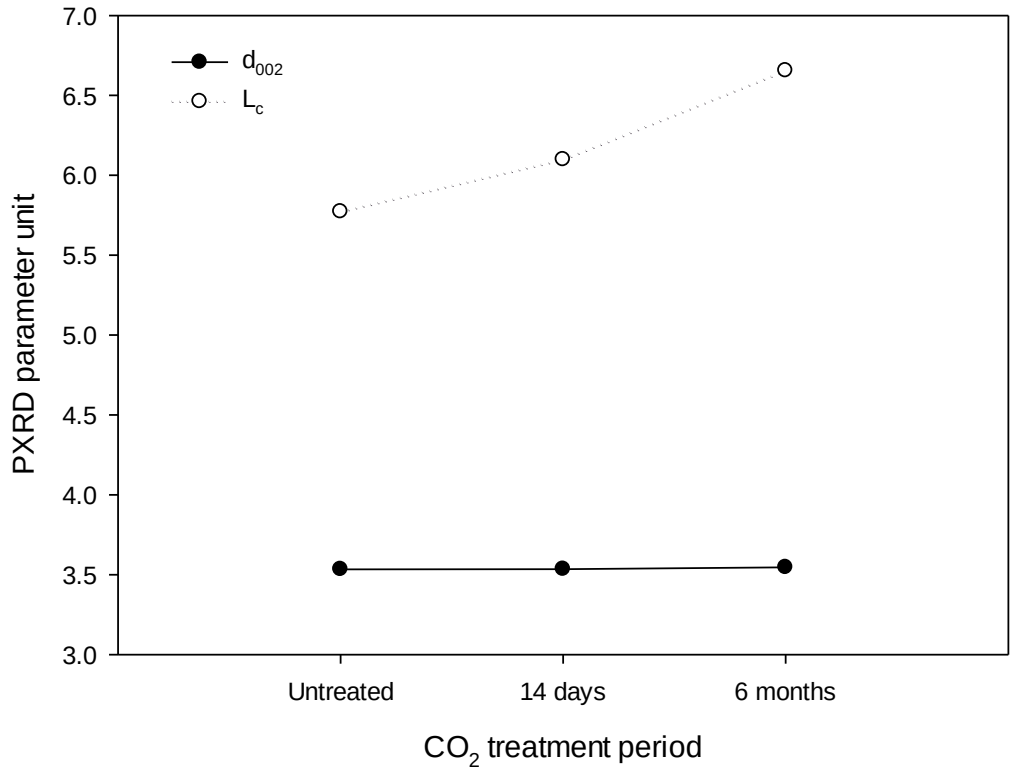

Figure 6-6: Structural parameters from powder XRD analysis for treated and untreated coal B.

From a structural point of view, an increase in the stacking height corresponds to an increase or opening of slit-shaped micropores, considering the fact that micropores of this type are basically formed by a misconfiguration among layers or stacks [219] . This observation would help explain the sorption properties observed in the PSD changes and the next section.

6.7 Summary and conclusion

This part of the study was undertaken to determine, at a fundamental level, the chemical and physical changes caused by CO_2 sorption in coal after 6 months of subcritical treatment, as summarised in Table 6-2.

Table 6-2: Summary of the effects on coal structural properties post subcritical CO_2 treatment

Property	Effects caused by CO_2 treatment	
	Coal A-Vitrinite rich	Coal B-Inertinite rich
Petrographic Reflectance	Slight changed	Slight change
Surface area	Increased	Unchanged
Pore structure	Increased	Unchanged
Functional groups	Minor increase on the adsorbed CO_2 peak	Increase in peak intensity at 1000cm^{-1}
d_{002} spacing	Undeterminable	Unchanged
L_c	Undeterminable	Increased

Petrographic reflectance analysis indicates a slight change in reflectance as observed by the extended v-classes and slight increase in mean random reflectance values; whether this change is significant is uncertain at this stage. BET analysis of treated and untreated coals showed that the vitrinite-rich coal samples have a greater surface area and change in pore structure, following subcritical CO_2 treatment, than the inertinite-rich coal samples used in this study. Functional group analysis indicated that there was no functionality change for the treated and untreated coals. Analysis of the crystalline part of the CO_2 treated and untreated inertinite-rich samples showed that there was slight increase in the average crystallite height, although no changes were observed for the d_{002} aromatic interplanar spacing.

It has been argued that surface areas measured by CO_2 adsorption may be in error because its adsorption may be influenced by the quadruple moment of the adsorbate molecule. The adsorption of CO_2 on carbons reported that the amount of CO_2, adsorbed per square meter of the surface area and the heat of adsorption of CO_2 increased with increase in the fraction of the surface covered by hydroxyl groups.

CHAPTER 7
EFFECTS ON COAL PROPERTIES UNDER SUPERCRITICAL CONDITIONS

7.1 Introduction

Following the results on the effects CO_2 under subcritical conditions in previous chapter and other studies [220], it was decided to focus on the vitrinite-rich sample for the study under supercritical conditions. This is because vitrain was found to be more affected by saturation with CO_2 at pressures up to 45 bar with regard to mesopore and micropore characteristics, specifically showing an increase in surface area and mesopore and micropore volume. This section presents and discusses results from analysis of vitrinite rich coal treated under CO_2 for 6 months at 125bar and 35°C.

7.2 Experimental

The testing of CO_2 effects under supercritical conditions were conducted according to the experimental scheme presented in Chapter 4, which also gives information on the equipment used and details on the characterisation techniques used.

7.3 Effects on Petrographic Properties

The vitrinite-rich samples were shown to include pseudovitrinite, a form of vitrinite with inherent desiccation cracks. Shown in Figure 7-1 are pictures, taken using a petrographic microscope, of the 6 months treated vitrinite rich-coal A samples under (a) subcritical and (b) supercritical conditions. On visual observation of the pictures in Figure 7-1, it is apparent that

the dimensions of the slits have not drastically changed from between the coal treated under subcritical conditions and the coal treated under supercritical conditions.

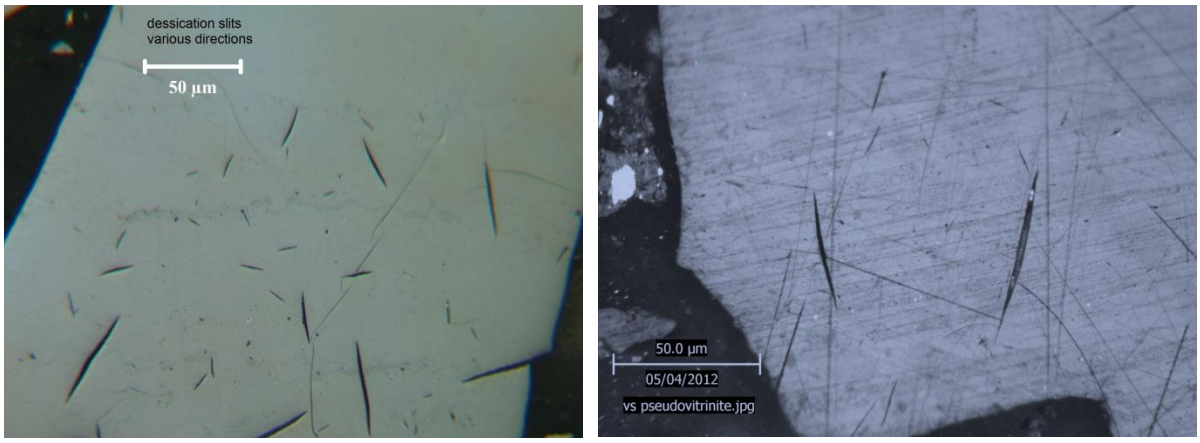

Figure 7-1: Pseudovitrinite particles showing desiccation slits in the 6 months treated coal A under subcritical (left) and supercritical (right) conditions (polarised reflected light, oil immersion, x500)

It was not expected that the treatment of coal with CO_2 treatment would affect the petrographic maceral content of the coal. However, it was found that supercritical treated coal had a higher pseudovitrinite content (17.8 wt%) than the untreated coal (7.8 wt%). This could, however, be due to coal heterogeneity, or the fact that enhanced CO_2 resulted in expansion of the inherent desiccation cracks. All other parameters were found to have remained constant. Overall, it can be concluded that there was no indication that CO_2 treatment under supercritical conditions affected the petrographic properties of the coal (see Appendix E.1)

7.4 Effects on Physical Properties

In Figure 7-2, the physical properties for untreated, 6 months treated under subcritical, and supercritical condition are shown. The surface area of the coals as determined by the BET method and the Langmuir model, and the micropore volume as determined by the D-A equation, are shown respectively. The data was obtained by fitting the models to low pressure adsorption isotherms with CO_2 used as the adsorbate. The different values obtained by the

different models are due to the assumption used underlying the different models (discussed in 2.4.1.3).

The trend across all models is comparable for the untreated and treated coals. There is an initial increase for the subcritical treated coal when compared to the untreated coal, followed by a sharp decrease for the supercritical sample.

This result shows that the relationship between the pressure of treatment and the physical properties is not linear, as initially thought. It seems to suggest that CO_2 treatment under supercritical conditions reduces the micropore capacity of the coal. It does, however, confirm other field studies, was CO_2 injectivity was seen to decrease over a period of time.

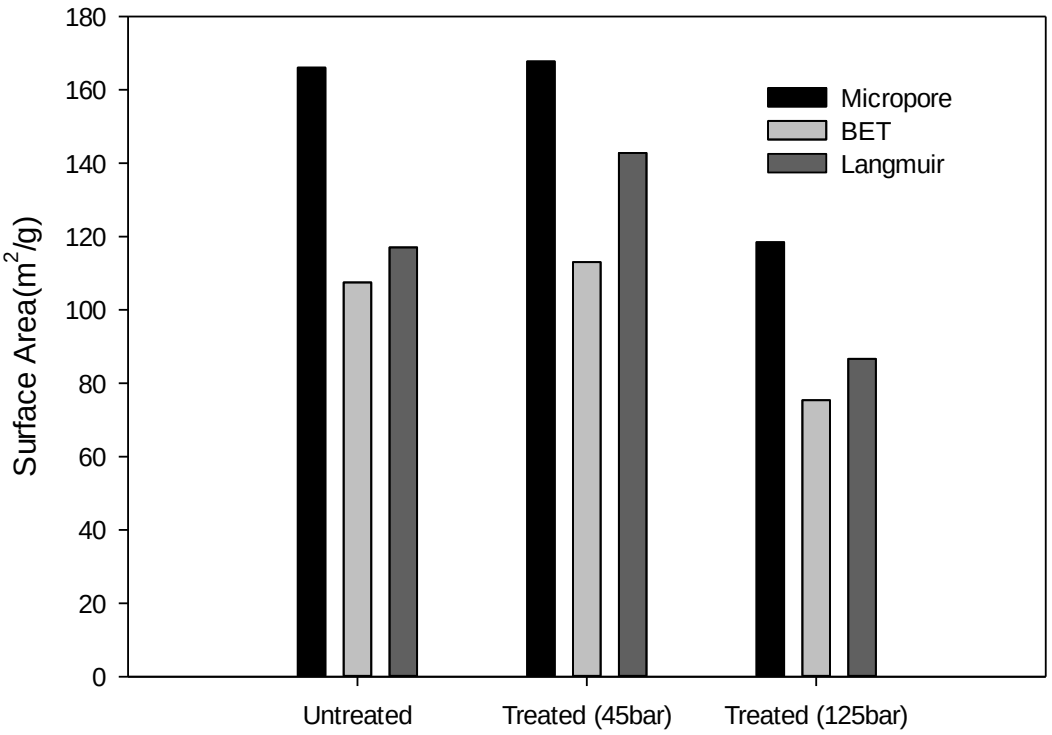

Figure 7-2: Physical properties for coal A: untreated, treated for 6 months under subcritical and supercritical conditions

From Figure 7-2, it is clear that this decrease could be explained by lower micropore and surface area. Also, considering that vitrinite has previously been found to swell more under

CO_2 treatment it [20, 32, 141] would explain the decrease in micropore surface area. This result would also suggest that the supercritical treated sample will have a lower adsorption capacity [221].

Because surface area is inherently linked to the pore size distribution of a sample, low pressure CO_2 sorption/desorption data was used to calculate pore size distribution using the Horvath – Kawazoe method [222]. Shown in Figure 7-3 is the differential PSD in the microporous region for the untreated, subcritical treated, and supercritical treated coal A sample (calculated by using the Horvath-Kawazoe method).

What is apparent from Figure 7-3 is that the pore size distribution for the supercritical treated coal sample is lower than both the untreated and subcritical treated coal samples. Also, more interesting, is how considerably lower the supercritical treated is for pore width (lower than 4.6 Å). The pore size distribution in this region (lower than 4.6 Å) was found to be significantly lower for supercritical treated than the other two samples.

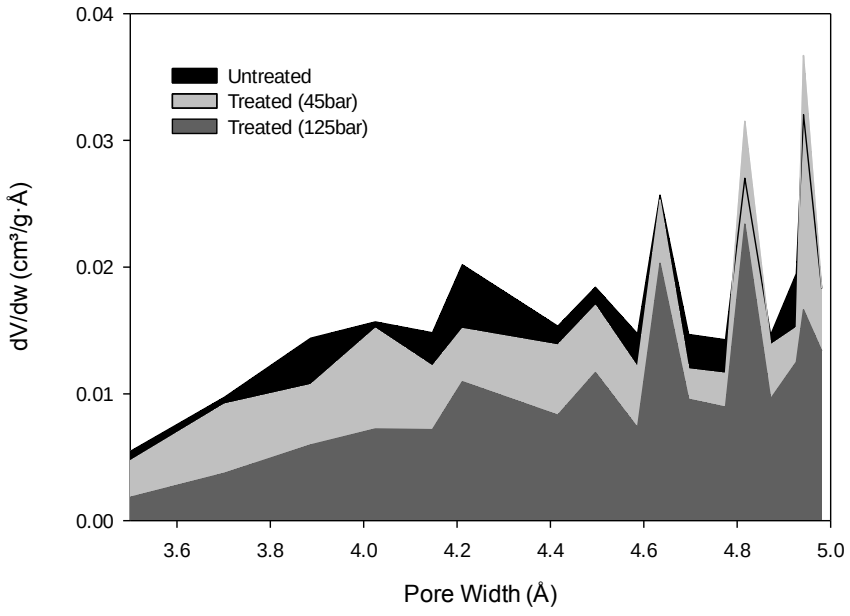

Figure 7-3: PSD analysis for the untreated, subcritical treated, and supercritical treated coal A sample.

This observation would suggest that the supercritical treated coal sample has lost its micropore structural integrity. As was the case with the subcritical treated coal discussion, this finding suggests that some structural deformation might have occurred due to the long term CO_2 saturation period. The deformation is greater under supercritical treatment over the same period of time (6 months for this study) than for the subcritical treated sample.

7.5 Effects on Chemical properties

Figure 7-4 is the FTIR spectra for the untreated, subcritical, and supercritical treated coal for the vitrinite-rich coal A. As was the case in the discussion in the previous chapter, special attention was paid towards the hydroxyl group (3200-3600cm^{-1}) and the adsorbed CO_2 peak at 2330cm^{-1}.

What is apparent from the spectra in Figure 7-4 is the more pronounced adsorbed CO_2 peak at 2330cm^{-1} for the supercritical coal. The circled peak in Figure 7-4 represents the absorbed CO_2 peak at about 2330cm^{-1}. Evident from the figure is that this peak has largely increased in intensity suggesting that the CO_2 "adsorbed" in the coal structure under supercritical conditions is incorporated into the coal structure, possibly "absorbed" into the matrix structure of the coal.

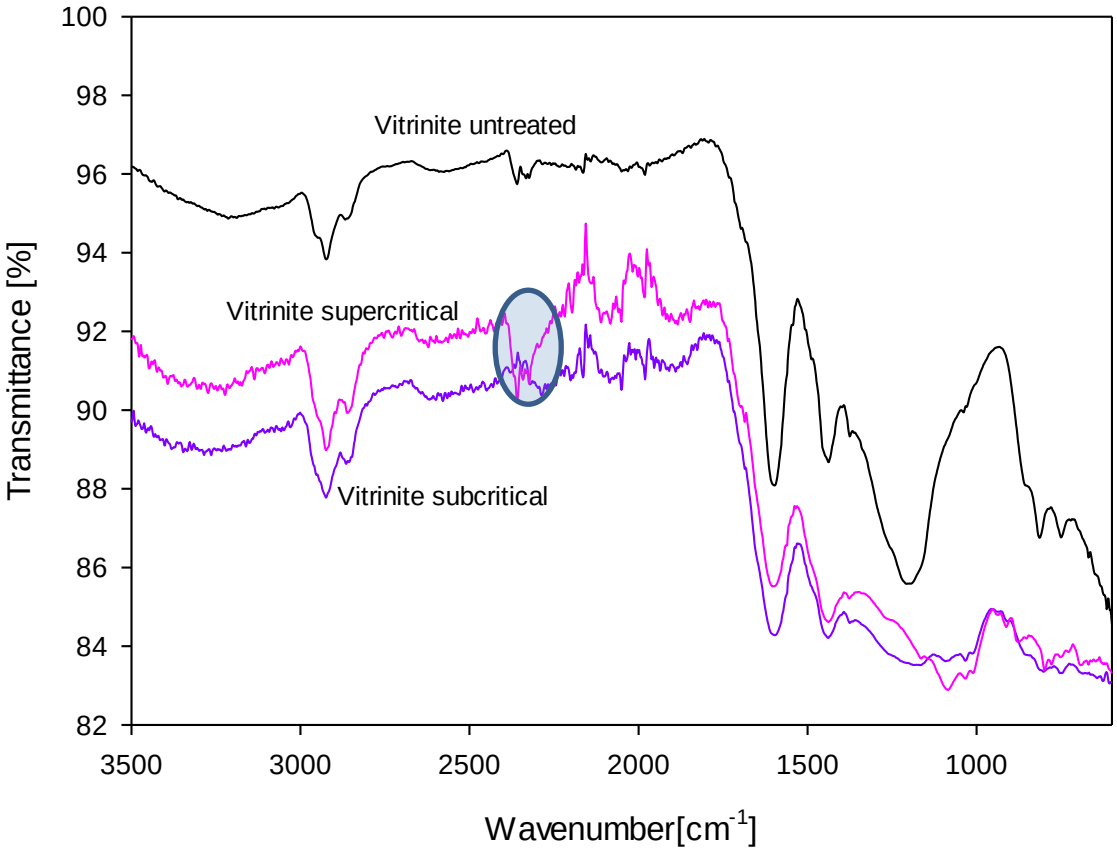

Figure 7-4: FTIR spectra of treated (subcritical and supercritical) and untreated Coal A (vitrinite-rich) sample

Also, there is a more pronounced peak at the 1050-1100 cm^{-1}. The absorption peak represents the C-O bond absorption and seems to have a higher intensity for the supercritical treated sample than for subcritical treated sample. Also evident from Figure 7-4 is the fact that the hydroxyl group peak shows no changes between the treated and untreated vitrinite-rich samples. The higher intensity of the characteristic aliphatic absorption peak at 2920–2850 cm^{-1} could indicate that the supercritical treated coal has a more "aliphatic" nature than the untreated and subcritical treated coals. The more aliphatic nature of the supercritical could be due to the realignment of the internal structure of the coal as corroborated by the change in PSD and micropore surface area change.

7.6 Effects on internal structure

An analysis on the d_{002} analysis similar to the one performed for inertinite coal could not be performed for the vitrinite-rich sample to due to the highly diffuse nature of the d_{002} peak in vitrinite. The plot in Figure 7-5 is the powder X-ray diffraction pattern for the untreated and 6 months subcritical and supercritical treated vitrinite rich coal A sample.

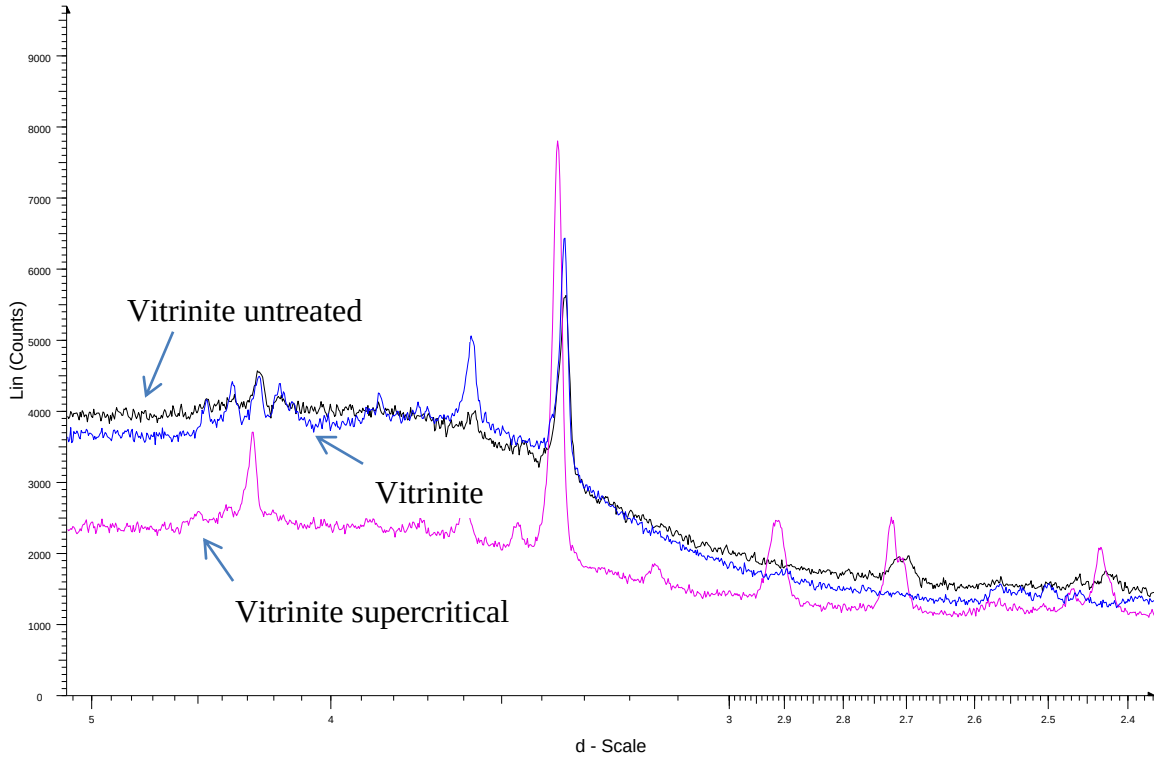

Figure 7-5: Powder XRD patterns for the untreated and 6 months treated coals under subcritical and supercritical conditions

It is not possible to draw the same conclusions about the effects on the internal structure based on the intensity of the PXRD peak without a deconvolution of the d_{002} peak. That is because the intensity is a factor of many variables, including the time and force for grinding the sample during sample preparation. However, some obvious observations can be made from Figure 7-5, the most apparent being the significantly higher intensities of mineral peaks for the supercritical treated sample. This is not to suggest that the supercritical treated coal sample has more mineral matter than the untreated and the subcritical treated sample.

The above shows the point mentioned earlier that deductions cannot be drawn from peak intensity as they are affected by multiple factors, one of those factors being the source tube for the X-ray wavelength. The untreated sample was measured using copper (Cu) as the tube for the X-rays and a cobalt (Co) tube was used for the supercritical sample. Hence, a d-scale was used instead of the 2θ as the former independent of the wavelength used. No final conclusions can be regarding the effect caused by CO_2 treatment on the internal structure of the supercritical treated coal.

7.7 Summary and Conclusion

This chapter presented results and a discussion on the effects of supercritical CO_2 on a vitrinite-rich coal compared to an untreated and subcritical treated coal sample. Table 7-1 summarises some of the results observed in this chapter.

With regards to the effects on petrographic properties, as suggested by the comparison of subcritical treated samples with those after supercritical treatment, the main conclusion was that these effects are very small. As for the the effects on the physical properties, it was found that the BET, Langmuir, and micropore (D-A) surface decreases sharply for the supercritical treated sample when compared to the untreated and subcritical treated coal.

Table 7-1: Summary on the effects of supercritical CO_2 treatment on vitrinite-rich coal A compared to the subcritical

Property	Effects caused by supercritical CO_2 treatment
Surface area	Decreased
Pore structure	Micropore volume decrease
Functional groups	Adsorbed CO_2 peak more intense
D_{002} spacing	Not determinable
L_c	Not determinable

It was also shown that the pore size distribution was considerably lower for the supercritical sample than for the other two coal samples. This was interpreted as loss of the micropore structure integrity of the coal due to the long term CO_2-coal interaction.

On the effects on the chemical properties as determined by FTIR, it was found that the treated coal showed distinctly more intense peaks for the adsorbed CO_2 peak. This was interpreted as indicative of the stronger incorporation of the CO_2 molecules into the coal matrix. However, it was noted that further work is required to confirm this. As for the effects on the internal structure, it was not determinable due to the diffuse nature of the d(002) peak.

CHAPTER 8
EFFECTS ON CO_2 SORPTION BEHAVIOUR

8.1 Introduction

High pressure sorption behaviour of the two coals was determined using the high pressure adsorption system on the untreated coals and on the CO_2 treated coals. The main reason for this exercise was to compare their respective sorption behaviours (i.e storage capacities, adsorption/desorption hysteresis). In determining the sorption behaviours, it was envisaged that it would then be possible to deduce the mechanisms of storage that were in operation in the coal-CO_2 system under study. In addition to be able to predict or deduce the expected behaviour of the coals on CO_2 sorption (see § 2.6.1). Carbon dioxide sorption behaviour was determined for both subcritical and supercritical conditions.

8.2 Experimental

A high pressure volumetric adsorption system was commissioned during this research for the determination of CO_2 treatment on the CO_2 sorption behaviour. The details of the instrument and the methodology are discussed in Section (§4.2), with further detail in APPENDIX D Only the results and discussion are presented in this section.

Although all necessary precaution was taken to minimise the exposure of the treated coals once removed from the long term storage reactor, they were exposed to atmospheric O_2 and pressures during transfer; as all samples were treated in the same manner, it is hoped that any effects of exposure to the atmosphere prior to CO_2 sorption studies were insignificant to the results. However, with samples having been exposed to the atmosphere, isothermal analyses

may therefore not be the same as isotherms generated on coal at depth in an O_2 deficient environment with pressure [223].

8.3 Subcritical CO_2 sorption behaviour

8.3.1 Untreated coals

As a base to the subcritical CO_2 sorption behaviour study, adsorption isotherms of untreated samples were determined for vitrinite-rich coal A and inertinite-rich coal B samples. Figure 8-1 shows the adsorption isotherms for the untreated inertinite and vitrinite coals plotted against pressure. As expected from literature [112, 215-216], untreated vitrinite-rich coal has higher CO_2 storage capacity (~2.0 mmol/g) than the inertinite-rich sample (~0.95 mmol/g). The CO_2 sorption results are also consistent with other adsorption studies that were performed on coals from the same coal field using the similar equipment [225]. In general, adsorption capacities in this range are within the general observed capacities for coals [112, 215-216].

This observation is consistent with earlier findings where inertinite-rich coal B was found to be more mesoporous and macroporous than vitrinite-rich coal A (§5.3.1). Coal B has a high non-reactive inertinite content (70.7% by volume, as shown in Table E-1) and previous studies have also indicated that non-reactive inertinite tend to have a lower adsorption capacity than reactive vitrinite (collotelinite, 13.7wt% by volume) [221].

This is because mesoporous to macroporous materials have less surface area than microporous material. This inversely proportional relationship between inertinite content and CO_2 sorption capacity is due to the positive correlation between inertinite and macroporosity. An inertinite-rich coal tends to have lower microporosity and high meso- and macroporosity, which reduces the surface area for sorption [221].

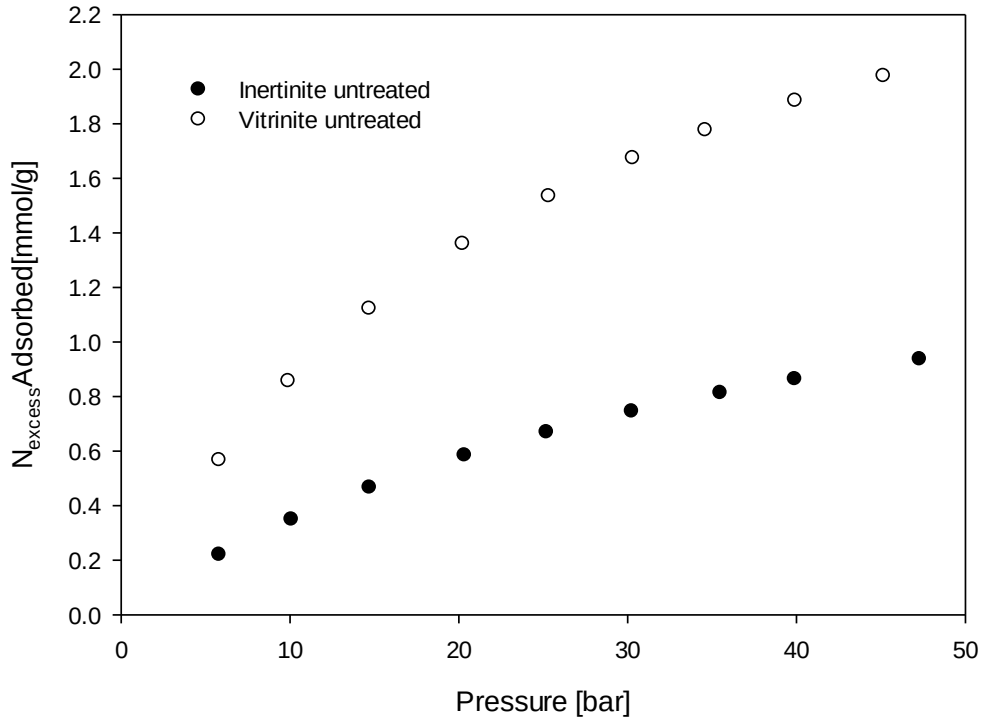

Figure 8-1: Untreated inertinite (coal B) and vitrinite-rich (coal A) adsorption isotherms

Reactive inertinite (such as reactive semi-fusinite) is chemically and structurally similar to vitrinite [50] and is more microporous than non-reactive inertinite. Therefore sometimes inertinite-rich coals produce CO_2 sorption capacities that are similar to those of vitrinite-rich coals [221]. The composition of reactive inertinite was 0% for the above sample used in this study, so the point doesn't apply here.

A commonly used standard for comparison of adsorption data is the Argonne Premium Coal Sample Programme, which consists of a selection of eight U.S. coals of different ranks ranging from 0.25% up to 1.68% VRr. These coals have been characterised comprehensively and have been used as standard and reference samples in numerous studies [69, 105, 167, 184]. The Argonne Premium coal with the most comparable properties in terms of petrographic composition to the current sample is the Illinois no.6 coal. Table 8.1 shows the comparison between the Illinois no.6 coal and the vitrinite-rich coal A sample.

Table 8-1: A comparison of properties for Illinois no. 6 coal and South African vitrinite-rich coal A sample (vol %)

Property	Illinois # 6	Coal A (Vitrinite-rich)
VRr (%)	0.46	0.67
Liptinite (%)	5	2.6
Inertinite (%)	10	4.4
Vitrinite (%)	85	91.8
Ash (%)	15.48	4.9
H_20 (%)	7.79	3.8
VM (%)	40.05	35.6
Langmuir Parameter N_o (mmol/g)	3.2	3.41

Both the coals have a high vitrinite content, but Illinois no.6 has a higher moisture and ash content (15.5% and 7.8% respectively). Both moisture and ash content have an adverse relationship with adsorption capacity [35-36], and would contribute to a lower adsorption capacity (and consequently lower Langmuir N_o parameter) for the Illinois no.6 coal. Also, Illinois no.6 has a slightly higher inertinite content than coal A, which might contribute to the lower Langmuir N_o parameter value. Although the difference in these parameters may contribute to the adsorption capacity, one could assume that the higher vitrinite-rich content and rank in coal A is the main contributor to the slightly higher N_o Langmuir parameter.

8.3.2 Subcritical CO_2 treated samples

Vitrinite-rich coal A and inertinite-rich coal B were treated under subcritical condition at 45bar and room temperature for 6 months, subsequently removed from the reactors and tested for CO_2 sorption behaviour in the volumetric adsorption system. Figure 8-2 shows excess adsorption isotherms for untreated and treated (a) coal A and (b) coal B.

From the plots in Figure 8-2, it is apparent that the treatment in CO_2 for 6 months did affect the absorption capacity for both coal samples. What is more interesting in the plots is the difference in the magnitude of the affect between 6 month treated samples for the two coals, where the vitrinite-rich coal A shows a greater effect than the inertinite-rich coal B.

This observation is consistent with a previous observation for vitrinite-rich coals, where the coals showed a significant change in adsorption capacity after being treated with CO_2 [118]. Where this study deviates from other studies, is in the magnitude of that change. In the current study, CO_2 adsorption capacity has more than doubled from untreated to 6 months treated coal (Coal A). This is significantly different to other observations, where the adsorption capacity of coal showed a maximum increase of 18% from untreated to one that was treated over a 13 months period [118].

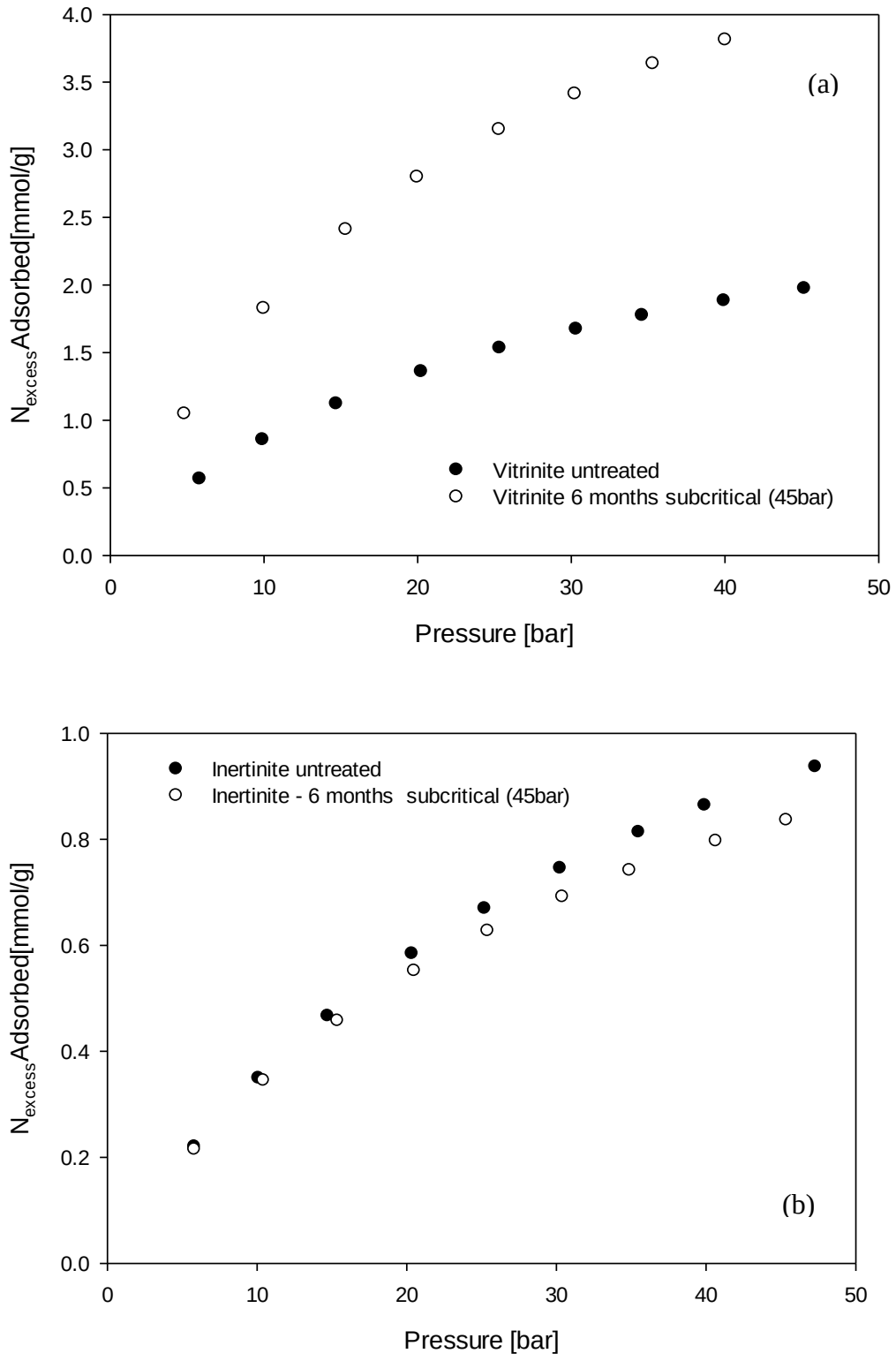

Figure 8-2: Excess adsorption isotherms for treated and untreated (a) coal A and (b) coal B

Prior studies have attributed the change in CO_2 adsorption capacity between untreated and treated coals to the loss of moisture in the treated coals [118, 212, 228].

As mentioned in the experimental section (see §3.2.1), samples were oven dried to remove the effect moisture prior to treatment. Moisture content of the coals after 6 months' subcritical treatment was determined, and found to have slightly decreased for both the samples (See Figure 8-3).

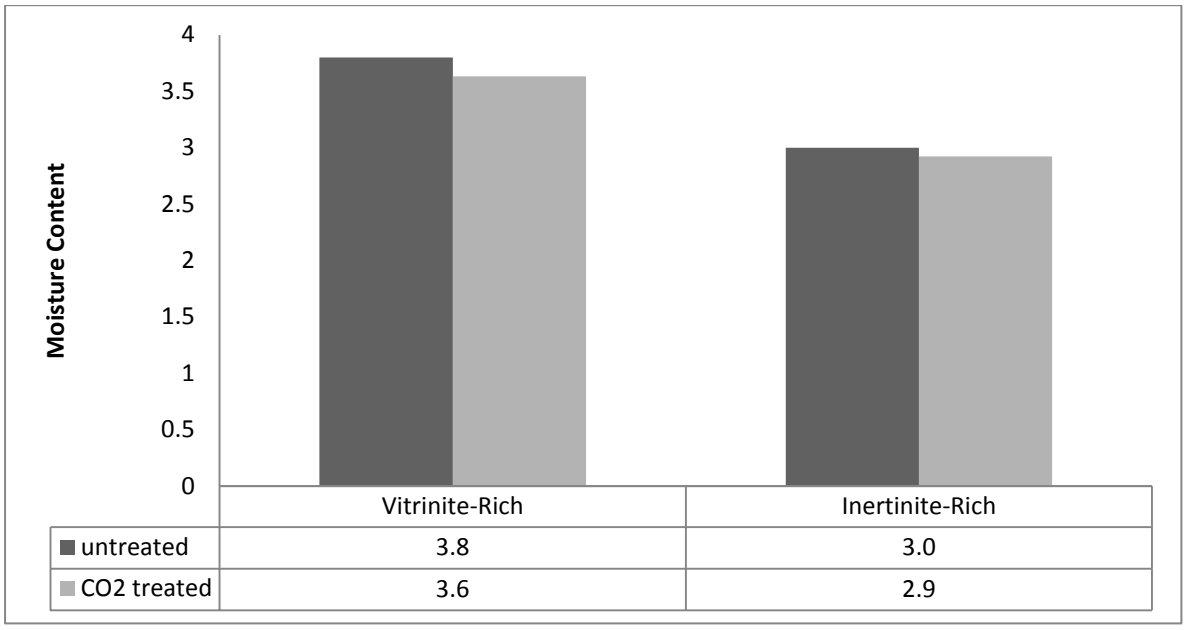

Figure 8-3: Moisture content (%) for treated and untreated vitrinite-rich coal A and inertinite-rich coal B

The loss of moisture does not explain why vitrinite has a higher increase in the adsorption capacity for the 6 months treated coals than the inertinite-rich coals, or why inertinite shows little to no change in the adsorption capacity after treatment. A more plausible explanation for the observed differences in coal A and coal B's response to CO_2 treatment is in their chemical and physical structure and properties. This also agrees with our earlier observations (see § 6.4), which showed a higher increase in the surface area and microposity of treated coal A and a very low to non-existent change in the coal B's surface and microposity.

In terms of chemical structure, vitrinite has a more "plastic" character due to its high aliphatic content when compared to the more "rigid" structure of inertinite, due to its higher aromatic content (see § 5.4.1). This plastic character of the vitrinite-rich coal A would also explain the higher capacity of the 6 months. In a plasticised coal A structure inaccessible pores would be more accessible to the CO_2 molecules thus reporting higher adsorption capacity.

Another alternative possibility for the observations in Figure 8-2(a) is the loss in pore integrity due to the high pressure CO_2 treated for 6 months. This could also explain the deviation observed for both coal A and B treated samples at high pressures. At such high pressures, the effect of CO_2 on coals would be similar to the "conditioning effect" observed in glassy polymer-liquid sorbate systems. For glassy polymers the "conditioning effect" has been demonstrated for small molecules like CO_2 [174] . A more in-depth discussion on the conditioning effect is provided in section 2.4.2.1.1.

Briefly, in the conditioning effect, pore deformation is brought about by the infusion of the sorbate into the sorbent at a concentration above the glass transition concentration of the sorbate. In this solid-liquid sorption system, conditioning first converts the sample to the rubbery state through the effect of plasticisation and causes the pores to disappear. Then, as the conditioning agent is removed and glass transition concentration is approached from the high-concentration side, "new pores" are created in the solid. This leaves the conditioned sample with a greater pore capacity than the original sample.

By this "conditioning effect" mechanism, the sorbate causes irreversible changes in the structure of internal micropores (holes) in the organic matrix upon its sorption [198; 199] . If it is assumed during the experimental conditions in this study, this transition concentration was reached, then the conditioning effect theory does explain the observed sorption

behaviour. To further investigate this possibility, adsorption-desorption hysteresis studies were performed on the untreated and treated samples.

8.3.3 Adsorption-desorption hysteresis

Desorption isotherms for CO_2 were measured immediately after the corresponding sorption isotherms for the treated and untreated samples. Ideally, desorption isotherms should not deviate from the sorption isotherms. However, as evident from Figure 8-4, desorption isotherms lie above the excess sorption isotherms, and this normally indicates that a significant hysteresis effect is associated with the sorption/desorption process [228]. An in-depth definition of adsorption-desorption hysteresis is provided in Section 2.6.1.

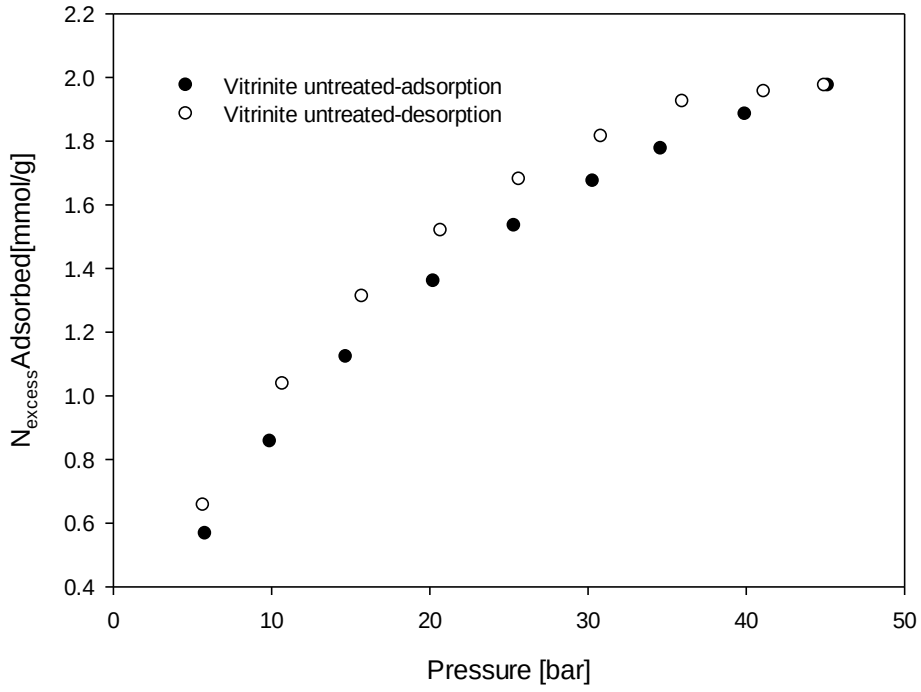

Figure 8-5Figure 8-4: Adsorption and desorption isotherms for coal A

Briefly, the adsorption-desorption hysteresis effect indicates that the sorbent-sorbate system is in a metastable state, and, as pressure decrease, the gas is not readily released to the extent corresponding to the thermodynamic equilibrium value [229]. In other words, hysteresis is

the same as *irreversible* sorption. Irreversible does not mean that the sorbate is irretrievable, but that sorption and desorption follow different mechanistic pathways; that is, sorption is irreversible because sorption and desorption occur to/from different physical environments [173].

8.3.3.1 Adsorption-desorption hysteresis for untreated and 6 months treated coals

Figure 8-5 shows the adsorption and desorption isotherms for untreated coal A and untreated coal B. The adsorption-desorption hysteresis for vitrinite-rich coal A samples is greater than the adsorption-desorption hysteresis for untreated inertinite-rich coal B, although it is only slightly so. The difference in the adsorption-desorption hysteresis can be explained by the difference in the coal-CO_2 interactions.

In the case of the coal A isotherm, the adsorption-desorption hysteresis can be explained by a firmer bond of the CO_2 molecules with carbon in the coal, possibly due to its higher oxygen and hydrogen content (15.31wt% and 5.14wt% respectively, see Table 5-1).

As in the case of untreated coals, the isotherms from the 6 months treated samples show different degrees of hysteresis. Here, relatively large deviations between the two isotherms are noticed for the vitrinite-rich coal A sample, while for the inertinite-rich coal B a closer agreement of the two curves is observed. For the inertinite rich coal B sample, the desorption process proceeded almost reversibly to the adsorption process, which means that CO_2 desorbs directly on pressure decrease [229].The large adsorption-desorption hysteresis for the vitrinite coal A sample is surprising, because it would suggest, from a chemical perspective, that the vitrinite-rich coal A matrix still has a stronger CO_2-coal interaction.

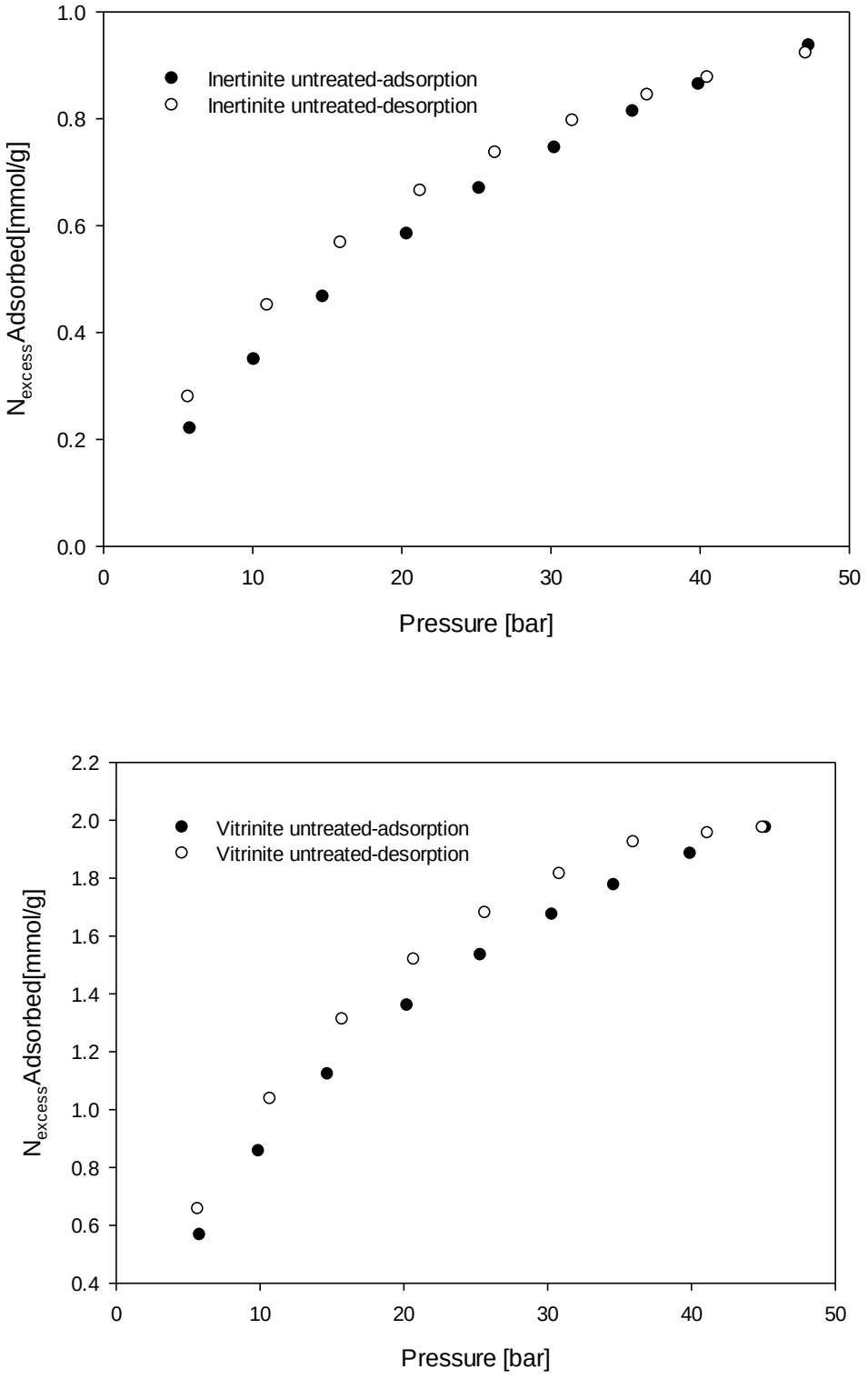

Figure 8-5: Adsorption and desorption isotherms for untreated vitrinite-rich coal A and inertinite-rich coal B sample.

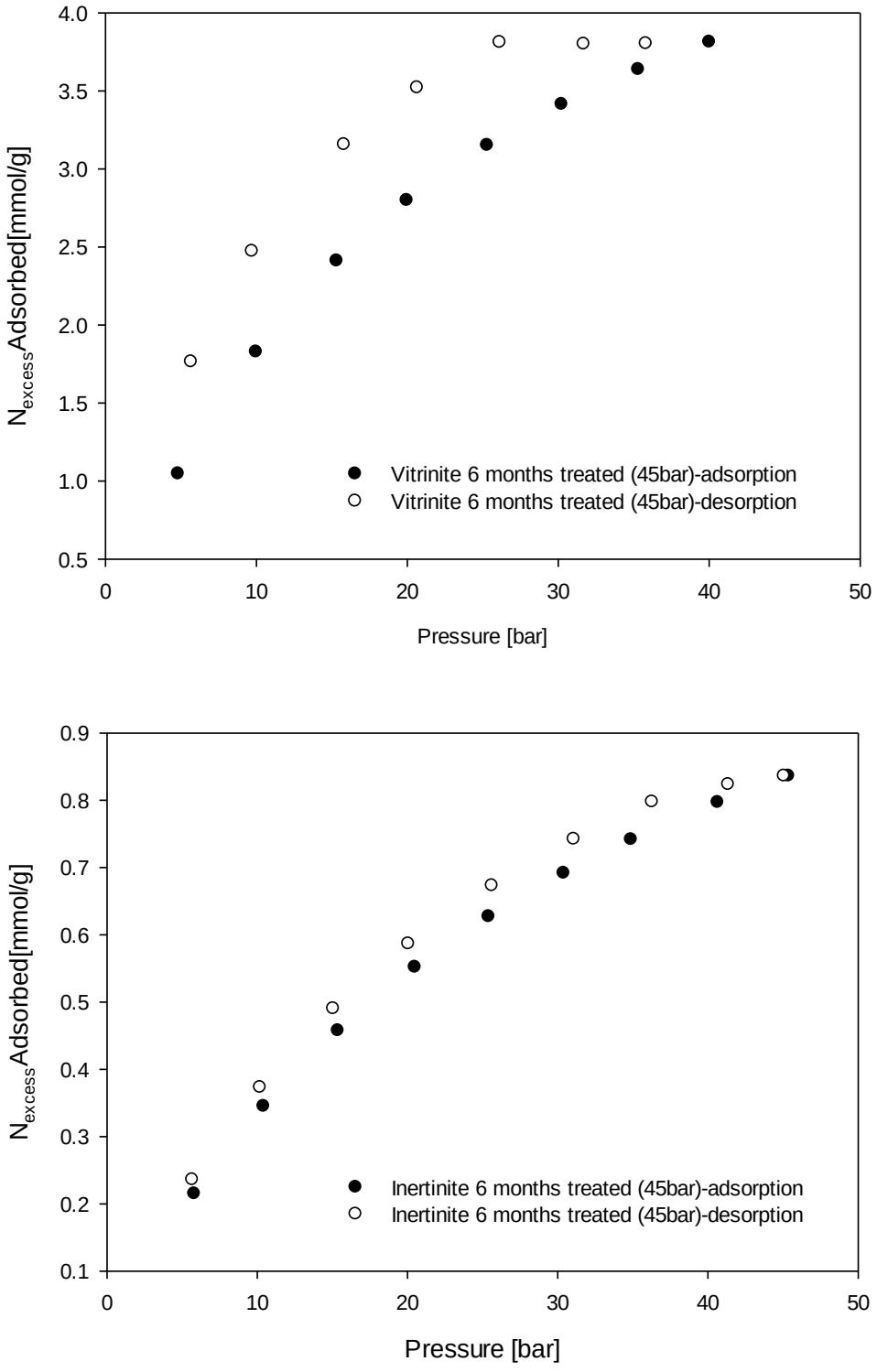

Figure 8-6: Adsorption and desorption isotherms for treated vitrinite-rich coal A and inertinite-rich coal B sample (subcritical conditions).

Based on the adsorption-desorption hysteresis results for the untreated coals, it was expect that, due to its slightly higher hysteresis and its higher hydrogen and oxygen content, the vitrinite-rich coal A would have stronger CO_2-coal interactions during the 6 months subcritical treatment period. As such, the vitrinite rich coal A's more "active" sites (possibly those that would form stronger van der Waal's forces with CO_2) would be saturated, making the coal less "reactive", or having lower CO_2-coal interaction "bonding".

An alternative explanation for the observed higher adsorption-desorption hysteresis is by considering the effect of the duration of CO_2 treatment on the physical properties, or more specifically, on the pore structure of the coal. When contact between the coal sample and the CO_2 molecules is as long as in this study, CO_2 molecules begin to diffuse through ultra micropores which it would otherwise not be able to over a shorter period of time. At pressures in excess of 20 bar, the CO_2 starts to accumulate in newly opened pores in the form of a free gas [230]. When the pressure is released, the free gas is released, leaving behind newly formed pores. It is possibly these newly formed pores that are used as the new "active sites", or new pathways, for the desorption isotherm. This theory would also explain the higher adsorption capacity observed for the 6 months treated vitrinite-rich coal when compared to the untreated coal corroborating the surface area and pore structure results.

Sometimes, in cases when the desorption branch lies over the adsorption branch within the total or bulk of the pressure range, it is an indication that the CO_2 molecules have stayed captured within the structure of solid phase and a percentage of the CO_2 molecules have been absorbed in addition to the physical adsorption [182].

8.3.3.2 Using adsorption-desorption isotherms to differentiate between absorption and adsorption

Using a method developed by Medek et al. [182], it is possible to separate the adsorption isotherm from the absorption isotherm. In doing so it would be possible to deduce the amount of CO_2 absorbed for each sorption isotherm. And, it would then be possible to infer the type of coal-CO_2 interactions and integrity of the coals pre and post-CO_2 treatment.

In developing the method for using adsorption/desorption isotherms for differentiating between adsorption from absorption, Medek et al. [182] suggested the following simplifying prerequisites for an ideal mechanism of both processes:

(a) The physical adsorption for the coal/CO_2 under given state conditions is realised predominantly on the principle of volume filling; it is reversible and represents the adsorption isotherm (AD).

(b) Absorption proceeds via dissolving of gas in solid phase according to Henry's law, the linear dependence of the dissolved amount of gas on pressure has a constant slope and represents the absorption isotherm (AB).

(c) The final absorbed amount absorbed (AB_f) for coal remains constant within the entire course of desorption.

The shared adsorption/ absorption branch (AD+AB) and the shared desorption branch or desorption absorption branch (DAB) represent sets of experimental values for adsorption isotherms and desorption isotherms respectively. When, under given conditions, the final amount (AB_f) absorbed at the final pressure (pf) is subtracted from the branch DAB at all pressure points, the separated adsorption isotherm (AD) is obtained, which will have a constant distance from the desorption branch (DAB).

At the first approximation, the value AB_f can be derived as distance between the desorption branch DAB and the branch AD+AB in the pressure range near to zero, where the curvature of both branches is very similar and the distance has only quite slightly fluctuating value.

Determination of AB_f is done numerically by fitting respective experimental points of branches AD+AB and DAB with mathematically defined curves, for example in the form of a polynomial. As the total absorbed amount AB_f does not change during desorption, the desorption branch DAB copies the shape of the reversible isotherm AD. The separated absorption branch AB is then obtained by subtracting the isotherm AD from the branch AD+AB. The following relations apply to the above operations:

$$AB_f = F(DAB) - F(AB + AD) \tag{8-1}$$

$$F(AD) = F(DAB) - AB_f \tag{8-2}$$

$$F(AB) = F(AB + AD) - F(AD) \tag{8-3}$$

The reconstructed isotherms for untreated and 6 months treated coals A and B are presented in Figure 8-7 (a-b) and Figure 8-8 (a-b) respectively. The upper most curve and the second upper curve represents the experimental desorption isotherm (DAB) and the experimental adsorption isotherm (AD+AB) curve, respectively. The curve below the experimental adsorption isotherm curve (AD+AB) is the calculated pure adsorption isotherm (AD). The straight line curve at the bottom of the plot represents the calculated absorption (AB) curve.

The contribution of absorption to the experimental adsorption isotherm is indicated by the width of the distance between DAB and AD. From the plots in Figure 8-7 (a) and (b), it is clear that the contribution of the experimental adsorption isotherm is higher for untreated coal A than for the 6 months treated sample.

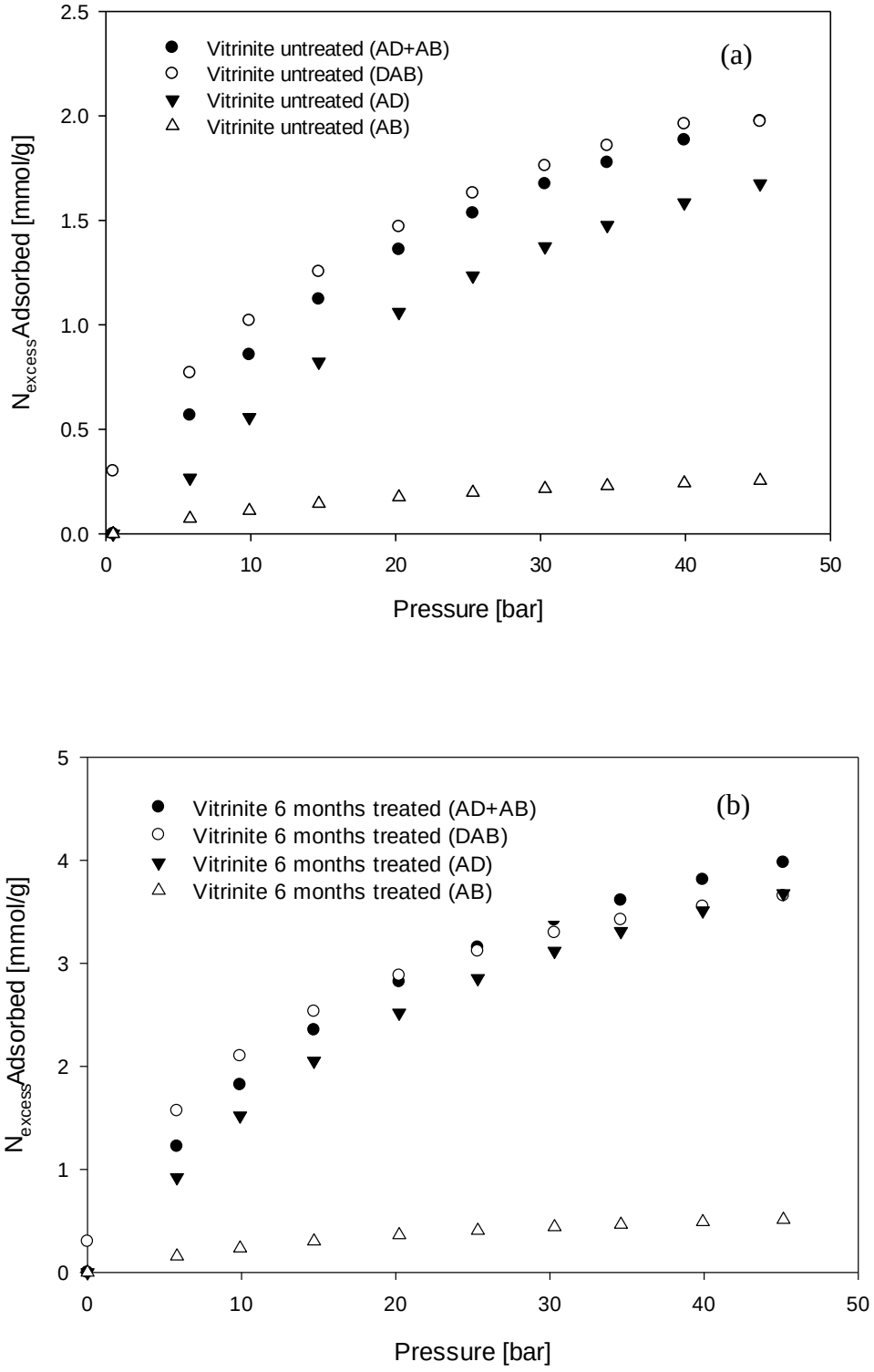

Figure 8-7: Reconstructed isotherms for (a) untreated and (b) 6 months treated coal A with separated absorption and adsorption isotherms

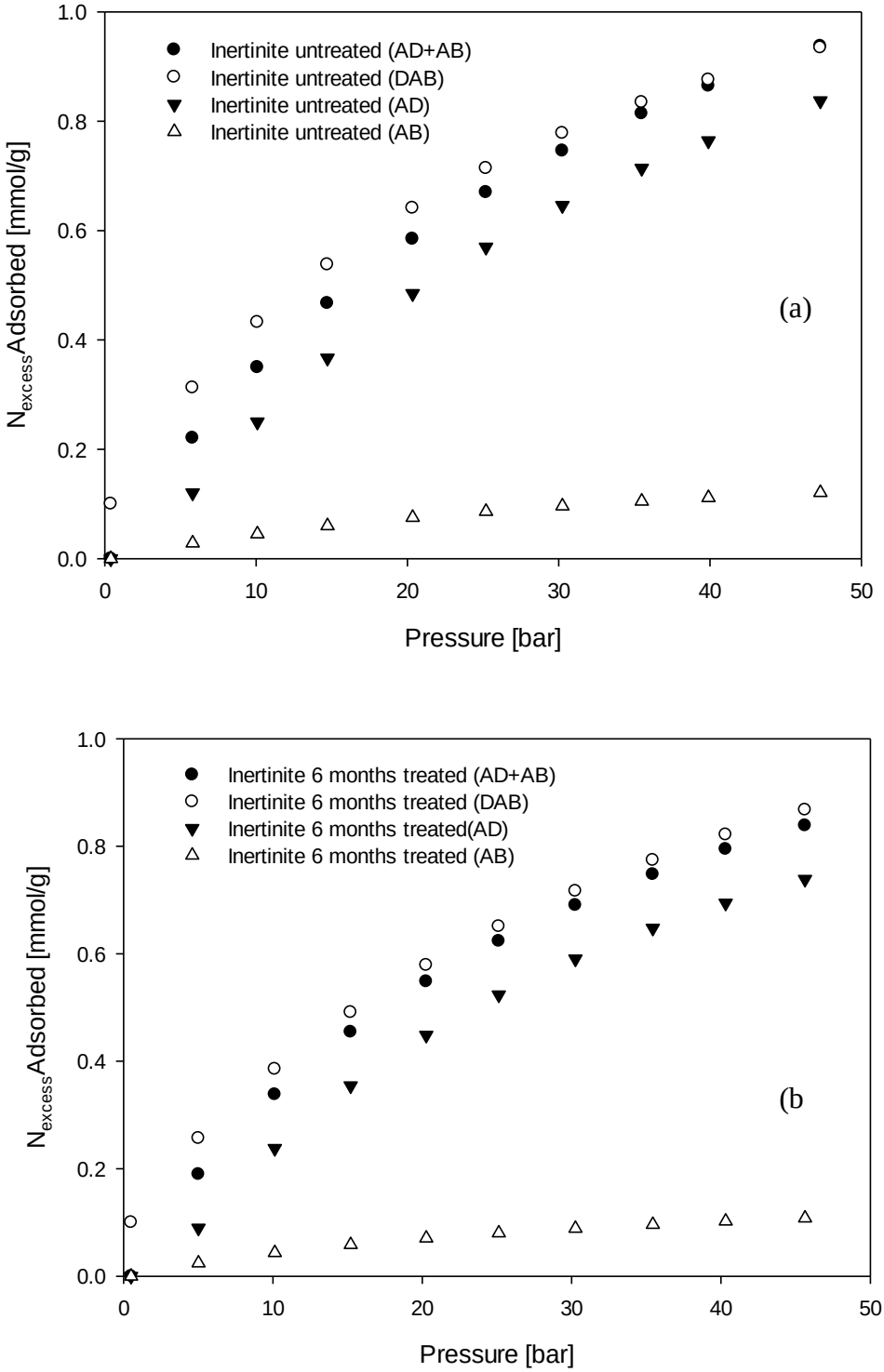

Figure 8-8: Reconstructed isotherms for (a) untreated and (b) 6 months treated coal B with separated absorption and adsorption isotherms

This does not necessarily represent the final absorbed amount (final absorbed amount is indicated by AB_f), but it does give an indication of degree of reversibility of the adsorption isotherm. This proves that reversibility of the 6 months treated adsorption isotherm, a testament to the higher polymer character or plasticity of vitrinite-rich coal and CO_2's ability to enhance that plasticity.

Interestingly, contrary to vitrinite-rich coal A, inertinite coal B shows very similar curves for both treated and untreated coal (see Figure 8-8 (a) and (b)). This result is consistent with the previous observation for inertinite-rich coal, whose adsorption behaviour seems to be unaffected by the 6 months CO_2 treatment at 45bar (Figure 8-2).

An analysis on the final absorbed amount (AB_f) for the untreated and treated coals of coal A and B yields similar results. In addition, an analysis on the reconstructed plots was on the absorbing behaviour of the treated and untreated coals of the coals. This was done by plotting the slope of the AB curve and assuming Henry's law applies. As seen in Figure 8-9, the absorbing behaviour of the coal B seems to remain unchanged.

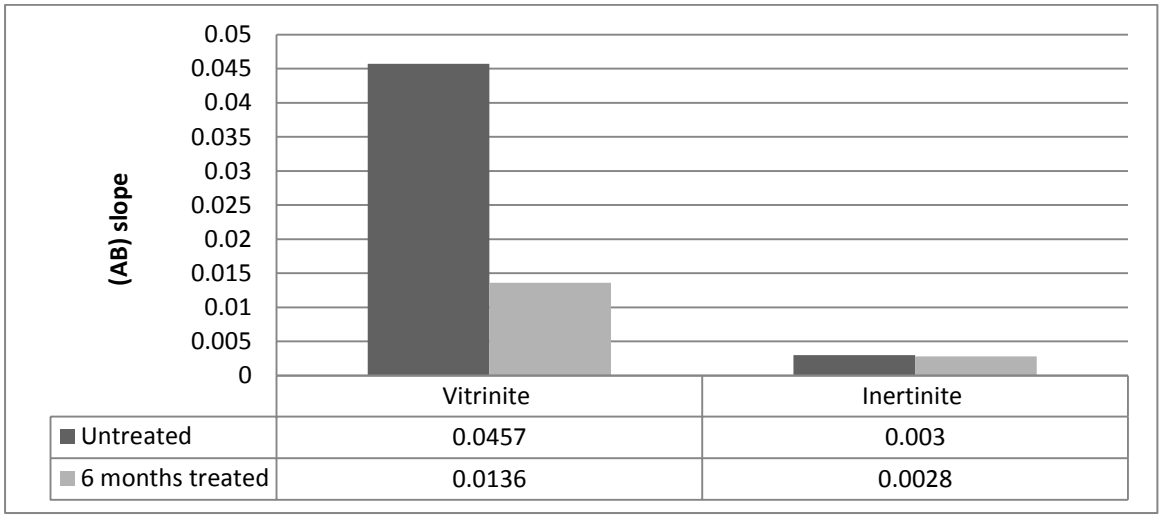

	Vitrinite	Inertinite
Untreated	0.0457	0.003
6 months treated	0.0136	0.0028

Figure 8-9: Absorption isotherm (AB) slope for untreated and treated coal A and coal B

Interestingly, for vitrinite the AB_f and the AB slope is higher for untreated coal than for the treated coal. Because absorption proceeds via diffusion of gas molecules into the macromolecular structure of coal matrix [202-203], it can be assumed that the amount of CO_2 absorbed is influenced by the contact time of gas with the coal, and should increase with more contact. This finding would suggest that the pore spaces in the coal matrix might have been closed due to the volumetric changes caused by the 6 months CO_2 treatment of coal.

It is noted that volumetric changes (or swelling) will be associated with the absorption of CO_2 in coal, as has been indicated in other studies [204-205]. This phenomenon was outside the scope of this study and thus has been excluded, but requires inclusion in future studies.

8.4 Supercritical CO_2 sorption behaviour

Untreated coal A was also treated under supercritical conditions at 35°C and 125bar over a 6 months period[18]. The plot in Figure 8-10 shows the adsorption isotherm for untreated and 6 months subcritical and supercritical treated coal A. What is interesting in this plot is that the adsorption capacity for the 6 months supercritical treated is lower than the 6 months subcritical treated coal.

These results seem to be consistent with actual field observations, where the injectivity of the CO_2 seems to decrease over time [26, 236-237]. The results would seem to suggest that the adsorption capacity increases with pressure only to a certain point when it either has a tipping point or plateaus and then drops.

[18] Coal B was also included in this part of the study, only to find that the sample had been mistakenly replaced with a vitrinite rich coal upon removal from the high pressure reactor and time did not allow for another 6 month test.

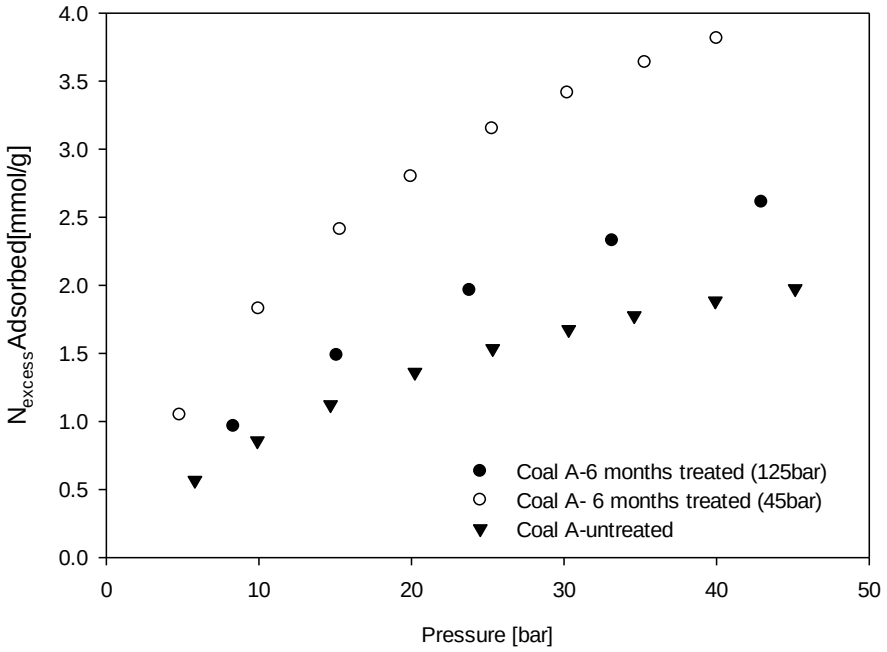

Figure 8-10: Adsorption isotherms for untreated and 6 months subcritical and supercritical treated coal A

Interestingly, this result corroborates an earlier finding on the analysis of low temperature BET surface area of supercritical treated CO_2 where it was found that a similar trend exists for surface area (see Figure 8-11). Figure 8-11 shows a plot of the Langmuir surface area of the untreated, subcritical and supercritical treated coal A as determined by the low pressure BET analysis superimposed by the adsorption capacity plot.

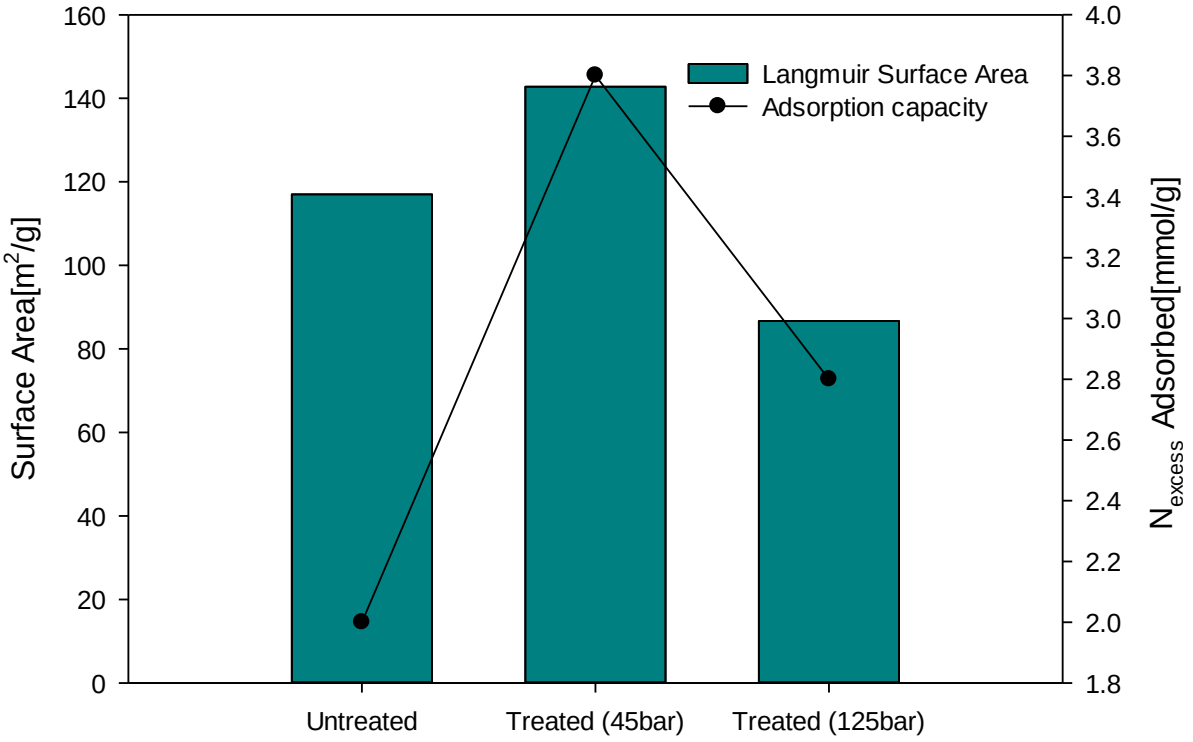

Figure 8-11: Adsorption capacity of supercritical treated coal A compared with the Langmuir surface as determined by low pressure CO_2 adsorption isotherm

It is clear from Figure 8-11 that the two plots follow a similar trend, and helps in explaining the sharp drop in CO_2 adsorption capacity for the supercritical treated coal compared to the subcritical treated coal. The drop is due to a much lower surface for the supercritical treated coal, which could be attributed to loss in micropore volume, as was found in section 7.4.

8.5 Summary and conclusion

The study determined that there was a significant increase in the sorption capacity of the treated vitrinite-rich coal A compared to the untreated sample under subcritical conditions. It was also found that CO_2 treatment over a 6 months period on the inertinite-rich coal sample had little to no effect on the sorption behaviour of the coal. A significant conclusion that can be drawn from these findings is that, in order to avoid the volumetric effects (e.g swelling)

that CO_2 sorption has on the coal, it might necessary to consider inertinite-rich coals as they respond minimally to CO_2 treatment, although they have a lower adsorption capacity. Vitrinite-rich coals show the most pronounced response to CO_2 treatment and contribute greatly to CO_2 treatment either by increasing or decreasing adsorption capacity. This means that a vitrinite-rich coal is more prone to structural changes under CO_2 treatment than an inertinite-rich coal.

The study further separated the adsorption isotherm into separate adsorption and absorption isotherms. This exercise was highly effective in that it determined the final amount of CO_2 that is absorbed in the coal structure. Surprisingly, it was found that the absorption slope, equivalent to Henry's constant, seems to be lower for the 6 months treated vitrinite-rich coal when compared to the untreated coals. It was suggested that this might be due to the pore spaces being closed due to volumetric changes caused by long term CO_2 treatment.

Finally, the study showed that the adsorption capacity of the supercritical treated coal is lower than the subcritical treated coal over the same period of 6 months for the vitrinite-rich coal A. This finding confirms field observations where the CO_2 injectivity decreases with time.

CHAPTER 9
SUMMARY, CONCLUSIONS AND RECOMMENDATIONS FOR FUTURE WORK

9.1 Summary

The main aims of the current study were to understand, at a fundamental level, CO_2-coal interactions over a long term period of time (up to 6-months) and how this CO_2-coal interaction would affect the coal structure and properties, as well as CO_2 uptake.

The study set out to achieve these aims by considering the long term effect of storing CO_2 in coal, on two well characterised samples, vitrinite-rich and inertinite-rich coal particles. Experimentally, the study was conducted by keeping both types of coal particles under pressure for up to a 6 months period under subcritical and supercritical CO_2 conditions. After treatment with CO_2, the samples were analysed to determine the petrographic, physical, chemical, and sorption characteristics of the treated coals.

A high pressure adsorption measurement instrument was commissioned during the study. It enabled the measurement of adsorption and desorption isotherms at high pressures (up to 60 bar). The adsorption and desorption isotherms formed a important part of the study as it enabled the determination of the nature of coal-CO_2 interactions, and how they were affected by long term CO_2 treatment. This was seen as crucial to understanding the coal-CO_2 interactions for CO_2 storage, and possibly ECBM, applications.

A pre-CO_2 treatment characterisation of the coals indicated, by petrographic analysis, a successful maceral separation, as coal A was found to have 97.0wt% vitrinite and coal B

having 80.9%wt inertinite. This analysis was used as a reference to coal A being referred to as the "vitrinite-rich coal" and coal B being referred to as "inertinite-rich coal".

The surface area analysis of the coals revealed that the surface area obtained is dependent on the adsorbate molecule used. For N_2 BET surface area analysis, coal B has a higher surface area than coal A particle. For CO_2 BET analysis, coal A has a higher surface area, than inertinite coal B sample. This was interpreted as indicative of a more microporous nature of the coal A. A PSD analysis confirmed this interpretation to be true. In terms of chemical properties, coal A was found to be more aliphatic than the coal B, which was more aromatic.

The next part of the study focused on the chemical and physical changes caused by CO_2 sorption in coal after 6 months of treatment for both coal A and coal B under subcritical conditions. BET analysis of the treated and untreated coal particles showed that coal A particles have a greater surface area and change in pore structure than the coal B samples. Functional group analysis (FTIR) indicated that there was no functionality change for the treated and untreated coals for both coal A and coal B. Analysis of the crystalline part of the CO_2 treated and untreated coal B samples showed that there was slight increase in the average crystallite height, although no changes were observed for the d_{002} aromatic interplanar spacing. The most significant result from this part of the study was the notable changes in post-CO_2 treated coal A coal properties in comparison to the relatively unchanged post-CO_2 treated coal B.

After considering the effects under subcritical conditions, the study further investigated the effects of supercritical CO_2 treatment on a coal A when compared to subcritical treated coal. With regards to the effects on petrographic properties, the main observation was that these effects are very small if not non-existent. On the effects on physical properties, it was found that the surface area decreases sharply when compared to the untreated and subcritical treated

coal. It was also shown that the PSD was considerably lower for the supercritical sample than for the untreated and subcritical treated coal samples. This was interpreted as a reduction or loss of the micropore structure integrity of the coal due to the long term CO_2-coal interaction. Using FTIR, it was found that the treated coal showed distinctly more intense peaks for the adsorbed CO_2 peak compared to untreated coals. This was interpreted as indicative of the stronger incorporation of the CO_2 molecules into the coal matrix. However, it was noted that further work is required to confirm this. As for the effects on the internal structure, it was not determinable due to the diffuse nature of the d_{002} peak.

The last part of the study was to determine the effects of subcritical and supercritical treatment on CO_2 sorption behaviour. It was determined that there was a significant increase in the sorption capacity of the treated coal A compared to the untreated sample. It was also found that CO_2 treatment over a 6 month period (subcritical conditions) on the coal B sample had little to no effect on the sorption behaviour of the coal. Ideally, the experiment should be run again to consider the effect under supercritical conditions. Additionaly, sorption isotherms were separated into adsorption and absorption isotherms. This exercise was highly effective in that it determined the final amount of CO_2 that is absorbed in the coal structure. Surprisingly, it was found that the absorption slope, equivalent to Henry's constant, seems to be lower for the 6 months treated vitrinite rich coal compared to untreated coals. It was suggested that this might be due to the pore spaces being closed due to volumetric changes caused by long term CO_2 treatment, correlating with the BET analysis.

Finally, the study showed that the adsorption capacity of the supercritical treated coal is lower than the subcritical treated coal over the same period of 6 months for coal A (vitrinite-rich).

9.2 Conclusions

Taking into consideration the summary provided in the previous section, it is now possible to draw the following conclusions by addressing the research questions posed in Chapter 1 (conclusions follow below the questions):

(i) What is the major coal-CO_2 interaction mechanism during CO_2 storage in coal?

- The major CO_2-coal interaction is definitely a physical interaction (as demonstrated by the adsorption behaviour study in Chapter 8), although it was found that a significant amount of the CO_2 gets absorbed in the coal structure. It can also be concluded that this interaction will be dependent on the maceral composition of the coal, whereby a vitrinite-rich coal has a stronger coal-CO_2 interaction than inertinite-rich coal.

(ii) What is the long term effect of CO_2 storage on the coal structure and properties?

- It was assumed that the CO_2 treatment under subcritical and supercritical conditions simulates, to a certain extent, the storage conditions of CO_2 in coal seams. If this assumption is held to be true, then the long term effects of CO_2 storage in coal were found to be dependent on the maceral composition of the coal, with a vitrinite-rich coal showing a much more pronounced structural and properties change after CO_2 storage. This change did, however, differ under subcritical and supercritical conditions. Inertinite rich coal was found to be less prone to changes under CO_2 storage. A major implication of this finding is the inclusion of maceral composition as major criteria for determining CO_2 storage capability. Until now, adsorption capacity has been the main criteria for CO_2 storage in coal. This study suggests that maceral composition should also be considered, as an inertinite, commonly with lower

adsorption capacity, might ensure the long term integrity of the coal structure and properties.

It can be concluded that the current research adds substantially to our understanding of CO_2-coal interactions, and it will serve as a basis for future studies in the field.

9.3 Recommendation for future work

Although this study was successful in advancing our understanding of CO_2-coal interactions, it has also thrown up many questions in need of further investigation. It is recommended that further research be undertaken in the following areas:

- The current study was done on maceral enriched coals and did not take into the effect that moisture content and mineral matter. So, it would be desirable that future studies include the effect of moisture and mineral matter on the CO_2-coal interactions in order to simulate actual storage conditions.
- The current study was also performed on small sized particles (1mm); this is not representative of actual storage reality, but was required for laboratory scale research. Future studies should investigate much larger particle sizes, as practically possible, that are more representative of in-situ storage conditions.
- It is also recommended that a non-invasive in-situ analytical technique for example a CT scan should be used to analyse the coals in-situ without taking the samples out of the pressurised treatment reactor. This would reduce the risks of oxidation of the coal structure prior to analysis.
- The study made inferences to volumetric changes based on observed changes on previous studies about the implications on volumetric changes (or swelling) in coal. Further investigation and experimentation into this is strongly recommended.

- From an experimental point of view, it would be interesting if the effects of CO_2 treatment could be extended to supercritical adsorption isotherms as they might reveal further CO_2-coal interaction behaviour.
- A more robust chemical analysis on the supercritical treated coals is required to investigate the chemical species from the coal matrix that might have been mobilised during supercritical CO_2 treatment.

Finally, although the study was a first in CO_2 treatment of coal under the conditions presented in the study, it is acknowledged that a longer period (1 year) is more likely reveal more about coal-CO_2 interactions and coal's behaviour under prolonged CO_2 treatment.

REFERENCES

[1] DOE, “Coal Resources,” 2010. [Online]. Available: http://www.energy.gov.za/files/coal_frame.html. [Accessed: 24-Feb-2011].

[2] B. MacColl, “An overview of Eskom’s Research Approach to Carbon Capture and Storage (CCS).” University of the Witwatersrand’s Coal School, Johannesburg, South Africa, p. 29, 2009.

[3] B. Naidoo, “South Africa pushes ahead with carbon dioxide storage Atlas project, but scepticism persists,” *Engineering News*, 2009. [Online]. Available: http://www.engineeringnews.co.za/article/south-africa-pushes-ahead-with-carbon-dioxide-storage-atlas-project-but-scepticism-persists-2009-01-16. [Accessed: 24-Feb-2011].

[4] S. Raubenheimer, “Long Term Mitigation Scenarios Strategic Options for South Africa,” *Department of Environment Affairs and Tourism Report*, p. 34, 2007.

[5] Intergovernmental Panel on Climate Change, *Carbon dioxide capture and storage*. New York: Cambridge University Press, 2005, pp. 1–443.

[6] C. M. White, D. H. Smith, K. L. Jones, A. L. Goodman, S. A. Jikich, R. B. Lacount, S. B. Dubose, E. Ozdemir, B. I. Morsi, and K. T. Schroeder, “Sequestration of Carbon Dioxide in Coal with Enhanced Coalbed Methane Recoverys-A Review,” *Energy & Fuels*, vol. 19, no. 3, pp. 659–724, 2005.

[7] S. Bachu, “Screening and ranking of sedimentary basins for sequestration of CO2 in geological media in response to climate change,” *Environmental Geology*, vol. 44, pp. 277–289, 2003.

[8] N. Kulichenko and E. Ereira, “Carbon Capture and Storage in Developing Countries : a Perspective on Barriers to Deployment,” Washington DC, 2011.

[9] M. Cloete, “Atlas on Geological Storage of CO2 in South Africa.” South African Centre for Carbon Capture and Storage, Pretoria, pp. 1–59, 2010.

[10] J. H. A. Viljoen, F. D. J. Stapelberg, and M. Cloete, “Technical report on the geological storage of carbon dioxide in South Africa,” Council for Geoscience, Pretoria, 2010.

[11] A. Engelbrecht, A. Golding, and B. Scholes, “The potential for sequestration of carbon dioxide in South Africa,” CSIR and Department of Minerals and Energy, Pretoria, 2004.

[12] L. S. Jeffrey, “Characterization of the coal resources of South Africa,” *The Journal of The South African Institute of Mining and Metallurgy*, no. 2, pp. 95–102, 2005.

[13] T. P. Machacha and B. N. Modie, “The Department of Geological Survey Coalbed Methane Study,” *Botswana Department of Geological Survey*, 2004.

[14] S. Wandrag, “Sustainable development report.” Sasol, Johannesburg, p. 89, 2007.

[15] BOPA, “Carbon Capture too risky,” *Botswana Daily News*, 2007. [Online]. Available: http://www.dailynews.gov.bw/cgi-bin/news.cgi?d=20071212. [Accessed: 29-Aug-2011].

[16] S. Bachu, “CO2 storage in geological media : Role, means, status and barriers to deployment,” *Progress in Energy and Combustion Science*, vol. 34, pp. 254–273, 2008.

[17] J. Gale, “Geological storage of CO2 : What do we know, where are the gaps and what more needs to be done?,” *Energy*, vol. 29, pp. 1329–1338, 2004.

[18] R. Shukla, P. Ranjith, A. Haque, and X. Choi, “A review of studies on CO2 sequestration and caprock integrity,” *Fuel*, vol. 89, no. 10, pp. 2651–2664, 2010.

[19] E. Ozdemir, “Modeling of coal bed methane (CBM) production and CO2 sequestration in coal seams,” *International Journal of Coal Geology*, vol. 77, no. 1–2, pp. 145–152, 2009.

[20] A. L. Goodman, R. N. Favors, M. M. Hill, and J. W. Larsen, “Structure Changes in Pittsburgh No. 8 Coal Caused by Sorption of CO2 Gas,” *Energy & Fuels*, vol. 19, no. 8, pp. 1759–1760, 2005.

[21] C. Ö. Karacan, “Swelling-induced volumetric strains internal to a stressed coal associated with CO2 sorption,” *International Journal of Coal Geology*, vol. 72, pp. 209 – 220, 2007.

[22] J. W. Larsen, “The effects of dissolved CO2 on coal structure and properties,” *International Journal of Coal Geology*, vol. 57, no. 1, pp. 63 – 70, 2004.

[23] J. W. Larsen, “Sorption of carbon dioxide by coals,” *Fuel Chemistry Division Preprints*, vol. 48, no. 1, pp. 112–113, 2003.

[24] M. Mirzaeian and P. J. Hall, “The interactions of coal with CO2 and its effects on coal structure,” *Energy & fuels*, vol. 20, no. 5, pp. 2022–2027, 2006.

[25] M. Fujioka, S. Yamaguchi, and M. Nako, “CO2-ECBM field tests in the Ishikari Coal Basin of Japan,” *International Journal of Coal Geology*, vol. 82, no. 3–4, pp. 287–298, 2010.

[26] F. V. Bergen, “Effect of coal matrix swelling on enhanced coalbed methane production A field and laboratory study,” *Utrecht University: PhD Thesis*, pp. 1–206, 2009.

[27] S. Mazumder, P. V. Hemert, J. Bruining, K. A. A. Wolf, and K. Drabe, “In situ CO2 – coal reactions in view of carbon dioxide storage in deep unminable coal seams,” *Fuel*, vol. 85, pp. 1904–1912, 2006.

[28] R. Sakurovs, S. Day, S. Weir, and G. Duffy, “Application of a Modified Dubinin−Radushkevich Equation to Adsorption of Gases by Coals under Supercritical Conditions,” *Energy & Fuels*, vol. 21, no. 2, pp. 992–997, 2007.

[29] V. Romanov and Y. Soong, “Long-Term CO Sorption on Upper Freeport Coal Powder and Lumps Long-Term CO2 Sorption on Upper Freeport Coal Powder and,” *Energy & Fuels*, vol. 22, no. 2, pp. 1167–1169, 2008.

[30] H. J. Siriwardane, R. Gondle, and D. H, “Influence of shrinkage and swelling properties of coal on geologic sequestration of carbon dioxide,” *Response*. National Energy Technology Laboratory, Morgantown, pp. 1–15, 2007.

[31] S. Day, R. Fry, R. Sakurovs, and S. Weir, “Swelling of Coals by Supercritical Gases and Its Relationship to Sorption,” *Energy & Fuels*, vol. 24, no. 4, pp. 2777–2783, 2010.

[32] C. Karacan, “Heterogeneous Sorption and Swelling in a Confined and Stressed Coal during CO2 Injection,” *Energy & Fuels*, vol. 17, no. 6, pp. 1595–1608, 2003.

[33] J. I. Joubert, T. Grein, and D. Bienstock, “Effect of moisture on the methane capacity of American coals,” *Fuel*, vol. 53, no. 3, pp. 186–191, 1974.

[34] J. Cervik, “An investigation of the behavior and control of methane gas,” *Min.Congr.J.*, vol. 53, no. 7, pp. 52–57, 1967.

[35] E. D. Thimons and F. N. Kissell, “Diffusion of methane through coal,” *Fuel*, vol. 52, no. 10, pp. 274–280, 1973.

[36] R. L. Every and L. Dell’osso Jr., “Method for removing methane from coal - Patent 4043395.” Jun-1976.

[37] P. F. Fulton, C. A. Parente, B. A. Rogers, N. Shah, and A. A. Reznik, “A laboratory investigation of enhanced recovery of methane from coal by carbon dioxide injection,” in *Unconventional Gas Recovery Symposium*, 1980, p. 65.

[38] W. D. Gunter, T. Gentzis, B. A. Rottenfusser, and R. J. H. Richardson, “Deep coalbed methane in Alberta, Canada: A fuel resource with the potential of zero greenouse gases,” in *Energy Convers. Mgmt*, 1997, vol. 38, no. 96, pp. 217–222.

[39] J. J. Chaback, W. D. Morgan, and D. Yee, “Sorption of nitrogen, methane, carbon dioxide and their mixtures on bituminous coals at in-situ conditions,” *Fluid Phase Equilibria*, vol. 117, no. 1–2, pp. 289–296, 1996.

[40] R. Span and W. J. Wagner, “A new equation of state for carbon dioxide covering the fluid region from the triple-point temperature to 1100K at pressures up to 800 MPa,” *Phys. Chem.*, vol. 25, no. 6, pp. 1509–1596, 1996.

[41] S. Day, R. Fry, and R. Sakurovs, “Swelling of Australian coals in supercritical CO2,” *International Journal of Coal Geology*, vol. 74, pp. 41 – 52, 2008.

[42] S. Day, R. Sakurovs, and S. Weir, “Supercritical gas sorption on moist coals,” *International Journal of Coal Geology*, vol. 74, no. 3–4, pp. 203 – 214, 2008.

[43] J. G. Kaldi, C. M. Gibson-Poole, Y. Cinar, P. Cook, T. Dance, R. Daniel, K. Dodds, J. Esterle, M. Faiz, R. Funnell, A. Golab, L. Gurba, A. Hennig, J. Kaldi, D. Kirste, L. Paterson, D. Sherlock, P. Tingate, J. Underschultz, B. Vakarelov, P. V. Ruth, M. Watson, and M. Werner, “Storage Capacity Estimation, Site Selection and Characterisation for CO2 Storage Projects,” *CO2CRC*, no. March. CO2CRC, Canberra, pp. 1–52, 2008.

[44] D. W. Holliday, G. M. Williams, S. Holloway, D. Savage, and M. P. Bannon, “A preliminary feasibility study for the underground disposal of carbon dioxide in the UK.” British Geological Survey, Nottingham, p. 25, 1991.

[45] S. Bachu, “Carbon dioxide storage capacity in uneconomic coal beds in Alberta, Canada : Methodology, potential and site identification,” *International journal of greenhouse gas control*, vol. 1, pp. 374–385, 2007.

[46] R. M. Bustin and C. R. Clarkson, “Geological controls on coalbed methane reservoir capacity and gas content,” *International Journal of Coal Geology*, vol. 38, no. 1–2, pp. 3–26, 1998.

[47] E. Stach, *Coal Petrology*, 3rd ed. Berlin: Gebruder Borntraeger, 1992, p. pp.87.

[48] T. Major, *Genesis and the origin of coal and oil*, 2nd ed. Montgomery: Apologetics Press Inc., 1996, p. 20.

[49] J. Schuyer, H. Dijkstra, and D. W. van Krevelen, *Coal*, 3rd ed., vol. 34. Amsterdam: Elsevier, 1955, p. 251.

[50] R. E. Winans and J. C. Crelling, “Chemistry and Characterization of Coal Macerals,” *ACS Symposium Series*, vol. 252, pp. 1–20, 1984.

[51] R. Menendez and A. G. Borrego, “Organic Petrology applied to materials and coal by-products characterization,” in *24th Annual International Pittsburg Coal Conference*, 2007.

[52] C. R. Ward and I. Suarez-Ruiz, “Basic Factors Controlling Coal Quality and Technological Behavior of Coal,” in *Applied Coal Petrology*, no. 1, 2008, pp. 19–59.

[53] A. Marzec, “Macromolecular and molecular model of coal structure,” *Fuel Processing Technology*, vol. 14, pp. 39–46, 1986.

[54] F. Derbyshire, A. Marzec, M. A. Wilsonj-, A. Davistf, P. Tekelyf, A. Jurkiewicz, C. E. Bronnimann, R. A. Wind, G. E. Maciel, K. Bartle, and C. Snape, “Molecular structure of coals : A debate,” *Fuel*, vol. 68, no. 9, pp. 1091–1106, 1989.

[55] P. H. Given, B. C. Gersteint, A. Bartok, and L. J. Lyncht, “The concept of a mobile or molecular phase within the macromolecular network of coals : A debate,” *Fuel*, vol. 65, no. 2, pp. 155–163, 1986.

[56] J. G. King and E. T. Wilkins, “The internal structure of coal,” in *Conference on Ultrafine Structure of Coals and Cokes*, 1944, pp. 46–56.

[57] J. W. Larsen, “Some thoughts on the organic structure of bituminous coal.” Oak Ridge National Lab, Menlo Park, Jan-1978.

[58] A. Jurkiewicz, A. Marzec, and N. Piślewski, “Molecular structure of bituminous coal studied with pulse nuclear magnetic resonance,” *Fuel*, vol. 61, no. 7, pp. 647–650, 1982.

[59] S. T. Hsieh and J. L. Duda, “Probing coal structure sorption with organic vapour,” *Fuel*, vol. 66, no. 2, pp. 170–178, 1987.

[60] J. W. Larsen, T. K. Green, and J. Kovac, “The nature of the macromolecular network structure of bituminous coals,” *The Journal of Organic Chemistry*, vol. 50, no. 24, pp. 4729–4735, 1985.

[61] D. V. Niekerk, J. P. Mathews, and P. M. Halleck, “Molecular representations of Permian-aged vitrinite-rich and inertinite-rich South African coals,” *Fuel*, vol. 89, no. 1, pp. 19–25, 2010.

[62] M. Nishioka, “The associated molecular bituminous coal,” *Fuel*, vol. 71, no. 9, pp. 941–948, 1992.

[63] L. M. Lucht, J. M. Lamon, and N. A. Peppas, “Macromolecular Structure of Coals . 9 . Molecular Structure and Glass Transition Temperature,” *Energy & Fuels*, vol. 1, no. 6, pp. 56–58, 1987.

[64] N. A. Peppas, “Swelling and dissolution coals of the macromolecular structure of bituminous,” *Polymer*, vol. 38, no. 13, pp. 3425–3427, 1997.

[65] J. W. Larsen and K. Jeffrey, “Polymer Structure of Bituminous Coals,” in *Organic Chemistry of Coal*, 1st ed., J. W. Larsen, Ed. American Chemical Society, 1978, pp. 36–49.

[66] N. A. Peppas and L. M. Luchtt, “Macromolecular structure of coals 2. Molecular weight between crosslinks from pyridine swelling experiments,” *Fuel*, vol. 66, no. 6, pp. 803–809, 1987.

[67] D. Bodzek and A. Marzec, “Molecular structure components of coal and coal,” *Fuel*, vol. 60, pp. 47–51, 1981.

[68] P. M. Klotzkin, “Solvent treatment of coals 1. Effect of microporosity at ambient temperature,” *Fuel*, vol. 64, pp. 1092–1096, 1985.

[69] J. W. Larsen, P. Hall, and P. C. Wernett, “Pore Structure of the Argonne Premium Coals,” *Energy & Fuels*, vol. 9, no. 2, pp. 324–330, 1995.

[70] P. L. Walker, “Pore Structure in Coals,” *Fuel*, vol. 7, no. 3, pp. 559–560, 1993.

[71] C. F. Rodrigues and M. J. L. De Sousa, “The measurement of coal porosity with different gases,” *International Journal of Coal Geology*, vol. 48, pp. 245 – 251, 2002.

[72] P. Mahajan and P. L. Walker, “Water adsorption on coals,” *Fuel*, vol. 50, no. 3, pp. 308–317, 1971.

[73] R. Sakurovs, S. Day, S. Weir, and G. Duffy, “Effect of Coal Properties on CO2 Sorption Capacity under Supercritical Conditions,” in *24th Annual International Pittsburgh Coal Conference*, 2007, pp. 1–18.

[74] D. Prinz, W. Pyckhout-hintzen, and R. Littke, “Development of the meso- and macroporous structure of coals with rank as analysed with small angle neutron scattering and adsorption experiments,” *Fuel*, vol. 83, pp. 547–556, 2004.

[75] Y. Toda, M. Hatami, S. Toyoda, Y. Yoshida, and H. Honda, “Micropore structure of coal,” *Fuel*, vol. 50, no. 2, pp. 187–200, 1971.

[76] J. W. Larsen and P. Wernett, “Pore structure of Illinois No. 6 coal,” *Energy & Fuels*, vol. 2, no. 5, pp. 719–720, 1988.

[77] A. D. Alexeev, T. A. Vasilenko, and E. V. Ulyanova, “Closed porosity in fossil coals,” *Fuel*, vol. 78, pp. 635–638, 1999.

[78] J. Medek, L. Kovar, and Z. Weishauptova, “Bond forms of methane in porous system of coal II,” *Fuel*, vol. 83, pp. 1759–1764, 2004.

[79] R. L. Bond, “Capillary Structure of Coals,” *Nature*, vol. 178, no. 4524, pp. 104–105, Jul. 1956.

[80] F. Rouquerol, J. Rouquerol, and K. Sing, *Adsorption by Powders & Porous Solids*, 1st ed. San Diego: Elsevier, 1999, p. 467.

[81] F. Unsworth, C. S. Fowler, L. F. Jones, C. Po, C. C. Uk, M. C. A. Services, U. Ia, M. S. Park, and M. Lane, “Moisture in coal 2. Maceral effects on pore structure,” *Fuel*, vol. 68, pp. 18–26, 1989.

[82] P. J. Crosdale, B. B. Beamish, and M. Valix, “Coalbed methane sorption related to coal composition,” *International Journal of Coal Geology*, vol. 35, no. 1–4, pp. 147–158, 1998.

[83] H. Gan, S. P. Nandi, and P. L. Walker, “Nature of the porosity in American,” *Fuel*, vol. 51, no. 4, pp. 272–277, Oct. 1972.

[84] C. R. Clarkson and R. M. Bustin, “Variation in micropore capacity and size distribution with composition in bituminous coal of the Western Canadian Sedimentary Basin potential,” *Fuel*, vol. 75, no. 13, pp. 1483–1498, 1996.

[85] D. Prinz and R. Littke, “Development of the micro- and ultramicroporous structure of coals with rank as deduced from the accessibility to water,” *Fuel*, vol. 84, pp. 1645–1652, 2005.

[86] G. R. Baker-Read and S. A. Radchenko, “Methane emission from coal and associated strata samples,” *International Journal of Mining and Geological Engineering*, vol. 7, pp. 101–126, 1989.

[87] S. A. Anderson, L. R. Radovic, P. G. Hatcher, and F. S. Program, “Effects of surface chemsitry on the porous structure of coal,” no. May. U. S. Department of Energy, Pennsylvania, pp. 1–225, 1997.

[88] C. R. Clarkson and R. M. Bustin, “The effect of pore structure and gas pressure upon the transport properties of coal : a laboratory and modeling study . 1 . Isotherms and pore volume distributions,” *Fuel*, vol. 78, no. 11, pp. 1333–1344, 1999.

[89] E. P. Barrett, L. G. Joyner, and P. P. Halenda, “The Determination of Pore Volume and Area Distributions in Porous Substances. I. Computations from Nitrogen Isotherms,” *Journal of the American Chemical Society*, vol. 73, no. 1, pp. 373–380, 1951.

[90] L. R. Radovic, V. C. Menon, C. A. Leon, Y. Leon, T. Kyotani, R. E. Danner, S. Anderson, and P. G. Hatcher, “On the Porous Structure of Coals : Evidence for an Interconnected but Constricted Micropore System and Implications for Coalbed Methane Recovery,” *Adsorption*, vol. 3, pp. 221–232, 1997.

[91] P. D. Gamson, B. B. Beamish, and D. P. Johnson, “Coal microstructure and micropermeability and their effects natural gas recovery,” *Fuel*, vol. 72, no. 1, pp. 87–99, 1993.

[92] A. D. Alexeev, T. A. Vasylenko, and E. V. Ul’yanova, “Phase states of methane in fossil coals,” *Solid State Communications*, vol. 130, pp. 669–673, 2004.

[93] V. Guillot, O. Goetz, and A. Pupier, “Carbon dioxide-methane mixture adsorption on activated carbon,” *Adsorption*, vol. 12, pp. 55–63, 2006.

[94] F. Dreisbach, R. Staudt, and J. U. Keller, “High Pressure Adsorption Data of Methane , Nitrogen , Carbon Dioxide and their Binary and Ternary Mixtures on Activated Carbon,” *Adsorption*, vol. 5, pp. 215–227, 1999.

[95] B. M. Krooss, F. V. Bergen, and Y. Gensterblum, “High-pressure methane and carbon dioxide adsorption on dry and moisture-equilibrated Pennsylvanian coals,” *International Journal of Coal Geology*, vol. 51, pp. 69 – 92, 2002.

[96] J. U. Keller and R. Staudt, *Gas Adsorption Equilibria- Experimental Methods and Adsorptive Isotherms*. Boston: Springer Science, 2005, p. 422.

[97] S. Gregg and K. Sing, *Adsorption, surface area and porosity*, 2nd ed. New York: Academic Press, 1982, p. 371.

[98] Y. Belmabkhout, M. Frère, and G. D. Weireld, “High-pressure adsorption measurements. A comparative study of the volumetric and gravimetric methods,” *Measurement Science and Technology*, vol. 15, no. 5, pp. 848–858, May 2004.

[99] R. W. Pohl, *Experimental Physics- mechanics, acoustics, thermodynamics*, Vol 1. Berlin: Springer, 1954.

[100] M. Kochsiek and M. Glaser, *Comprehensive Mass Metrology*. Berlin: WILEY-VCH, 2000, p. 610.

[101] D. D. Do, *Adsorption Analysis: Equilibria and Kinetics*, 2nd ed., vol. 2. London: Imperial College Press, 1998, p. 913.

[102] I. Langmuir, "The constitution and fundamental properties of solids and liquids," *J. Am. Chem. Soc.*, vol. 38, no. 11, pp. 2221–2295, 1916.

[103] S. Brunauer, P. H. Emmett, and E. Teller, "Adsorption of gases in multimolecular layers," *Journal of the American Chemical Society*, vol. 60, no. 2, pp. 309–319, 1936.

[104] M. M. Dubinin, "The Potential Theory of Adsorption of Gases and Vapors for Adsorbents with Energetically Nonuniform Surfaces," *Chem. Rev.*, vol. 60, no. 2, pp. 235–241, 1969.

[105] E. Ozdemir, "Chemistry of the adsorption of carbon dioxide by Argonne premium coals and a model to simulate CO2 sequestration in coal," University of Pittsburgh (PhD Thesis), 2004.

[106] A. Dabrowski, "Adsorption - from theory to practice," *Advances in Colloid and Interface Science*, vol. 93, pp. 135–224, 2001.

[107] M. S. A. Perera, P. G. Ranjith, S. K. Choi, A. Bouazza, J. Kodikara, and D. Airey, "A review of coal properties pertinent to carbon dioxide sequestration in coal seams : with special reference to Victorian brown coals," *Environ Earth Sci*, no. 2000, 2010.

[108] A. Kim, "Estimating Methane Content of Bituminous Coalbeds From Adsorption Data," *US Bureau of Mines Report of Investigations*. Bureau of mines, Washington DC, p. 22, 1977.

[109] P. J. Crosdale, T. A. Moore, and T. E. Mares, "Influence of moisture content and temperature on methane adsorption isotherm analysis for coals from a low-rank , biogenically-sourced gas reservoir," *International Journal of Coal Geology*, vol. 76, pp. 166–174, 2008.

[110] C. R. Clarkson, R. M. Bustin, and J. H. Levy, "Application of the mono/multilayer and adsorption potential theories to coal methane adsorption isotherms at elevated temperature and pressure," *Carbon*, vol. 35, no. 12, pp. 1689–1705, 1997.

[111] J. Koresh, "The Langmuir Model in Ultramicroporous Adsorbents," *Journal of Colloid and Interface Science*, vol. 88, no. 2, pp. 398–406, 1982.

[112] K. S. W. Sing, D. H. Everette, R. A. W. Haul, L. Moscou, R. A. Pierotti, J. Rouquerol, and T. Siemieniewska, "Reporting Physisortion Data for Gas/Solid Systems with Special Reference to the Determination of Surface Area and Porosity," *Pure & Appl. Chem.*, vol. 57, no. 4, pp. 603–619, 1985.

[113] J. Medek, L. Kova, L. Kovar, and Z. Weishauptova, “Bond forms of methane in porous system of coal II,” *Fuel*, vol. 83, pp. 1759–1764, 2004.

[114] B. P. Bering, M. M. Dubinin, and V. V. Serpinsky, “Theory of volume filling for vapor adsorption,” *Journal of Colloid and Interface Science*, vol. 321, no. 4, pp. 378–393, 1966.

[115] G. R. R. Barker-Read and S. A. Radchenko, “The relationshio between the pore structure of coal and gas dynamic behaviour of coal seams,” *Mining Science and Technology*, vol. 8, pp. 109–131, 1989.

[116] G. D. Mitchell, “Behavior and effect of different coal microlithotypes during gas transport for carbon dioxide sequestration into coal seams,” *International Journal of Coal Geology*, vol. 53, pp. 201 – 217, 2003.

[117] G. R. L. Chalmers and R. M. Bustin, “The organic matter distribution and methane capacity of the Lower Cretaceous strata of Northeastern British Columbia , Canada,” *International Journal of Coal Geology*, vol. 70, pp. 223 – 239, 2007.

[118] M. Mastalerz, W. Solano-acosta, A. Schimmelmann, and A. Drobniak, “Effects of coal storage in air on physical and chemical properties of coal and on gas adsorption,” *International Journal of Coal Geology*, vol. 79, no. 4, pp. 167–174, 2009.

[119] R. E. Carroll and J. C. Pashin, “Relationship of Sorption capacity to coal quality: CO2 sequestration potential of coalbed methane reseviours in the Black Warrior Basin,” in *International Coalbed Methane Symposium Proceedings*, 2003, p. 11.

[120] C. Laxminarayana and P. J. Crosdale, “Role of coal type and rank on methane sorption characteristics of Bowen Basin , Australia coals,” *International Journal of Coal Geology*, vol. 40, no. 4, pp. 309–325, 1999.

[121] J. Milewska-Duda, J. Duda, A. Nodzeñski, and J. Lakatos, “Absorption and Adsorption of Methane and Carbon Dioxide in Hard Coal and Active Carbon,” *Langmuir*, vol. 16, no. 12, pp. 5458–5466, 2000.

[122] Z. Qing-ling, “Adsorption mechanism of different coal ranks under variable temperature and pressure conditions,” *J China Univ Mining & Technol*, vol. 18, no. 3, pp. 0395–0400, 2008.

[123] I. Ettinger, I. Eremin, B. Zimakov, and M. Yanovskaya, “Natural factors influencing coal sorption properties: I. Petrography and sorption properties of coals,” *Fuel*, vol. 45, no. 4, pp. 267–275, 1966.

[124] B. B. Beamish and P. J. Crosdale, “Instantaneous outbursts in underground coal mines : An overview and association with coal type,” *International Journal of Coal Geology*, vol. 35, no. 1–4, pp. 27–55, 1998.

[125] M. Mastalerz, H. Gluskoter, and J. Rupp, “Carbon dioxide and methane sorption in high volatile bituminous coals from Indiana , USA,” *International Journal of Coal Geology*, vol. 60, pp. 43 – 55, 2004.

[126] J. C. Pashin, “Stratigraphy and structure of coalbed methane reservoirs in the United States: An overview,” *International Journal of Coal Geology*, vol. 35, no. 1–4, pp. 209–240, 1998.

[127] G. Amarasekera, M. J. Scarlett, and D. E. Mainwaring, “Micropore size distributions interactions in coals,” *Fuel*, vol. 74, no. 1, pp. 115–118, 1995.

[128] E. Ozdemir and K. Schroeder, “Effect of Moisture on Adsorption Isotherms and Adsorption Capacities of CO2 on Coals,” *Energy & Fuels*, vol. 23, no. 5, pp. 2821–2831, 2009.

[129] J. H. Levy, S. J. Day, and J. S. Killingley, “Methane capacities of Bowen Basin coals related to coal properties,” *Fuel*, vol. 76, no. 9, pp. 813–819, 1997.

[130] D. H. Everett, “Adsorption Hysteresis,” in *The Solid-Gas Interface*, 2nd ed., E. A. Flood, Ed. New York: Marcel Dekker, Inc., 1967, pp. 1055 – 1113.

[131] J. I. Joubert, C. T. Grein, and D. Bienstock, “Sorption of methane in moist coal,” *Fuel*, vol. 52, no. 3, pp. 181–185, 1973.

[132] A. L. Goodman, A. Busch, G. J. Duffy, J. E. Fitzgerald, K. A. M. Gasem, Y. Gensterblum, B. M. Krooss, J. Levy, E. Ozdemir, Z. Pan, R. L. Robinson, K. Schroeder, M. Sudibandriyo, and C. M. White, “An Inter-laboratory Comparison of CO2 Isotherms Measured on Argonne Premium Coal Samples,” *Energy & Fuels*, vol. 18, no. 7, pp. 1175–1182, 2004.

[133] A. L. Goodman, A. Busch, R. M. Bustin, L. Chikatamarla, S. Day, and G. J. Duffy, “Inter-laboratory comparison II: CO2 isotherms measured on moisture-equilibrated Argonne premium coals at 55 ° C and up to 15 MPa,” *International Journal of Coal Geology*, vol. 72, pp. 153 – 164, 2007.

[134] R. C. Hartman and T. J. Pratt, “A preliminary study of the effect of moisture on the carbon dioxide storage capacity in coal,” in *International Coalbed Methane Symposium Proceedings*, 2005.

[135] P. L. Walker, Jr, 0 P. Mahajan, and M. Morishita, “Dynamic adsorption of carbon dioxide on microporous carbons,” *Carbon*, vol. 8, pp. 167–179, 1970.

[136] Z. Majewska and J. Ziętek, “Changes of acoustic emission and strain in hard coal during gas sorption–desorption cycles,” *International Journal of Coal Geology*, vol. 70, no. 4, pp. 305–312, May 2007.

[137] A. L. Goodman, R. N. Favors, J. W. Larsen, and R. N. Favors, “Argonne Coal Structure Rearrangement Caused by Sorption of CO2,” *Energy & Fuels*, vol. 20, no. 7, pp. 2537–2543, 2006.

[138] E. M. Suuberg, S. C. Deevi, and Y. Yun, “Elastic behaviour of coals studied mercury porosimetry by,” *Fuel*, vol. 74, no. 10, pp. 1522–1530, 1995.

[139] T. K. Green and T. D. Selby, “Pyridine Sorption Isotherms of Argonne Premium Coals : Dual-Mode Sorption and Coal Microporosity,” *Energy & Fuels*, vol. 8, no. 6, pp. 213–218, 1994.

[140] H. Briggs and R. P. Sinha, “Expansion and Contraction of Coal Caused Respectively by the Sorption and Discharge of Gas,” *Proc.R.Soc.Edinburgh*, vol. 53, pp. 48–53, 1933.

[141] H. Patel and P. J. Reucroft, “Gas-induced swelling in coal,” *Fuel*, vol. 65, pp. 816–820, 1986.

[142] S. Day, G. Duffy, R. Sakurovs, and S. Weir, “Effect of coal properties on CO2 sorption capacity under supercritical conditions,” *International j ournal of greenhouse gas control*, vol. 2, pp. 342–352, 2008.

[143] V. Romanov and Y. Soong, “Long-Term CO2 Sorption on Upper Freeport Coal Powder and Lumps,” *Energy & Fuels*, vol. 22, no. 2, pp. 1167–1169, 2008.

[144] M. Sander and J. J. Pignatello, “On the Reversibility of Sorption to Black Carbon: Distinguishing True Hysteresis from Artificial Hysteresis Caused by Dilution of a Competing Adsorbate,” *Environmental Science & Technology*, vol. 41, no. 3, pp. 843–849, 2007.

[145] J. W. Larsen, R. A. Flowers, P. J. Hall, and G. Carlson, “Structural Rearrangement of Strained Coals,” *Energy & Fuels*, vol. 11, no. 5, pp. 998–1002, 1997.

[146] B. A. Miller-chou and J. L. Koenig, “A review of polymer dissolution,” *Prog. Polym. Sci.*, vol. 28, pp. 1223–1270, 2003.

[147] P. J. Hall, K. M. Thomas, and H. Marsh, “The relation between coal macromolecular structure and solvent diffusion mechanisms,” *Fuel*, vol. 71, no. 11, pp. 1271–1275, 1992.

[148] A. S. Argon, R. E. Cohen, and A. C. Patel, “A mechanistic model of case II diffusion of a diluent into a glassy polymer,” *Polymer*, vol. 40, no. 25, pp. 6991–7012, 1999.

[149] A. Turner, Jr, E. F. Gurnee, and G. Lloyd, “Diffusion in Glassy Polymers,” *Journal of Polymer Science. Part C.*, vol. 261, no. 12, 1966.

[150] P. Opaprakasit and P. Painter, “Concerning the Glass Transition Temperature of Coal,” *Energy & Fuels*, vol. 17, no. 2, pp. 354–358, 2003.

[151] M. R. Khan and R. G. Jenkins, “Thermoplastic properties of coal at elevated pressures: Effects of gas atmospheres,” in *Proceedings of Conference on Coal Science*, 1985, p. 5.

[152] R. G. Wissinger and M. E. Paulaitis, “Swelling and sorption in polymer–CO2 mixtures at elevated pressures,” *Journal of Polymer Science Part B: Polymer Physics*, vol. 25, no. 12, pp. 2497–2510, 1987.

[153] V. Romanov, “Coal Chemistry for Mechanical Engineers : From Macromolecular Thermodynamics to Reservoir Simulation,” *Energy & Fuels*, vol. 21, no. 3, pp. 1646–1654, 2007.

[154] P. C. Painter, J. Graf, and M. M. Coleman, “Coal Solubility and Swelling . 1 . Solubility Parameters for Coal and the Flory Parameter,” *Energy & Fuels*, vol. 4, no. 14, pp. 379–384, 1990.

[155] P. J. Flory, *Principles of Polymer Chemistry*, 1st ed. Cornell University Press, 1953, p. 672.

[156] P. C. Painter, J. Graf, and M. M. Coleman, “Coal Solubility and Swelling. 3. A Model for Coal Swelling,” *Energy & Fuels*, vol. 4, no. 4, pp. 393–397, 1990.

[157] P. J. Reucroft and K. B. Patel, “Surface area and swellability of coal,” *Fuel*, vol. 62, no. March, pp. 279–284, 1983.

[158] C. O. Karacan and E. Okandan, “Adsorption and gas transport in coal microstructure : investigation and evaluation by quantitative X-ray CT imaging,” *Fuel*, vol. 80, pp. 509–520, 2001.

[159] T. Kiyama, S. Nishimoto, M. Fujioka, Z. Xue, Y. Ishijima, Z. Pan, and L. D. Connell, “Coal swelling strain and permeability change with injecting liquid/supercritical CO2 and N2 at stress-constrained conditions,” *International Journal of Coal Geology*, vol. 85, no. 1, pp. 56–64, 2011.

[160] E. Ozdemir, B. I. Morsi, and K. Schroeder, “Importance of Volume Effects to Adsorption Isotherms of Carbon Dioxide on Coals Importance of Volume Effects to Adsorption Isotherms of,” *Langmuir*, vol. 19, no. 23, pp. 9764–9773, 2003.

[161] Z. Pan and L. D. Connell, “A theoretical model for gas adsorption-induced coal swelling,” *International Journal of Coal Geology*, vol. 69, pp. 243 – 252, 2007.

[162] J. C. Jones, “Comments on recently reported results for solvent-induced swelling of coals,” *Fuel*, vol. 88, no. 5, p. 959, 2009.

[163] Y. Wu, J. Liu, D. Elsworth, Z. Chen, L. Connell, and Z. Pan, “Dual poroelastic response of a coal seam to CO2 injection,” *International Journal of Greenhouse Gas Control*, vol. 4, no. 4, pp. 668–678, 2010.

[164] W. R. Vieth, J. M. Howell, and J. H. Hsieh, “Dual sorption theory,” *Journal of Membmne Science*, vol. 1, pp. 177–220, 1976.

[165] J. Schuyer, H. Dijkstra, and D. W. van Krevelen, “Coal Science,” *Fuel*, vol. 33, p. 409, 1954.

[166] P. L. Walker, Jr, J. Rivera-utrillat, S. K. Verma, and A. Davis, “Densities , porosities and surface areas of coal macerals as measured by their interaction with gases , vapours and liquids,” *Fuel*, vol. 67, pp. 1615–1623, 1988.

[167] R. J. Pugmire, M. S. Solum, and D. M. Grant, “13C Solid-state NMR of Argonne Premium Coals,” *Energy & Fuels*, vol. 3, pp. 187–193, 1989.

[168] L. Lu, V. Sahajwalla, C. Kong, and D. Harris, “Quantitative X-ray diffraction analysis and its application to various coals,” *Carbon*, vol. 39, pp. 1821–1833, 2001.

[169] P. C. Painter, M. M. Coleman, R. G. Jenkins, P. W. Whang, and P. L. W. Jr, “Fourier Transform Infrared study of mineral matter in coal. A novel method for quantitative mineralogical analysis,” *Fuel*, vol. 57, no. 6, pp. 337–344, 1978.

[170] E. Yalcum and S. Durucan, “Methane capacities of Zonguldak coals and the factors affecting methane adsorption,” *Mining Science and Technology*, vol. 13, pp. 215–222, 1991.

[171] I. Ettinger, G. Lidin, and I. Eremin, “Natural factors influencing coal sorption properties: II. Gas capacity of coals found in weathering zone of coal deposits,” *Fuel*, vol. 45, no. 4, pp. 277–283, 1966.

[172] C. T. Miller and J. A. Pedit, “Use of reactive surface-diffusion model to describe apparent sorption-desorption hysteresis abiotoc degradation of lindane in a subsurface model,” *Environ. Sci. Technol.*, vol. 26, no. 7, pp. 1417–1427, 1992.

[173] J. J. Pignatello and Y. Lu, “Demonstration of the ‘ Conditioning Effect ’ in Soil Organic Matter in Support of a Pore Deformation Mechanism for Sorption Hysteresis,” *Environmental Science & Technology*, vol. 36, no. 21, pp. 4553–4561, 2002.

[174] Y. Kamiya, K. Mizoguchi, K. Terada, Y. Fujiwara, and J. Wang, “CO2 Sorption and Dilation of Poly (methyl methacrylate),” *Macromolecules*, vol. 9297, no. 97, pp. 472–478, 1998.

[175] B. Y. A. Bailey, D. A. Cadenhead, D. H. Everett, and A. J. Miles, “Low Pressure Hysteresis in the Adsorption of Organic Vapours by Porous Carbons,” *Trans. Faraday Soc.*, vol. 67, pp. 231–243, 1971.

[176] K. S. Rao, “Hyteresis in sorption I. Permanence of the Hysyteresis Loop. Titania gel-Water system,” *J. Phys. Chem.*, vol. 45, no. 4, pp. 500–506, 1941.

[177] K. S. Rao, “Hysteresis in sorption II. Scanning of the Hysteresis loop. Titania gel-water system,” *J. Phys. Chem*, vol. 45, no. 4, pp. 506–512, 1941.

[178] K. S. Rao, “Hysteresis in sorption III. Permanence and Scanning of the Hysteresis loop. Silica gel-water system,” *J. Phys. Chem.*, vol. 45, no. 4, pp. 513–517, 1941.

[179] K. S. Rao, “Hysteresis in Sorption. IV. Permanence and Scanning of the Hysteresis Loop. Silica Gel–Carbon Tetrachloride System.,” *J. Phys. Chem.*, vol. 45, no. 4, pp. 513–517, 1941.

[180] K. S. Rao, “Hysteresis in sorption V. Permanence, Scanning and Drift of the Hysteresis Lopp. Ferric Oxide Gel-Carbon Tetrachloride and Ferric Oxide gel-Water system,” *J. Phys. Chem.*, vol. 45, no. 4, pp. 522–531, 1941.

[181] K. S. Rao, “Hysteresis in sorption. VI Disappearance of the Hysteresis Loop. The role of elasticity of organogels in hysteresis in sorption. Sorption of some cereals,” *J. Phys. Chem*, vol. 45, no. 4, pp. 531–539, 1941.

[182] J. Medek, Z. Weishauptova, and L. Kovar, “Combined isotherm of adsorption and absorption on coal and differentiation of both processes,” *Microporous and Mesoporous Materials*, vol. 89, pp. 276–283, 2006.

[183] A. L. Goodman, L. M. Campus, and K. T. Schroeder, “Direct Evidence of Carbon Dioxide Sorption on Argonne Premium Coals Using Attenuated Total Reflectance-Fourier Transform Infrared Spectroscopy,” *Energy & Fuels*, vol. 19, no. 10, pp. 471–476, 2005.

[184] B. Cairncross, “An overview of the Permian (Karoo) coal deposits of southern Africa,” *African Earth Sciences*, vol. 33, no. 2001, pp. 529–562, 2006.

[185] C. J. Liu, G. X. Wang, S. X. Sang, and V. Rudolph, “Changes in pore structure of anthracite coal associated with CO2 sequestration process,” *Fuel*, vol. 89, no. 10, pp. 2665–2672, 2010.

[186] ISO 7404 - 2, “Methods for the petrographic analysis of bituminous coal and anthracite, Part 2: Method of preparing coal samples.,” *International Standards Organization*. Standards Organization International, South Africa, 1985.

[187] ISO 7404 - 3, “Methods for the petrographic analysis of bituminous coal and anthracite, Part 3: Method of determining maceral group composition.” International Standards Organization, South Africa, 1985.

[188] SABS SM 924, “Moisture content of coal sam-ples intended for general analysis: Vacuum oven method.” South African Bureau of Standards, South Africa, 1978.

[189] ISO 1171, “Solid mineral fuels – Determina-tion of ash content. Standards South Africa.” International Standards Organization, South Africa, 1997.

[190] ASTM D3176 - 09, “Standard Practice for Ultimate Analysis of Coal and Coke.” ASTM International, West Conshohocken, PA, 2006.

[191] S. Saha, B. K. Sharma, S. Kumar, G. Sahu, and Y. P. Badhe, “Density measurements of coal samples by different probe gases and their interrelation,” *Fuel*, vol. 86, pp. 1594–1600, 2007.

[192] M. Viana, P. Jouannin, C. Pontier, and D. Chulia, “About pycnometric density measurements,” *Talanta*, vol. 57, pp. 583– 593, 2002.

[193] S. Brunauer, P. H. Emmett, and E. Teller, “Adsorption of gases in multimolecular layers,” *Journal of the American Chemical Society*, vol. 60, no. 2, pp. 309–319, May 1938.

[194] E. L. Fuller, Jr, “Physical and Chemical Structure of Coals: Sorption Studies,” in *Coal Structure*, Vol 192., vol. 192 SV - 1, Oak Ridge: American Chemical Society, 1981, pp. 293–309.

[195] J. D. N. Pone, P. M. Halleck, and J. P. Mathews, “3D characterization of coal strains induced by compression , carbon dioxide sorption , and desorption at in-situ stress conditions,” *International Journal of Coal Geology*, vol. 82, no. 3–4, pp. 262–268, 2010.

[196] M. Inagaki, “Relations between structural parameters obtained by X-ray diffraction of various carbon materials,” *Carbon*, vol. 31, no. 7, pp. 1107–1113, 1993.

[197] M. Maphada, “Automation and validation of Volumetric Adsorption System,” University of the Witwatersrand (MSc Dissertation, under examination), 2012.

[198] P. V. Hemert, H. Bruining, E. S. J. Rudolph, K. A. A. Wolf, and J. G. Maas, “Improved manometric setup for the accurate determination of supercritical carbon dioxide sorption,” *Review of Scientific Instruments*, vol. 80, no. 035103, pp. 1–11, 2009.

[199] D. Li, Q. Liu, P. Weniger, Y. Gensterblum, A. Busch, and B. M. Krooss, “High-pressure sorption isotherms and sorption kinetics of CH4 and CO2 on coals,” *Fuel*, vol. 89, no. 3, pp. 569–580, 2010.

[200] P. Dutta, S. Harpalani, and B. Prusty, “Modeling of CO2 sorption on coal,” *Fuel*, vol. 87, pp. 2023–2036, 2008.

[201] National Institute of Standards and Technology, “NIST Chemistry WebBook,” 2011. [Online]. Available: http://webbook.nist.gov/chemistry/. [Accessed: 08-Sep-2011].

[202] J. Medek, “Possibility of micropore analysis of coal and coke from the carbon dioxide isotherm,” *Fuel*, vol. 56, no. 2, pp. 131–133, 1977.

[203] J. Clifford and W. O. Stacy, “The swelling and adsorption characteristics of Victorian brown coals,” *Fuel*, vol. 65, pp. 1171–1173, 1986.

[204] C. Tien, “Adsorption Calculation and Modeling,” in *Series in Chemical Engineering*, London: Butterworth–Heinemann, 1994.

[205] L. Cartz and P. B. Hirsch, “A Contribution to the Structure of Coals from X-Ray Diffraction Studies,” *Phil. Trans. R. Soc. Lond. A*, vol. 252, pp. 557–602, 1960.

[206] P. B. Hirsch, “X-Ray Scattering from Coals,” *Proc. R. Soc. Lond. A*, vol. 226, pp. 143–169, 1954.

[207] D. V. Niekerk, R. J. Pugmire, M. S. Solum, P. C. Painter, and J. P. Mathews, “Structural characterization of vitrinite-rich and inertinite-rich Permian-aged South African bituminous coals,” *International Journal of Coal Geology*, vol. 76, no. 4, pp. 290–300, 2008.

[208] G. R. Barker-Read and S. A. Radchenko, “The relationship between the pore structure of coal and gas-dynamic behaviour of coal seams,” *Mining Science and Technology*, vol. 8, pp. 109–131, 1989.

[209] B. K. Saikia, R. K. Boruah, and P. K. Gogoi, “XRD and FT–IR investigations of sub-bituminous Assam coals,” *Bull. Mater. Sci.*, vol. 30, no. 4, pp. 421–426, 2007.

[210] M. Mastalerz, A. Drobniak, R. Walker, and D. Morse, “Coal lithotypes before and after saturation with CO2 ; insights from micro- and mesoporosity , fluidity , and functional group distribution,” *International Journal of Coal Geology*, vol. 83, no. 4, pp. 467–474, 2010.

[211] M. Mastalerz, A. Drobniak, D. Strąpoć, W. Solano, and J. Rupp, “Variations in pore characteristics in high volatile bituminous coals : Implications for coal bed gas content,” *International Journal of Coal Geology*, vol. 76, pp. 205–216, 2008.

[212] P. Massarotto, S. D. Golding, J. Bae, R. Iyer, and V. Rudolph, “Changes in reservoir properties from injection of supercritical CO2 into coal seams — A laboratory study,” *International Journal of Coal Geology*, vol. 82, no. 3–4, pp. 269–279, 2010.

[213] S. U. Rege and R. T. Yang, “Pore size distribution of microporous materials using corrected Horvath-Kawazoe models,” *Journal of the Chinese Institute of Chemical Engineers*, vol. 33, no. 1, pp. 1–7, 2002.

[214] P. Kowalczyk, A. Ciach, and A. V. Neimark, “Adsorption-induced deformation of microporous carbons: pore size distribution effect.,” *Langmuir : the ACS journal of surfaces and colloids*, vol. 24, no. 13, pp. 6603–8, Jun. 2008.

[215] T. T. Tsotsis, H. Patel, B. F. Najafi, D. Racherla, M. A. Knackstedt, and M. Sahimi, “Overview of Laboratory and Modeling Studies of Carbon Dioxide Sequestration in Coal Beds,” *Ind. Eng. Chem. Res.*, vol. 43, no. 12, pp. 2887–2901, 2004.

[216] Y. Guo and R. M. Bustin, “Micro-FTIR spectroscopy of liptinite macerals in coal,” *International Journal of Coal Geology*, vol. 36, pp. 259–275, 1998.

[217] J. R. Connolly, “Introduction Quantitative X-Ray Diffraction Methods,” 2010.

[218] M. Inagaki and N. Iwashita, “Relations between structural parameters obtained by X-ray diffraction of various carbon materials,” *Carbon*, vol. 31, no. 7, pp. 1107–1113, 1993.

[219] N. Yoshizawa and K. Maruyama, “Stacking Structure Of Aromatic Layers In DTF Coal Chars And Its Relation To Gasification Property,” *National Institute of Advanced Industrial Science and Technology*, vol. 49, no. 1, pp. 37–38, 2004.

[220] X. Cao, M. Mastalerz, M. a. Chappell, L. F. Miller, Y. Li, and J. Mao, “Chemical structures of coal lithotypes before and after CO2 adsorption as investigated by advanced solid-state 13C nuclear magnetic resonance spectroscopy,” *International Journal of Coal Geology*, vol. 88, no. 1, pp. 67–74, Aug. 2011.

[221] G. R. L. Chalmers and R. M. Bustin, “On the effects of petrographic composition on coalbed methane sorption,” *International Journal of Coal Geology*, vol. 69, no. 4, pp. 288 – 304, 2007.

[222] R. J. Dombrowski, C. M. Lastoskie, and D. R. Hyduke, “The Horvath – Kawazoe method revisited,” *Colloids and Surfaces A: Physicochemical and Engineering Aspects*, no. 187–188, pp. 23 – 39, 2001.

[223] B. Ryan, “Pseudovitrinite : Possible Implications for Gas Saturation in Coals and Surrounding Rocks,” *British Columbia Geological Survey*, no. 2002. British Columbia Geological Survey, pp. 203–212, 2003.

[224] R. Sakurovs, S. Day, and S. Weir, “Causes and consequences of errors in determining sorption capacity of coals for carbon dioxide at high pressure,” *International Journal of Coal Geology*, vol. 77, no. 1–2, pp. 16–22, 2009.

[225] R. M. Gertenbach, “Methane and carbon dioxide studies on South African studies,” University of Stellenbosch (MSc Dissertation), 2009.

[226] G. K. W. Dawson, S. D. Golding, P. Massarotto, and J. S. Esterle, “Experimental supercritical CO2 and water interactions with coal under simulated in situ conditions,” *Energy Procedia*, vol. 4, pp. 3139–3146, 2011.

[227] P. J. J, “Conditioning-annealing studies of natural organic matter solids linking irreversible sorption to irreversible structural expansion Environ,” *Sci. Technol.*, vol. 40, p. 170, 2006.

[228] A. Busch, Y. Gensterblum, and B. M. Krooss, “High-Pressure Sorption of Nitrogen, Carbon Dioxide, and their Mixtures on Argonne Premium Coals,” *Energy & Fuels*, vol. 21, no. 3, pp. 1640–1645, 2007.

[229] A. Busch, Y. Gensterblum, and B. M. Krooss, “Methane and CO2 sorption and desorption measurements on dry Argonne premium coals: pure components and mixtures,” *International Journal of Coal Geology*, vol. 55, no. 2–4, pp. 205–224, Aug. 2003.

[230] K. Zarebska and G. Ceglarska-stefanska, “Sorption of carbon dioxide – methane mixtures,” *International Journal of Coal Geology*, vol. 62, pp. 211 – 222, 2005.

[231] A. D. Alexeev, E. P. Feldman, and T. A. Vasilenko, “Alteration of methane pressure in the closed pores of fossil coals,” *Fuel*, vol. 79, pp. 939–943, 2000.

[232] A. D. Alexeev, E. P. Feldman, and T. A. Vasilenko, “Methane desorption from a coal-bed,” *Fuel*, vol. 86, pp. 2574–2580, 2007.

[233] N. Siemons and A. Busch, “Measurement and interpretation of supercritical CO2 sorption on various coals,” *International Journal of Coal Geology*, vol. 69, no. 4, pp. 229 – 242, 2007.

[234] F. van Bergen, P. Winthaegen, H. Pagnier, P. Krzystolik, B. Jura, J. Skiba, and N. van Wageningen, “Assessment of CO2 storage performance of the Enhanced Coalbed Methane pilot site in Kaniow,” *Energy Procedia*, vol. 1, no. 1, pp. 3407–3414, Feb. 2009.

[235] A. Marzec, “Towards an understanding of the coal structure : a review,” *Fuel Processing Technology*, vol. 77–78, pp. 25 – 32, 2002.

[236] J. W. Larsen, C. S. Pan, and S. Shawver, “Effect of demineralization on the macromolecular structure of coals,” *Energy & Fuels*, vol. 3, no. 5, pp. 557–561, 1989.

[237] M. Polat, H. Polat, and S. Chander, “Physical and chemical interactions in coal flotation,” *Int. J. Miner. Process.*, vol. 72, pp. 199 – 213, 2003.

APPENDIX A
EFFECT OF SEPARATING MEDIA ON COAL SURFACE PROPERTIES

Inorganic and organic solvents are commonly used as separating media for laboratory scale sample preparation. Both techniques have advantages and disadvantages from safety to cost but both are effective at separating coal macerals based on density (commonly known as heavy media separation). However, the major potential disadvantage of both techniques is the possibility of the separating media (organic or inorganic) interacting with the coal's chemical and physical structure and thus altering its properties. In order to ensure that the separating media did not affect the coal structure, a study was undertaken on organic and inorganic solvents. The coal structure was analysed before and after separation using the inorganic and organic solvent respectively.

A.1 General procedure and solvents used

The organic solvents used in this project were chloroform and benzene. Benzene has a specific gravity (S.G) of 0.88 g/cm^3 and chloroform an S.G. of 1.48 g/cm^3. The inorganic solvent used was zinc chloride. The zinc chloride came in the form of a salt and was diluted with water and a S.G. of 1.3 g/cm^3 was obtained.

The chemicals were mixed accordingly to achieve the required S.G's of 1.3 g/cm^3 and 1.5 g/cm^3 for both the organic and inorganic solvents. The mass of the coal was weighed and firstly separated using the mixture with a S.G. of 1.3 g/cm^3. The coal was left in the mixture until it separated into a float and sink product with a clear band of liquid between the two. The floats were then removed and dried using filter paper, a Buchner funnel and a pump to remove residual chemicals.

The same procedure was followed for the sink sample. When both the float and the sink samples were dry the mass of each was recorded again. The sink generated at S.G. 1.3 g/cm^3 was placed in a solution with a S.G. of 1.5 g/cm^3. The 1.5 g/cm^3 solution was left until there was a clear distinction between the float sink and float samples. The float and sink were removed and dried, and their mass was taken.

Organic solvents are highly volatile, so the samples were left overnight in the fume hood and were dry the next morning; no washing was required. After the sink and float were obtained, it was necessary to wash the zinc chloride off the coal, as unlike the organic solvents, zinc chloride could possibly remain on the coal surface affecting the properties of the coal. After being washed thoroughly with distilled water, the samples were dried overnight in a drying oven.

In analysing for any change in surface properties it was decided that the coal sample needed to be put back together according to the mass percentages that were obtained during the separation. This would mean that the petrographic constituents of the parent coal and those of the separated and re-mixed sample would be more comparable, thus making it possible to detect and compare any changes in surface properties between the parent and the re-mixed coal. It was for this very reason that the mass fractions of every separation were recorded. Figure A-1 shows a flow diagram for the experimental method used to determine the best solvent for isolating maceral-enriched samples with minimal structural changes.

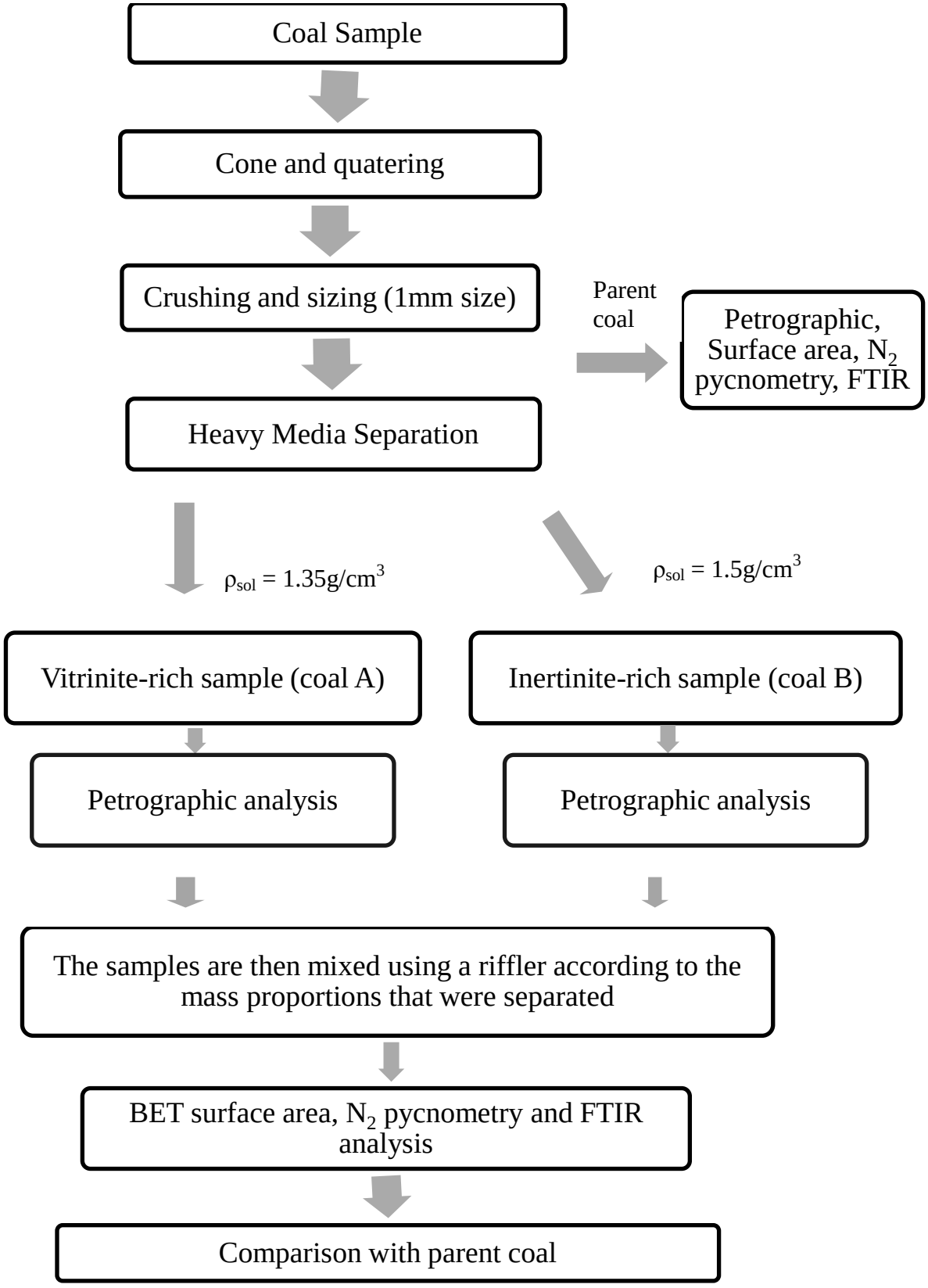

Figure A-1: Flow diagram for experimental method used to determine the best solvent for isolating maceral-enriched samples with minimal coal structural changes.

A.1.1 Results

Petrographically the separation using both the solvent types was effective, with a vitrinite-rich fraction obtained at S.G. of 1.3 g/cm3 and inertinite-rich fraction obtained at 1.5 g/cm3 (see Appendix E.1for results).

A.1.2 BET Surface properties

The results from the BET surface measurements are presented in

Figure **A-2** and Figure A-3 for average pore diameter and surface area, respectively.

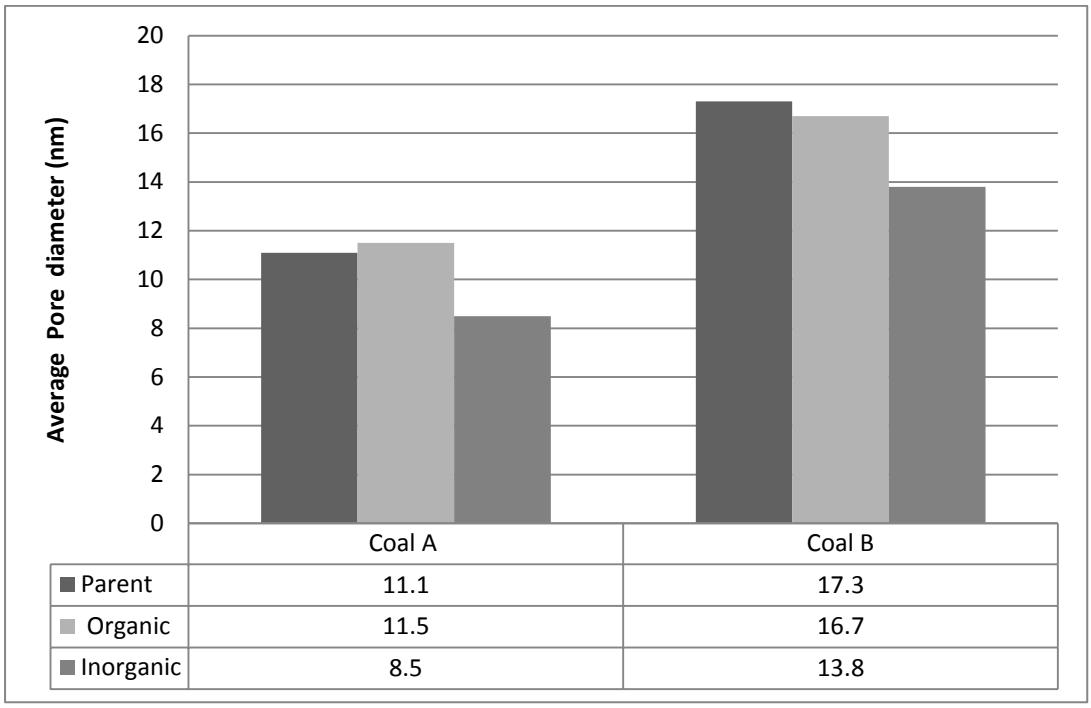

Figure A-2: Average pore diameter as measured by N_2 Surface area of coal A and coal B samples before and after density separation with organic and inorganic solvents.

In Figure A-2, the average pore diameter of both coal A and coal B are slightly affected by both organic and inorganic solvents. However, the organic solvent shows a much smaller variance (average 3.5%) to the parent coal's pore diameter than the inorganic solvent (average 22%).

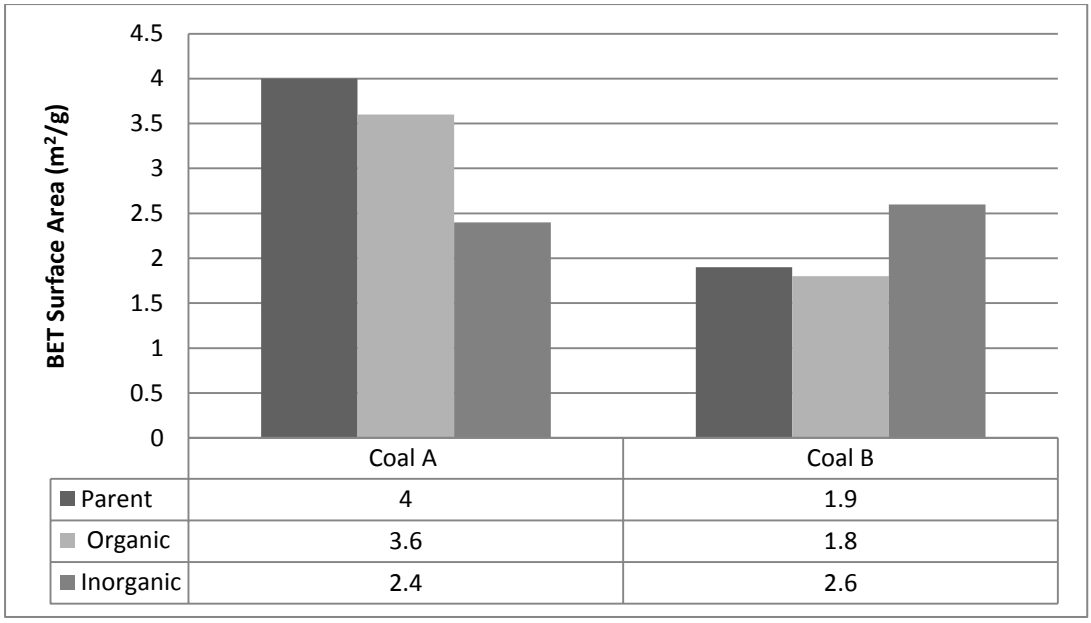

Figure A-3: BET surface area of coal A and coal B samples before and after density separation with organic and inorganic solvents

In Figure A-3, a similar trend for the BET surface area is observed where the variance for the organic solvent was found much lower than the variance for inorganic solvent at an average of 7.6% and 38.4%, respectively. Interestingly, the inorganic sample shows a different effect on coal A surface area when compared to coal B's surface area. Coal A inorganically separated sample surface area is lower than the parent coal's whereas coal B's organically separated sample is much higher than parent coal surface are.

It is evident from Figure A-2 and Figure A-3 that the organically separated samples have a better deviation from the parent coal's surface properties. The results also indicate that there is some slight effect on the coal properties but that the effect is negligible for the organically separated samples.

A.1.3 Density pycnometry (N_2) measurements

The density of the different parent and composite coals (organically and inorganically separated samples) was measured by a pycnometer. The gas used was nitrogen and density of

each sample was measured twice for accuracy. The results obtained are presented in Table A-1 and

Table **A-2**.

Table A-1: Nitrogen pycnometry analysis for coal A

Sample ID	Density ($g.cm^{-3}$)			%Change
	1st run	*2nd run*	*average*	
Parent	3.58	3.39	3.485	-
Organic	3.06	3.02	3.04	12.76901
Inorganic	2.91	2.98	2.945	15.49498

Table A-2: Nitrogen pycnometry analysis for coal B

Sample ID	Density ($g.cm^{-3}$)			% Change
	1st run	*2nd run*	*Average*	
Parent	3.22	3.25	3.235	-
Organic	2.98	3.02	3	7.2643
Inorganic	2.9	2.89	2.895	10.51

Table A-1 and

Table **A-2** show that both solvents decrease the density of the coal. The inorganic solvents however decrease the density more than the organic solvents. The decrease in coal A density is slightly higher than coal by about 5%. Since density is mass divided by volume it means that at constant mass the solvents increased the volume of the coal.

The reason the organic solvent shows a lower density change can be attributed to its non-polar character, which means that it does not interact as much with the coal structure as the inorganic solvent does.

A.1.4 FTIR

The parent coal and composite coals were also analysed for surface functionality effects. In Figure A-4, the FTIR results for (s) coal A and (b) coal B's parent, organically separated and inorganically separated samples are presented.

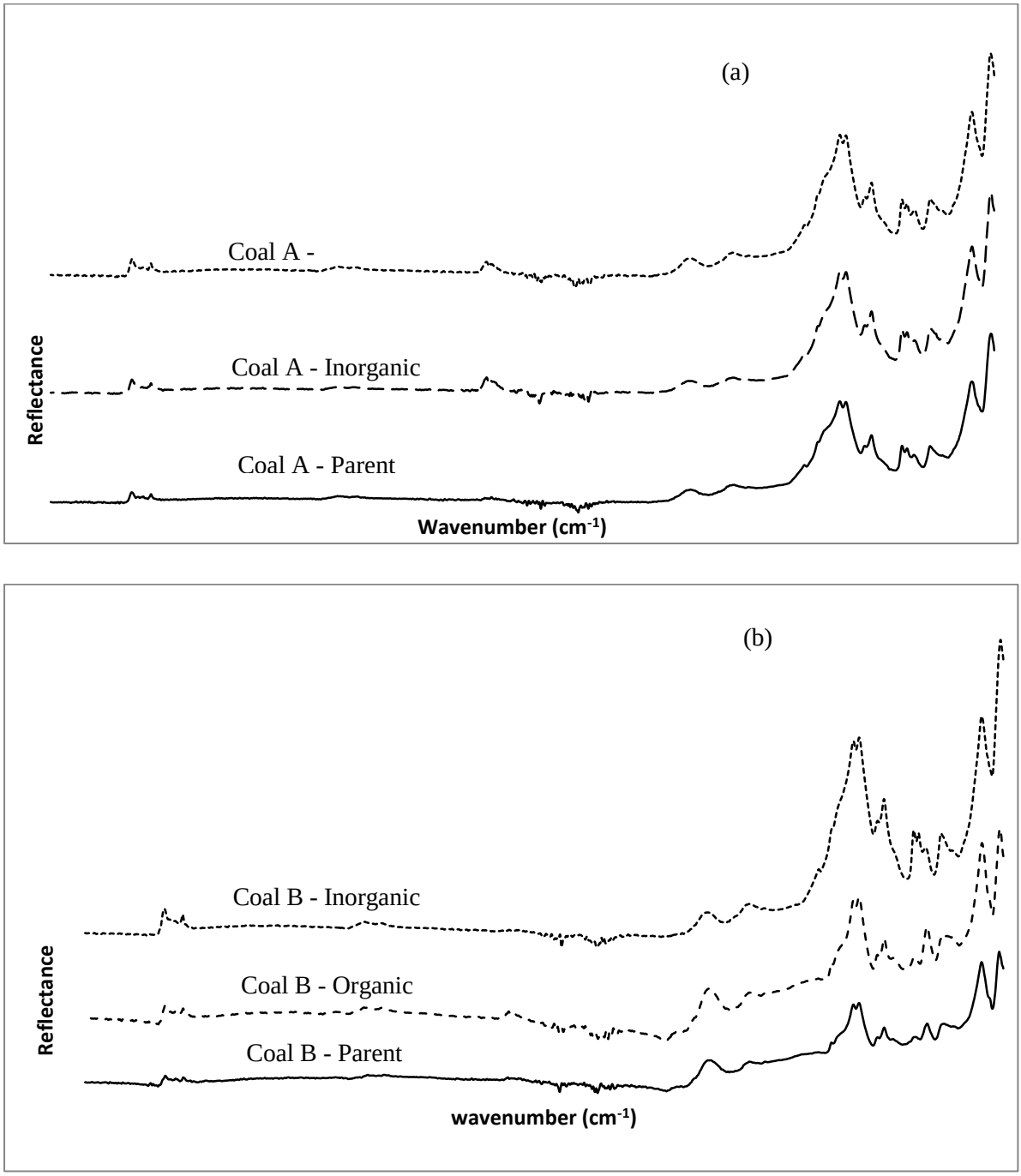

Figure A-4: A comparison of the FTIR spectra for different (a) coal A and (b) coal B samples

From Figure A-4 it can be seen that all of the coals have the same trend of reflectance, this means that they all have the same functional groups. The identical trends indicate that both the organic and inorganic separating media did not affect the functional groups present in coal.

A.2 Conclusion

The aim of this sub-study was to determine the effects of separating media on coal properties and to determine the suitable solvent for performing density separation. It can now be concluded that the separating media does have a slight effect on the coal's properties. More specifically, on the average pore diameter, surface area and density. There was no change observed for surface functionality for both organically separated and inorganically separated coals. Where a change was observed, it was found to be small, at 10% or less, for organically separated samples. Thus it was decided to use the organically separated samples for the rest of the study.

APPENDIX B

HELIUM DENSITY PYCNOMETRY

B.1.1 Theory

A Stereopycnometer is an instrument specifically designed to measure the volume of solid objects. This is accomplished by employing Archimedes' principle of fluid displacement to determine the volume. The displaced fluid is a gas which can penetrate the finest pores to assure maximum accuracy. For this reason, helium is recommended since its small atomic dimension assures penetration into crevices and pores approaching one Angstrom (10^{-10}m). Its behaviour as an ideal gas is also desirable. Other gases such as nitrogen can be used, often with no measurable difference.

Pycnometry is a technique that measures the true volume of solid objects. The material is, after preparation and possible activation, i.e. degassing at elevated temperatures, put in a cell of known volume which after evacuation is filled with a known mass of Helium gas. Assuming helium neither to be adsorbed nor absorbed, the volume of the sorbent material (mass: which is impenetrable to the helium molecules, i. e. the so-called helium volume of the material, can be calculated from a mass balance of this gas expansion experiment.

$$m_{He} = \rho_{He}(V_{SC} - V_{He}^{s}) \qquad (1.3)$$

Viz:

$$V_{He}^{s} = V_{SC} - m_{He}/\rho_{He} \qquad (1.4)$$

Where m_{He} is the mass of helium gas, V_{SC} is the volume of the sample cell, $\rho_{He} = \rho_{He}(p,T)$ is the density of the helium gas which can be determined from measured data of pressure (P) and temperature (T) normally by using the ideal gas equation of state (EOS) or a standardized real gas EOS, and V_{He}^{s} is the helium true density of the solid.

B.1.2 Sources of Errors

Sources of errors include non-ideal gas behaviour. Equations used in Helium pycnometry are derived using the equation of state for an ideal gas; therefore, dry helium is recommended for use in a stereopycnometer. However, dry nitrogen can also be used at room temperature. When analysing vegetable matter, materials containing cellulose or low density polymers (including foams) it is recommended that nitrogen or sulphur hexafluoride (SF6) be used instead of helium because helium can diffuse into the solid matter and across cell walls. If air or other gases which contain absorbable impurities are used, the pressure readings will be affected due to adsorption on the powder surface.

The extent of the resulting error depends upon the amount and nature of the impurities as well as the solid's surface area. Many samples contain impurities on their surface and within pores. The presence of these impurities can affect the results in several ways: (i) The actual weight of the sample is less than the weight indicated when weighed. (ii) Contaminants fill pores causing a larger sample volume to be observed. (iii) Volatile impurities will cause erroneous readings. Successive density determinations yielding results trending in one direction usually can be taken to mean that contaminants are being removed after each depressurization. Measurements should be continued until two or three successive determinations are made to within 0.2%. Another indication of the presence of volatile contaminants is a gradual pressure increase when the sample is isolated after purging with clean He. This occurs as the contaminants leave the surface and establish an equilibrium partial pressure.

An additional source of error caused by high surface area powders is the annulus volume created between the powder surface and the centre of mass of the gas phase molecules at the interface. Assuming that the closest approach of the centre of mass of the gas molecules to the powder surface is 0.5Å, 5×10^{-11} meter, and that the powder surface is in the order of 1000 square meters per gram, there will exist an annulus volume of 5×10^{-8} cubic meters (5×102 cm^3) per gram of powder. Thus, with the large samples, 10 grams or so of high specific surface area, volume errors of 0.5 cm^3 can occur. Corrections for this error can be made with knowledge of the gas molecules' effective diameter (i.e., Van der Waals diameter) and the powder's specific surface area.

APPENDIX C

VOLUMETRIC ADSORPTION SYSTEM

C.1 Components description and specifications

A volumetric instrument for measurements of pure gas adsorption basically consists of a gas storage cell and an adsorption cell being connected by a tube bearing a valve. Both cells are completely placed within a thermostat (air) and provided with tubes for gas supply and evacuation as well as with thermometers and manometers to measure the temperature and pressure inside the cells.

C.1.1 Piping and Fittings

Each cell is provided with four pipes of ¼" allowing instrumentation (tubing, device inputs etc). For pressures above ambient all cells and tubes were manufactured of stainless steel, inside surfaces were electropolished. CO_2 is non-corrosive but the high pressures necessitated the use of metallic sealings (stainless steel).

C.1.2 Cells

The same kind of cell was used for fluids which are subcritical at the ambient temperature and supercritical at the experimental temperature. CO_2 is super critical at ≈31.1˚C and 7.39MPa (73.9 bar). In cases when the experiment is performed above these supercritical conditions, the cell is filled with liquid–vapour equilibrium at ambient temperature, and then put into the incubator at the experimental temperature. The quantity to be introduced is estimated beforehand so that the pressure of the supercritical gas at the experimental

temperature is high enough to provide the maximum pressure required at the end of the experimental procedure (generally 13 000 kPa for a final pressure of 10 000 kPa).

The adsorption cell includes a sample of sorbent material of mass which prior to measurement should have been "activated" (i.e degassed) at higher temperature and in vacuum for several hours to reduce the amount of pre-adsorbed molecules. When lump coals or drill core coal samples are the adsorbent, a cell with a higher volume is used. This stainless steel cell has an internal volume of about 1201cm^3 and was specially designed to withstand high temperature and pressure conditions (333 K and 16 000 kPa). For pulverized coals, smaller cells are used so that the void is proportionally reduced. The cell has an internal volume of about 53cm^3

C.1.3 The Oven

A ventilated incubator ensures a constant temperature in the whole installation (adsorption cell/cell, piping circuit, gas cell/cell), providing temperatures from ambient to 333 K. The oven had a regulation accuracy of 0.3 K. The maximum temperature gradient in the incubator was 1 K. The internal wall of the incubator is thermally insulated. Hole(s) in a wall were necessary to allow for physical connections between the installation and the components located outside the incubator, i.e. temperature measurements the pressure transducers, the pipe to the vacuum pump, the pipe to the gas cylinder, the electrical connections of the temperature sensor, and electrovalves.

C.1.4 The temperature sensor

For temperature measurement, a 4 wire Pt100, RTD sensor with ¼" NPT was used for temperature measurements working between 233 and 493 K with an absolute accuracy of 0.1 K. It was located in the reference cell and sample cell.

C.1.5 The pressure transducers

The experimental procedure required the use of two pressure transducers (PT-1 and PT-2). The transducer has a sensor working on the piezoresistive principle using a polysilicon sensor (Endress + Hauser, Cerabar S PMP 71). It can operate between 0 and 25MPa (0-250bar). The relative measurement accuracy is 0.075% of the operating range, i.e. 0.75 to 18.75 kPa. It was supplied by a 24 V DC voltage and it provides a 4–20 mA DC output current. Any temperature change is responsible for a shift which can be estimated to 300 Pa/10 K. The pressure transducer can operate at process temperatures up to 473 K. However, its use is not advised in the case of simultaneous high temperature and low pressure (lower than 20 kPa).

C.1.6 Valves, electrovalves and piping equipment

High-pressure pneumatic-valves (WIKA) with special solenoids for high temperatures were used. They can operate with maximum differential and absolute pressures of 200 000 kPa and for ambient temperatures ranging from 253 K to 423 K. They limit the use of the experimental device at a maximum temperature of 423 K. They are supplied by a 24V DC voltage and play an important role in the automation of the experimental procedure.

Stainless steel mixing valve (Swagelok), operating at ambient temperatures up to 588 K and for differential and absolute pressures up to 20 000kPa, was used for the parts of the experiment which are not automated.

A filter (Swagelok) protects the installation against adsorbent dust. It is made of stainless steel with a filtering matrix consisting of wire mesh which retains particles of diameter larger than 7 μm. It can operate at pressures up to 41 300 kPa and at ambient temperatures up to 755 K.

C.1.7 The vacuum pumping system

A classical two-stage vacuum pump was used. The lowest achievable pressure is 1 Pa (dynamic vacuum). Such a pressure cannot be measured by either PT-1 or PT-2. Given we do not want to measure adsorption data at low pressure, our only requirement during this pumping process is the cleanness of the sample. Studies have shown that a 1 kPa vacuum level is sufficient if the other outgassing parameters (temperature, time) are optimized. Tests will be done to optimize these parameters.

C.2 The data acquisition and control system

The main part of the experimental procedure was semi-automated. A computer equipped with a data acquisition system (I/O – NI 9203 8-Channel +/-20mA, 200kS/s, 16-Bit analog Input Module) and a control unit (CPU – cRIO-9073 8-slot Integrated 266Mhz 17,990.00 Real-Time Controller and 2M Gate FPGA) permits automated acquisition of the temperature, pressure and valve signals. LabView was used as the software to monitor and control the experiment. Figure C-1 shows a data flow diagram for the whole system (devices and control systems)

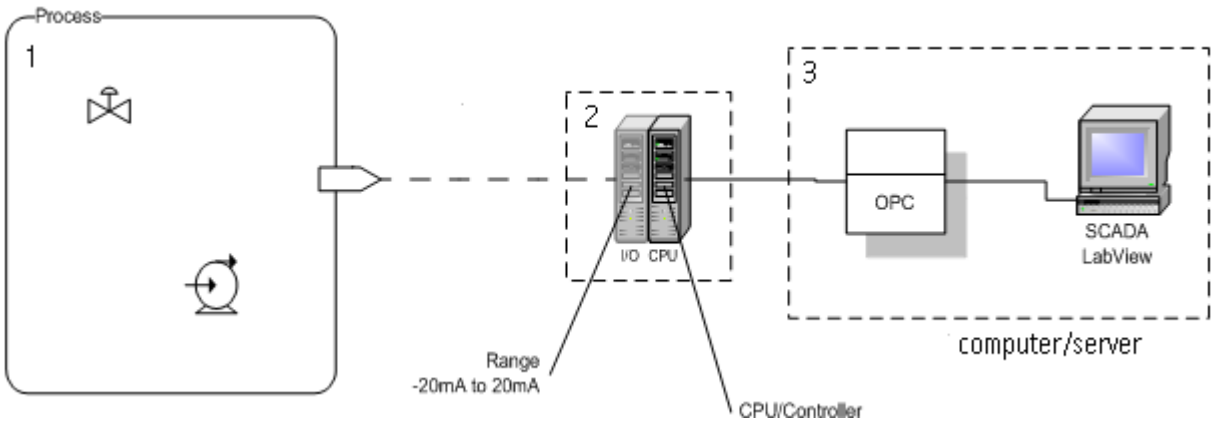

Figure C-1: Data flow diagram from devices and control system. 1-data collected from devices, 2-then signal is converted from digital to analog using an 8 channel module

I/O, 3-the data is then processed and controlled by a CPU via OPC[19] and using LabView as the software

The algorithm for data acquisition and control was developed in-house in collaboration with JAD systems.

C.3 Automated Operation

The automated operation enables the equipment to operate automatically (see Figure C-2). The volumetric adsorption system is supported by a pc and a control panel for control and data acquisition.

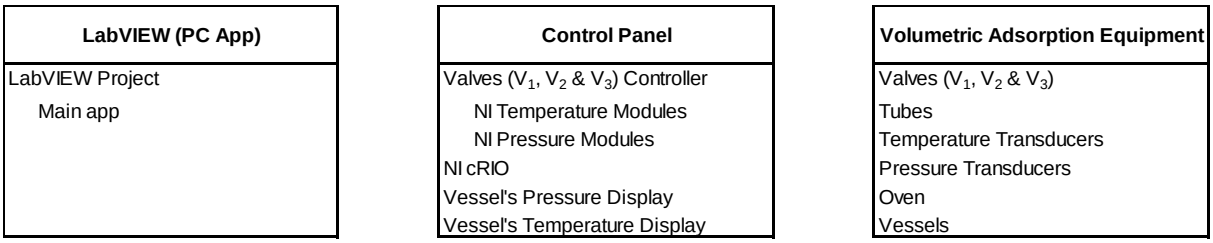

Figure C-2: Systematic View of the Controlled Experimental Setup

The NI cRIO used in this project is labelled NI-cRIO9073-0142A90D with the IP Address 192.168.0.191 in the network of the University of the Witwatersrand. The cRIO can only connect to the designated desktop pc in order to avoid corruption.

In order to operate the system automatically, the operator switches the control panel key on so that the compact RIO (NI cRIO) can be turned on. Connects the pc and the cRIO using a network cable to enable the link of the two and then launch the LabVIEW software. Then, opens the project labelled abspro.lvproj in the desktop of LabVIEW.

[19] OPC – OLE for Process Control, is an industry standard created with the collaboration of a number leading worldwide automation hardware and software suppliers, working in cooperation with Microsoft. The standard defines methods for exchanging realtime automation data between PC-based clients using Microsoft operating system

After this, deploy the cRIO in the project and then open the VI (Virtual Interface) labelled main.vi. While all the valves' control buttons in the control panel are off, switch the mode trigger from manual to LabVIEW to enable the pc automatic control of the volumetric adsorption system. **Figure C-3** below shows the interface of main VI:

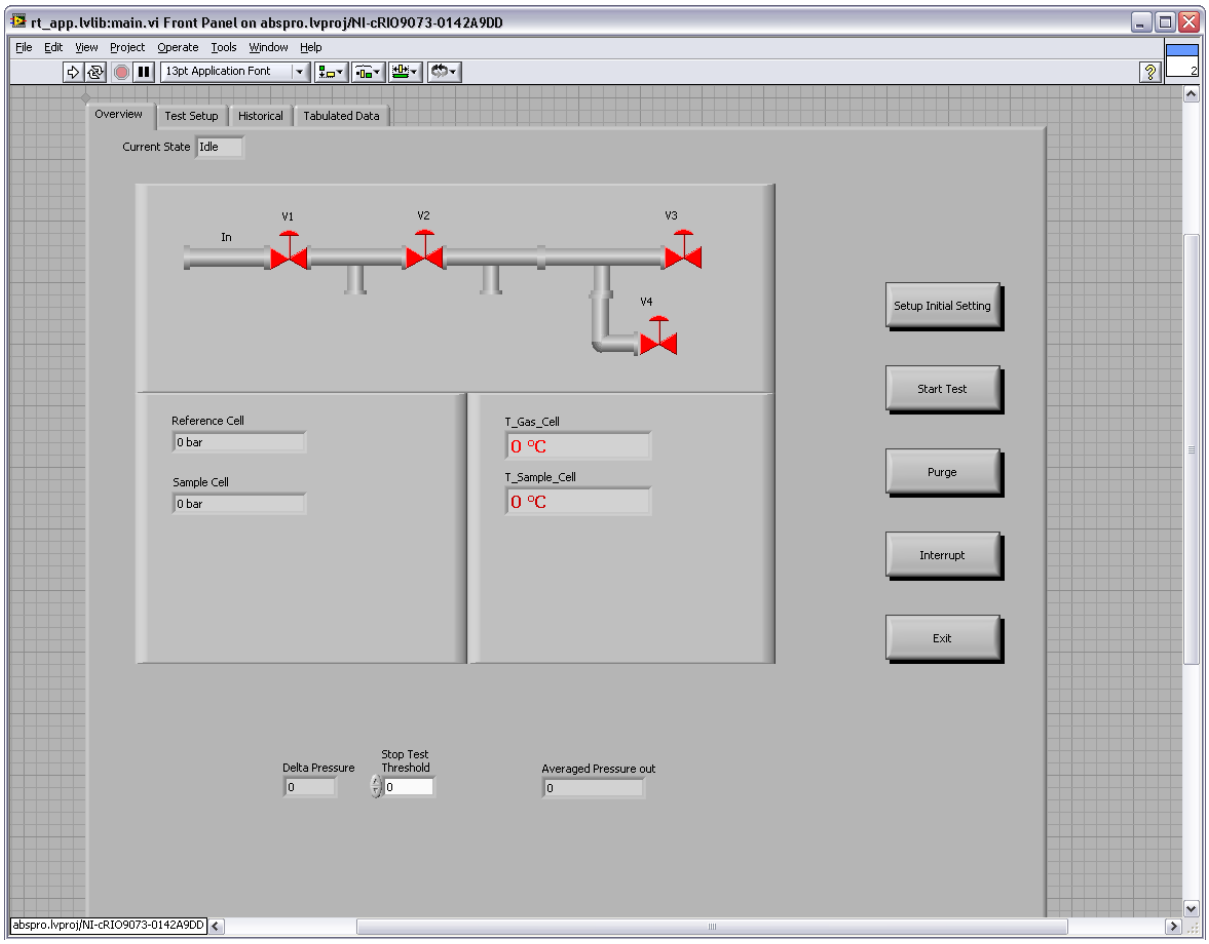

Figure C-3: View of the main.vi interface

C.3.1 Automated data collection

An automated operation of the equipment enables the equipment to function with less human intervention. Figure C-4 to Figure C-8 show the pressure-temperature profiles of each experimental point against time. Each experimental point of the run was set to operate for up to 90 minutes (1800 seconds), although higher equilibration times were for the . However, Figure C-4 to Figure C-8 only shows data in the first 150 seconds of the run. This was done

to show the temperature and pressure profiles from the beginning and the other part of the period is not shown because the changes are small. According to Figure C-4 to Figure C-8 shows the reference cell pressure decreases while the sample cell temperature increases to a value almost equal to that of the reference cell. Note T_1 and P_1 are the Temperature and Pressure of the reference cell respectively, while T_2 and P_2 are the Temperature and Pressure of sample cell respectively. The temperature difference is due to the regulation [197].

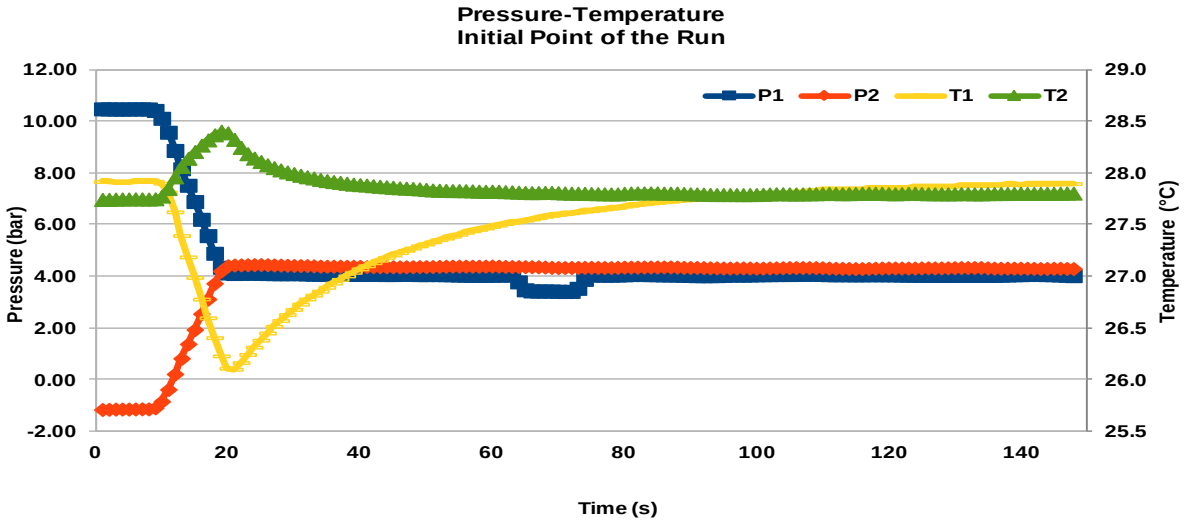

Figure C-4: Pressure-Temperature profile of the first point at 28 °C and reference pressure of 10 bar (the 1st 150 seconds of this pressure step) and the equilibration pressure amounting to 4 bar

The negative pressure (P_2 = -1.1 bar) is a gauge pressure and indicates the sample cell is approximately equals to 0 bar (vacuum = absolute pressure). The hook between the 60 and 80 seconds can be attributed to the beginning of the adsorption process.

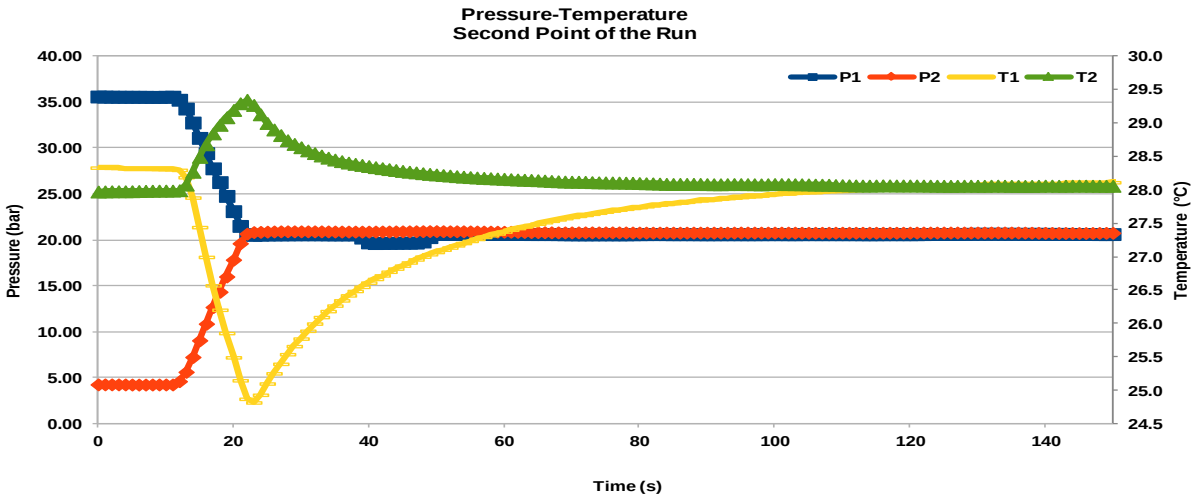

Figure C-5: Pressure-Temperature profile of the second point at 28 °C and reference pressure of 35 bar (the 1st 150 seconds of this pressure step) and the equilibration pressure amounting to 20 bar

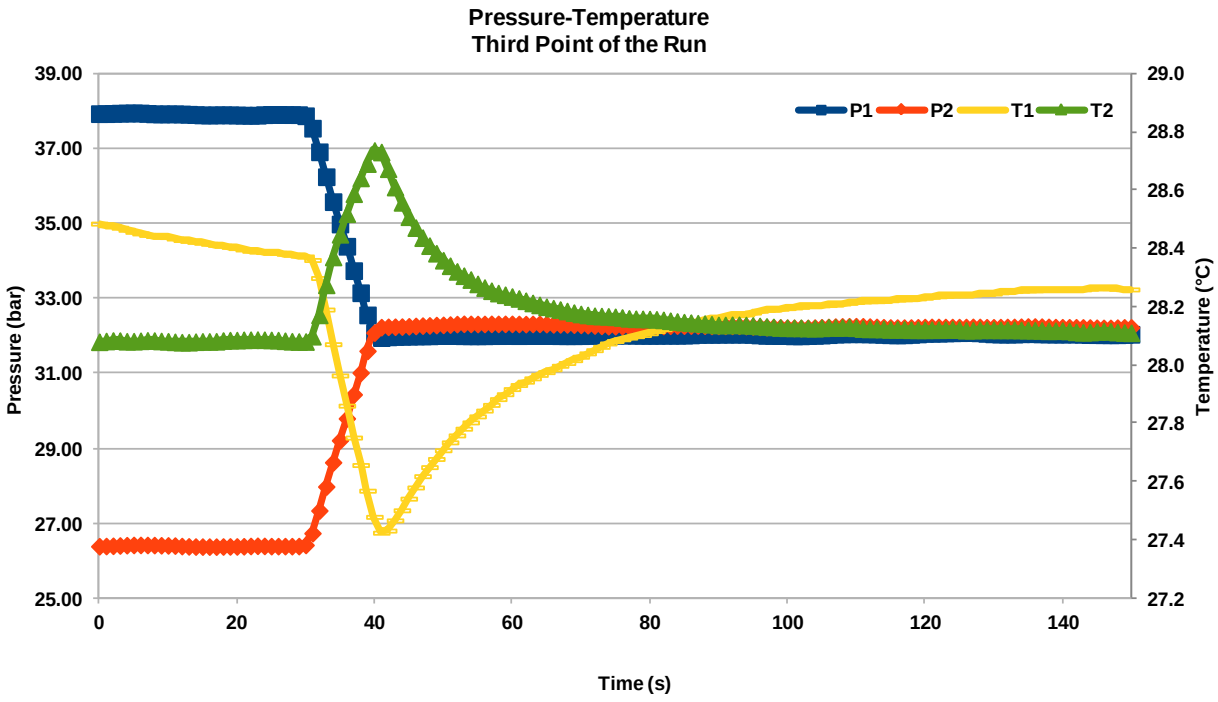

Figure C-6: Pressure-Temperature profile of the third point at 28 °C and reference pressure of 38 bar (the 1st 150 seconds of this pressure step) and the equilibration pressure amounting to 32 bar

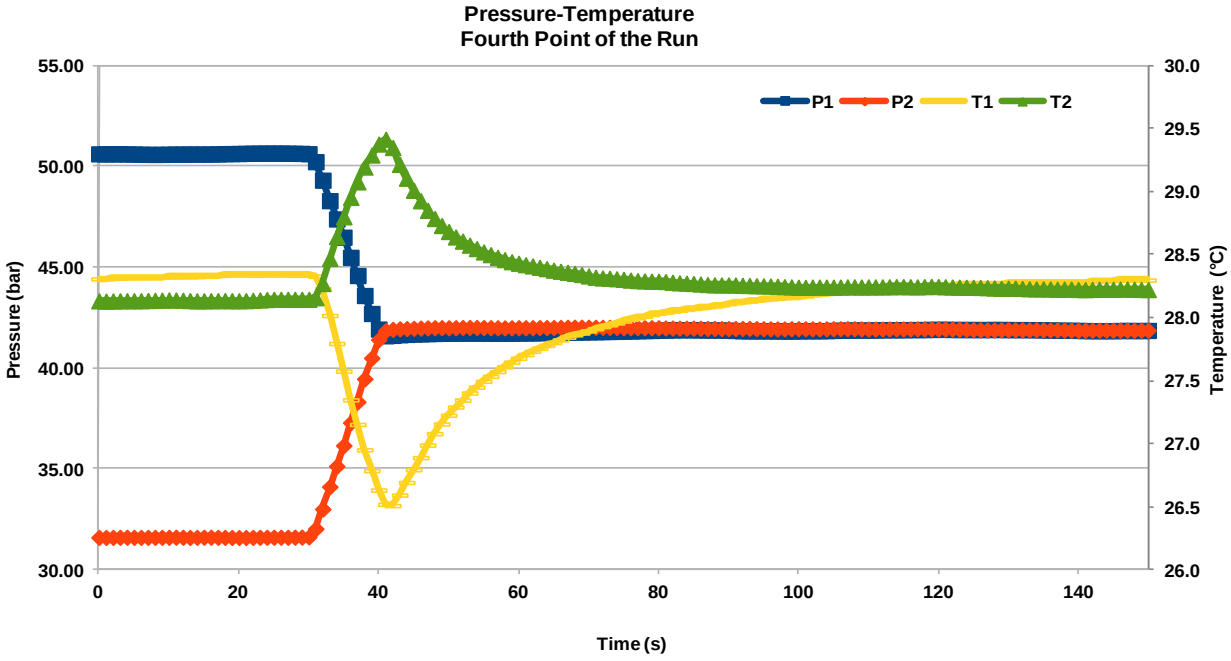

Figure C-7: Pressure-Temperature profile of the fourth point at 28 °C and reference pressure of 50 bar (the 1st 150 seconds of this pressure step) and the equilibration pressure amounting to 45 bar

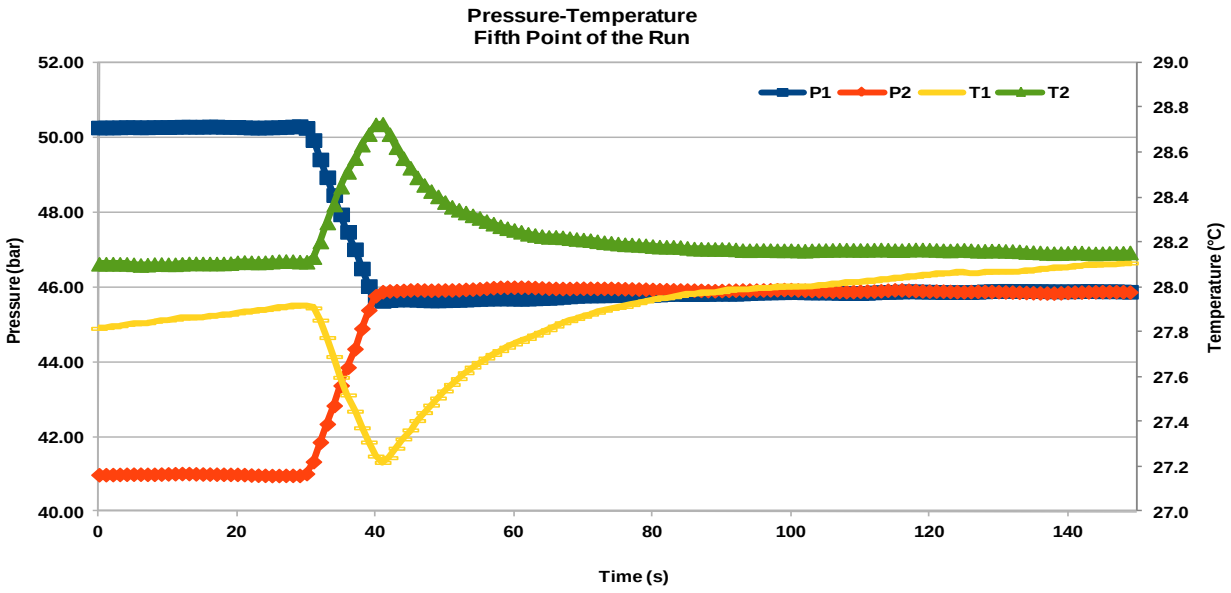

Figure C-8: Pressure-Temperature profile of the fifth point at 27 °C and reference pressure of 50 bar (the 1st 150 seconds of this pressure step) and the equilibration pressure amounting to 45 bar

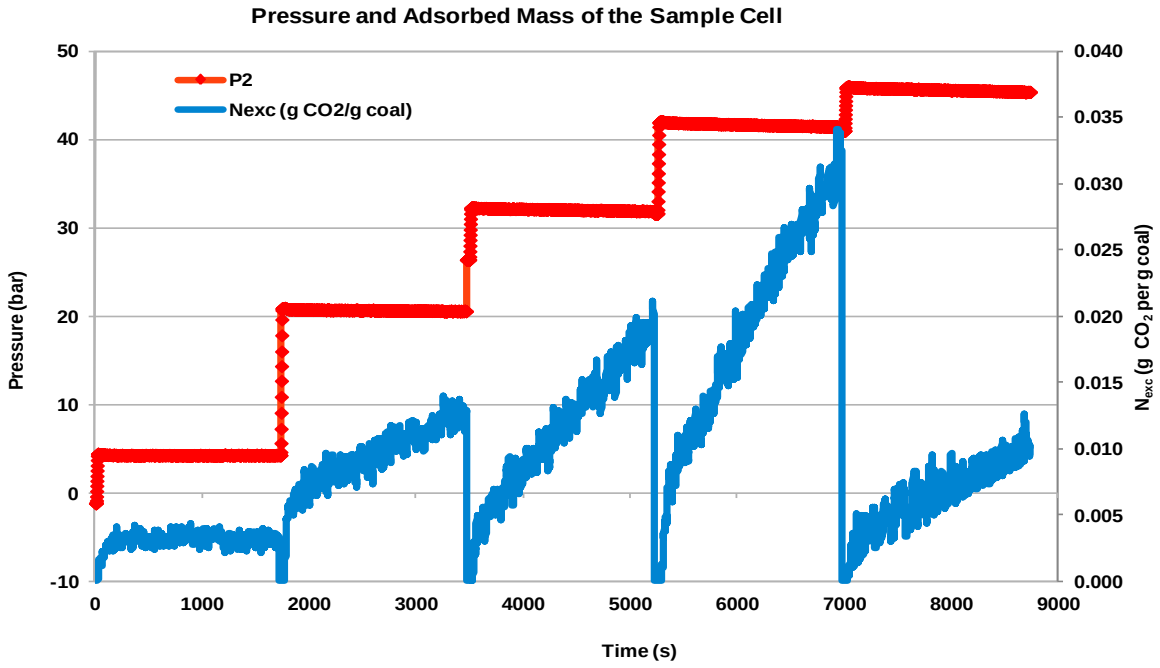

Figure C-9: Pressure and Adsorbed amount profile as a function of time.

Figure C-9 shows the adsorbed amount change with respect to time and pressure at constant temperature of 28 °C. Negative pressure means the sample sell was sucked to vacuum. P_2 = -1.1 bar is a gauge pressure. P_2 is the sample cell gas pressure. n^{exc} (g CO_2 per g coal) is the excess number of moles in the sample cell, which is the adsorbed amount. The run shown in Figure A-3 has five experimental steps which can also be viewed in the form of Figure C-4 to Figure C-8 excess isotherms. The data for the initial point is between 0 and 1723 seconds, the second point is between 1722 and 3470 seconds, the third point between 3469 and 5230 seconds, the fourth point between 5229 and 6980 seconds, and the fifth point is between 6979 and 8745 seconds. Each point of the run was operated for 30 minutes from the time adsorption is N_{exc} greater than zero [197].

C.4 Commissioning of the Volumetric Adsorption System

The following are experiences which were encountered during the commissioning phase of the project, which were taken as learning's to improve the equipment and the analytical procedure.

C.4.1 Leaks and Pressure

V_1 leaked the gas into the reference cell at pressures of greater than 100 bar and constant temperature of 28 °C; below 90 bar the leak rate was more stable. However, leaks were stopped by changing the seal in the sample cell regularly (after three runs), and ensuring the nuts of the cell and line were tightened. Leaks were tested by the use of the soap solution test method.

C.4.2 Oven

The oven is dependent on the room temperature air and is therefore unable to cool to operate at temperatures below the room temperature. Hence, it is recommended that the experiments should be performed at temperatures greater than room temperature, which may be seasonal. The operational temperature was 28 °C in the winter period and was kept constant by frequently venting the 'hot' air with a compressed air hose.

C.4.3 LabVIEW

If LabVIEW is frozen, the solution is to reboot cRIO (compact RIO), but if the dilemma persists restart cRIO and the pc. When cRIO and the script in the main.vi are running, the indicator turns light green.

C.4.4 Inequality of pressures between the reference and sample cells

The pressures read by the pressure transducers in the reference and sample cells are unequal due to the fact that the volume between V_1 and V_2 and between V_2 and V_3 are not equal. However, the pressure magnitudes are not greatly different when the cells are empty. The pressure set-up in the reference cell filling has magnitudes approximately equals to the desired whole numbers. This is due to the system not being fully automated, but the values are not greater than 1 % from the desired.

It is recommendable that the ratio of the reference cell to the sample cell should be greater than 1; hence the system will be modified to the ratio of 2. The actual volume of the cells will also be reduced ± 10 ml. The inequality of pressures dilemma resulted in longer pressurisation of the sample cell by the reference cell.

C.4.5 Pump

A syringe pump is strongly not recommended when it comes pressurising the reference cell, for it requires a lot of manual work to control the syringe. Due to this dilemma an automatic pump D260 from Teledyne was purchased towards the end of the project, thus enabling an automatic control of the pump, and far less physical exertion.

C.5 Measurement of cell volumes

The volumes of the empty reference and sample cells were obtained by allowing the gas, helium, to expand from the reference cell into the sample cell or vice versa, in a fashion similar to the technique described in the Helium pycnometry section (APPENDIX B). This procedure was performed with both the empty sample cell was empty and with the sample cell filled with aluminium sphere of a known volume for calibration. Table C-1 shows the data for cell volume measurements for run 1 and run 2.

Table C-1: Data for cell volume measurements

Parameters	**Run 1**	**Run 2**
P_1 (bar)	12.97	12.94
P_2 (bar)	6.46	6.33
P_3 (bar)	12.99	12.97
P_4 (bar)	6.55	6.46
V_x (cm3)	1.79	1.79
P_1/P_2	2.007	2.044
P_3/P_4	1.983206	2.008
V_B/V_A	1.00774	1.0179

C.6 Reproducibility

In order to determine the reproducibility of the adsorption isotherm data, 2 runs were performed the untreated samples. As shown in **Figure C-10**, the reproducibility for both samples is good.

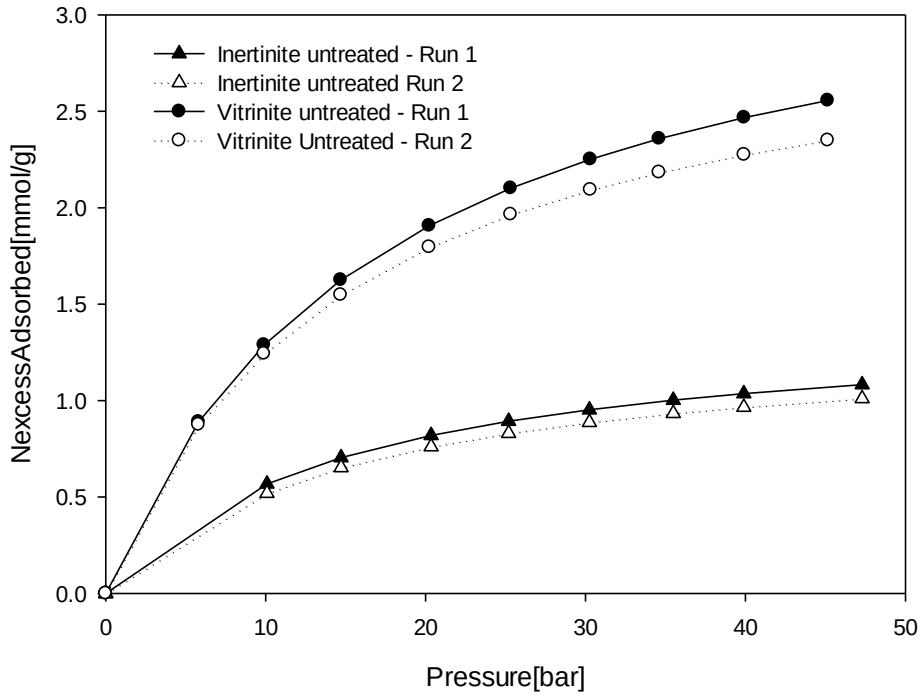

Figure C-10: Reproducibility of adsorption isotherms

C.7 Algorithm for measurements

set_v1,O

set_v2,C

set_v3,C

display_message, Setting pump pressure to start pressure

set_pressure, 24.000000

wait_pressure, 10.000000, up

set_v1, C

stop_pump

gosub, do_test

set_v1, O

display_message, Setting pressure to next pressure step

set_pressure, 34.000000

wait_pressure, 20.000000, up

set_v1, C

stop_pump

gosub, do_test

set_v1, O

display_message, Setting pressure to next pressure step

set_pressure, 44.000000

wait_pressure, 30.000000, up

set_v1, C

stop_pump

gosub, do_test

set_v1, O

display_message, Setting pressure to next pressure step

set_pressure, 54.000000

wait_pressure, 40.000000, up

set_v1, C

stop_pump

gosub, do_test

set_v1, O

display_message, Setting pressure to next pressure step

set_pressure, 64.000000

wait_pressure, 50.000000, up

set_v1, C

stop_pump

gosub, do_test

set_v1, O

display_message, Setting pressure to next pressure step

set_pressure, 74.000000

```
wait_pressure, 60.000000, up

set_v1, C

stop_pump

gosub, do_test


display_message, Venting

set_v1, C

set_v3, O

set_v2, O

wait, 30

set_v1, C

set_v3, C

set_v2, C

display_message, Stopped

stop


:do_test

start_logging

display_message, Logging

set_v2, O

wait, 10

set_v2, C

wait, 0
```

```
stop_logging

display_message, Stopped logging

return
```

APPENDIX D

ADSORPTION ISOTHERMS

D.1 NIST Webbook data

Table D-1: NIST webbook isothermal data for CO_2 at 28.5°C (subcritical) and 32.4°C (Supercritical)

28.5°C					32.4°C				
Temperature (C)	**Pressure (bar)**	**Density (mol/l)**	**Volume (l/mol)**	**Phase**	**Temperature (C)**	**Pressure (bar)**	**Density (mol/l)**	**Volume (l/mol)**	**Phase**
28.5	0	0	infinite	vapor	32.4	0	0	infinite	vapor
28.5	1	0.040063	24.961	vapor	32.4	2	0.079456	12.586	vapor
28.5	2	0.080516	12.42	vapor	32.4	4	0.16042	6.2336	vapor
28.5	3	0.12137	8.2393	vapor	32.4	6	0.24297	4.1157	vapor
28.5	4	0.16263	6.1488	vapor	32.4	8	0.32718	3.0564	vapor
28.5	5	0.20432	4.8944	vapor	32.4	10	0.41314	2.4205	vapor
28.5	6	0.24643	4.058	vapor	32.4	12	0.50094	1.9962	vapor
28.5	7	0.28899	3.4604	vapor	32.4	14	0.59068	1.693	vapor
28.5	8	0.332	3.0121	vapor	32.4	16	0.68248	1.4652	vapor
28.5	9	0.37548	2.6633	vapor	32.4	18	0.77645	1.2879	vapor
28.5	10	0.41943	2.3842	vapor	32.4	20	0.87272	1.1458	vapor
28.5	11	0.46389	2.1557	vapor	32.4	22	0.97145	1.0294	vapor
28.5	12	0.50884	1.9652	vapor	32.4	24	1.0728	0.93215	vapor
28.5	13	0.55432	1.804	vapor	32.4	26	1.1769	0.84968	vapor
28.5	14	0.60034	1.6657	vapor	32.4	28	1.284	0.7788	vapor
28.5	15	0.64692	1.5458	vapor	32.4	30	1.3943	0.71718	vapor
28.5	16	0.69406	1.4408	vapor	32.4	32	1.5081	0.66308	vapor
28.5	17	0.74179	1.3481	vapor	32.4	34	1.6256	0.61515	vapor
28.5	18	0.79013	1.2656	vapor	32.4	36	1.7472	0.57235	vapor
28.5	19	0.8391	1.1918	vapor	32.4	38	1.8731	0.53386	vapor
28.5	20	0.88871	1.1252	vapor	32.4	40	2.0039	0.49902	vapor
28.5	21	0.939	1.065	vapor	32.4	42	2.14	0.46729	vapor

28.5	22	0.98997	1.0101	vapor	32.4	44	2.282	0.43822	vapor
28.5	23	1.0417	0.96	vapor	32.4	46	2.4304	0.41145	vapor
28.5	24	1.0941	0.91399	vapor	32.4	48	2.5862	0.38667	vapor
28.5	25	1.1473	0.8716	vapor	32.4	50	2.7502	0.36362	vapor
28.5	26	1.2013	0.83242	vapor	32.4	52	2.9235	0.34205	vapor
28.5	27	1.2562	0.79608	vapor	32.4	54	3.1077	0.32178	vapor
28.5	28	1.3119	0.76228	vapor	32.4	56	3.3044	0.30262	vapor
28.5	29	1.3685	0.73075	vapor	32.4	58	3.5161	0.28441	vapor
28.5	30	1.426	0.70127	vapor	32.4	60	3.7457	0.26697	vapor
28.5	31	1.4845	0.67363	vapor	32.4	62	3.9975	0.25016	vapor
28.5	32	1.544	0.64766	vapor	32.4	64	4.2774	0.23379	vapor
28.5	33	1.6046	0.62321	vapor	32.4	66	4.5944	0.21766	vapor
28.5	34	1.6663	0.60014	vapor	32.4	68	4.9631	0.20149	vapor
28.5	35	1.7291	0.57833	vapor	32.4	70	5.4097	0.18485	vapor
28.5	36	1.7932	0.55767	vapor	32.4	72	5.9897	0.16695	vapor
28.5	37	1.8585	0.53806	vapor	32.4	74	6.8665	0.14564	vapor
28.5	38	1.9252	0.51942	vapor	32.4	74	6.8665	0.14564	supercritical
28.5	39	1.9933	0.50168	vapor	32.4	74	6.8665	0.14564	supercritical
28.5	40	2.0629	0.48476	vapor	32.4	76	9.5518	0.10469	supercritical
28.5	41	2.134	0.46859	vapor	32.4	78	13.692	0.073035	supercritical
28.5	42	2.2069	0.45313	vapor	32.4	80	14.509	0.068921	supercritical
28.5	43	2.2814	0.43832	vapor	32.4	82	15.008	0.066629	supercritical
28.5	44	2.3579	0.42411	vapor	32.4	84	15.377	0.065034	supercritical
28.5	45	2.4363	0.41045	vapor	32.4	86	15.672	0.063809	supercritical
28.5	46	2.5169	0.39731	vapor	32.4	88	15.92	0.062813	supercritical
28.5	47	2.5997	0.38465	vapor	32.4	90	16.136	0.061973	supercritical
28.5	48	2.685	0.37243	vapor	32.4	92	16.327	0.061247	supercritical
28.5	49	2.7729	0.36063	vapor	32.4	94	16.5	0.060606	supercritical
28.5	50	2.8637	0.3492	vapor	32.4	96	16.657	0.060033	supercritical
28.5	51	2.9575	0.33812	vapor	32.4	98	16.802	0.059515	supercritical
28.5	52	3.0547	0.32736	vapor	32.4	100	16.937	0.059042	supercritical
28.5	53	3.1555	0.3169	vapor	32.4	102	17.063	0.058606	supercritical

28.5	54	3.2604	0.30671	vapor	32.4	104	17.181	0.058202	supercritical
28.5	55	3.3697	0.29676	vapor	32.4	106	17.293	0.057826	supercritical
28.5	56	3.4839	0.28703	vapor	32.4	108	17.399	0.057475	supercritical
28.5	57	3.6037	0.27749	vapor	32.4	110	17.5	0.057144	supercritical
28.5	58	3.7297	0.26812	vapor	32.4	112	17.596	0.056832	supercritical
28.5	59	3.8629	0.25887	vapor	32.4	114	17.688	0.056537	supercritical
28.5	60	4.0042	0.24974	vapor	32.4	116	17.776	0.056257	supercritical

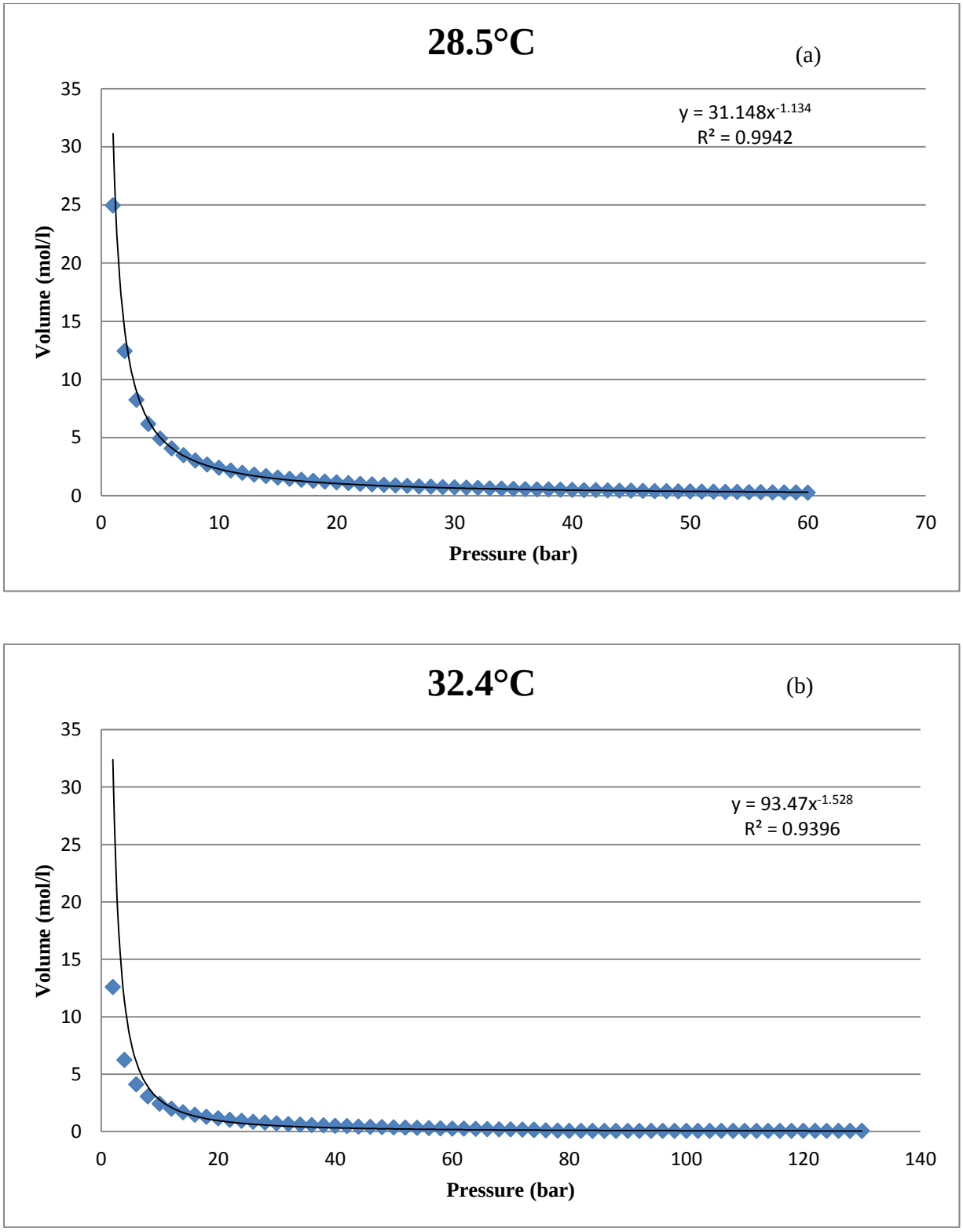

Figure D-1: An NIST Webbook plot of pressure against molar volume plot for CO_2 at (a) 28.5°C and (b) 32.4°C

D.2 Adsorption isotherms experimental Data

Table D-2: Parameters for adsorption isotherm measurements

	Experimental Conditions				
Sample	**Isothermal Temp(°C)**	**True density (cm^3/g)**	**Sample mass(g)**	**$Void_{sample}$ Volume(l)**	**Vapour Pressure(P_0)**
Inertinite nondemineralised untreatreated	28.86	1.65	1.689	0.0389	70.75
Vitrinite untreated nondemineralised	28.65	1.35	0.53	0.0396	70.40
Inertinite CO_2 treated 6 months at 45bar	28.68	1.45	0.565	0.0396	70.45
Vitrinite CO_2 treated 6 months at 45bar	28.86	1.33	0.55	0.0396	70.75
Inertinite CO_2 treated 6 months at 125 bar	32.2	1.65	0.76	0.0395	77.83
Vitrinite CO_2 treated 6 months at 125 bar	32.6	1.35	0.577	0.0396	77.94

Table D-3: Experimental adsorption isotherm data for subcritical CO_2 treated

Sample	**Initial Pressure(bar)**	**N_{exc} (mmol/g)**
Inertinite untreatreated	0	0
	10.0887	0.567460684
	14.7193	0.703998627
	20.3502	0.819154247
	25.1973	0.892570676
	30.2424	0.952351966
	35.4817	1.001836873
	39.8954	1.036220396
	47.2917	1.082950099

Vitrinite untreated	0	0
	5.81	0.889661961
	9.90586	1.288208963
	14.6988	1.624900732
	20.2212	1.906091499
	25.3216	2.10101811
	30.2995	2.250954665
	34.6008	2.357334039
	39.9144	2.466652533
	45.1458	2.556095767
Inertinite CO_2 treated 6 months at 45bar	0	0
	5.81	0.332112037
	10.4187	0.512118089
	15.3727	0.656725227
	20.4873	0.771033402
	25.4036	0.857890882
	30.3903	0.929489231
	34.8779	0.983278197
	40.6443	1.041167088
	45.357	1.081169257
Vitrinite CO_2 treated 6 months at 45bar	0	0
	4.81248	1.63548082
	9.97421	2.676165288
	15.3164	3.374410195
	19.9603	3.805739397
	25.2843	4.176491424
	30.2264	4.441739143
	35.2937	4.659089286
	40.0093	4.825085312

Vitrinite rich Supercritical - 6 months	0	0
	8.332128	0.964699
	15.10558	1.486064
	23.80616	1.963021
	33.15759	2.32904
	42.94087	2.611454
	53.52409	2.842429
	64.71348	3.030472
	70.2416	3.107875

APPENDIX E

PETROGRAPHIC AND PROXIMATE ANALYSIS DATA

E.1 Petrographic Analysis

Table E-1: Petrographic analysis data

untreated and treated	V2 -Coal A treated		V1- Coal A untreated		I2 – Coal B treated		I1 – Coal B untreated	
MACERAL (vol%)	inc. mm vol%	mmf vol%	inc. mm vol%	mmf vol%	inc. mm vol%	mmf vol%	inc. mm vol%	mmf vol%
telinite	1.4	1.4	7.2	7.8	1.0	1.0	0.0	0.0
collotelinite	41.2	41.7	44.4	47.8	16.3	16.3	13.7	14.0
vitrodetrinite	0	0.0	0.0	0.0	1.8	1.8	0.0	0.0
collodetrinite	0	0.0	0.0	0.0	2.3	2.3	0.0	0.0
corpogelinite	4.2	4.3	3.6	3.9	0.0	0.0	0.3	0.3
gelinite	0.6	0.6	0.0	0.0	0.0	0.0	1.0	1.0
pseudovitrinite	17.6	17.8	34.8	37.5	0.0	0.0	0.3	0.3
fusinite	4.8	4.9	0.4	0.4	4.0	4.0	6.3	6.5
reactive semifusinite	1.6	1.6	0.0	0.0	5.3	5.3	0.0	0.0
inert semifusinite	9.8	9.9	1.2	1.3	45.0	45.1	38.0	38.9
micrinite	0.2	0.2	0.0	0.0	1.0	1.0	1.0	1.0
macrinite	0.2	0.2	0.0	0.0	1.5	1.5	0.7	0.7
secretinite	1	1.0	0.0	0.0	2.0	2.0	0.3	0.3
funginite	0	0.0	0.0	0.0	0.0	0.0	0.0	0.0
inertodetrinite	14.4	14.6	0.0	0.0	17.0	17.1	32.7	33.4
sporinite	0.8	0.8	0.0	0.0	0.5	0.5	0.7	0.7
cutinite	0.4	0.4	1.2	1.3	2.8	2.8	1.7	1.7
resinite	0.4	0.4	0.0	0.0	0.2	0.2	0.3	0.3
alginite	0	0.0	0.0	0.0	0.3	0.3	0.0	0.0
liptodetrinite	0	0.0	0.0	0.0	0.0	0.0	0.0	0.0
suberinite	0	0.0	0.0	0.0	0.0	0.0	0.0	0.0
exsudatinite	0.2	0.2	0.0	0.0	0.1	0.1	0.7	0.7
silicate	0.4		1.6		0.3		2.3	
sulfide	0.2		5.6		0.0		0.0	
carbonate	0.6		0.0		0.0		0.0	
quartz	0		0.0		0.0		0.0	
other	0		0.0		0.0		0.0	
TOTAL								
VITRINITE	65	65.8	90.0	97.0	21.4	21.5	15.3	15.7
INERTINITE	32	32.4	1.6	1.7	75.8	76.0	79.0	80.9
LIPTINITE	1.8	1.8	1.2	1.3	3.9	3.9	3.3	3.4
MINERAL MATTER	1.2		7.2		0.3		2.3	
Rmax	0.73		0.7		0.8		0.7	
st. dev.	0.07		0.0		0.1		0.0	
Rrandom	0.69		0.67		0.72		0.6	
st. dev.	0.06		0.04		0.08		0.1	
V classes	v5 - v9		v6 - v7		v6 - v9		v6 - v7	
RANK CATEGORY	Medium Rank C		Medium Rank C		Medium Rank C		Medium Rank C	

E.2 Proximate Analysis

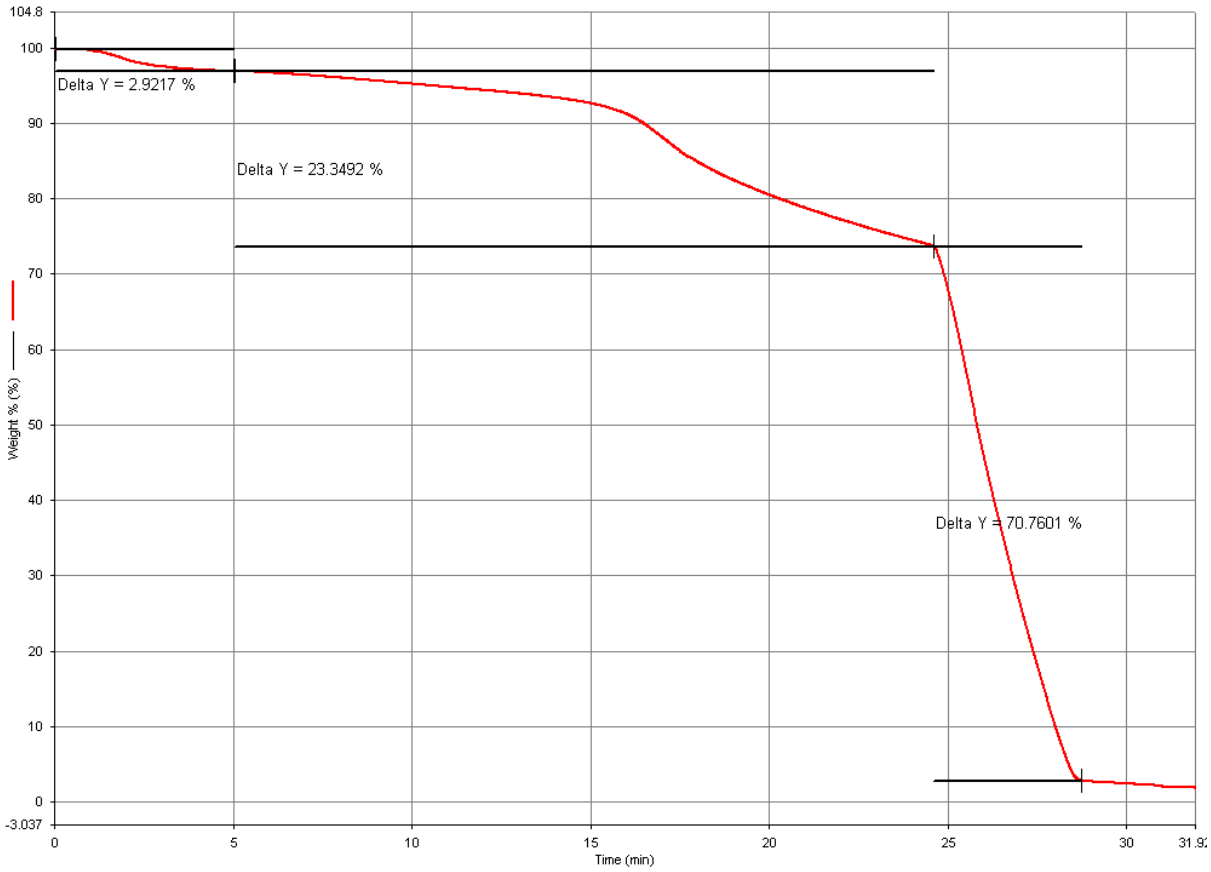

Figure E-1: Proximate analysis plot from TGA for coal A untreated sample

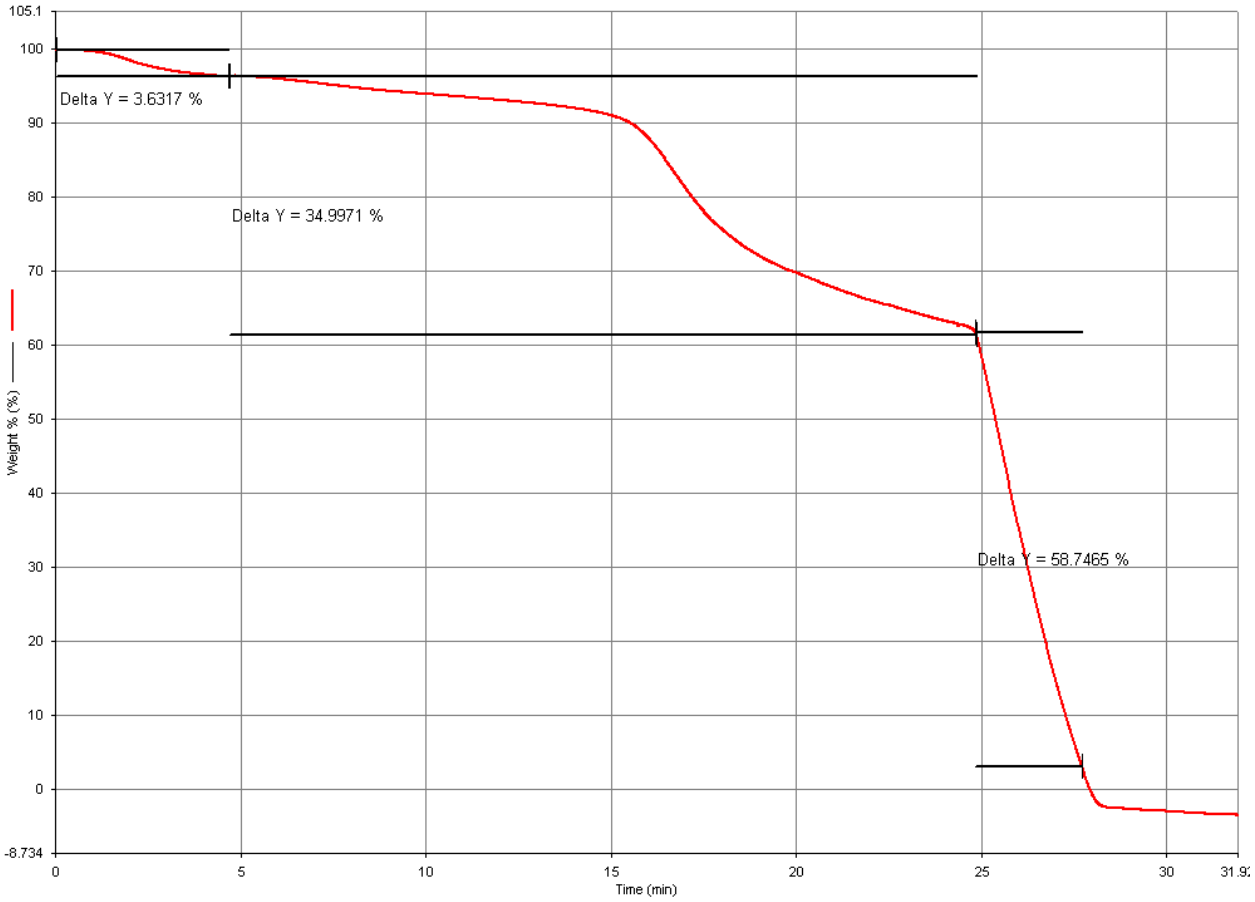

Figure E-2: Proximate analysis plot from TGA for coal B untreated sample